The University Of Sheffield.

An Investigation into the use of Coated Vanadium Alloys for the Purpose of Hydrogen Separation

By:

Stephen McCord

Yajue Wu, Vida Sharifi, Jim Swithenbank

A thesis submitted in partial fulfilment of the requirements for the degree of Doctor of Philosophy

The University of Sheffield
Faculty of Engineering
Department of Chemical and Biological Engineering

31st October 2017

Summary

A need for a new energy vector is highlighted, as carbon-based transport fuels are identified as producing sub-micron particulate causing both environmental and health issues. It is suggested that this energy vector should be hydrogen, however current commercial hydrogen production relies on the use of expensive hydrogen separation technologies such as amine separation and pressure swing adsorption.

It is suggested in this work that a focus be put on the development of hydrogen separation membranes, and in particular a focus on metallic membranes due to their potential for delivering a large hydrogen flux at a high purity and low operating cost. The major barrier to utilisation is identified as cost and thus motivation is provided for the need to develop a new generation of membrane.

The problem is identified as having two parts: identifying suitable surface catalysts and bulk membrane materials. Theoretical modelling was used to investigate the design of idealised membranes before tests were conducted.

A number of membranes were tested in a bespoke enclosure under conditions designed to mimic real-life operation, with tests undertaken under non-dilute hydrogen conditions and with a mixed CO_2/H_2 feed. Tests on a non-palladium containing surface catalyst, oxidised silver, proved to show no positive results. Pd-Ag Coated V-Ni and V-Ni-Al membranes are shown to have a maximum apparent permeability of 3.3 $x10^{-8}$ mol m^{-1} s^{-1} $Pa^{-0.5}$ and 4.1 $x10^{-8}$ mol m^{-1} s^{-1} $Pa^{-0.5}$ when tested at 300 °C with a binary feed mixture of CO_2 and H_2. In both instances the purity of the permeate was found to be 99.9% hydrogen. The permeability of both membranes under these conditions warrants further study.

Acknowledgements

I would like to thank my supervisors Jim, Yajue and Vida for your invaluable guidance and support over the last four years. It has been a privilege to work with you all on a new challenging topic for us all. You have each been an inspiration. I'd also like to thank Adrian for his support in trying to understand the world of material science and his infectious energy for the field.

I would also like to thank the technical staff out in Buxton, Dave and Mike. I was always amazed by your skills in the workshop and how you could fabricate things out of almost nothing and I will always be grateful for you being able to interpret my ramblings and drawings and turn them into something of the highest quality.

I would like to thank my family for being there whenever needed, not just now but forever. Mum & Dad, from the first day you took me to school to the present day you have always been interested in what I am doing. I apologise that it's gotten more progressively boring over the years – I promise this is the last of it!

Finally, I'd like to thank my wife, Ana. If nothing else was to come of the last four years it would still be the best of times as I will always be able to look back on the day we met, even if you insist "I looked at you a bit funny". Nothing brightened up my day more over the last four years of than being able to look up and see your face across the office. Your support and your love has been monumental, and I can't wait to start the next adventure together – Te amo mucho. Vamos, mi amor! Es hora de una nueva Aventura!

"New knowledge is the most valuable commodity on earth. The more truth we have to work with, the richer we become." – Kurt Vonnegut

Contents

List of Figures

List of Tables

List of Abbreviations

CS: Cryogenic separation

CVD: Chemical vapour deposition

EBVPD: Electron beam physical vapour

EDA: Ethylene-diamine

EDS: Energy dispersive x-ray analysis spectroscopy

DFT: Density functional unit

DoE: Department of Energy

GC: Gas chromatography

GHG: Greenhouse gases

MDS: Molecular dynamics simulation

MDEA: Methyl diethanolamine

MEA: Monoethanolamine

NMVOC: Non-methane volatile organic compounds

PM: Particulate matter

PSA: Pressure swing adsorption

PVD: Physical vapour deposition

SEM: Scanning electron microscopy

SMR: Steam reformation of natural gas

TCD: Thermal conductivity detector

TEM: Transmission electron microscopes

TR: Thermally rearranged

Nomenclature

Symbol	Name	Unit
J	hydrogen flux	[mol H] m^{-2} s^{-1}
D	diffusion coefficient	m^2 s^{-1}
t	membrane thickness	m
c_f	concentration of hydrogen atoms in the membrane	mol m^{-3}
c_u	hydrogen concentration	mol m^{-3}
K_S	Sievert constant	dimensionless
P	pressure	Pa
b	constant for the gas-metal system	dimensionless
k_{ri}	rate constant	
Θ	surface coverage	dimensionless
Θ_{eq}	surface component	dimensionless
k_{ads}	rate constants for adsorption	m^2 mol^{-1} s^{-1}
k_{des}	rate constants for desorption	m^2 mol^{-1} s^{-1}
D_0	pre-exponential factor for diffusion	m^2 s^{-1}
E_{dif}	activation energy for diffusion	kJ mol^{-1}
R	gas constant	J mol^{-1} K^{-1}
ΔS^0	standard molar entropy of solution	J K^{-1} mol^{-1}
ΔH^0	molar enthalpy of solution	kJ mol^{-1}
α_m	adsorption probability	dimensionless
μ	kinetic factor	dimensionless
k_b	Boltzmann constant	m^2 kg s^{-2} K^{-1}
m_h	molecular mass of hydrogen	g mol^{-1}
Υ	proportionality constant	dimensionless
ω	proportionality constant	dimensionless
δ	rate constant for desorption	
N	metal density	Kg m^{-3}
Γ_j	interstitial lattice sites for hydrogen	dimensionless
E_{bs}	activation energy for a hydrogen atom moving from a bulk to surface site	kJ mol^{-1}
E_{dif}	activation energy for hydrogen diffusion in the bulk	kJ mol^{-1}
c_s	saturation concentration of hydrogen in the metal	([mol H] m^{-3}
E_d	activation energy for desorption	kJ mol^{-1}
E_A	activation energy for surface to bulk transition	kJ mol^{-1}
E_B	activation energy for bulk to surface transition	kJ mol^{-1}
h	mass transfer coefficient	m s^{-1}
C	concentration of hydrogen in the bulk	[mol H] m^{-3}
	atomic adsorption rate	[mol H] m^{-2} s^{-1}
$S(\Theta)$	coverage dependant sticking coefficient	dimensionless
Γ	bombardment rate	[mol H] m^{-2} s^{-1}
R	ideal gas constant	J K^{-1} mol^{-1}
K	constant that is dependent on the probability of adsorption and desorption over empty and occupied sites	dimensionless
θ_{00}	modification of the surface coverage	dimensionless
w	pair-wise interaction energy	kJ mol^{-1}
N_{xx}	number of OO, AA and OA pair sites available	mol pairs m^{-2}
N_s	metal surface atom concentration	[mol Pd] m^{-2}

N_b	bulk metal atom concentration	[mol Pd] m^{-3}
v_d	rate constant for surface to bulk transfer	m^3 [mol H]$^{-1}$ s^{-1}
X_s	hydrogen-metal atomic ratio in the bulk metal	dimensionless
v_0	pre-exponential factor	m^3 [mol H]$^{-1}$ s^{-1}
ρ_m	membrane metal density	g m^{-3}
M_m	membrane metal atomic mass	g mol^{-1}
β_d	bulk-to-surface rate constant	m^3 [mol H]$^{-1}$ s^{-1}
β_0	pre-exponential factor for bulk-to-surface transfer	m^3 [mol H]$^{-1}$ s^{-1}
α_c	diffusion coefficient	dimensionless
a	lattice parameter	m
Γ_j	diffusive jump frequency	s^{-1}
Γ_{j0}	pre-exponential factor	s^{-1}
E_j	activation energy for a jump	kJ mol^{-1}
BDJ	bulk diffusive jump	s^{-1}
k_d	activated rate constant	m^2 mol^{-1} s^{-1}
k_0	pre-exponential factor for the desorption rate	m^2 [mol H]$^{-1}$ s^{-1}
N_{AA}	concentration of occupied nearest neighbour sites	mol pairs m^{-2}
z	number of nearest neighbour sites on the surface	dimensionless
F(θ)	coverage factor	dimensionless
$\Delta\overline{G_H}$	relative partial Gibbs free energy of dissolution	kJ [mol H]$^{-1}$
$\Delta\bar{S}_H^0$	relative partial molar entropy	kJ [mol H]$^{-1}$
$\Delta\overline{H_H^0}$	relative partial molar enthalpy	kJ [mol H]$^{-1}$
W_{HH}	hydrogen interactions in the solid	kJ [mol H]$^{-1}$
ε	support porosity	dimensionless
τ	tortuosity	dimensionless
r	characteristic pore diameter	m
t_p	porous layer thickness	m
P_m	mean pressure	Pa
θ_k	Knudsen surface coverage	dimensionless
μ	gas viscosity	mPa s^{-1}
γ_H	activity coefficient	dimensionless
μ_H	hydrogen chemical potential	kJ mol^{-1}
μ_H^0	chemical potential at infinite dilution	kJ mol^{-1}
σ	hydrostatic pressure of hydrogen in the metal lattice	Pa
Y	stress parameter	Pa
Sh	sherwood number	dimensionless
K_c	film mass transfer coefficient	m s^{-1}
t_f	film thickness	m
D_{gb}	binary gas diffusivity	m^2 s^{-1}
g(Re)	function of the Reynolds number	dimensionless
Sc	Schmidt number	dimensionless
K_c	matrix of the mass transfer coefficients	dimensionless
Z	matrix of the correction factors used to account for the high transfer rates	dimensionless
ϕ	permeability	mol m^{-1} s^{-1} $Pa^{-0.5}$
E_c	activation energy for dissociation	kJ mol^{-1}
$\Delta\overline{S_0^0}$	entropy of hydrogen absorption under standard conditions	J mol^{-1}

Extended Summary

A need for a new energy vector is highlighted, as existing carbon-based transport fuels have been shown to have negative impacts both the environment and on public health. Whilst the environmental impacts of carbon-based fossil fuels are widely cited and discussed, the impacts on health are not always as visible. The combustion of carbon-based fuels has been shown to produce sub-micron size particulate matter (PM), which has been shown to cause over 29,000 deaths annually and worsen existing respiratory diseases.

This thesis suggests using hydrogen as this new low-carbon energy vector. Hydrogen is a promising alternative fuel as it is versatile both in its production and utilisation. Hydrogen production is currently dominated by steam methane reformation (SMR) of natural gas, with coal/biomass gasification and electrolysis of water also potential sources. For utilisation as fuel, hydrogen can be combusted through gas engines, burners or utilised in fuel cells. The use of hydrogen fuel cells in the transport sector has achieved some success in limited programmes, however hydrogen currently remains prohibitively expensive for use in this manner.

A contributing factor to this problem is the separation of hydrogen from other gases (predominantly carbon dioxide) remains expensive in existing SMR processes. Existing hydrogen-carbon dioxide separation technology is dominated by “active” process such as chemical and physical adsorptive processes, examples include amine and zeolite capture processes, and cryogenic separation. These processes are typically capitally intensive and require significant operating expenses due to being energy intensive, alongside requiring replenishment of capture materials (particularly for amine separators) and extensive maintenance. An argument is made for the requirement to develop more “passive” separation technology, with lower operating costs (less replenishment and maintenance) and a smaller energy penalty.

It is suggested that membranes could provide this, and a review of membrane technology was completed in this work. Current membrane systems are not widely used for hydrogen separation due to their prohibitive cost making them an unattractive alternative to existing technologies. At this point the aim of the project was set: to develop and design an economically viable membrane separation system in which hydrogen can be separated at high purity form other gaseous products of SMR and gasification, primarily carbon dioxide.

Upon reviewing polymer, ceramic and metallic membranes, a decision was made to focus on metallic membranes for further investigation due to their unmatched ability to produce both a high flux (permeate flow rate) and a high hydrogen selectivity. Traditionally metallic membranes for hydrogen

separation have been dominated by palladium and palladium alloy (primarily palladium-silver) membranes due to palladiums natural affinity for hydrogen permeation. Whilst these membranes offer excellent selectivity and deliver a reasonable permeate flow rate, they remain prohibitively expensive. It is identified that to become economically feasible, palladium use in membranes needs to be minimised or eliminated.

A focus was put onto the design of new “thick”, free-standing membranes – considering both bulk material and surface catalysts. It was found that an ideal bulk membrane material would have excellent hydrogen diffusivity and solubility properties – with the group Vb metals (vanadium, niobium, tantalum) and their alloys identified as ideal candidates. As these metals and their alloys do not dissociate hydrogen a need for a surface coating to catalyse this reaction was identified. The bulk membrane materials tested were palladium, niobium, vanadium and two vanadium alloys (vanadium-nickel and vanadium-nickel-aluminium).

It was found that an ideal surface catalyst would promote dissociation (re-association on the permeate side) without limiting the bulk transport of hydrogen in conditions which should lead to bulk-limited diffusion. The coatings identified and utilised in this work were: palladium, palladium silver alloys of varying silver content and oxidised silver. The coatings were adhered to the membranes using electroless plating and physical vapour deposition techniques.

A review of existing permeation models was conducted. With the Ward and Dao model for hydrogen permeation highlighted and utilised in this work for the modelling of thick palladium membranes (as was done by Ward and Dao). Subsequently, effort was made in modifying the existing model to predict the behaviour of coated vanadium-nickel membranes.

A membrane test enclosure was designed for the testing of various metallic membranes – palladium, niobium, vanadium and vanadium alloy membranes were all tested this. Tests were conducted with both a pure hydrogen feed and a mixed hydrogen (40% vol.) and carbon dioxide (60% vol.) feed. The group Vb metal membranes were coated with the catalytic coatings identified above. Palladium membranes were used to provide “yardstick” measurements and to verify the experimental procedure and set-up. The oxidised silver coatings on niobium and vanadium membranes were found to be unsuitable for use, due to their low apparent permeabilities (with little flux evolved), instability and their need to operate outside the required temperature range.

Niobium membranes were tested with various pure palladium (Pd 100) and two palladium-silver alloy coatings (containing 76% palladium (Pd 76) and 55% palladium (Pd 55)) to investigate the impact on minimising the use of palladium. The performance of the Pd 100 and Pd 76 coatings was found to be

comparable on both pure hydrogen and mixed hydrogen-carbon dioxide feeds. A significant drop-off was found for the Pd 55 coating, which is possibly explained by a loss of active surface permeation sites causing the membrane to become surface and not bulk diffusion limited. The permeability of hydrogen through niobium was found to be lower than that predicted in Gorsky-type studies, this finding is consistent with other experimental data collected in non-dilute conditions.

The Pd-Ag coated V-Ni membrane tested in pure hydrogen was found to have a maximum permeability of 4.55 x 10^{-8} mol m^{-1} s^{-1} $Pa^{-0.5}$ a value similar to that found for other tests on the same membrane. The Pd-Ag coated V-Ni-Al membrane was found to have a maximum permeability of 6.35 x 10^{-8} mol m^{-1} s^{-1} $Pa^{-0.5}$ in pure hydrogen test conditions, with this value being comparable to that of other published data for similar membranes.

Pd-Ag Coated V-Ni and V-Ni-Al membranes are shown to have a maximum apparent permeability of 3.3 x10^{-8} mol m^{-1} s^{-1} $Pa^{-0.5}$ and 4.1 x10^{-8} mol m^{-1} s^{-1} $Pa^{-0.5}$ when tested at 300 °C with the mixed carbon dioxide/hydrogen feed. In both instances the purity of the permeate was found to be 99.9% hydrogen. The permeability of both membranes under these conditions warrants further study, at higher pressures on thinner membranes to produce the required molar flux for commercialisation.

1 Introduction

1.1 Background

1.1.1 Current UK Energy Supply and Trends

Fossil fuels are the primary source of energy worldwide. Between 2006-2013, the percentage of total energy consumed provided by fossil fuels remained steady at around 81% (World Bank, 2016).

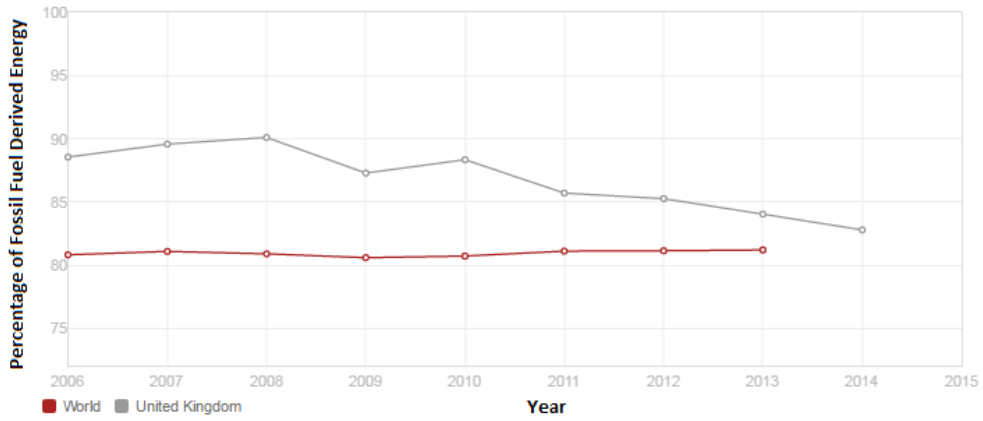

Figure 1.1 – World-wide and UK fossil fuel energy consumption (World Bank, 2016)

As can be seen in figure 1.1 the UK has been consistently above this worldwide average, although a decreasing trend has been established since 2010. Looking in greater detail at the UK energy picture allows for a deeper understanding of the energy consumption per sector.

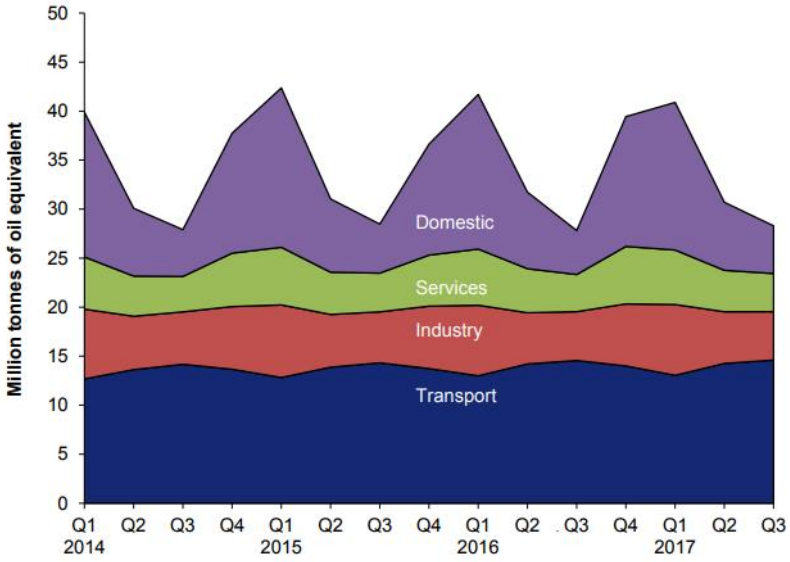

Figure 1.2 – UK total energy consumption by sector (Evans and Harris, 2018)

Figure 1.2 shows that energy consumption in the transport, industry and service sectors is relatively constant throughout the year, with domestic use being more seasonal; the increase in quarters one and four are attributed to the use of central heating systems during the winter. The figure also shows the oil equivalent consumption through the year, for 2015 the peaks average out at approximately 33 million tonnes of oil equivalent. Figures 1.1 and 1.2 can be combined to show the large-scale dependency on fossil fuels within the UK.

It has been long understood that the combustion of fossil fuels has a negative impact, both on the environment and on human health. The impacts of anthropogenic climate change are well documented, both in critical reviews and globally in political summits, such as the 2015 UN conference on climate change in Paris. The health impacts of the use of fossil fuels will be discussed in greater detail later section 1.1.4.

Highly visible events such as the Paris conference are vital for increasing global co-operation, and for improving public perception on the threat of climate change. Alongside this, national legislation is required.

The UK energy act 2013 states that the UK will produce 30% of its energy from renewable sources by 2020 (Parliament of the United Kingdom, 2013). Alongside this the report also states that the UK will cut greenhouse emissions by 50% on 1990 levels before 2025 and 80% before 2050 (Parliament of the United Kingdom, 2013).

1.1.2 Environmental Impacts of Fossil Fuel Usage

As briefly mentioned in section 1.1.1, the combustion of fossil fuels has a significant negative impact on the environment. Whilst the primary justification for this research is the improvement of human health it would be incomplete to not discuss the other major benefit of moving from traditional fossil fuel combustion; a reduction in the contribution towards anthropogenic climate change.

Greenhouse gases are those mainly responsible for changes in global temperatures, a gas is considered a greenhouse gas if it absorbs and emits radiation within the thermal infrared range. 2014 UK emissions are reported in millions of tons of carbon dioxide equivalent ($MtCO_2e$) as follows in table 1.1 below.

Table 1.1 – UK emissions of greenhouse gases (DECC, 2015a)

Species	2014 Emissions ($MtCO_2e$)	Change from 2013
Carbon dioxide	422	-8.9%
Methane	53.5	-4.1%
Nitrous oxide	21.9	+2.3%
Hydrofluorocarbons	16.3	+1.9%
Perfluorocarbons	0.3	0
Sulphur hexafluoride	0.5	0
Nitrogen trifluoride	0	0
Total	514.4	-7.7%

Of this total value for greenhouse gas (GHG) emissions, transport and energy supply account for 54% of the total, with a further 29% linked to residential and business properties (DECC, 2015a). Whilst total emissions of greenhouse gases have decreased it is important to note that some individual species have seen either an increase or a continuation of their level of emission. The DECC reports that the amount of greenhouse gas emissions in the UK has decreased continuously since 2012, where before this it remained largely stable, significantly below the UKs Kyoto Protocol target (DECC, 2015a). Whilst this decrease is encouraging the amount of emissions is still significant, alongside this it can be seen that global greenhouse gas emissions have continued to climb steadily. A major area of growth is Asia which has seen a significant increase in carbon dioxide emissions (US EPA, 2014).

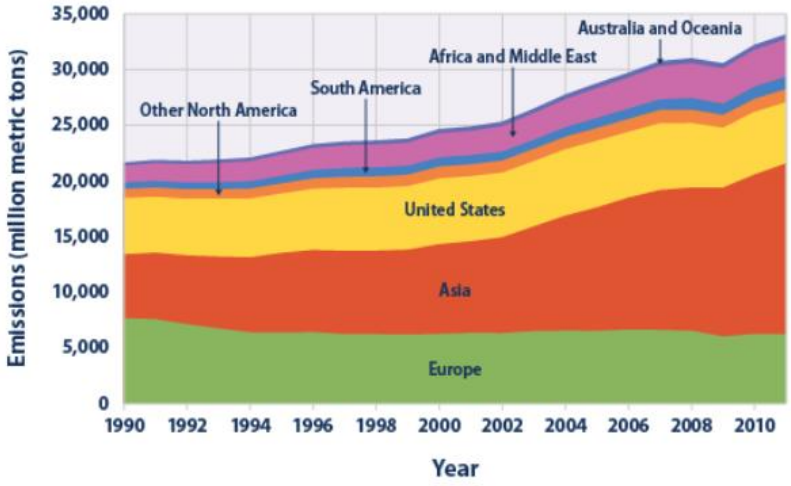

Figure 1.3 – Global greenhouse gas emissions by continent (US EPA, 2014)

Figure 1.3 shows that although efforts are being made to reduce greenhouse emissions, particularly in Europe, the steady climb in total emissions has not stopped and thus the impacts of greenhouse emissions will continue to grow.

The impacts of ever increasing greenhouse emissions are wide spread and varied; one well documented impact is the increase of average global temperatures, with 2015 being a significant year as global average temperatures have reached an average of 1 °C above the pre-industrial age temperature (1850) (Met Office, 2015). This increase in temperature has been linked with the decrease in polar ice, a potentially disastrous increase in sea levels (with an annual increase of 3.4mm measured for 2016) (NASA, 2016), unpredictable and unstable weather and a wide range of other human impacts.

This section has focussed primarily on the greenhouse effect, however combustion of fossil fuels can produce NOx and SOx compounds resulting in the formation of photoactive smog, the eutrophication of soils and the formation of acid rain (DEFRA, 2015).

One possible solution to combat the climate change problem would be a step change in the reduction of greenhouse emissions by using alternative energy sources or through the utilisation of carbon capture and storage systems.

1.1.3 Alternatives to Fossil Fuels

Due to the damaging nature of fossil fuels efforts have long been made to support alternative fuel sources. Numerous alternatives to fossil fuels exist, with the amount of energy produced through renewable sources increasing four-fold in the decade between 2004 and 2014 (DECC, 2015b).

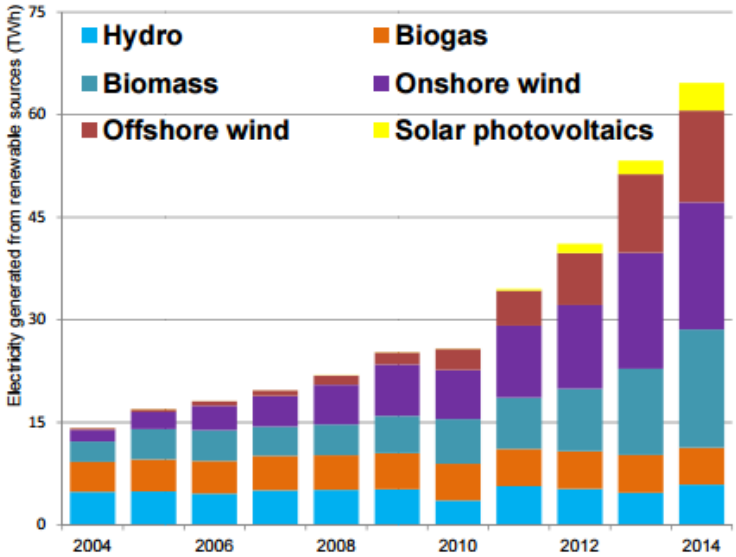

Figure 1.4 – Renewable energy sources in the UK (DECC, 2015b)

Of particular interest is the growth in the use of biomass as a fuel source, where at Drax power station biomass has begun to replace coal (with 3 of 6 furnaces now fired with this). Biomass itself is largely

seen as carbon neutral due to its absorption of carbon dioxide during its growth, however due to the emissions associated with transportation and preparation it is important to note that current biomass usage accounts for only an 80% decrease in carbon dioxide emissions for the fraction of coal replaced (Drax, 2014). As the UK begins to phase out coal by 2025 (BBC, 2015) it could be anticipated that the gasification or combustion of biomass will become more widespread due to the success Drax has had with its conversion.

Other alternative energy sources, including nuclear which is not listed above, will continue to play an increasing role in the UK energy sector, particularly if the planned construction of the Hinkley Point C plant is complete. However, alternative sources such as nuclear will not be discussed in detail here as they fall outside of the focus of this project.

1.1.4 Health Implications of Fuel Combustion

As mentioned in section 1.1.1, a major issue with the use of fossil fuels is the negative aspects that combustion products can have on human health. This can be extended to alternative energy sources too, as biomass and biogas produce similar combustion products due to the similarity in the chemical composition of these fuels to oil, gas and coal.

The products of combustion are wide ranging and vary depending on the fuel used and the combustion system itself. Volumes of text could be devoted to both these pollutants and methods of treatment for each, however for the sake of brevity only a summary of these are included in this report. Table 1.2 below summarises some of the key emissions, with species known to cause detriment to human health italicised.

Table 1.2 – Summary of the major emissions and impacts from fuel combustion in the UK

Species	Quantity emitted	Impact	Sources
CO_2	422 Mt (2014)	Greenhouse gas. Effects of emission are less significant if the source is biomass.	(DECC, 2015a)
CO	2 Mt (2013)	Toxic gas, binds to haemoglobin in the blood, can be fatal. In smaller doses breathing problems can develop.	(DEFRA, 2014a)
SO_2	0.31 Mt (2014)	Can cause acidification resulting in damage to soils, vegetation and buildings.	(DEFRA, 2015)
NO_x	0.95 Mt (2014)	Combine with NMVOCs to produce low level smog, resulting in increased incidences of breathing difficulty, asthma, reduced lung function & lung disease occurrence. Can cause acidification resulting in damage to soils, vegetation and buildings.	(DEFRA, 2015)

Species	Quantity emitted	Impact	Sources
NMVOCs	0.82 Mt (2014)	Combine with NO_x to produce low level smog, resulting in increased incidences of breathing difficulty, asthma, reduced lung function & lung disease occurrence.	(DEFRA, 2015)
NH_3	272 kt / 6kt (2014)	Produced mainly through agriculture but 6kt is formed through road transport. Can cause eutrophication damage to the environment.	(DEFRA, 2015)
PM_{10}	148 kt	Particulates in the size range of 2.5 to 10 µm, long term exposure to PM increases risk of developing cardiovascular disease and lung cancer.	(DEFRA, 2015)
$PM_{2.5}$	105 kt	Particulates in the size range of 1 to 2.5 µm, long term exposure to PM increases risk of developing cardiovascular disease and lung cancer.	(DEFRA, 2015)

Setting aside carbon dioxide, it can be seen that emissions of each of the other products has followed a downward trend from 1970 (DEFRA, 2015), (DEFRA, 2014a). This has been due to a range of advancements in combustion technology, flue gas treatment technology and process control.

1.1.5 The Sub-Micron Particulate Matter Problem

Of particular interest in this report is particulate matter (PM), particularly sub-micron particulates (PM_1), due to the varied and significant hazards posed by these to the population. Transport has been shown to be a major source of PM (Lee *et al.*, 2015), (Gowers, Miller and Stedman, 2014), with other sources including domestic gas appliances such as boilers (US EPA, 1995) and diesel generators (US EPA, 1996). The three sources listed for PM are of particular interest due to their wide spread domestic and commercial use and thus they contribute a significant amount to the health problems linked to exposure to PM.

Whilst emissions of PM may be decreasing, the threat to the health of the population still persists.

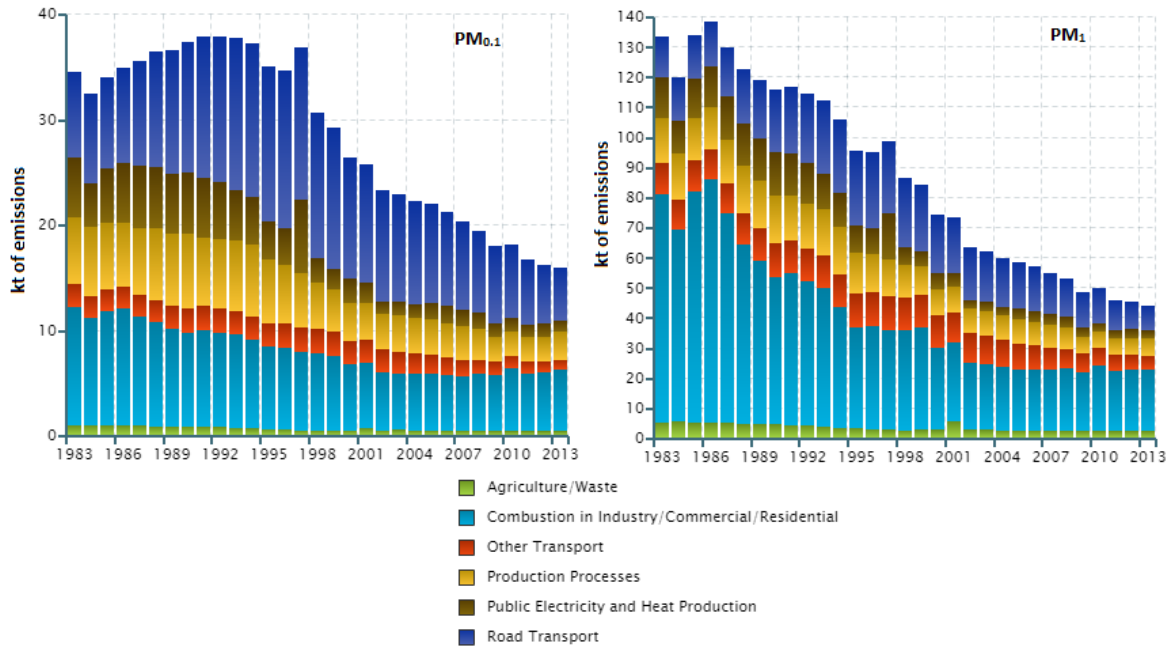

Figure 1.5 – Graphs showing UK emissions of $PM_{0.1}$ and PM_1 and sources (DEFRA, 2014b)

Submicron particulate matter has been shown to have a negative impact on human health; it is estimated that particulate air pollution causes 29,000 deaths in the UK every year (Gowers, Miller and Stedman, 2014). The production of carbon submicron particles from incomplete combustion in vehicles is particularly problematic, with smaller particles being able to penetrate deeper into the respiratory system (Katoshevski *et al.*, 2011). This is particularly a problem for those that live in urban areas or those near high volumes of traffic. Studies have been conducted to show that those who live within a "critical distance (275m)" of major road networks have a higher occurrence of respirational diseases (Jephcote and Chen, 2013), (Yim and Barrett, 2012) than those that do not.

Figure 1.4 shows that combustion of fuels in industrial, commercial and domestic locations is the UKs primary source of submicron PM, this has the potential to be even more problematic than transport emissions, as the critical distance suggested for transport is significantly larger than the typical residential and commercial property size.

The current worldwide solution lies in limiting the production of sub-micron particles (Katoshevski *et al.*, 2011) due to the difficulty in efficient capture of these particles. One potential solution to reduce potential submicron particulate emissions would be to not combust carbon-based fuels and use an alternative fuel source or energy vector; it is proposed in this study to use hydrogen. The combustion of hydrogen does not produce any particulate matter, as the only product is water vapour.

1.1.6 Hydrogen as a Fuel Source

Technology for the combustion of hydrogen varies from traditional burners to modern fuel cells; the use of fuel cells often requires high purity hydrogen, typically with purity of greater than 99.99%. This diversity has the potential to be an advantage to the use of hydrogen, as existing burners in the UK are designed to accept fuel in the same Wobbe band as hydrogen (Dodds and Demoullin, 2013); with the Wobbe Index being an indicator of the interchangeability of fuel gases. However other studies show more research must be undertaken to ensure this (Haeseldonckx and D'haeseleer, 2007). Studies suggest that conversion of the current gas grid would be feasible but concerns exist due to a reduction in grid capacity and reduced capability of in-grid storage (Dodds and Demoullin, 2013).

As mentioned above, a major source of health damaging emissions is transport. Conversion to usage of a hydrogen fuel would eliminate the production of particulate matter. Brazil has launched a fuel cell powered bus and has also constructed the necessary hydrogen fuelling station (Lucas, 2009), the station is currently capable of supplying hydrogen for three buses to travel 300 km a day. It has also been recently revealed that mass produced hydrogen powered cars have "arrived" on British roads (Vaughan, 2015); however the vehicles remain prohibitively expensive even with government grants.

There are still barriers to overcome with regards to the wide-spread use of hydrogen as a fuel source within the UK and the world in general. Economic factors evidently still play a significant role in this, hence efforts to make hydrogen more affordable and accessible must be made.

1.1.7 Production of Hydrogen

Hydrogen can be produced via numerous different pathways, this gives the potential for diversification of production which can increase security of supply. (Dodds and Mcdowall, 2012) list the hydrogen production technologies as:

- Steam reformation of natural gas (methane) (SMR)
- Coal gasification
- Biomass gasification
- Anaerobic digestion of biomass
- Electrolysis of water
- Thermochemical cracking of water (using the waste heat from nuclear power)

Currently the majority of hydrogen in the UK, and the world, is produced through SMR. However, gasification, particularly of biomass, is also technologically and economically feasible. Figure 1.5 shows

a timeline for the estimated evolution of hydrogen production in the US, it is expected that the pattern will be similar in the UK. SMR and gasification will be the hydrogen sources focussed on within this report due to their immediacy for production.

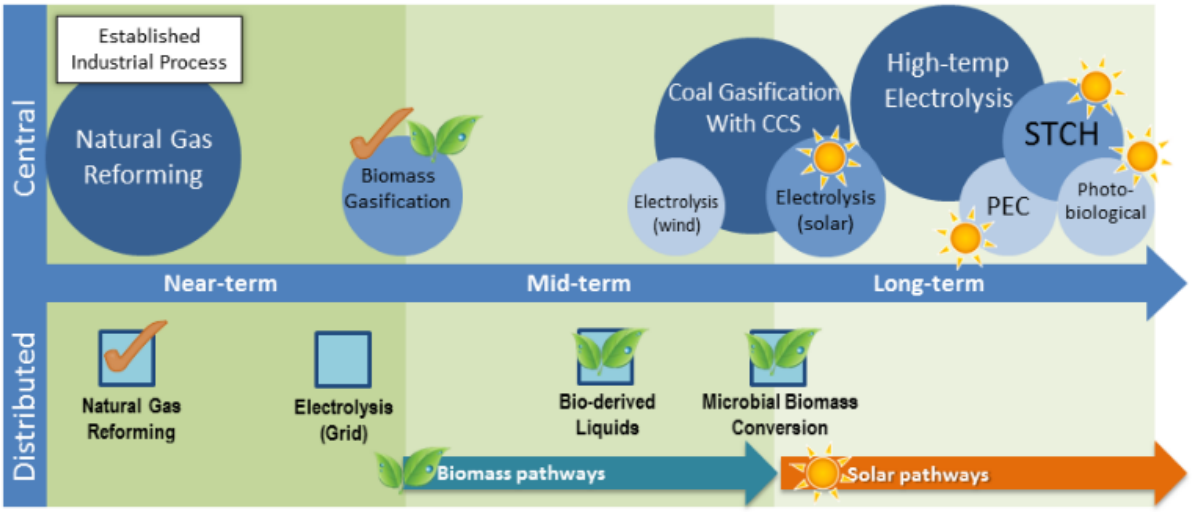

Figure 1.6 – Timeline of hydrogen production sources (US OEERE, 2016)

SMR consists of two stages, reformation of methane with steam to form hydrogen and carbon monoxide, some of this carbon monoxide continues to react with the steam to produce more hydrogen and carbon dioxide. SMR requires high temperature operation (800 °C) and the presence of a nickel catalyst (Air Products, 2013).

The process of gasification allows for solid or liquid hydrocarbon fuel sources to be transformed into a gaseous mixture, consisting primarily of hydrogen, carbon dioxide and carbon monoxide. This mixture is referred to as “syngas”; the source of the hydrocarbons can vary greatly – from fossil fuels to renewable or sustainable biomass. By separating hydrogen from the other products of gasification one can have a potentially renewable, clean combusting hydrogen fuel source.

Both SMR and the gasification of coal/biomass produce a similar chemical feedstock, syngas consisting primarily of hydrogen, carbon monoxide and carbon dioxide. Thus, it may be possible to use a universal hydrogen separation technology for both.

1.1.8 Current and Future Separation Technologies

Current hydrogen separation technologies are dominated by active processes, such as cryogenic separation (CS), and pressure swing adsorption (PSA).

Cryogenic separation is a long standing and well understood technology, with cryogenic separation of air being completed in the 19th century (Sreenivasulu *et al.*, 2015). A number of cryogenic processes have been developed; however the underlying theory behind them all is essentially the same. Cryogenic separation is undertaken by exploiting the differences between gas species phase transition properties through the use of a number of compression, cooling and expansion steps (Xu *et al.*, 2012).

Cryogenic separation of hydrogen and carbon dioxide can achieve the removal of over 90% of the carbon dioxide from the hydrogen stream (Xu *et al.*, 2012), the removed carbon dioxide can reach purities of over 99% and little of the hydrogen is lost during the process (Sreenivasulu *et al.*, 2015). As cryogenic separation is energy intensive it is important that minimal hydrogen loss occurs, or the energy penalty will be greater than expected. Cryogenic systems have high initial capital costs and incur a significant running cost due to the electrical demand for compression (Faraji, Sotudeh-Gharebagh and Mostoufi, 2005). Estimates for post-combustion capture of carbon dioxide in power plants are typically reported at between $30-42 per tonne of CO_2 avoided dependent on the cryogenic system used (Scholes *et al.*, 2013).

PSA is widely considered as a versatile method for separation and purification of gas mixtures (Sircar, 2002); and has been used for a variety of industrial gas separation processes. These include: gas drying, solvent vapour recovery, fraction-ation of air, *production of hydrogen from steam-methane reformation*, separation of CO_2 from landfill gas and *carbon monoxide/hydrogen separations* (Sircar, 2002).

Carbon capture rates for PSA can be as high as 99-100% with the use of monoethanolamine (MEA) as the solvent (Sreenivasulu *et al.*, 2015). Hydrogen purification from carbon dioxide and carbon monoxide using PSA can result in hydrogen purities of 99.98% (Lopes, Grande and Rodrigues, 2011); however at this purity losses of hydrogen in the waste stream were as high as 28% (Lopes, Grande and Rodrigues, 2011). This can be reduced to around 20% by applying optimal cycle times (Rahimpour *et al.*, 2013), but this loss is still potentially crippling for any hydrogen generation process. This is problematic in terms of overall efficiency as this must be added to the process energy penalty.

There are disadvantages to the use of PSA however; once again, like cryogenics, there is a need to vary both pressure and temperature thus creating an energy penalty. Alongside this there is a requirement to recharge the solvent causing further loss of overall efficiency.

The solvent used has a significant effect on the energy required for CO_2 capture; amine based solvents may require up to 4.8 MJ/kg of CO_2, whilst alternatives such as zeolites can reduce this to 1.7 MJ/kg (Sreenivasulu *et al.*, 2015) – the problem being that zeolite produces a significantly less pure CO_2

stream, suggesting loss of hydrogen. It must also be noted that these losses do not account for the need to replace solvent over time to keep removal efficiency at these levels.

PSA incurs significant capital costs due to the large amount of plant required alongside significant operational costs; for example, capture of carbon dioxide using MEA, amine solvents and vacuum swing adsorption are $55, $46 and $51 respectively per tonne of CO_2 (Scholes *et al.*, 2013). These prices are still somewhat optimistic especially for large scale applications, the carbon capture plant installed on the Boundary Dam power plant in Canada has doubled the cost of power (Langenegger, 2016). The Boundary Dam plant was the world's first commercial scale carbon capture and storage (CCS) plant and gives arguably the best reflection on what can be expected with current technology.

A computational study based on the recovery of hydrogen from a refinery off-gas stream suggests that the operating expenditure of such a plant would be around 7.5% of its capital expenditure per year – with an initial capital cost of around $2 million (Mivechian and Pakizeh, 2013); whilst recovering only around half of the hydrogen present on a per mole basis.

As stated at the start of this section both cryogenic separation and PSA are active processes that largely depend on the use of external energy sources to drive separation. Membranes have the potential to be passive in nature, provided they are designed to withstand and operate in the conditions typically found in a gasification or SMR process. Gasification and SMR processes typically produce syngas at temperatures well above 600 °C and pressures up to 30 bar (van Holt *et al.*, 2014), (Liu, Song and Subramani, 2010). These conditions are potentially very advantageous for membrane separation, where a gas pressure/concentration gradient is required to drive the process and higher temperatures often produce higher separating efficiencies (Ockwig and Nenoff, 2007). Whilst much research has been focussed into the development of suitable membranes, very few market ready membrane separation systems are available (EERC, 2010), (Al-Mufachi, Rees and Steinberger-Wilkens, 2015), (Iulianelli *et al.*, 2016). This is due to a variety of reasons, however most prominent are: a lack of membrane reliability and stability, and the prohibitive cost of the materials and manufacture.

Thus, further research must be carried out to develop a new generation of membranes, which are not only robust but economically feasible and fit for purpose.

1.2 Problem Statement and Project Aim

1.2.1 Problem Statement

The combustion of carbon-based fuels has a number of effects that are detrimental to the health of the general population of the UK and the wider world. Of particular concern is the emission of sub-micron particulate matter (PM); which has been shown to have a negative effect on human health. A major source of sub-micron PM is transport emissions – generated by private vehicles or public transport; research has shown that PM is a major contributor to respiratory disease and ultimately death in the UK. Alternative fuel sources must be found, one potential fuel source is hydrogen due to its clean combustion to water vapour. A major barrier to the use of hydrogen as a fuel is the difficulty in separating it from other gaseous products of steam reformation of methane and the gasification of biomass or coal. Current separation technologies are prohibitively expensive or do not provide hydrogen at a high enough purity for use within fuel cells.

1.2.2 Project Aim

This project aims to develop and design an economically viable membrane separation system in which hydrogen can be separated at high purity from the other gaseous products of gasification or steam methane reformation; primarily carbon dioxide.

1.3 Project Objectives

To achieve the aim stated in section 1.2.2 the following objectives were addressed:

- The identification of a suitable membrane separation technology
- The development of a suitable model to predict membrane flux and selectivity
- The determination of material(s) of construction of the membrane
- The determination of a suitable method of construction for the membrane
- The design and operating conditions of the membrane enclosure and membrane
- The completion of analytical tests to ensure purity of the permeate is acceptable
- The determination of the expected operational life of the membrane developed

1.4 Outline of the Thesis

This thesis consists of seven chapters, chapter one is an introduction and a justification for the research undertaken. Chapter two consists of a review of the relevant literature including: a brief summary of the SMR and gasification processes, a general review of membrane technologies and its alternatives and a more detailed review of metallic membranes, with particular attention paid to palladium-based and niobium/vanadium-based membranes.

Chapter three details the theoretical concepts that are core to membrane operations, with a broad spectrum of models considered, alongside a detailed explanation of a composite model developed by Timothy Ward & Tien Dao.

Chapter four details the theoretical concepts that are core to the production of the membranes tested as part of this PhD project. The chapter also includes a summary of the details the design and set up of the membrane enclosure and the experimental procedure.

Chapter five contains the computational modelling undertaken, including a general model for permeation of hydrogen in metals alongside a more detailed model based on the concepts discussed in chapter three.

Chapter six contains the experimental body of work undertaken as part of this PhD, the chapter can be split into two sections. The first part of the chapter reports the results from testing palladium membranes under various conditions, with the second part following the same formula as the second but with vanadium and niobium-based membranes.

Chapter seven contains a detailed comparison and discussion of the modelling and experimental results from chapters five and six, along with other notable results found within the literature. The merits and benefits of the work are discussed with a focus given to potential applications and the economic feasibility of implementing the tested membranes on a larger scale.

Conclusions are drawn and suggestions for future work to be undertaken are made at the end of the thesis.

1.5 Chapter One Reference List

Air Products (2013) *Steam methane reformer overview*. Available at: http://www.airproducts.com/~/media/Files/PDF/industries/energy-hydrogen-steam-methane-reformer-datasheet.pdf.

Al-Mufachi, N. A., Rees, N. V. and Steinberger-Wilkens, R. (2015) 'Hydrogen selective membranes: A review of palladium-based dense metal membranes', *Renewable and Sustainable Energy Reviews*. Elsevier, 47, pp. 540–551. doi: 10.1016/j.rser.2015.03.026.

BBC (2015) *UK's coal plants to be phased out within 10 years*. Available at: http://www.bbc.co.uk/news/business-34851718 (Accessed: 19 May 2016).

DECC (2015a) '2014 UK Greenhouse Gas Emissions', (March), pp. 1–33. Available at: https://www.gov.uk/government/uploads/system/uploads/attachment_data/file/416810/2014_stats_release.pdf.

DECC (2015b) *DUKES Renewables 2014*. Available at: https://www.gov.uk/government/uploads/system/uploads/attachment_data/file/449426/Chapter_6_Renewables.pdf.

DEFRA (2014a) *About Carbon Monoxide*. Available at: http://naei.defra.gov.uk/overview/pollutants?pollutant_id=4 (Accessed: 19 May 2016).

DEFRA (2014b) *About PM2.5,1.0,0.1*. Available at: http://naei.defra.gov.uk/overview/pollutants?pollutant_id=PMFINE (Accessed: 20 May 2016).

DEFRA (2015) *Emissions of Air Pollutants in the UK , 1970 to 2014*. Available at: http://webarchive.nationalarchives.gov.uk/20130123162956/http:/www.defra.gov.uk/statistics/files/Emissions-of-air-pollutants-statistical-release_updated-figures.pdf%5Cnhttps://www.gov.uk/government/uploads/system/uploads/attachment_data/file/388195/Emission.

Dodds, P. E. and Demoullin, S. (2013) 'Conversion of the UK gas system to transport hydrogen', *International Journal of Hydrogen Energy*, 38(18), pp. 7189–7200. doi: 10.1016/j.ijhydene.2013.03.070.

Dodds, P. E. and Mcdowall, W. (2012) 'A review of hydrogen production technologies for energy system models', *UCL Energy Institute, University College London*, (6), pp. 1–22.

Drax (2014) *Carbon Factsheet*. Available at: http://www.drax.com/media/56593/carbon-factsheet.pdf.

EERC (2010) 'Hydrogen separation membranes', *Advanced Membrane Technology and Applications*. EERC. Available at: http://www.undeerc.org/ncht/pdf/eercmh36028.pdf (Accessed: 20 November 2013).

Evans, W. and Harris, K. (2018) *Total Energy Statistics: Section 1*. Available at: https://www.gov.uk/government/uploads/system/uploads/attachment_data/file/669696/Total_Energy.pdf.

Faraji, S., Sotudeh-Gharebagh, R. and Mostoufi, N. (2005) 'Hydrogen recovery from refinery offgases', *Journal of Applied Sciences*, 5(3), pp. 459–464. Available at: http://scialert.net/qredirect.php?doi=jas.2005.459.464&linkid=pdf.

Gowers, A. M., Miller, B. G. and Stedman, J. R. (2014) *Estimating Local Mortality Burdens associated with Particulate Air Pollution*, *Public Health England*. Available at: http://www.hpa.org.uk/webc/HPAwebFile/HPAweb_C/1317141074607.

Haeseldonckx, D. and D'haeseleer, W. (2007) 'The use of the natural-gas pipeline infrastructure for hydrogen transport in a changing market structure', *International Journal of Hydrogen Energy*, 32(10–11), pp. 1381–1386. doi: 10.1016/j.ijhydene.2006.10.018.

van Holt, D., Forster, E., Ivanova, M. E., Meulenberg, W. a., Müller, M., Baumann, S. and Vaßen, R. (2014) 'Ceramic materials for H2 transport membranes applicable for gas separation under coal-gasification-related conditions', *Journal of the European Ceramic Society*. Elsevier Ltd, pp. 1–9. doi: 10.1016/j.jeurceramsoc.2014.03.001.

Iulianelli, A., Liguori, S., Wilcox, J. and Basile, A. (2016) 'Advances on methane steam reforming to produce hydrogen through membrane reactors technology: A review', *Catalysis Reviews*, 4940(January), pp. 1–35. doi: 10.1080/01614940.2015.1099882.

Jephcote, C. and Chen, H. (2013) 'Geospatial analysis of naturally occurring boundaries in road-transport emissions and children's respiratory health across a demographically diverse cityscape', *Social Science and Medicine*. Elsevier Ltd, 82, pp. 87–99. doi: 10.1016/j.socscimed.2013.01.030.

Katoshevski, D., Ruzal-Mendelevich, M., Hite, I. and Sher, E. (2011) 'Environmental and Health Risk Associated with Air pollution Emitted by Public Transportation, and a New Methodology for Reducing the Risk', *Procedia - Social and Behavioral Sciences*, 20, pp. 687–692. doi: 10.1016/j.sbspro.2011.08.076.

Langenegger, S. (2016) *Sask. carbon capture plant doubles the price of power*. Available at: http://www.cbc.ca/news/canada/saskatchewan/carbon-capture-power-prices-1.3641066 (Accessed: 6 June 2017).

Lee, B. P., Li, Y. J., Yu, J. Z., Louie, P. K. K. and Chan, C. K. (2015) 'Characteristics of submicron particulate matter at the urban roadside in downtown Hong Kong—Overview of 4 months of continuous high-resolution aerosol mass spectrometer measurements', *Journal of Geophysical Research : Atmospheres*, 120(14), pp. 7040–7058. doi: 10.1002/2015JD023311.

Liu, K., Song, C. and Subramani, V. (2010) *Hydrogen and syngas production and purification technologies*. Available at: http://onlinelibrary.wiley.com/doi/10.1002/9780470561256.fmatter/summary (Accessed: 4 February 2014).

Lopes, F. V. S., Grande, C. a. and Rodrigues, A. E. (2011) 'Activated carbon for hydrogen purification by pressure swing adsorption: Multicomponent breakthrough curves and PSA performance', *Chemical Engineering Science*, 66(3), pp. 303–317. doi: 10.1016/j.ces.2010.10.034.

Lucas, L. (2009) 'Brazil launches first fuel cell bus, with hydrogen station', *Fuel Cells Bulletin*, 2009(9), p. 2. doi: 10.1016/S1464-2859(09)70273-1.

Met Office (2015) *Global Average Temperature*. Available at: http://www.metoffice.gov.uk/research/news/2015/global-average-temperature-2015 (Accessed: 26 May 2016).

Mivechian, A. and Pakizeh, M. (2013) 'Hydrogen recovery from Tehran refinery off-gas using pressure swing adsorption, gas absorption and membrane separation technologies: Simulation and economic evaluation', *Korean Journal of Chemical Engineering*, 30(4), pp. 937–948. doi: 10.1007/s11814-012-0221-y.

NASA (2016) *Sea Level Rise*. Available at: http://climate.nasa.gov/vital-signs/sea-level/ (Accessed: 26 May 2016).

Ockwig, N. W. and Nenoff, T. M. (2007) 'Membranes for hydrogen separation.', *Chemical reviews*, 107(10), pp. 4078–110. doi: 10.1021/cr0501792.

Parliament of the United Kingdom (2013) *Energy Act 2013*, *HM Government*.

Rahimpour, M. R., Ghaemi, M., Jokar, S. M., Dehghani, O., Jafari, M., Amiri, S. and Raeissi, S. (2013) 'The enhancement of hydrogen recovery in PSA unit of domestic petrochemical plant', *Chemical Engineering Journal*. Elsevier B.V., 226, pp. 444–459. doi: 10.1016/j.cej.2013.04.029.

Scholes, C. A., Ho, M. T., Wiley, D. E., Stevens, G. W. and Kentish, S. E. (2013) 'Cost competitive membrane-cryogenic post-combustion carbon capture', *International Journal of Greenhouse Gas Control*. Elsevier Ltd, 17, pp. 341–348. doi: 10.1016/j.ijggc.2013.05.017.

Sircar, S. (2002) 'Pressure Swing Adsorption', pp. 1389–1392.

Sreenivasulu, B., Gayatri, D. V., Sreedhar, I. and Raghavan, K. V. (2015) 'A journey into the process and engineering aspects of carbon capture technologies', *Renewable and Sustainable Energy Reviews*. Elsevier, 41, pp. 1324–1350. doi: 10.1016/j.rser.2014.09.029.

US EPA (1995) *Natural Gas Combution*, *Emissions Factors & AP 42, Compilation of Air Pollutant Emission Factors*. Available at: http://www.epa.gov/ttnchie1/ap42/ch01/final/c01s04.pdf.

US EPA (1996) *3.4 Large Stationary Diesel And All Stationary Dual-fuel Engines*, *Compilation of Air Pollutant Emission Factors, Volume I: Stationary Point and Area Sources, AP-42*. Available at: http://www.epa.gov/ttn/chief/ap42/ch03/index.html.

US EPA (2014) 'Climate Change Indicators in the United States: Global Greenhouse Gas Emissions Global Greenhouse Gas Emissions', (May), pp. 1–6. Available at: www.epa.gov/climatechange/indicators.

US OEERE (2016) *Hydrogen Production Pathways*. Available at: http://energy.gov/eere/fuelcells/hydrogen-production-pathways (Accessed: 20 May 2016).

Vaughan, A. (2015) *The future is here: mass-market hydrogen cars take to Britain's roads*, *Guardian*. Available at: http://www.theguardian.com/environment/2015/nov/04/the-future-is-here-mass-market-hydrogen-cars-take-to-britains-roads (Accessed: 19 May 2016).

World Bank (2016) *Fossil Fuel Energy Consumption (% of total)*. Available at: http://data.worldbank.org/indicator/EG.USE.COMM.FO.ZS/countries/1W-GB?display=graph.

Xu, G., Li, L., Yang, Y., Tian, L., Liu, T. and Zhang, K. (2012) 'A novel CO2 cryogenic liquefaction and separation system', *Energy*, 42(1), pp. 522–529. doi: 10.1016/j.energy.2012.02.048.

Yim, S. H. L. and Barrett, S. R. H. (2012) 'Public health impacts of combustion emissions in the United Kingdom', *Environmental Science & Technology*, 46, pp. 4291–4296. doi: 10.1021/es2040416.

2 Literature Review

2.1 Syngas Production: SMR & Gasification

Chapter one of this thesis alluded briefly to various methods of hydrogen production, this section will explore in greater depth both Steam Methane Reformation (SMR) and gasification. Both of these technologies are established and mature and provide a similar end product in terms of syngas.

2.1.1 Steam Methane Reformation

Methane is the primary constituent of natural gas, a major feedstock for SMR. Typically, over 90% of natural gas consists of methane, with ethane and propane being the next most common species. Small amounts of larger hydrocarbons, carbon dioxide and nitrogen and sulphur compounds are also notably present (BOC, 2013).

Steam methane reformation is the source of the majority of the world's hydrogen, SMR accounts for approximately 95% of hydrogen used in the USA (US Department of Energy, 2013). It is worthwhile to note that the SMR moniker is frequently retained even when other light hydrocarbon feedstocks are used (Farid *et al.*, 2009), alternatively a more general term of steam reformation can be used (Holladay *et al.*, 2009).

2.1.1.1 Process Outline

SMR facilities generally consist of four major process units, plus several smaller heaters and coolers to permit heat integration in larger or more advanced plants (Nexant Inc., 2006)(Farid *et al.*, 2009). The four major processes units consist of:

- **Desulphurisation**: The feedstock is scrubbed of sulphur compounds to prevent damage to downstream equipment using a solid adsorbent.
- **Steam Reformer**: The feedstock is heated and mixed with high temperature steam to produce a mixture of carbon monoxide and hydrogen. The temperature inside the reactor is typically 500-900 °C, with pressures of 20 – 35 bar and a steam to carbon ratio of 2.5-3.0 (Voldsund, Jordal and Anantharaman, 2016). Typically the reaction is conducted over a nickel based catalyst that can be susceptible to hydrogen disulphide poisoning (Voldsund, Jordal and Anantharaman, 2016).

- **Shift Reactor**: The next unit is responsible for further reaction of the carbon monoxide with steam to boost the hydrogen yield through the water gas shift (WGS) reaction), a catalyst of copper promoted iron-chromium is used. The product gas is typically at a temperature of around 270 °C and a pressure of 30 bar (Nexant Inc., 2006). To increase carbon monoxide conversion, high temperature and low temperature shift reactors are often used. Higher rates of carbon monoxide conversion are favoured thermodynamically at lower temperatures as the conversion reaction is slightly exothermic. However, the WGS reaction is kinetically favoured at higher temperatures. As such, a high temperature reactor is used to react most of the carbon monoxide before a low temperature reactor is used to convert the remaining fraction of the feed carbon dioxide.
- **Hydrogen Separation**: Typically this is done through the use of pressure swing adsorption (PSA) (Nexant Inc., 2006)(Farid *et al.*, 2009) – the technology has been used in plants from the early 1980s. Many systems utilise an amine absorption step to remove a fraction of the carbon dioxide prior to the PSA system (Rath, 2010)(Rostrup-Nielsen and Rostrup-Nielsen, 2002). Alternatives systems exist, including other forms of adsorption and absorption along with cryogenic separation and membrane separations (Voldsund, Jordal and Anantharaman, 2016)(Bartels, Pate and Olson, 2010)(Terrien *et al.*, 2014).

Table 2.1 below gives an example of some typical process conditions for large and small scale SMR designs, the data was collected from numerous commercially operational and aggregated by (Nexant Inc., 2006). Small scale refers to an operation/plant producing around 4.5 kg/hr of hydrogen; with large scale producing 45 tonnes/hr.

Table 2.1 Operational Conditions for an SMR process; adapted from (Nexant Inc., 2006)

Process Condition	Small scale	Large scale
Reforming pressure (bar)	20	30
Steam to carbon ratio	3	2.8
Reformer inlet temperature (°C)	450	540
Reformer outlet temperature (°C)	800	880
Methane Conversion (%)	71	77
Shift inlet temperature (°C)	450	450
Shift outlet temperature (°C)	250	275
CO concentration in shifted gas (%)	0.3	0.8
PSA hydrogen recovery (%)	75	86

Process Condition	Small scale	Large scale
Natural gas feed/hydrogen product (vol. ratio)	0.47	0.36
Steam/hydrogen product (vol. ratio)	1.4	0.97

The steam to carbon ratio given in the above source is larger than in other sources (Rostrup-Nielsen and Rostrup-Nielsen, 2002); where a higher ratio of steam is beneficial for hydrogen production but incurs a higher cost.

As can be seen, process conditions vary with scale; other sources suggest similar temperature ranges, carbon to steam ratios and operational pressures (Voldsund, Jordal and Anantharaman, 2016)(Holladay *et al.*, 2009)(Huang and T-Raissi, 2007b).

2.1.1.2 The Chemical Reactions of SMR

A general chemical reaction can be given for the steam reformation of hydrocarbons as:

$$C_mH_n + mH_2O \rightarrow mCO + (m + \tfrac{1}{2}n)H_2 \quad \text{(Equation 2.1)}$$

Where the reaction enthalpy (ΔH) is dependent on the hydrocarbon used, in all cases ΔH will be negative as the reaction is endothermic. Applying the general formula to methane gives:

$$CH_4 + H_2O \rightarrow CO + 3H_2 \quad \text{(Equation 2.2)}$$

Where ΔH = -206 kJ/mol at 15 °C (Farid *et al.*, 2009). As the reaction is endothermic heat must be supplied to the reactor; typically, an externally-heated packed bed reactor is used (Voldsund, Jordal and Anantharaman, 2016).

Further reaction of the carbon monoxide, completed in the shift reactor, gives a higher hydrogen yield through the WGS reaction:

$$CO + H_2O \leftrightarrow CO_2 + H_2 \text{ (Equation 2.3)}$$

Where ΔH = +41.2 kJ/mol at 15 °C (Farid *et al.*, 2009). Thus, one mole of methane can in principle provide up to potentially four moles of hydrogen if fully reacted (with no recycling), this ratio changes slightly dependent on the feedstock composition.

The amount of hydrogen produced per mole of feedstock is typically lower than the maximum, particularly with methane used as a feedstock. As equation 2.2 shows, the initial reaction is endothermic and thus requires heat energy to proceed; for SMR, the feedstock can be used as a fuel

through combustion and the overall efficiency (of methane conversion to hydrogen) is more useful as a metric. Typical efficiencies for SMR are between 65% and 74% (Rath, 2010).

2.1.1.3 Industrial Units

As mentioned previously SMR provides a large majority of the total amount of hydrogen produced. Many of the world's major gas suppliers have industrial/commercial SMR operations.

Air Liquide began production of hydrogen through SMR in France in 1973, supplying hydrogen through a 30 km long pipeline that was later (1985) extended to 140 km in length, leading to Belgium (Air Liquide, 2008). Further expansion of this grid continued in the 1990s; the grid became 800 km in length and connected to the Netherlands as well, along with the installation of Air Liquides first large scale hydrogen production facility capable of producing 10,000 m^3/hr of hydrogen (Air Liquide, 2008). Expansion has continued to include projects in Asia and North America and the construction of a 100,000 m^3/hr plant in Belgium during 2004.

Since 1992 Technip & Air Products have formed a successful partnership in hydrogen production and supply; completing 35 projects in locations ranging from Canada (Alberta) to the US (Texas, California) to China (Sichuan). Many of these plants are capable of producing 90,000 m^3/hr of hydrogen (Air Products, 2012).

Progress continues to be made with SMR plants, Air Liquide recently opened a state-of-the-art SMR plant in Cologne, Germany, capable of producing 22,000 tonnes of hydrogen and 120,000 tonnes of carbon monoxide annually (Air Liquide, 2015). This was a major investment (€100 million) and shows that SMR is expected to continue to play a growing role in hydrogen production. Air products announced in 2016 a plan to invest $350 to $400 million in the construction of a "world-scale" SMR facility in Baytown, Texas. Air products believe this facility, when it opens in 2018, will be capable of producing 3.54 million cubic metres (125 million standard cubic feet) of hydrogen per day (Air Products, 2016).

2.1.1.4 Academic Research in SMR

Research into SMR is widespread, with a particular focus on improving both the hydrogen yield and the development of a "one step method" for producing high purity hydrogen without the need for a separation unit.

Enhancement of hydrogen production is of particular interest as this will increase the economic viability of the process. The use of a combination of permeable nickel tubes and zirconium-vanadium-iron alloys have been utilised to produce an effective and continuous method of CH_4 to H_2 conversion (Fukada, Shimoshiraishi and Katayama, 2014). A heat pump, consisting of two types of metal hydride, is operated amongst three different temperatures to enhance heat utilisation efficiency in the system and a "$ZrV_{1.9}Fe_{0.1}$" alloy is used to adsorb and desorb hydrogen at different pressures between two process beds.

Due to the catalytic nature of the SMR reaction it is not surprising to find multiple studies working on wildly varying catalysts. Another example can be seen in a study centred around the steam reformation of ethanol, where a nickel catalyst, on a support of lanthanum modified alumina was studied. It is theorised that the presence of lanthanum in the support improves the dispersion of nickel throughout the support (Melchor-Hernández, Gómez-Cortés and Díaz, 2013). The result of this was noticeably higher ethanol conversion in La-containing supports, where ethanol conversion peaked at 95-100 % at 600 °C.

A modified SMR reaction for hydrogen production has been studied, where sodium hydroxide is added to the methane and steam, resulting in the following reaction:

$$CH_4 + 2NaOH + H_2O = Na_2CO_3 + 4H_2 \qquad \text{(Equation 2.4)}$$

The researchers claim this modified reaction has several advantages as the reaction does not require catalysis, the temperature of the reaction is reduced and the by-products are also of industrial importance (Saxena, Kumar and Drozd, 2011). However, even the authors themselves acknowledge that this scheme is for limited use and tests conducted were only of a small scale (25 ml/min of methane). Suggestions of use alongside existing chlor-alkali plants warrant further investigation, with the authors claiming that retrofitting the modified SMR technology to each of the current 50 chlor-alkali plants in the US could produce 35,040 tonnes of hydrogen annually.

Other studies have focused on the use of computational modelling, using packages such as ASPEN to predict potential improvements to the SMR process. One such study suggests that the application of a calcium oxide sorption to the SMR process could produce hydrogen at purity of over 92% without the use of any separation stage (Zhu, Li and Fan, 2015). Whilst this is impressive, until proven experimentally questions will remain about feasibility, especially around the calcium sorption system and its potential longevity.

2.1.2 Gasification of Biomass & Coal

Gasification is the process of converting solid fuels into syngas, with small amounts of solid and liquid waste by-products also created. Gasification of coal is a well-established technology, with patents for long-standing processes such as the Lurgi dry ash process dating back to 1927 (Higman and Van Der Burgt, 2008). Traditionally gasification focused primarily on the use of coal as a feedstock, however some modern developments have focused on the use of biomass as a fuel.

2.1.2.1 Gasification Feedstock

Unlike the light hydrocarbon feedstock of most SMR processes, coal and biomass have much more complex molecules and a variety of significantly undesirable elements. Often these elements are referred to in whole as ash; this group consists of various metal oxides, silicon dioxide, and sulphur compounds (Yeboah *et al.*, 2014). The products of gasification vary greatly dependent on the feedstock, of significant concern is the presence of sulphur due to the likelihood of forming hydrogen sulphide which is capable of causing problems for any gas reformation process and various hydrogen separation technologies. Table 2.2 contains a summary of typical coal compositions and indicates that gas scrubbing technology is certainly required. It is important to note that the percentages shown are on an ash-free basis and this must also be accounted for.

Table 2.2 – Average component weight percentage of various types of coal. Adapted from (Higman and Van Der Burgt, 2008)

Component (wt %)	**Lignite**	**Bituminous**	**Anthracite**
Carbon	69.5	77.3	92.1
Hydrogen	4.87	5.9	2.6
Sulphur	0.43	4.3	3.9
Nitrogen	0.75	1.4	0.3
Oxygen	24.45	11.1	1.1

The composition of biomass is even more varied than that of coal, due to the wide range of biomass sources available. Typically biomass consists of the organic materials cellulose, hemicellulose and lignin (Yaman, 2004), with the amount of each component varying on the biomass. Table 2.3 below gives a brief summary of each of the components and typical compositions of each.

Table 2.3 – Typical biomass organic components. Data taken from (Yaman, 2004)

Component	Description	Abundance
Cellulose	• General formula – $(C_6H_{10}O_5)_n$ • Large molecule consisting of thousands of mono-metric units. • Forms the skeletal structure of most biomass.	• Cotton is almost pure cellulose • Wood cellulose always occurs in association with hemicellulose and lignins. • Cellulose makes up a minimum of 30% of the total mass
Hemicellulose	• General formula – $(C_5H_8O_4)_n$ • Typically 50 - 200 mono-metric units in size. • Branched chemical structures unlike cellulose.	• Up to 10% of the dry mass of softwood species. • Up to 30% of the dry mass in hardwood species.
Lignin	• Highly branched, substituted, mononuclear aromatic polymers.	• Between 20 – 40% of the dry mass of softwood and hardwood species. • Between 10 – 40% of the dry mass of other biomass wastes such as corncobs, peanut shells, rice husks and straw.

Analysis of a wide range of biomass sources ranging from wood/woody biomass to agricultural biomass to animal biomass (such as chicken litter and meat-bone meal) highlighted that whilst the majority of biomass consists of carbon, hydrogen and oxygen both nitrogen and sulphur are present in varying amounts. Mean values for the data collected were found to be 1.25% and 0.19% of the total weight for nitrogen and sulphur respectively (Vassilev *et al.*, 2010).

The same study shows that the mass of ash and it's composition for both coal and biomass varies dependent on source, with table 2.4 below showing selected average values. Details of specific species can be found in (Vassilev *et al.*, 2010).

Table 2.4 – Ash mass percentage and composition for selected fuel sources. Adapted from (Vassilev *et al.*, 2010)

Feedstock	Ash Content (weight %)	Details
Coal	19.8	Ash % varies from 5 - 48.9% depending on the feedstock. Major ash species include: SO_2, Al_2O_3, Fe_2O_3 and CaO.
Wood	2.7	Ash % varies from 0.1 - 8.4% depending on the feedstock. Major ash species include: SO_2, Al_2O_3, K_2O and CaO.
Straw	7.8	Ash % varies from 4.3 – 18.6% depending on the feedstock. Major ash species include: SO_2, Al_2O_3, K_2O and CaO.
Grass	4.3	Ash % varies from 0.8 – 9.4% depending on the feedstock. Major ash species include: SO_2, Al_2O_3, K_2O and CaO.
Shells/husks/other residues	4.4	Ash % varies from 0.9 – 16.1% depending on the feedstock. Major ash species include: SO_2, P_2O_5, K_2O and CaO.
Biomass (all varieties)	6.0	Ash % varies from 0.1 – 43.3% depending on the feedstock. Major ash species include: SO_2, MgO, K_2O and CaO.

Ash produced in gasification can become entrained in the flue gas, thus cleaning of the gas is often required before it is processed further. Ash production can cause serious disposal problems (Thind *et al.*, 2012), efforts continue to be made in the processing of ash into useful products through recycling (Qiu *et al.*, 2010) or using it improve soil conditions for crop growth (Thind *et al.*, 2012).

2.1.2.2 Products of Gasification

Whilst gasification produces mainly syngas, both liquid and solid by-products are also produced. Char is primarily un-reacted carbon that remains after the process, whilst tar consists of "condensable" hydrocarbons including single ring to 5-ring aromatic compounds, oxygen-containing hydrocarbons and polycyclic aromatic hydrocarbons (Emami Taba *et al.*, 2012).

The amount of each product produced is dependent on the temperature of gasification, the fuel source, the fuel to air/oxygen/steam ratio, the fuel particle size and the gasifier design amongst other conditions (Emami Taba *et al.*, 2012).

General figures for each are reported above. However, with gas components making up typically 80-85% of the product and the remaining 15-20% taken by char and tar, the exact ratio of the two varies dependent on the gasifier design (Roos, 2010). Updraft gasifiers typically produce more tar whilst downdraft gasifiers typically produce more char (Roos, 2010).

The composition, of the syngas produced is also dependent on the conditions stated above. The primary concern for the amount of hydrogen present is obviously the amount of hydrogen present in the fuel source, which acts as a limit for the amount of hydrogen produced. Hydrogen concentration in syngas also appears to be affected by temperature, where higher temperatures produce a higher hydrogen gas concentration (Kumar, Jones and Hanna, 2009)(Emami Taba *et al.*, 2012)(Wei *et al.*, 2007), higher temperatures also see a decrease in methane and carbon dioxide concentration alongside an increase in carbon monoxide concentration.

2.1.2.3 The Chemical Reactions of Gasification

Gasification has a significantly more extensive and complex reaction path than SMR. This section will focus primarily on those reactions that produce gas due to the nature of the project. The following reaction scheme is taken from (Spaeth, 2012), where the initial reaction is described as primary de-volatilisation:

$$\text{Coal/Biomass} \rightarrow \text{Primary tar} + \text{Char} + CO + CO_2 + CH_4 + C_2H_4 + H_2O + H_2 \quad \text{(Equation 2.5)}$$

After the production of the primary tar through this initial reaction these chemicals continue to react in cracking and reforming reactions:

$$\text{Primary tar} \rightarrow \text{Secondary tar} + CO + CO_2 + CH_4 + C_2H_4 + H_2 \quad \text{(Equation 2.6)}$$

Secondary tar can also be cracked to produce:

$$\text{Secondary tar} \rightarrow C + CO + H_2 \quad \text{(Equation 2.7)}$$

Char and the initial fixed carbon in the coal/biomass react with a number of different species to produce a variety of products:

$$C + O_2 \rightarrow CO_2 \quad \text{(Equation 2.8)}$$

$$C + \tfrac{1}{2}O_2 \rightarrow CO \quad \text{(Equation 2.9)}$$

$$C + H_2O \rightarrow CO + H_2 \quad \text{(Equation 2.10)}$$

$$C + 2H_2 \rightarrow CH_4 \quad \text{(Equation 2.11)}$$

Gas phase reactions also occur throughout the process:

$$H_2 + \tfrac{1}{2}O_2 \rightarrow H_2O \quad \text{(Equation 2.12)}$$

$$CO + O_2 \rightarrow CO_2 \quad \text{(Equation 2.13)}$$

$$CH_4 + CO_2 \rightarrow 2CO + 2H_2 \quad \text{(Equation 2.14)}$$

$$CH_4 + H_2O \rightarrow CO + 3H_2 \quad \text{(Equation 2.15)}$$

$$CO + H_2O \rightarrow CO_2 + H_2 \quad \text{(Equation 2.16)}$$

The extent to which these reactions are carried out is, as previously mentioned, dependent on the process conditions, the feedstock and the amount of oxygen available. As many of these reactions compete or exist in equilibrium it is clear that process conditions will have a controllable impact on the composition of the syngas, as discussed in section 2.1.2.2 above.

2.1.2.4 Gasification Technologies

Whilst SMR technology is relatively similar across the industry, gasification technology varies greatly with numerous process methods. Gasifier technologies can be divided into three broad categories: moving-bed, fluidised-bed and entrained flow (Higman and Van Der Burgt, 2008)(Phillips, 2006).

Moving-bed gasifiers are the oldest processes, the outlet gas temperature is typically low and hydrocarbons are expected to be found in the syngas produced (Higman and Van Der Burgt, 2008).

Further categorisation can be made of moving-bed gasifiers by considering where the fuel and oxidising agent are added. In updraft/counter-current gasifiers fuel is added at the top of the gasifier with the oxidant added at the bottom, this leads to the syngas moving upwards and exiting the gasifier at the top(Kumar, Jones and Hanna, 2009). In downdraft/co-current gasifiers the fuel and the oxidant

are added at the top and move downward, with the products exiting from the bottom of the gasifier (Kumar, Jones and Hanna, 2009).

In updraft gasifiers gasification takes place at the bottom of the bed which is the hottest part of the gasifier (up to 1200 °C). As the gas exits from the top it leaves at a lower temperature, around 500 °C, and due to this lower temperature, more tar is found in the syngas when compared to downdraft designs (Kumar, Jones and Hanna, 2009)(Roos, 2010).

In downdraft gasifiers gasification occurs as the fuel and oxidant travel downwards, and the gas exits at a higher temperature, around 800 °C, as the higher temperature region of the gasifier is near the gas exit (the bottom of the gasifier). This results in significantly less tar in the syngas (Kumar, Jones and Hanna, 2009) but can result in higher particulate matter entrainment due to the increased amount of char (Roos, 2010).

Examples of moving-bed gasifier designs include the Lurgi, Ruhr 100 and British Gas-Lurgi (BGL) gasifiers (Higman and Van Der Burgt, 2008). These designs are mature processes that can be found throughout the world industrially. A comparison of the technologies showed that the Lurgi dry ash gasifier produced the highest amount of hydrogen (on a per mole basis) from a feedstock of coal, where 42% of the syngas produced was found to be hydrogen, in comparison to 32% produced in the BGL gasifier (Higman and Van Der Burgt, 2008).

In fluidised-bed gasifiers the fuel is fed into the bottom of the gasifier and is fluidised using air, nitrogen and/or steam, the syngas moves upwards and exits the gasifier at the top (Kumar, Jones and Hanna, 2009). Fluidisation improves heat transfer and thus results in higher conversion efficiencies; this is a major advantage as the typical particle residence time in a moving-bed gasifier may be hours (Phillips, 2006). Fluidisation must be controlled to prevent entrainment of fuel and ash particles, and different gasifier designs incorporate different gas velocities and different fluidisation properties. The lowest gas velocities are used in stationary bed designs, with circulating fluid beds being an intermediate and transport reactors having the highest gas velocities (Higman and Van Der Burgt, 2008). Fluidised bed gasifiers are a popular choice for the gasification of biomass or co-gasification of biomass with coal (Emami Taba *et al.*, 2012)(Higman and Van Der Burgt, 2008)(Phillips, 2006). The syngas outlet temperature is significantly higher than that of moving-bed gasifiers; with temperatures of over 900-1000 °C being typical for the process (Emami Taba *et al.*, 2012).

Similar to moving-bed gasifiers, fluidised bed gasifiers have a long history of use, with early designs by Winkler being developed in the 1920s (Higman and Van Der Burgt, 2008). Other designs in use industrially include the high temperature Winkler (HTW), Circulating fluidised bed (CFB), the Kellogg

Brown and Root (KBR) and U-Gas gasifiers. Alongside providing electrical power, gasifiers have been used to provide chemical feedstocks for other processes. One such example is a HTW gasifier operated in Germany, where during a 20 year operational period it produced 800,000 tonnes of methanol (Renzenbrink, Wischnewski and Engelhard, 1998). Other examples of similar HTW processes can be found in Germany, Finland & Japan operated by ThyssenKrupp (Radtke, 2011), where the various biomass/waste feedstocks have been used for both methanol and electrical power production.

The wide scale use of biomass in these designs suggests a robust ability to produce syngas worldwide, it is important to note however that the hydrogen content in the gas may not be particularly high. Reviews of the technology show that hydrogen content in the syngas varies greatly, from 10-45% on a molar basis (Emami Taba *et al.*, 2012).

The final classification of gasifier is the entrained flow type, where fine particles of fuel are injected at the top of the gasifier co-currently with an oxidant. The fuel particles fed here are significantly smaller than those used in either of the other two designs and the residence time of the particles is also shorter, typically in the order of seconds (Phillips, 2006). Typically these gasifiers produce syngas at the highest outlet temperatures, with 1250 – 1600 °C being reported as typical values (Higman and Van Der Burgt, 2008).

Industrial designs of entrained flow gasifier include the Shell, Texaco, E-Gas, Noell and KT designs (Higman and Van Der Burgt, 2008). Large-scale examples have been in operation since the 1970s to process coal. A major advantage to the entrained gasifier design is that it produces significantly less tar than most designs (Strezov and Evans, 2014), however it must be noted that, due to the slagging nature of the ash formed in the gasifier, feeds of low ash content are required.

Sections 2.1.1 and 2.1.2 above illustrate that both SMR and gasification are well-established, large-scale technologies, capable of providing significant amounts of hydrogen through the processing of both fossil fuels and biomass. This is in line with the thinking of other interested groups, where both are seen as current and future energy sources (International Energy Agency, 2006)(U.S Department of Energy, 2010)(US OEERE, 2016) and (UK H2Mobility, 2013), the last of which is an agglomeration of UK government departments and businesses. Efforts will continue to be made on advancing the technologies both commercially and through research, where large volumes of work are produced on both gasification and SMR annually.

2.2 Gas Separation Technology

Separation of hydrogen from the other components of syngas is viable in a multitude of different ways, some of which were alluded to in the introduction section of this thesis. It is stated in (CO2 Capture Project, 2008) that gas separation technologies can be split into three major classifications: separation through solvents/sorbates (through the use of PSA and related technologies), cryogenic separation and membrane separation. The technologies featured in this section are of either commercial/industrial relevance or research interest for the separation of hydrogen from carbon monoxide/dioxide.

2.2.1 Cryogenic Separation

Cryogenic separation is a well-established technology, the principles for which were explored extensively from the 19th century, leading to Carl von Linde developing the first air separation plant in 1902 and eventually the double-column rectification system for cryogenic separation in 1910 (Linde Engineering, 2014). These early systems were primarily for the production of oxygen, but the principle remains largely similar for any gas.

The process for separating hydrogen using cryogenics is well established, with various patents stating that the compression and cooling of hydrogen containing refinery gas was a well-established principle from as early as the 1960s (Schaefter, 1981)(Bolez and Pryor, 1967).

Cryogenic separation is undertaken by exploiting the differences between gas species phase transition properties through the use of a number of compression, cooling and expansion steps (Xu *et al.*, 2012). Using phase diagrams like the one for carbon dioxide seen in figure 2.1, a cryogenic process can be set up to separate individual species of gases from mixtures.

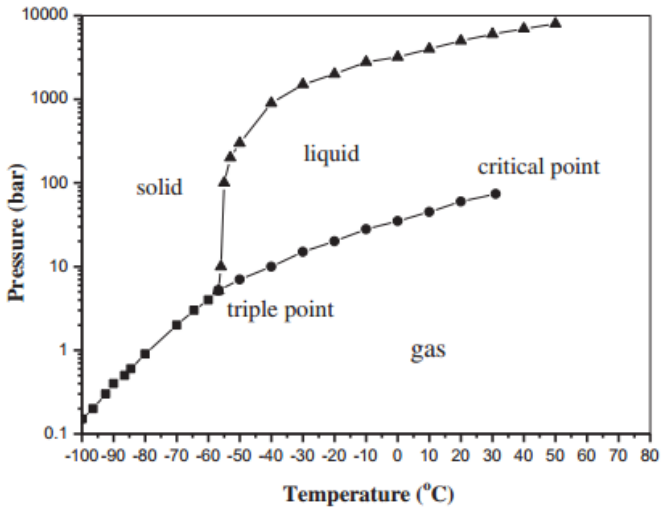

Figure 2.1 – Phase diagram of CO_2 (Xu *et al.*, 2012)

Cryogenic systems have an advantage in that they are capable of accepting feed gases with a high range of hydrogen purity, between 30 – 80% but are limited in the sense that separation is difficult to achieve if the other gas components do not condense at cryogenic temperatures (Grashoff, Pilkington and Corti, 1983). This isn't a problem for the aforementioned industrial processes above as hydrogen has a high relative volatility compared to hydrocarbons (such as methane) but problems arise if large amounts of carbon monoxide and carbon dioxide are present (Adhikari and Fernando, 2006).

Another major drawback is that the process is expensive, especially when higher hydrogen purities are required (Porter, Hinchliffe and Tighe, 1997)(Hinchliffe and Porter, 2000). This is due to the energy intensive nature of the separation (Adhikari and Fernando, 2006) described above. It is suggested that for hydrogen permeate purities of over 95% a cryogenic system for separation is technically possible but is not practical for industrial use (NETL, 2003).

More recent examples include cryogenic separation of hydrogen and carbon dioxide, that can achieve the removal of over 90% of the carbon dioxide from the hydrogen stream (Xu *et al.*, 2012), and the removed carbon dioxide can be reach purities of over 99% meaning that little of the hydrogen is lost during the process (Sreenivasulu *et al.*, 2015). As cryogenic separation is energy intensive it is important that minimal losses of hydrogen occur, or the energy penalty will be even greater.

The paper by (Xu *et al.*, 2012) includes examples of typical cryogenic separation system layouts, where there are several compression, expansion and cooling stages to ensure maximum capture of the carbon dioxide. Multiple stages are required as a single stage would not produce a high enough separation. Figure 2.3 shows how the amount of CO_2 removed from the hydrogen stream per stage changes with pressure, temperature and CO_2 concentration:

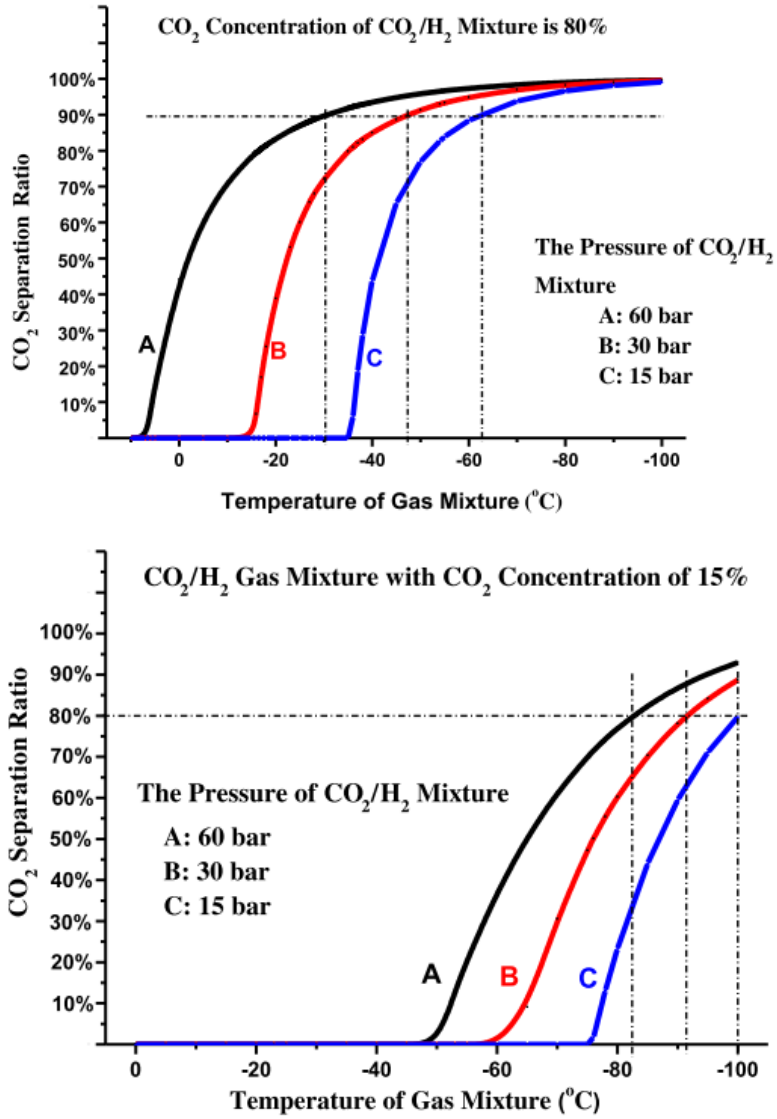

Figures 2.2 & 2.3 – Stage separation ratio for cryogenic separation at varying temperatures, pressures and CO_2 concentrations (Xu *et al.*, 2012)

As figures 2.2 and 2.3 illustrate, decreasing the temperature and increasing the pressure results in a more successful separation. As the concentration of CO_2 decreases, the conditions required for successful separation become more intensive; lower temperatures are needed - even at high pressure. Care must be taken to find the balance in the number of stages required for separation and the conditions of each stage; it is feasible to have fewer stages of separation at higher pressures and lower temperatures, or to have more stages that are less efficient per stage. The limit for separation of carbon dioxide from hydrogen in cryogenic systems is the acceptable "energy penalty". Since separation requires an input of energy for compression and cooling there is a direct offset of the energy generated through gasification and through combustion of the product gases. This energy penalty is a direct hit on efficiency and, understandably, efforts have been made to maximise the efficiency of cryogenic systems to reduce this overall energy loss.

The following are examples of the energy penalty in using a cryogenic system to remove CO_2:

- Theoretical loss of 0.395 MJ/kg of CO_2 removed from a CO_2/H_2 stream (Xu *et al.*, 2012).
- 10% overall energy loss in a 30% efficient cryogenic system for a $CH_4/CO2/H_2$ separation system (Huang and T-Raissi, 2007a).
- 9-12% energy loss for 70-90% CO_2 recovery post combustion in a coal power plant (Sreenivasulu *et al.*, 2015).

Figure 2.4 below shows the theoretical energy penalty as a function of the initial molar concentration of carbon dioxide as a percentage in hydrogen. As these are theoretical they represent values close to the minimum possible, real systems are likely to be less efficient as shown in the references above.

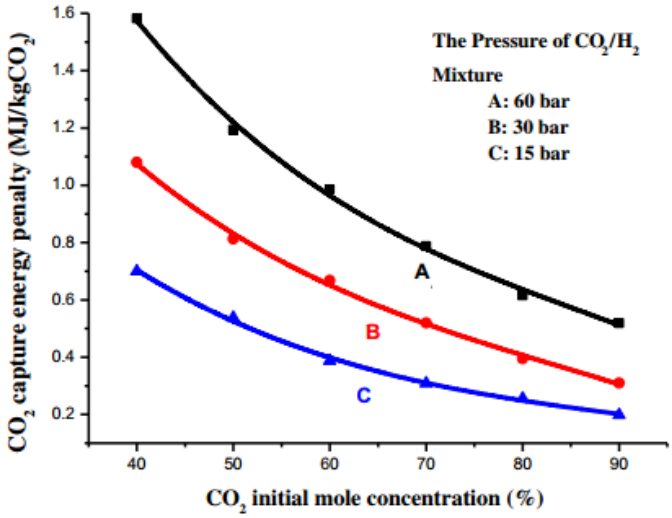

Figure 2.4 – CO_2 capture penalty as a function of initial molar concentration of CO_2 (Xu *et al.*, 2012)

As can be seen the energy loss is significant, with values around 10% being somewhat commonplace in operational systems. This is significantly higher than the energy loss for membrane separation; membranes only require a concentration/pressure gradient to achieve separation. As covered in the previous chapter, many gasifiers operate at pressures in the region of 25-30 bar (BGL, Lurgi Dry Ash) thus providing the driving force for membrane separation; if more than one membrane stage is required this gas can be re-pressurised and the energy penalty will still only be a fraction of that required for cryogenic separation, the total energy penalty being dependent on the type of compressor and the pressure compressed to.

2.2.2 Pressure Swing Adsorption (PSA)

PSA is widely considered as a versatile method for separation and purification of gas mixtures (Sircar, 2002); and has been used for a variety of industrial gas separation processes. These include: gas drying, solvent vapour recovery, fractionation of air, *production of hydrogen from steam-methane reformation*, separation of CO_2 from landfill gas and *carbon monoxide/hydrogen separations* (Sircar, 2002).

PSA is a cyclical process where products are selectively adsorbed and separated from a feed gas mixture. PSA operations can be split into four basic process steps (Linde Group, 2013):

1. Adsorption
2. Depressurisation
3. Regeneration
4. Repressurisation

The adsorption stage is typically done at high pressures, where selected gas species are adsorbed onto the surface of an adsorbent (Linde Group, 2013); these adsorbents tend to be highly porous materials, with pores sizes being in the micro/mesoporous region (Sircar, 2002). Units typically run in tandem, where steps 1 & 3 and then 2 & 4 are ran in parallel to allow for constant operation.

PSA was first used for gas separation in the 1950s (Sreenivasulu *et al.*, 2015)(Turnock and Robert H. Kadlec, 1971)(Honeywell UOP, 2016). PSA processes for hydrogen separation from the products of SMR are well established (Xiao *et al.*, 2015)(Tavan, Hosseini and Olazar, 2015)(Yang *et al.*, 2008)(Wiheeb *et al.*, 2016), primarily these works focus on the removal of carbon monoxide, carbon dioxide and methane. PSA processes are commonly of the stripping-type, where the lighter component is the one to be purified, in this case hydrogen, but rectifying-type PSA is also possible if not commonly used (Kostroski and Wankat, 2009).

A number of factors have an effect on the PSA process and its overall separation efficiency, these include: the reactor design, the adsorbent, the operating temperature and the adsorption pressure.

Ideal adsorbents should have high capture capacity, easy regenerability, large pore dimensions, high recyclability and they should have good chemical stability (Sreenivasulu *et al.*, 2015). A large range of materials have been used as adsorbents, these can be generally classified as: activated carbon, zeolites, metal oxides, silicas & alumina (Wiheeb *et al.*, 2016)(Sreenivasulu *et al.*, 2015).

The carbon dioxide separation characteristics of metal oxides, lithium metal oxides and hydrotalcite are all summarised in (Wiheeb *et al.*, 2016). Metal oxides are stated as having good adsorption

capacity and kinetics along with poor chemical stability. Lithium metal oxides offer average levels of adsorption capacity and stability and good kinetics. Hydrotalcite offers good chemical and physical stability but poor adsorption capacity and kinetics. Zeolites such as calcium chabazite, 13X zeolites and K_2CO_3 based HTC zeolite amongst others are summarised in (Sreenivasulu *et al.*, 2015); where they are reported to show excellent thermal stability and activity over a wide range of temperatures. Their adsorption capacity is stated to be 2.5 mmol/g of adsorbent (Sreenivasulu *et al.*, 2015), this would suggest that for use with large scale energy production plants would have to be of a significant size.

Hydrogen purification from carbon dioxide and carbon monoxide using PSA can result in hydrogen purities of 99.98% (Lopes, Grande and Rodrigues, 2011); however, at this purity losses of hydrogen in the waste stream were as high as 28% (Lopes, Grande and Rodrigues, 2011). This can be reduced to around 20% by applying optimal cycle times (Rahimpour *et al.*, 2013), but this loss is still potentially crippling for any hydrogen generation process. This is problematic in terms of overall efficiency as this must be added to the process energy penalty.

Large scale commercial systems for hydrogen separation through PSA have been available for several decades; there are over 1000 such examples in operation today, constructed by Honeywell-UOP (Honeywell UOP, 2016) - with competitors such as Air Products, Air Liquide & BOC also offering commercial systems (Air Products, 2015a)(BOC, 2007). Refinery operations account for 65% of all installed PSA systems with SMR accounting for a further 15% (Honeywell UOP, 2016). Research efforts are also being made in research to integrate PSA with a wider range of industries, including the use of hydrogen production from coke oven gas in steel mills where the separated hydrogen could feasibly be used as transport fuel or fed into a gas network (Joseck, Wang and Wu, 2008)(Tavan, Hosseini and Olazar, 2015).

As with cryogenic separation and many other hydrogen separation technologies, one potential disadvantage is the energy penalty for separation. For separation of hydrogen from methane, energy penalties are stated at around 260kJ/mol of feed (Kostroski and Wankat, 2009). For capture of carbon dioxide the energy penalty varies, with values of 1.79-2.14 MJ per kg of CO_2 separated stated for 5A zeolite, and 1.78 MJ per kg of CO_2 separated for activated carbon and 4.8 MJ per kg of CO_2 captured for amine based adsorbents (Sreenivasulu *et al.*, 2015). However, it is stated that the current energy penalty is competitive (Tavan, Hosseini and Olazar, 2015).

Another concern for some PSA systems is the amount of hydrogen that is recovered; whilst the product can be very pure, the rate of recovery of hydrogen can be significantly lower. Zeolites are shown to recover around 60-70% of the hydrogen feed (Xiao *et al.*, 2015)(Yang *et al.*, 2008), whilst

(Rahimpour *et al.*, 2013) report that recovery rates of up to 80% are possible through optimisation of the process.

An alternative adsorption-based separation technology to PSA is temperature swing adsorption (TSA). As would be expected from the name, temperature is used as the driving force of separation for TSA. TSA uses similar adsorbents to PSA but has major drawbacks in comparison to PSA due to the longer desorption times, higher energy requirements and rapid adsorbent deactivation (Sreenivasulu *et al.*, 2015).

Alongside adsorption, absorption processes can be used for separation of gases, with absorption of carbon dioxide being the most widely used of carbon capture technologies (Sreenivasulu *et al.*, 2015). Absorbents are typically liquid and can be used in PSA processes or in packed spray tower processes (Verma *et al.*, 2015)(Sreenivasulu *et al.*, 2015). Examples of absorbents include Selexol, amines such as MDEA and MEA (Verma *et al.*, 2015), with other studies looking at ammonia and ionic liquids alongside the aforementioned chemicals (Sreenivasulu *et al.*, 2015). Typically, these are stripping processes where carbon dioxide is absorbed. Typically the process captures up to 95% of the carbon dioxide in a stream (Sreenivasulu *et al.*, 2015)(Verma *et al.*, 2015), however this can be increased with the use of specific absorbents and reactor designs at the cost of a greater energy penalty.

2.2.3 Membrane Separation

The final gas separation technology to be discussed is that of membranes. Membranes can be defined as “an interphase separating two phases and selectively controlling the transport of materials between those phases” (Sinnott, 1996). This section will focus solely on gas-gas separation membranes, although it is important to note that many liquid-gas and liquid-liquid separations also use membrane technology.

Membranes offer a number of potential advantages, included amongst the most widely reported (Al-Mufachi, Rees and Steinberger-Wilkens, 2015)(Ockwig and Nenoff, 2007)(Phair and Badwal, 2006) are:

- Low energy consumption: membranes are typically a passive technology requiring no external energy input.
- Capable of carrying out continuous separation.
- Mature processes (for example the separation of oxygen from air) are relatively low cost in both operating and capital terms.
- Membranes can easily be combined with other separation technologies.

- Easy to scale & easy to operate.
- Extreme operating conditions are not required.

It is important to note that problems exist with the use of membranes for gas separation; some membranes are prone to excess fouling (dependent on process conditions) and concerns persist around the lifetime of membranes in other processes (Al-Mufachi, Rees and Steinberger-Wilkens, 2015). Other problems persist in ensuring that membranes deliver acceptable levels of selectivity and permeate flux.

Similar to PSA, there is a wide range of competing membrane technologies with the material of construction varying greatly. Gas separation membranes constructed from polymers have been widely used for the last three decades for a variety of gas separation applications (Sanders *et al.*, 2013). Permeation of gases through metals has been studied in great detail for many years, detailed studies such as (Fowler and Smithells, 1937) prove this; included in the study are references back to the discovery that hydrogen can diffuse through platinum made in 1866. Permeation of hydrogen through palladium has been studied in depth since the 1970s, with the suggestion that this phenomenon could be used as the basis for the development of metallic membranes (Ockwig and Nenoff, 2007)(Al-Mufachi, Rees and Steinberger-Wilkens, 2015). Over time the search for metal membranes has diversified with other metals and alloys being of increasing interest for use in membrane separation (Dolan, 2010)(Ockwig and Nenoff, 2007). Other materials such as ceramics and carbon have also been researched and developed for the potential use of hydrogen separation (Ockwig and Nenoff, 2007)(Lu *et al.*, 2007) (Phair and Badwal, 2006).

Another important distinction to make, alongside material of construction, is that membranes can be classified as either porous or non-porous (dense). The separation mechanism for both classifications varies greatly, with porous membranes typically separating through a molecular sieving mechanism (MS) and dense membranes separating through the use of a solution-diffusion mechanism (SD) (Ockwig and Nenoff, 2007)(Phair and Badwal, 2006).

Table 2.5 below gives a summary of some of the properties of each membrane class, a more detailed review of membranes will be presented in section 2.3 of this thesis.

Table 2.5 – Table containing a summary of the physical properties (Ockwig and Nenoff, 2007)(EERC, 2010)

Property	Metallic	Ceramic	Carbon	Polymer
Temperature range (°C)	300 – 600	Dense: 600 – 900 Porous: 200 – 600	500 – 900	<100
Selectivity	High	Dense: High Porous: Medium	Low	Low
Flux	High	Dense: Low Porous: High	Medium	Low
Mechanical Issues	Phase transitions of metals	Brittle	Very brittle	Swelling and compaction
Chemical Stability	Poisoned by HCl, H_2S SOx	Potential degradation with H_2O, H_2S	Susceptible to oxidisation, organic vapours	Degraded by H_2S, HCl, CO_2, SOx
Transport Mechanism	SD	Dense: SD Porous: MS	SD/MS	Dense: SD Porous: MS

The properties found in table 2.5 are amongst the key attributes to consider when deciding upon a membrane for hydrogen separation. Permeate flux and membrane selectivity are arguably the most used indicators for determining the feasibility of a potential membrane, with chemical & mechanical stability also being noteworthy.

Commercial membrane separation units are available and continue to be produced. Air Liquide produces the MEDAL system, primarily used for refinery operations and for separating hydrogen from nitrogen (EERC, 2010)(Air Liquide, 2010). MEDAL uses a polymer membrane, where hydrogen is the "fast" gas that permeates through the membrane as the nitrogen is rejected. Whilst no value for the separation factor/selectivity is given by Air Liquide, work by (Robeson, 2008) suggests that the theoretical limit for H_2/N_2 selectivity (α) is in the order of thousands, 2,000-29,000 dependent on the material used. This would mean that hydrogen purity can be well above the 99.999% figure often quoted for use in hydrogen fuel cells. However, the same work suggests that separation of H_2/CO_2 using polymers is nowhere near as effective.

Other examples of commercial systems in the small scale are Pd-Cu membranes by Wah-Chang (EERC, 2010), however these are susceptible to degradation by H_2S and HCl, and Air Products PRISM membrane systems. PRISM is another example of a polymer membrane, similar to the MEDAL system above, where low temperatures are required. PRISM is used primarily in hydrocracker situations to separate CO and H_2, other examples can be found in ammonia plants (Air Products, 2015b). Hydrogen from the PRISM system is produced at a purity of 97% (Air Products, 2015b) limiting its use in fuel cell applications.

Commercial research into metal alloy membranes persists, with one of the most impressive proponents being Eltron Research & Development who, in partnership with the US Department of Energy, are developing a membrane that they claim is “ten times cheaper than palladium and ten times more effective” (Eltron R&D, 2008)(Evenson and Waters, 2011)(Tennant and Evenson, 2011)(Evenson and Jack, 2009). Comparisons of this system to PSA separation are very favourable, with the system capable of producing highly pure hydrogen at a reasonable cost. Currently the major drawback is the longevity of the membrane, which is significantly below DoE targets (Evenson and Jack, 2009).

2.2.4 Justification for Selecting Membranes for Further Review

This review has now considered the major classifications of gas separation technology and at this point it is prudent to give an explanation on why a focus on membrane technology was chosen for this project.

After considering the merits and opportunities within each technology, membranes were chosen as a focus. This was done for a number of reasons:

- **Membranes offer a low energy penalty for operational use:** Membranes can act as a passive technology, in this instance the conditions of the syngas can be exploited to drive separation. The operational conditions of SMR and gasification processes produce a syngas at temperatures and pressures ideal for driving membrane separation.
- **Low maintenance, low operating cost:** Membrane processes provide the option of a “low tech” choice for separation, unlike cryogenic separation and PSA systems where the increased complexity of the system is likely to lead to increased maintenance requirements. Membranes are capable of continuous operation without much interference or downtime. Membranes do not require replenishment unlike adsorption and absorption processes.
- **Membranes offer the option of providing highly pure hydrogen with minimal losses:** Whilst modern PSA technologies are now capable of competing with membranes in terms of hydrogen permeate purity these systems still have limitations with regards to the amount of hydrogen recovered from the process streams.
- **The continued interest in the development of membrane reactors:** Membrane shift reactors are of great interest to many researchers (Voldsund, Jordal and Anantharaman, 2016)(Bernardo, Drioli and Golemme, 2009)(Dolan, 2010)(Liu, Song and Subramani, 2010), as they offer the potential for a single stage for production of hydrogen and its separation.

Alongside offering the potential to lower plant footprint sizes and reduce capital costs, membrane shift reactors also offer the potential to increase the amount of hydrogen produced per mole of feed.

- **The ease of scaling:** As mentioned briefly in section 2.2.3, membranes are easy to scale. As stated in (Liu, Song and Subramani, 2010), the area of the membrane required scales linearly with the volume of gas to be separated. A two-fold increase in membrane area results in a two-fold increase of gas volume treated, if all other factors are held constant. This does not hold true for the volume-based processes of PSA and CS.

2.3 A Review of Membranes for Hydrogen Separation

After briefly discussing membrane technology in the previous section, a more detailed review of the technology will now be presented. The aim of this review is to analyse the general membrane classifications and identify a classification for further review and experimental study. As this section is a review it would be prudent to consider a number of performance targets that could be used to compare membranes. One widely accepted, and frequently mentioned set of targets is set by the US department of energy (DoE); these targets contain numerous criteria that have evolved and tightened over time. The aim of these targets is to develop a competitive system for the production of hydrogen for use in fuel cells.

Many reviewers and researchers in the field have referenced these targets to some extent (EERC, 2010)(Ockwig and Nenoff, 2007)(McLeod, 2008)(Al-Mufachi, Rees and Steinberger-Wilkens, 2015)(Evenson and Jack, 2009); table 2.6 below contains the values for the 2010 and the more relevant 2015 values.

Table 2.6 – US DoE membrane performance targets adapted from (Evenson and Jack, 2009)

Performance Criteria	**2010 Target**	**2015 Target**
Flux (SCFH/ft^2)	200	300
Operating temperature (°C)	300-600	250-440
Sulphur tolerance (ppm vol)	2	20
System cost ($/ft^2)	500	<250
ΔP operating capability (psi)	400	800-1000
CO tolerance	Yes	Yes
Hydrogen purity	99.5	99.99
Stability/Durability (years)	3	>5

The criteria in table 2.6 give an indication of what the key membrane performance factors are, whilst the tightening targets give an idea of what level of performance is required to ensure that membranes are operationally and economically viable for real world use. It is also important to note that none of the reviews listed above have identified a membrane capable of delivering the required level of performance as of yet; further reviewers such as (Dolan, 2010)(Viano *et al.*, 2015)(Tao *et al.*, 2015)(Phair and Badwal, 2006) also suggest that there is currently no membrane that meets the targets.

Discussed in this section are polymer and ceramic membranes, with a brief note on metallic membranes which are all discussed in significantly greater detail in the following section.

2.3.1 Polymer Membranes

As discussed in the previous section polymer-based membranes have been the most widely used for industrial gas separation processes, with industrial-scale examples for the separation of hydrogen from carbon monoxide and from nitrogen.

As shown in table 2.5 in section 2.2.3; polymer membranes can be porous or non-porous, with current market-ready technologies dominated by porous types. Other key factors to note from the table include the low operational temperature, the potential for plasticisation due to CO_2 contamination (Ockwig and Nenoff, 2007) and the potential for degradation by CO_2, H_2S and HCl. Each of these can be seen as problematic; pre-treatment to prevent sulphur compound contamination may be required, dependent on the process feedstock. The potential for degradation or plasticisation with CO_2 is also potentially problematic as care must be taken to ensure that any polymer selected will be capable of operating in an atmosphere rich in CO_2, CO and H_2. Finally, it must be noted that the low operating temperature could be seen as somewhat problematic for use with syngas taken straight from an SMR reactor or gasifier. Polymer membranes will never meet the current DoE targets due to their low maximum operating temperature; however, it could be argued that if future polymer membranes can meet the demands for selectivity and flux, commercial use would arise.

Whilst a large number of polymers have been investigated for use as membranes, only a limited number of materials have been used in commercial systems. Table 2.7 gives a number of examples of these polymers, splitting them polymers into two groups: “rubbery” and “glassy”.

Table 2.7 – Examples of industrially used polymer membrane materials adapted from (Bernardo, Drioli and Golemme, 2009)

Polymer Type	Examples
Rubbery	• Poly(dimethylsiloxane) • Ethylene oxide-amide copolymers • Propylene oxide-amide copolymers
Glassy	• Cellulose acetate • Polyperfluorodioxoles • Polycarbonates • Polyimides • Polysulfone

A membrane is classified as glassy or rubbery dependant on whether the membrane operates at a temperature above or below the glass transition temperature of the polymer. When below the glass transition temperature the polymer chains are fixed and do not rotate as easily; this makes the

material tough and rigid; these are glassy polymers (Baker, 2004). At temperatures above the glass transition temperature, sections of the polymer chains have enough energy to be able to undertake some limited rotation around the main chain of polymer (Baker, 2004). The result of this is that the polymer begins to behave as a rubber instead of a rigid glassy material.

This difference between glassy and rubbery polymers becomes significant when one begins to look at the diffusion coefficients of gases through the membrane. The selectivity of a membrane is normally given in binary terms and is the ratio of the permeabilities of two gases through the membrane (Baker, 2004):

$$\alpha_{ij} = \frac{\Phi_i}{\Phi_j} \qquad \text{(Equation 2.17)}$$

Where α is the selectivity and $\Phi_{(i,j)}$ is the permeability of the gases, in this example the two gases being represented with the subscripts i and j. The selectivity can be treated as a ratio of the products in the permeate stream of the membrane, for example a selectivity of 4 would suggest a ratio of 4 molecules of gas i per molecule of gas j in the product or an i purity of 80%.

The permeability of a gas is a product of its diffusion coefficient (D) and its gas sorption coefficient from the Sievert equation (K) (Baker, 2004). Thus, applying this to equation 2.1 gives:

$$\alpha_{ij} = \left[\frac{D_i}{D_j}\right]\left[\frac{K_i}{K_j}\right] \qquad \text{(Equation 2.18)}$$

In polymer materials the diffusion coefficient of a gas decreases as the molecular size increases, regardless of whether the polymer is rubbery or glassy in nature (Baker, 2004). This is due to larger molecules interacting with more sections of the membrane polymer chains. As expected, this means that smaller gas molecules pass through the membrane more easily whilst larger are impeded significantly. However this impedance of larger gas molecules is not equal in both glassy and rubbery states. (Baker, 2004) shows through an example of a glassy polymer (PVC) and a rubbery polymer (natural rubber) how significant an effect gas molar volume can have on the diffusion coefficient (and thus the selectivity of the membrane). By considering the diffusion coefficients of hydrogen and carbon dioxide in both materials, it can be seen that in natural rubber the coefficients are separated by approximately a factor of 10; in PVC the difference is closer to a factor of 1000. This could potentially result in a significantly different level of membrane performance dependent on the state of the material.

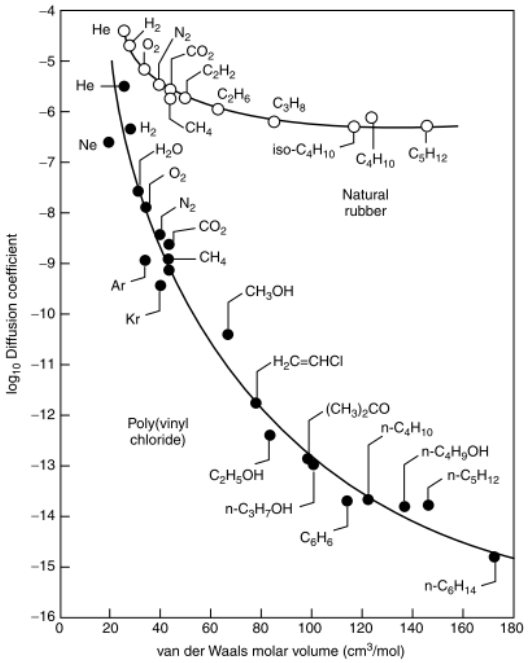

Figure 2.5 – Graph showing relationship of diffusion coefficient and volume (Baker, 2004)

However, as can be seen in equation 2.2 there are two terms of influence with the second one being the sorption coefficient. The sorption coefficient is a measure of the energy required for the permeate to be sorbed by the polymer (Baker, 2004); this coefficient increases as the condensability of the gas increases. This trend translates to the coefficient increasing as molecular diameter increases, larger molecules are generally more condensable than smaller ones (Baker, 2004).

It is worthwhile reflecting that the effect each term has varies depending on the type of polymer used, in glassy polymers the diffusion coefficient is the dominant term whilst in rubbery polymers the sorption term is dominant term (Baker, 2004). This difference in dominant terms results in variation of how gas mixtures are separated. Table 2.8 contains selected permeability data for various glassy and rubbery polymers.

Table 2.8 – Table containing permeability data adapted from (Baker, 2004)

Polymer	**Type**	**H_2 permeability (Barrer)**	**CO_2 permeability (Barrer)**	**Selectivity (α)**	**Operational temperature (°C)**
Silicone rubber	Rubbery	550	2700	4.91 (CO_2)	25
Natural rubber	Rubbery	41	153	3.73 (CO_2)	30
Cellulose acetate	Glassy	24	10	2.4 (H_2)	25
Polysulfone	Glassy	14	5.6	2.5 (H_2)	35
Polyimide	Glassy	50	13	3.84 (H_2)	60

Where Barrer is the unit of permeability, expressed in CGS units as g cm s^{-1} cm^{-2} bar^{-1}, with the length measurements included representing the membrane thickness and area.

Temperature data is included since the diffusion coefficient is temperature dependent. For rubbery polymers, where the sorption coefficient is dominant, permeability generally increases with increasing molecular volume. For glassy polymers, where the diffusion coefficient is dominant, permeability generally reduces with increasing molecular volume. Thus, whilst both types of polymer will separate a gas mixture, they are more selective to different molecules; this must be considered when designing a membrane separation system, as the permeate will either be H_2 or CO_2 rich.

Further context to the permeability numbers presented above can be given by (Bernardo, Drioli and Golemme, 2009), where it is stated that the polymer free-volume, "the fraction of the volume not occupied by the electronic clouds of the polymer", is a key factor in determining the transport properties of gases. Rubbery polymers have larger amounts of free volume due to the high mobility of the polymer chains, whilst glassy polymers exhibit more rigidity and less space for gas transportation. This can be seen to some extent in the table, where the highest permeabilities are seen for the rubbery polymers. Almost all current commercial systems utilise glassy polymers (Bernardo, Drioli and Golemme, 2009), thus further complicating the maximum temperature problem as it is important to keep these polymer membranes significantly below their glass transition temperature.

What can also be seen in table 2.10 is a very low selectivity for the chosen polymers; it is important to note that other researchers have found polymers with significantly higher selectivities. This can be seen in the commercial systems available (PRISM) and by other works.

One key, and potentially limiting, aspect of polymer membranes however is the "upper bound" first described by Lloyd Robeson in (Robeson, 1991) and then revisited in (Robeson, 2008). As discussed above, polymer membrane separation is governed by both the van der Waals molar volume of a gas and the polymer free-volume. A relationship can be drawn from this, where it is expected that a smaller gas will travel with less inhibition through a polymer than larger one, and a polymer with larger free-volume will allow for a greater permeability than one with a lower free-volume. However, an added complexity to this relationship is that the sorption and diffusion coefficients of gases of differing van der Waal molar volume in any given polymer are not first order linear, as demonstrated in figure 2.5. This complexity means that the nature of the separation is not one that is easily quantifiable in a purely theoretical sense.

The upper bound is described as an empirical relationship that acts as a supposed limit of the selectivity of a polymer membrane for various binary gas separations. The upper bound was initially plotted on a graph of the selectivity (α_{ij}) versus permeability of the more permeable gas (Φ_i), where the slope of the upper bound (n) is given by the following relationship (Robeson, 1991):

$$\Phi_i = k_f \alpha_{ij}^n \qquad \text{(Equation 2.19)}$$

The only previously undefined value here is k_f a constant called the front factor. This relationship can also be related to the difference between the molecular diameters (Lennard-Jones kinetic diameter) of the two gases to be separated, where a plot of -1/n against the difference in the diameters can be used to verify the validity of the upper bound as it passes through the origin (0,0) (Robeson, 1991).

Whilst Robeson studied many separations, only a couple are deemed relevant to this work, the data included here is taken from (Robeson, 2008), a later review of the previous paper where new empirical data is added and the upper bound was adjusted to a new higher level. This increase in the upper bound is cause for optimism as it shows that, whilst the empirical relationship holds, newer polymers may push the limitations of technology even further. The change in the upper bound in the newer paper reflects a change in the value for k_f. Robeson states that whilst a change has occurred to the upper bound there is not a significant shift in any case (Robeson, 2008).

The data from Robeson deemed useful are the (methane) H_2/CH_4 and carbon dioxide (H_2/CO_2) separations, in both instances Robeson collected large volumes of data for various polymer membranes.

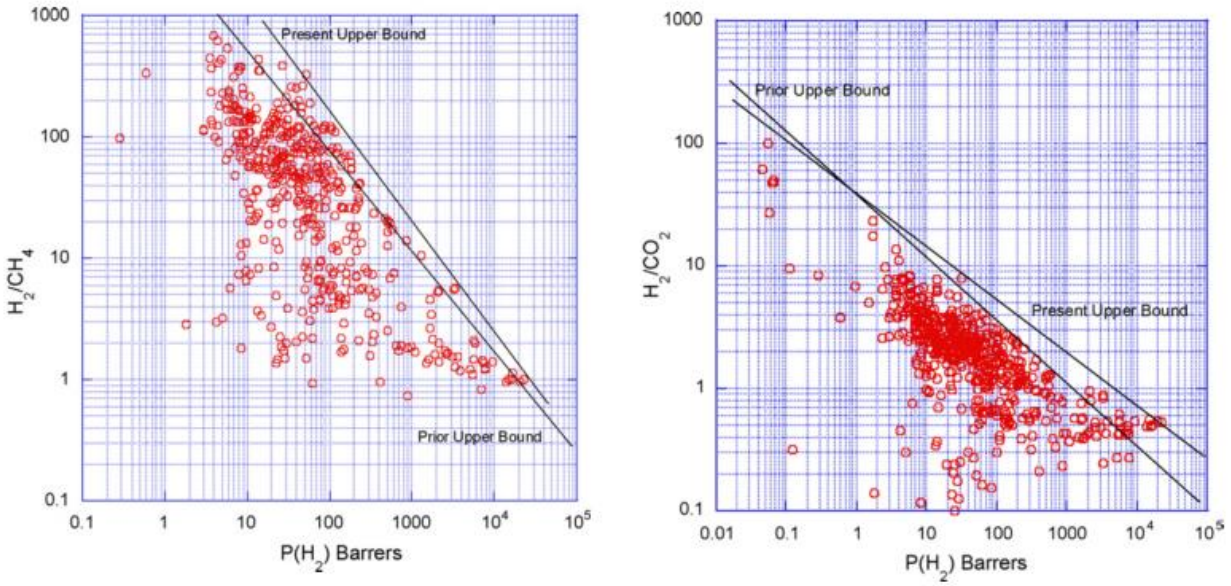

Figure 2.6 – Upper bound graphs for the separations H_2/CH_4 (left) and H_2/CO_2 (right) (Robeson, 2008)

One trend that is immediately clear from both graphs is that materials with higher hydrogen permeability flux tend to have a lower selectivity, suggesting that in general if hydrogen permeability increases then one can expect a greater increase in the second gases permeability. This would suggest that the materials with higher permeability are polymers with a higher free-volume and would also suggest that as these are likely to be rubbery in nature that they are of less interest on an industrial scale for high purity hydrogen separation. The relationship between selectivity and permeability creates an interesting dynamic, where a decision must be made on what level of permeate purity can be sacrificed for an increase in permeate yield.

The graphs in figure 2.6 show the data collected by Robeson and the adjusted upper bounds. What can be seen immediately is that hydrogen selectivity is typically much lower for the H_2/CO_2 separation than for H_2/CH_4. The upper bound for the H_2/CO_2 separation shows clearly why polymer membrane permeate is unfit for purpose; even at the lowest flux, separation is maximised at a selectivity of around 100 giving a hydrogen permeate purity of 99.01%. Table 2.9 below shows selected results from the graph, including the liquid crystalline polyester membrane that gives the highest selectivity on the chart. What can be seen is that the permeability of hydrogen for this material is very low, at 0.0545 Barrer, well below the target flux stated by the DoE.

Table 2.9 – Selected experimental data close to the Robeson upper bound for the H_2/CO_2 separation, selected from (Robeson, 2008)

Polymer	**Permeability (Barrer)**	**Selectivity (H_2/CO_2)**
Liquid crystalline polyester (HBA/HNA 30/70)	0.0545	100.9
Polyaniline (re-doped)	1.753	23.1
Polyimide (1,1-6FDA-DIA)	31.4	8.05
Poly(trimethylsilylpropyne-co-phenylpropyne) (95-5)	20,400	0.538
Poly(trimethylsilylpropyne)	23,300	0.53

Efforts continue to be made to improve the performance of polymer membranes. One way of improving current membranes is to modify the polymers by treating them chemically, one example of this is the treatment of polyimide membranes with vaporised ethylenediamine (EDA) (Shao, Lau and Chung, 2009), where polyimide membranes are dense polymer membranes. The EDA is vaporised at room temperature in a sealed container and the membranes exposed for a specified amount of time, resulting in the formation of a vapour modified layer on each side of the membrane. Treatment with EDA changes the chemistry at the surface of the membrane, where imide groups have been reacted into amide groups (Shao, Lau and Chung, 2009) thus resulting in a change in the rate of interaction

with gases at the surface. Tests were conducted on membranes exposed for zero, five and ten minutes; where single (H_2 or CO_2 only) and binary (H_2 and CO_2) gas environments were used. Longer exposure to EDA resulted in higher hydrogen selectivity, 0.33 to 16.6, but a significantly reduced hydrogen permeability, 194 to 19.4 Barrer.

Another option to increase performance is to blend polymers and create dual-layer hollow fibres to produce new polymeric membranes with higher separation efficiency. One example of this is the blending of PBI and Matrimid polymers, as done by (Hosseini, Peng and Chung, 2010). The hollow fibres were produced using a dry-jet wet spinning process and were doped with an outer silicon rubber layer, with the fibres manufactured to be significantly longer than their diameter of around 1 mm. A mixture of $H_2/CO_2/CH_4$ was fed into the fibres and the permeabilities of each gas recorded, the results of which are included here in table 2.10.

Table 2.10 – Selected results for blended polymer membranes, adapted from (Hosseini, Peng and Chung, 2010)

Material	**Permeability (Barrer)**			**Selectivity**	
	H_2	**CH_4**	**CO_2**	**H_2/CO_2**	**CO_2/CH_4**
Matrimid	27.16	0.21	7.00	3.88	33.33
PBI/Matrimid	13.06	0.045	2.16	6.05	48.00
PBI	0.60	0.0018	0.16	3.75	88.88

As can be seen the blended polymer reduces hydrogen permeability in comparison to Matrimid; however, it restricts permeability of CH_4 and CO_2 even more, thus increasing selectivity. The blended membrane also shows significant improvement over the PBI membrane, this is an interesting result as it suggests that future polymer combinations may lead to further improvements of membrane permeability and selectivity.

Alongside less than desirable permeability and selectivity, a more general review of polymer membranes highlights details around some other issues that polymeric membranes face. Plasticisation of the membrane can occur when the concentration of gas inside a polymer increases, hence plasticised membranes tend to have an increased free volume and this can change gas diffusion coefficients significantly (Sanders *et al.*, 2013). A significant problem for CO_2 separations is that many studies use CO_2 for plasticisation studies (Sanders *et al.*, 2013), due to it being readily absorbed by the polymers, suggesting that plasticisation of the membranes is likely to occur. As plasticisation causes changes to the gas diffusion coefficients it is worth noting that this is likely to result in a shift in selectivity and (dependent on the polymer in question) this may result in an enhanced or reduced performance. Once again the temperature issue is raised, (Sanders *et al.*, 2013) states that H_2 and CO_2

separations are likely to be linked to water gas shift reactors and SMR where the gas produced will be at temperatures where polymer separation is “impossible” (Sanders *et al.*, 2013).

Both Sanders and Robeson state that thermally rearranged (TR) polymers offer the best balance of permeability and selectivity, and that these materials are responsible for the shift in the upper bound (Robeson, 2008)(Sanders *et al.*, 2013). However, as it currently stands, polymer membranes are far from reaching the DoE stated standard.

2.3.2 Ceramic Membranes

An alternative to polymer membranes are ceramic membranes. Ceramic membranes are made of a variety of materials; with different ceramics using different separation methods. The range of materials investigated as ceramic membrane materials includes Alumina, Titania and Zirconia which are all examples of metallic oxide based ceramics - with silicon carbide being an example of a non-metallic based ceramic membrane material (EERC, 2010). All of the ceramics listed above have been investigated for use as hydrogen separation membranes, showcasing the diverse nature of the technology.

Dense ceramics use diffusion-solution to separate hydrogen and micro-porous ceramics use molecular sieving to separate hydrogen from other gas species; this allows for the drawing of parallels between polymer and ceramic membranes as in both the separation mechanism is dependent on the material of construction.

Referring back to table 2.5, some basic properties can be highlighted and compared with the DoE criteria. The ideal operating temperature for both porous and dense membranes is reasonable, if not a little high in the case of dense membranes. The flux for porous membranes is stated as “high” and for dense membranes as “medium” – this suggests a significant improvement on polymers, but individual ceramics must be considered for further details. The selectivity for dense membranes is significantly higher than that of porous, where the selectivity is significantly reduced to levels more akin to polymer membranes. Other issues are emphasized in table 2.6, including potential degradation from sulphur containing compounds and the brittle nature of ceramics are highlighted for consideration.

Commercial applications for ceramics membranes exist although their use in hydrogen separation is significantly limited in comparison to polymers. One example is the separation of hydrogen from nitrogen (Norby and Haugsrud, 2006), where dense ceramics are used as a permeation barrier. Like

metallic membranes dense ceramics are selective to hydrogen ions and allow them to permeate across (in ionic form); however, unlike pure metallic membranes, many ceramics also permeate oxygen ions (Norby and Haugsrud, 2006). This ability to permeate hydrogen in a way similar to metallic membranes may explain how the high selectivity is achieved; however metallic membranes produce a much higher flux per unit area.

A number of companies exist that produce ceramic membranes, although the majority of these appear to be relatively small. One such example is Cerametec, a US based company that has used its experience in producing ceramic materials for a range of industries (fuel cells, batteries and structural ceramics) to produce both dense and porous membranes for gas separations and enrichment (Cerametec, 2014). One product developed by Cerametec is a cermet (ceramic-metal composite) that has been used as a "pressure driven hydrogen separation membrane to remove hydrogen from syngas" (Cerametec, 2014).

In terms of separation mechanism, porous membranes separate gases through restricting the flow through their pores; gas molecules smaller than the pores flow through whilst those larger do not. This essentially means that separation and selectivity are a function of the membrane pore size and the size of the gas molecule. A number of theories are used to describe separation, where pore size is the determining factor on which of these is dominant, for gas separations such as H_2/N_2 where pores tend to be small the theories of Knudsen diffusion, laminar flow and surface diffusion are used to describe transportation through the membrane (Keizer, Vuren and Burggraaf, 1988). Knudsen separation is only possible when the diameter of the pores is shorter than the mean free path of the gas (Keizer, Vuren and Burggraaf, 1988); if this is true the Knudsen diffusion mechanism predicts that lighter gases permeate faster than heavier ones. Separation can be improved by activating the membrane to interact with specific species to impede their permeation or diffusion (Keizer, Vuren and Burggraaf, 1988).

Dense ceramics use the solution-diffusion method of separation; however, within this there are a number of variations on how gases are transported, dependant on the species of gas and material of construction. The most established use for dense ceramics is for oxygen separation, with hydrogen separation becoming of increasing interest. For either, hydrogen or oxygen transportation across the membrane is in ionic form – either H^+ or O^{2-} ions migrate across the membrane. H^+ ions are transported through the crystal lattice via free transport of protons (van Holt *et al.*, 2014), in a fashion similar to that used by metallic membranes. This is arguably due to the presence of metals in the cermet membranes that are commonly found in dense ceramic research; if a non-porous layer of a metallic material is present it is reasonable to assume that the material is likely to act similar to a metallic

membrane. Unlike oxygen transferring membranes hydrogen separation using dense ceramics is driven only by a chemical potential gradient (a difference in gas partial pressure on either side of the membrane); whilst oxygen membranes can be driven by chemical or electrical potential, with a voltage applied from an external source (Sunarso *et al.*, 2008).

A range of porous ceramic membranes are currently being investigated as potential hydrogen separation tools. One such example is being looked at by the University of Twente, where micro-porous silica membranes are being constructed on support layers of alumina. The silica layer is approximately 30-100nm thick to help produce a higher flux, the silica layer is also responsible for being hydrogen selective. The silica layer has pores that are only a few angstroms in size; allowing for effective gas separation (U. Twente, 2014) – even for small gas molecules. H_2/CO_2 selectivity is in the region of 100, whilst H_2/CH_4 selectivity can be as high as 1000 at a temperature of 623K (U. Twente, 2014), putting the membrane in the region of the best performing polymer membranes.

Other studies of work on micro-porous silica composites (Nwogu, Kajama and Gobina, 2015)(Nwogu, Anyanwu and Gobina, 2016) show that membrane thickness has a significant impact on the permeability of individual gases, as expected, and give an indication on hydrogen flux. Tests were run to investigate flux values through silica treated membranes for a gas mixture of H_2, N_2, CH_4 and Ar, where the silica fabricated membrane exhibited a four-fold increase in hydrogen flux but no increase for the other gases. Hydrogen flux is recorded at 0.76 mol m^{-2} s^{-1} (Nwogu, Anyanwu and Gobina, 2016) but the selectivity over CH_4 is only around 2.3 (CH_4 flux reported at 0.33 mol m^{-2} s^{-1}), this is poor and when considering that typically membranes are more selective to carbon dioxide then methane; it is plausible to imagine that the separation of H_2 and CO_2 is not feasible.

(Zhang *et al.*, 2014) have also completed an extensive study testing a number of porous “cement” membranes, where membranes of various thicknesses (5, 10 and 20mm) were tested with two different gas mixtures containing hydrogen and carbon dioxide. Two membranes were each coated with micro-silica and fly ash, whilst one remained uncoated. The average pore diameter of each membrane tested was below 100nm, which is relatively large for gas molecules, which may explain why selectivity was so poor. Selectivity for the porous membranes was higher at lower temperatures (below 50 °C), maxing at a relatively meagre 3.5, most membranes tested had an almost constant selectivity of around 2.5-2.0 regardless of operating temperature, with a minor downward trend as temperature increases. This would suggest that the pores are too large for effective separation, and that care must be taken when increasing the operational temperature, as an increase in gas kinetic energy can change the selectivity of the membrane.

With regards to the DoE targets, it is fair to assume that porous ceramic membranes are unlikely to be able to deliver the required selectivity; one possible reason why separation of gas mixtures containing H_2, CO_2 and CO is difficult with porous membranes is due to the similarity in size of all 3 molecules. The kinetic diameters of the gases are:

H_2 – 0.29nm CO_2 – 0.33nm CO – 0.37nm (Jüttke *et al.*, 2013)

As can be seen, to separate these gases with a very high selectivity pores would need to be created with an accuracy down to 0.01nm ($1x10^{-11}$m); mechanically this is very difficult to achieve (if not impossible) and whilst random pore sizes may create enough pores with a small enough diameter (0.32nm would block the CO_2 and CO molecules) it remains to be seen if this could be useful industrially.

In a similar vein to the porous ceramics already discussed, a wide range of dense ceramics have been investigated for use as potential hydrogen separation membranes.

Dense membranes made of cermets, consisting of a mixture of 50-60% vol. of Pd and yttria (Y_2O_3) stabilised zirconia (ZrO_2) were investigated by (Balachandran *et al.*, 2014) as potential hydrogen separation membranes. Membranes as thin as 18 µm were used (with a porous support layer present for stability), and a variety of hydrogen concentrations in the feed gas were investigated. The highest flux achieved was with pure hydrogen (Balachandran *et al.*, 2014), however of much more interest is the result of a test run with a gas mixture of 50%H_2, 30% CO_2, 19% H_2O and 1% CO and a membrane of 150µm thickness; conducted at a temperature of 400 °C. Hydrogen permeate purity was in the range of 98.0 - 99.5% even after 700 hours of operation. The membrane tested was 150 µm thick, with tests conducted at 400 °C and a feed pressure of 18.8 bar (200psi); the flux of the membrane varied between approximately 3.5 to 5.0 cm^3 min^{-1} cm^2 (6.5 to 9.5 SCFH ft^{-2}) over the 700-hour operation. Comparison to the DoE targets in table 2.6 at the beginning of this section shows that whilst this result may be promising, the flux is still significantly below the target. Questions remain around whether the requisite level of hydrogen purity can be reached. Another significant barrier is cost; whilst not considered much so far, as polymer membranes are typically cheap in comparison, and concerns are held about the viability of using expensive and scarce metals for wide spread applications.

However, even with concerns around cost, yttria stabilised zirconia appears to be a popular choice for ceramic membranes, this is likely due to YSZ being an excellent conductor of ions in fuel cells; the traditional use for many of the materials used in modern ceramic membranes. (Kim *et al.*, 2011) investigated a Perovskite structured BaCeYO that was augmented with a Zr based alloy to investigate hydrogen permeation in the temperature range of 773K – 1073K. The membrane is constructed on a

porous zirconia support and is approximately 10 µm thick. Tests by Kim consisted of only pure hydrogen feed (no binary gas mixtures), where the hydrogen flux increased with increasing temperature, between 500 and 800 °C. The flux delivered however was only between 0.1 and 0.175 $cm^3\ min^{-1}\ cm^{-2}$, significantly below the level required.

Palladium is a material that is commonly found in both metallic and ceramic membranes. Of particular interest are studies where hydrogen has been separated from carbon dioxide, such as (Tsai *et al.*, 2015). Tsai developed a cermet membrane consisting of palladium and BCZGD, a ceramic compound containing various transition metals. The membrane was manufactured by pressing and sintering a mixture of Pd and BCZGD powders at 1450 °C; at 400 µm thick, the membrane does not need a support layer unlike the previously discussed membranes. This allows for a simpler manufacturing process that may be useful for larger scale production. Tests were conducted over 10 hours with pure hydrogen as a feed, where an average permeate flux of approximately 2.9 $cm^3\ min^{-1}\ cm^{-2}$ was recorded. Tests of a 50% H_2 50% CO_2 feed were also performed; over 120 hours the average hydrogen permeate flux was around 1.25 $cm^3\ min^{-1}\ cm^{-2}$, with a selectivity approaching infinity (i.e. no CO_2 in the permeate) (Tsai *et al.*, 2015). This result is excellent in terms of hydrogen purity yet, once again, problems can be seen with the rather meagre flux permeated. Alongside this, the materials used are rather specialised and expensive, raising questions about larger scale use.

Low hydrogen permeate flux is a consistent problem, even in other separations containing hydrogen. Tests were conducted on an asymmetrical ceramic membrane consisting of barium, zirconium, cerium and yttrium oxides; with the intention of separating hydrogen from nitrogen (Zhu *et al.*, 2016). Whilst successful, the membrane only achieved a hydrogen flux of 1.71×10^{-7} mol $cm^{-2}\ s^{-1}$ significantly below the level required for operation. Separations of hydrogen from helium (T. Wang *et al.*, 2016), show similar fluxes for a strontium-cerium-yttrium-zirconia based ceramic, suggesting that the problem is rather consistent across much of the field.

After reviewing both porous and dense ceramics it can be seen that efforts need to be made to improve the performance of both types of membrane. Questions remain around the cost of specialised ceramics or cermets, particularly those that contain expensive metals such as palladium. The feasibility of using porous ceramics for producing highly pure hydrogen is low, the gas molecules are too similar in size for effective separation as can be seen in the low selectivities. Whilst dense ceramics and cermets are capable of producing highly pure hydrogen from H_2/CO_2 binary mixtures efforts must be made to increase permeate flux, which is far below a level to make the membranes cost effective. One significant advantage of ceramics is their apparent durability, where tests conducted over significant time spans show little diminishment of performance.

2.3.3 A Note on Metallic Membranes

Metallic membranes are discussed in significant detail in the next section of this review; to prevent repetition it was decided that it was not worthwhile to repeat details as part of section 2.3. A major objective of this literature review was to highlight where, in the vast field of hydrogen membrane research, the focus of this Ph.D. thesis should be directed. With such a broad goal to identify a potentially suitable hydrogen membrane, it was deemed necessary to primarily establish an area in which experimental and computational efforts could be concentrated. It was decided that metallic membranes should become that focus, due to their unmatched ability to provide both relatively high permeate flux rates and high selectivities.

2.4 A Review of Metallic Membranes

2.4.1 Reasoning for the Selection of Metallic Membranes

The limitations of both polymeric and ceramic membranes are presented clearly in the last section, where questions around both selectivity and/or permeate flux persist for both materials. Whilst metallic membranes are still under development for the use of separating hydrogen, advantages can be seen relatively easily. Table 2.11 contains a recap of previously displayed data, from which the advantages of metals become somewhat apparent.

Table 2.11 – Generic properties of metallic membranes (Ockwig and Nenoff, 2007), (EERC, 2010)

Property	**Values**
Operating Temperature (°C)	300-600
Hydrogen selectivity (α)	Very High (>1000)
Hydrogen flux	High
Mechanical issues	Phase transitions
Chemical issues	Poisoned by H_2S, HCl, CO_2, CO, SO_x
Example materials	Pd-Cu, Pd-Au, Pd-Ag, Ta, V, Nb, Ni, Fe
Transport mechanism	Solution-diffusion

Metallic membranes offer both the highest selectivities and the highest fluxes of all current hydrogen/carbon dioxide separation membranes, whilst other membranes may be capable of producing either a high flux or a high selectivity, metallic membranes combine both the most successfully. This was a key factor in the decision to continue with a focus on metallic membranes.

Issues still remain to be solved, these are discussed within this section, but an important note here is that many of the issues facing metallic membranes are similar to those that both polymer and ceramic membranes face; such as poisoning by sulphur species and the capital cost of membrane production (expensive raw materials). One unique mechanical issue to be concerned with is phase changes, however this typically means that minimum or maximum operating temperatures have to be observed to prevent such problems. The problem is limited somewhat as the ideal temperatures for avoiding phase changes are in the same range as the temperature of the syngas produced through SMR.

2.4.2 A Brief Introduction to the Separation Mechanism of Metallic Membranes

Chapter three contains a much more detailed study of the mechanism for hydrogen transport across the membrane. Here, a simplified model can be explained in seven steps as follows (Ockwig and Nenoff, 2007)(Phair and Donelson, 2006) (Andrew and Haasz, 1992):

1. The raw gas (in this case syngas; a mixture of hydrogen and the undesired carbon oxides) moves randomly in the vicinity of the membrane.
2. The gas contacts the membrane (adsorption), with the hydrogen gas dissociating into hydrogen ions and electrons catalysed by the active surface catalyst (typically palladium or a palladium alloy). Other gases present are not dissociated as readily.
3. The hydrogen ions are absorbed into the bulk of the membrane material.
4. The hydrogen ions and free electrons diffuse through the membrane bulk.
5. The hydrogen ions are desorbed to the surface of the membrane on the product side.
6. The hydrogen ions and free electrons re-associate into hydrogen molecules.
7. The hydrogen molecules are diffused from the surface of the membrane (desorption).

The seven steps stated above outline a solution-diffusion mechanism, a unique one in which hydrogen atoms can be transported across the bulk of the metallic grain alongside transportation through the grain boundaries.

For successful separation of gases dense metallic membranes require the ability to conduct free electrons and the presence of specific catalysts on the membrane surface to dissociate hydrogen gas molecules into atoms on the feed side (Ockwig and Nenoff, 2007). The hydrogen ions and free electrons are then re-associated upon exiting the membrane material, forming hydrogen molecules. Due to the dense structure of the membranes the larger gas molecules such as CO, CO_2, O_2, N_2 and CH_4 cannot pass through the membrane, hence the high purity (99.9999+%)(Lewis *et al.*, 2013) of hydrogen produced.

It is this unique behaviour of hydrogen that provides the most promise for future developments, shown in both the metals and the cermets discussed previously.

In most instances the step that is considered the most important is step 4, as the bulk diffusion of hydrogen is stated as the rate limiting step for membranes thicker than 10 µm (Ward and Dao, 1999). Similar to previously discussed membranes types, permeability and/or diffusivity and solubility are often used to compare different membrane materials.

2.4.3 Palladium and Palladium Alloys as Membranes for Hydrogen Separation

Historically, the metal of most interest in hydrogen separation membranes is palladium (Pd). Thomas Graham studied palladium and hydrogen extensively in 1866, where he discovered that palladium had an unmatched ability to absorb hydrogen and transport it across thin foils (Grashoff, Pilkington and Corti, 1983). However, it was the development of palladium-silver alloys in the 1950s that significantly furthered interest in the concept as it overcame a number of the issues that made the use of pure palladium membranes unfeasible (Grashoff, Pilkington and Corti, 1983). Other palladium based alloys have also been explored in detail, with particular interest in palladium-copper and palladium-silver-copper alloys (Knapton, 1977)(Dolan, 2010)(Tarditi and Cornaglia, 2011). Palladium membranes have seen limited use in the production of ultra-pure hydrogen for the semiconductor industry (Al-Mufachi, Rees and Steinberger-Wilkens, 2015).

Before delving into the broad range of palladium alloys available it may be worthwhile to briefly discuss palladium as a metal with a view of gaining an understanding on what makes it so unique in its uptake of hydrogen.

Palladium is a transition block metal and it is part of a group of metals commonly referred to as the platinum group metals (along with platinum, rhodium, osmium, iridium and ruthenium). It is interesting to note that whilst the platinum group metals have similar physical properties, none of the others offer the same level of hydrogen permeability. For example, in the paper (Phair and Donelson, 2006), the permeability of pure palladium at 500 °C is stated as 1.9×10^{-8} mol m^{-1} s^{-1} $Pa^{1/2}$, in the same study for platinum (Pt) is 2.0×10^{-12} mol m^{-1} s^{-1} $Pa^{1/2}$, the Pt value is four orders of magnitude smaller. To continue this comparison, the same source shows more data about the two metals; both metals exhibit face centred cubic (fcc) structures, both metals have similar enthalpies of formation for hydride production (+20 kJ/moil for Pd, +26 kJ/mol for Pt) and both metals have similar activation energies for bulk diffusion of hydrogen (+24 kJ/mol for Pd, +24.7 kJ/mol for Pt) (Phair and Donelson, 2006). However, there is a significant and notable divergence in one property listed by Phair & Donelson, hydrogen solubility is significantly higher in palladium than in platinum. Phair & Donelson give the data as a ratio of H atom/metal atom in equilibrium with the hydride at room temperature, Pt has a low solubility, with a H/Pt ratio of 1×10^{-5} to 1, whilst palladiums solubility is significantly greater with a ratio 0.03 to 1.

Other sources show that the hydrogen solubility of the other platinum group metals is more in line with that of platinum rather than palladium (Antonov *et al.*, 1984). What is important also to note

however is that some other metals exhibit higher solubilities than palladium (Oates, 1979)(Fowler and Smithells, 1937)(Lee, 1979), particularly the group Vb transition metals, yet these metals do not share the same readiness to permeate hydrogen. This suggests that palladiums unique rate of permeability relies on more than solubility alone, with the surface of the material also playing a key role. As discussed briefly in the model above, hydrogen must dissociate (step 2) before being absorbed into the bulk. Palladium has the ability to readily dissociate molecular hydrogen into monoatomic hydrogen (Al-Mufachi, Rees and Steinberger-Wilkens, 2015)(Tierney *et al.*, 2009)(Ockwig and Nenoff, 2007). Whilst other platinum group metals also dissociate hydrogen readily (Tierney *et al.*, 2009)(Ludwig *et al.*, 2006)(Gross, 1998), they do not have the same solubility as discussed above.

As mentioned previously palladium has an fcc crystal structure, where hydrogen will occupy either the tetrahedral (T) or octahedral (O) interstitial sites with a preference for occupying the more stable O site (Latge, Ribeiro-Teixeira and Iglesias, 1984). It is also worth noting that fcc crystals typically contain less O and T sites than bcc metals; as shown in table 2.12.

Table 2.12 – Comparison of fcc and bcc structures, data from (Dolan, 2010)

Site type	**FCC**	**BCC**
Space group	Lm3m	Fm3m
Tetrahedral	2	6
Octahedral	1	3

Less sites available typically means less sites for occupation which can act as a limiting factor for hydrogen diffusion. The nature of the crystal structure is also important to consider when forming alloys, as this will have an impact on the diffusion properties.

Whilst palladium does demonstrate excellent hydrogen permeability properties there are several draw backs to its use as a membrane material, both from both an economic and a technological stand point. Economically, palladium is scarce and prohibitively expensive; at the time of writing the price of palladium was $22.16 per gram (APMEX, 2016). This price appears to be volatile, with increases during times of economic hardship due to external investment into commodities such as precious metals. Also of concern is the limited availability of the material, sourced mainly from South Africa and Russia, alongside its high demand for use in the auto industry for catalytic converters.

Moving away from the economic feasibility and potential performance, problems can be highlighted. Whilst palladium has been used successfully as a pure metal for hydrogen separation there is evidence to suggest damage can be caused by carbon monoxide (EERC, 2010)(Ockwig and Nenoff, 2007), carbon

PM (Albers, Pietsch and Parker, 2001), sulphur containing compounds (Jones *et al.*, 2003)(Albers, Pietsch and Parker, 2001) and chlorine (Ockwig and Nenoff, 2007). Pure palladium appears to be more inhibited by carbon dioxide than when alloyed with another metal (Lewis *et al.*, 2013).

Palladium membranes also suffer when the feed gas contains carbon monoxide alongside hydrogen, where hydrogen can react with the carbon monoxide (producing methanol, for example) creating further problems for usage, however the addition of silver has been shown to reduce this effect (Phair and Badwal, 2006)(Cheng, Pena and Fierro, 2002)(Carapellucci and Milazzo, 2003).

A more significant problem for palladium membranes, but one that is not confined to only palladium, is the formation of hydrides which can result in irreversible damage and degraded performance. Metal-hydrogen systems undergo phase change dependent on a number of conditions, factors that can alter the phase of the system include temperature, pressure and H/M atomic ratio (Oates, 1979). Studies conducted by Sieverts, Bruning, Gillespie and Downs in the 1930s began to reveal the nature of metal-hydrogen systems, including that of palladium (Grashoff, Pilkington and Corti, 1983). Details of the palladium-hydrogen system are widely reported with (Lewis, 1982) providing a more detailed review and (Antonov *et al.*, 1984)(Shu *et al.*, 1991)(Oates, 1979)(Araki *et al.*, 2004)(Zaginaichenko *et al.*, 2011) providing further information; thus only a superficial overview will be included here.

Palladium forms a fcc host lattice in which hydrogen occupies the O sites as discussed previously, with palladium found in its alpha or beta phase, or a combination of both (Oates, 1979). It is reported that palladium membranes operating in the two phase area suffer from degradation (Ockwig and Nenoff, 2007). This is a problem as the two phase area is present in a range of conditions, the two phase area is present at temperatures of up to approximately 300 °C when the H/Pd ratio is between 0 and 0.65 (Oates, 1979), pressures of up to 10 atmospheres can also contain the two phase system (Lewis, 1982). The critical temperature for operation is stated at 292 °C (Antonov *et al.*, 1984) or 298 °C (Lewis, 1982) where above this only a single alpha or beta phase exists dependent on the H/Pd ratio. Operating in the mixed phase region leads to an increase in embrittlement (Liu, Song and Subramani, 2010), which will ultimately lead to the failure of the membrane. The high hydrogen solvency of palladium can also cause problems such as blistering and increased brittleness due to high hydrogen content (Lewis, 1990)(Oates, 1979), this is due to the formation of hydrides which can be found in many metals when hydrogen solubility is high. Hydride production occurs when the limits of solid solution are exceeded (Lewis, 1990) and can result in permanent physical damage to the membrane.

Combining the expense of palladium and these performance limitations it is clear to see why researchers have long searched for alternative materials, these range from palladium alloys to a range

of other transition metals. Palladium still remains a useful yardstick for testing, as results for permeability are widely reported and the system is broadly understood.

The earliest palladium alloys were developed for use in the 1950s and masses of permeability data exist, with studies such as (Knapton, 1977) providing a wealth of permeability data. Knapton ran tests on palladium and various alloys, comparisons to literature sources are also drawn at the same conditions. Tests were run at 350 °C and at feed pressures of 24.13 bar(g) (350 psig); selected results can be found in table 2.13.

Table 2.13 – Selected hydrogen flux figures, adapted from (Knapton, 1977)

Weight (%) and Material	Flux ($cm^3/cm^2/s$)
100Pd	1.43
80Pd/20Ag	2.46
77Pd/23Ag	2.48
70Pd/30Ag	1.46
48Pd/52Ag	0.13
95Pd/5Au	1.52
80Pd/20Au	1.37
60Pd/40Au	0.6
45Pd/55Au	0.13
90Pd/10Cu	0.69
70Pd/30Cu	0.12
60Pd/40Cu	1.52
55Pd/45Cu	0.25
45Pd/55Cu	0.01
90Pd/10Ni	0.27
95Pd/5Ru	0.47

As can be seen, alloying with other metals has a significant impact on flux, and it is clear to see why silver alloys are so popular, with a two-fold increase in hydrogen permeability. Alloying with gold also produced a slight bump in flux at low percentages of gold whilst dropping significantly at higher percentages, however of more significance is that Pd-Au alloys show less susceptibility to sulphur poisoning (Knapton, 1977). Alloying with copper, nickel and ruthenium generally sees a significant drop in flux; however an anomaly can be found with alloys of 60Pd/40Cu. Slight changes in

composition see a significant drop off of flux, this is explained by a change in crystal structure where at low copper concentrations the alloy displays a fcc structure, but at 40% copper this changes to a bcc structure resulting in an increase in permeability (Hatlevik *et al.*, 2010). The same author provides permeability data for a range of gold, silver and copper palladium alloys with some of this data available in figure 2.7.

In a similar fashion to the data collected by Knapton, it can be seen that silver alloys with around 23% silver are the most permeable. The slight increase with small amounts of alloyed gold is observable and the peak at 60Pd/40Cu is visible as before. Further examples of permeabilities of hydrogen in binary alloys of palladium with silver and copper are given in (Al-Mufachi, Rees and Steinberger-Wilkens, 2015) where similar values of permeability can be seen.

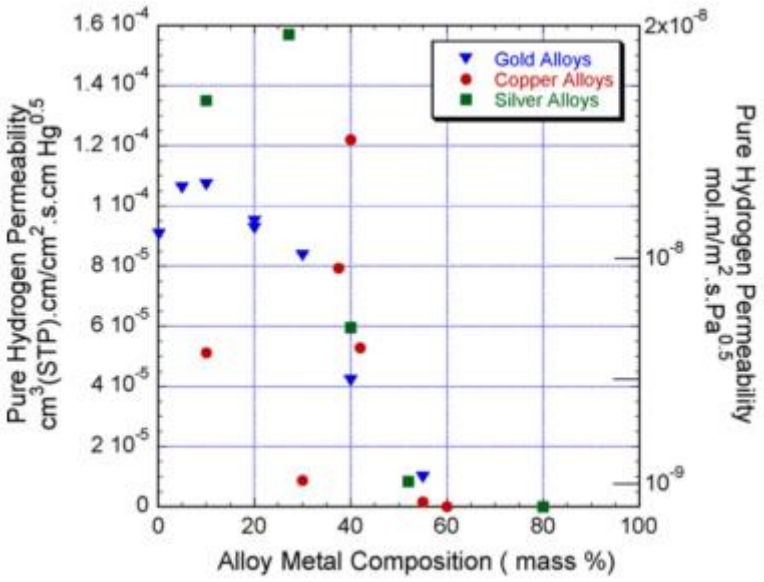

Figure 2.7 – Permeability data for palladium alloyed with gold, silver and copper taken from (Hatlevik *et al.*, 2010)

It has now been observed multiple times in this review that alloying with silver sees an increase in membrane permeability, provided the palladium to silver ratio is in the correct range. The alloying of palladium with silver can suppress the critical temperature (for co-existence of the α and β phases in the Pd-H system) of palladium to room temperature values, reducing the miscibility gap that causes hydride formation in pure palladium (Al-Mufachi, Rees and Steinberger-Wilkens, 2015). Another interesting theory can be drawn from looking at the surface of palladium and silver palladium membranes. SEM images found in (Hatlevik *et al.*, 2010) show the surface of a pure palladium and a palladium silver membrane, both are produced through electroplating of the material onto a ceramic substrate but it is clear to see that the surface area of the Pd-Ag membrane is significantly greater on a unit area basis. As hydrogen diffusion is a surface dependent process it is expected that a greater

surface area will provide an increase in permeation if more active sites for adsorption, dissociation and absorption are available. This suggests that the advantage of adding silver is two-fold, both allowing for greater membrane stability and improved performance. However Pd-Ag alloys also have disadvantages; the alloy is relatively low strength and has a typically short life span due to grain coarsening at high temperatures (Al-Mufachi, Rees and Steinberger-Wilkens, 2015). Another problem is that the membrane is still primarily palladium, meaning that the likelihood of it meeting the DoE target for cost is still low.

Pd-Cu alloys offer a higher permeability than pure palladium (provided the 60% Pd 40% Cu alloy is used) whilst exhibiting increased mechanical stability, being more durable to hydrogen cycling and being more resistant to damage by H_2S (Al-Mufachi, Rees and Steinberger-Wilkens, 2015)(Tarditi and Cornaglia, 2011)(Decaux *et al.*, 2013). Studies show that sulphur adsorption on the surface of the Pd-Cu alloy is more reversible, whereas pure palladium is more prone to nucleation and the formation of the irreversible Pd_4S structure (Opalka *et al.*, 2011)(Opalka *et al.*, 2007).

Palladium alloyed with yttrium has also been reviewed extensively (Shu *et al.*, 1991)(Al-Mufachi, Rees and Steinberger-Wilkens, 2015)(Ockwig and Nenoff, 2007)(Al-Mufachi, Rees and Steinberger-Wilkens, 2015)(Knapton, 1977). Experimental work conducted on yttrium (Burkhanov *et al.*, 2011)(Doyle and Harris, 1988)(Fort, Farr and Harris, 1975) shows that yttrium containing membranes offer unmatched permeability over other Pd membranes, with 93Pd-7Y membranes showing permeabilities around four times greater than palladium at temperatures between 350 and 450 °C.

This is due to the high solubility of yttrium in palladium at concentrations of up to 12%. As the yttrium percentage is increased from 0 to 12% the nature of the alloy reportedly changes from predominantly Y-substitutional (yttrium replacing palladium in the fcc structure) to Y interstitial (yttrium occupying the O sites) resulting in a significant changing of the lattice properties (Yoshihara, Pharr and McLellan, 1987).

The lack of development of commercial membranes is likely to be due to the fact that Pd-Y alloys suffer from work hardening during cold work, resulting in a requirement for multiple annealing stages before use (Al-Mufachi, Rees and Steinberger-Wilkens, 2015). The increase in hardness is reported in (Burkhanov *et al.*, 2011), where comparing the Vickers hardness (HV) figures of 100Pd and 93Pd/7Y shows an increase from 40 to 172, along with a doubling of the tensile strength and a reduction in relative elongation (ductility). Such physical conditions may lead to an increased brittleness of the membrane.

Other binary palladium alloys include ruthenium, with references as far back as (Knapton, 1977) available, many other reviews also mention ruthenium alloys (Ockwig and Nenoff, 2007)(Al-Mufachi, Rees and Steinberger-Wilkens, 2015). Typically, ruthenium alloys have been reported to show a significant drop off in permeability compared to pure palladium. Recent efforts have been made to produce Pd-Ru membranes, as the ruthenium alloys typically exhibit greater mechanical strength (Gade *et al.*, 2009), especially at higher temperatures. Electroless co-deposition of 95Pd-5Ru, 94.5Pd-4.5Ru membranes has produced membranes capable of producing similar fluxes to that of pure palladium, with a high hydrogen selectivity (>35,000) against nitrogen (Gade *et al.*, 2009).

Ruthenium is significantly cheaper than palladium but is typically more expensive than the alternatives of silver and copper thus limiting interest in its wider use. Ruthenium offers an advantage as the membranes can be operated at temperatures as low as 150 °C and in systems that contain contaminants such as HCl, $SiCl_4$ and gaseous hydrocarbons (Burkhanov *et al.*, 2011), some of these compounds would result in the destruction of many palladium-based membranes.

Ternary alloys have also been explored to a significantly lesser extent. A palladium-copper-silver alloy was investigated in (Tarditi and Cornaglia, 2011) and (Tarditi, Braun and Cornaglia, 2011), with one paper giving details on synthesis and the other giving details on surface characteristics and hydrogen permeation. The alloy consisted of 68% Pd, 7% Ag and 25% Cu constructed through sequential electroless plating layers placed onto a porous substrate. The membranes were used to separate hydrogen from nitrogen, so there is no information on their stability in the presence of carbon species, but selectivity was as high as 10,000 (99.9999%) for hydrogen at temperatures of 450 °C. The permeability was measured as 5.4×10^{-9} mol m s^{-1} m^{-2} $Pa^{-0.5}$ a value which is higher than the ultrathin (<10 µm) Pd-Cu membranes it is compared to in the paper.

A second ternary alloy of some interest consists of palladium, indium and ruthenium, with a composition of 93.5% Pd, 6% In and 0.5% Ru. Adding small amounts of ruthenium to a palladium-indium alloy allows for an increasing of the strength of the alloy and provides increased stability in a hydrogen-containing atmosphere in comparison to a binary Pd-In alloy (Burkhanov *et al.*, 2011). This ternary alloy has a higher permeability than pure palladium along with the aforementioned physical improvements, however the permeability is still significantly lower than the Pd-Ag, Pd-Y and Pd-Cu systems (Burkhanov *et al.*, 2011).

To draw conclusions from this section, it can be seen that palladium and its alloys offer excellent permeability and selectivity, with the DoE figures given in this report within the range of feasibility for various alloys, such as Pd-Ag and Pd-Y. However, the cost of using palladium as a bulk material for

membranes is unfeasible, leading to a cost far above what is seen to be of interest by the US DoE. Whilst small scale applications are available commercially it is hard to see a way in which large scale palladium usage can be realised. Alternatives to using palladium in the bulk must be found if metallic membranes are ever to become available on a larger scale. Other performance issues, such as longevity which is a major problem in itself due to the short life span of existing Pd based membranes (Phair and Badwal, 2006)) are also concerning, but it is the belief of this reviewer that the economic and availability hurdles are by far the most prevalent and permanent. One way to circumvent the cost issue is to create ultrathin (<10 μm) membranes, and many of the works discussed in this section utilise this technique. However, whilst this may reduce the cost it does not remove a secondary problem in that palladium is a relatively rare metal deemed "strategic" in its value (Phair and Badwal, 2006).

2.4.4 A Brief Discussion of Other Factors That May Affect Membrane Performance

Before discussing non-palladium-based membranes it may be worthwhile to use the vast amount of studies completed on palladium alloys to investigate the effects of other physical properties.

Grain Size

Studies into grain size have been widely undertaken for crystalline membranes, and the effects on permeate flux and membrane selectivity have been discussed. Metallic grain structure is an important feature of the atomic structure of metals and it is one that can have an effect on the performance of crystalline metallic membranes.

The effects of grain size on nanostructured (<1 μm thick) Pd-Ag membranes was investigated by (McCool and Lin, 2001), where the permeation properties were measured at various temperatures. At lower temperatures (100 – 200 °C), results suggested that surface reaction steps dominated the permeability rate. At higher temperatures, bulk diffusion became more important and here McCool and Lin found that grain size is a critical parameter affecting hydrogen flux. Increasing the grain size from 20 to 60 nm provided an increased rate of hydrogen flux, suggesting that hydrogen permeability in the bulk phase increases as grain size increases (McCool and Lin, 2001). Hydrogen was separated from helium (with a selectivity of about 4000, producing a hydrogen flux of 99.999% purity), where helium flux decreased as the temperature increased. Helium flux also decreased with increasing hydrogen partial pressure. It is important to note that the behaviour of non-nanostructured (amorphous) membranes is different to that of those studied in this work, as described later in this section.

Another study of interest was conducted by (Heinze *et al.*, 1999) on cold-worked 77Pd-23Ag membranes, where the relationship between grain size and the hydrogen diffusion coefficient was explored. The study proposes that two different diffusion mechanisms are displayed, with the dominant mechanism being dependent on the grain size.

For an apparent grain size of less than 40nm hydrogen diffusion through the grain boundary is dominant, whilst inter-granular diffusion is dominant at the larger sizes (100 nm plus) with intermediate sized (40-100 nm) grains showing a combination of both the mechanisms (Heinze *et al.*, 1999).

(Heinze *et al.*, 1999) also found that unlike in pure metals the diffusion in the boundaries is slower than through the grain bulk, although they state that they believe that this is due to the presence of impurities in the grain boundaries interacting with hydrogen. Theoretically, a single crystal membrane would be ideal, as no intergranular diffusion of undesired species could occur.

This test was conducted with a pure hydrogen feed which limits the usefulness of the study in terms of selectivity, but ideas can be extrapolated from this. If larger grains in the Pd-Ag system lead to an increase in bulk diffusion and lower boundary diffusion, it can be expected that permeate purity will increase; as only hydrogen can diffuse through the bulk material.

A study by (Lemier and Weissmüller, 2007) explored the nature of how hydrogen solubility affects the grain boundary, where it was found that at small grain sizes the interaction between grain boundaries has a significant effect on adsorption.

The study found that in the α (low hydrogen) phase the superficial density of hydrogen at the grain boundaries is positive, causing tensile stress, whereas in the β (high hydrogen) phase the density is negative resulting in a compressive stress on the grains. This shift in hydrogen density from the grain boundary to what is presumably the bulk is interesting, with (Lemier and Weissmüller, 2007) suggesting that hydrogen solubility is localised. As the palladium lattice expands when hydrogen is absorbed, smaller grain sizes with increased localised crystal expansion could lead to increased damage as the membrane expands in an “increasingly non-linear fashion”.

Other works suggest that grain boundaries in palladium supress the hydride formation temperature, resulting in the formation of less hydrides during high temperature testing (Iwaoka and Horita, 2013). The authors suggest grain boundaries allow for diffusion but do not act as sites for hydride formation. The study also suggests there is little difference between coarse and ultrafine grained membranes in terms of hydrogen permeability (Iwaoka and Horita, 2013). The “ultrafine” grain size discussed in the study was approximately 330nm which is actually larger than several of the other grain sizes discussed

in this section and this study and therefore should not be considered as contradictory to the findings of those such as Lemier and Weissmüller or Heinze et al. Once again only pure hydrogen was tested, giving no data on selectivity.

Amorphous and Crystalline Structures

It must also be noted however that not all metallic membranes are polycrystallic in structure; amorphous metals have also been studied. Amorphous metals, sometimes referred to as glassy metals, do not exhibit the typical ordered structure of their crystalline counterparts; most amorphous metals are alloys. Initially, amorphous metals were produced by cooling liquid metal mixtures rapidly, with a cooling rate of $10^5 – 10^6$ °C/s (Johnson, 2002), over time this has been reduced to as low as 1 °C/s where alloys yield lower critical/glass-transition temperatures. The suppression of the required cooling rate has led to an increase in interest of using these materials for separation, as they have become increasingly technologically and economically viable.

Amorphous metals offer a tightly packed but random structure on the atomic level, thus differing from the regularly arranged structure of crystalline metals. The random structure eliminates grain boundaries, which in theory should result in a higher selectivity as this removes the grain boundary diffusion mechanism that can lead to non-hydrogen impurities passing through the membrane. The major differences between crystalline and amorphous metals have been summarised in table 2.14.

Table 2.14 – A summary of the differing properties of amorphous and crystalline metals. Adapted from (Phair and Donelson, 2006)

Crystalline Metal	**Amorphous Metal**
Presence of plateau in pressure- hydrogen concentration isotherm	Absence of a plateau in pressure-hydrogen concentration isotherm
Sieverts law obeyed at high H_2 concentrations	Positive deviations from Sieverts law at high H_2 concentrations
Arrhenius behaviour of H_2 diffusion	Non-Arrhenius behaviour of H_2 diffusion
Hydrogen embrittlement caused through dislocation transport	Hydrogen embrittlement caused through the filling of the free volume
Hydrogen diffusivity remains constant with increasing dissolved hydrogen content	Hydrogen diffusivity depends on dissolved hydrogen content
Stable at high temperatures	May crystallise at high temperatures
Possesses weaker mechanical strength	Possesses higher mechanical strength

As can be seen, a number of key properties are significantly different, the most interesting is that the amorphous membranes need low temperature operation, or risk becoming crystalline. This is not ideal in terms of use for separating hydrogen from SMR or gasification processes, however as previously stated, if the permeability and selectivity of these membranes at low temperatures is significantly high enough, attitudes to low temperature operation will change. Another interesting feature is the lack of Arrhenius behaviour; this would suggest that the behaviour of the membranes is somewhat less predictable than their crystalline counterparts.

Examples of amorphous membranes used for hydrogen can be found readily in literature, with a wide range of materials studied. Amorphous alloys based on iron were studied by (Evard *et al.*, 2001), where comparison to similar crystalline membranes was undertaken. Both types of membrane encountered similar problems of a lack of catalysis for hydrogen dissociation, limiting flux, but the study found the activation energy for hydrogen diffusion in the amorphous alloy was around half of the value for the crystalline membranes.

Nickel based amorphous alloys, coated in palladium, were studied by (Wang *et al.*, 2013) with the results compared to the permeability, diffusivity and hydrogen solubility of pure palladium which was also tested by the researchers. The results suggest that the diffusivity of the nickel alloys is below that of palladium but the solubility is significantly higher, resulting in a higher permeability overall. The highest permeability was delivered by a nickel (28%), cobalt (5%), niobium (18%) and zirconium (50%) alloy, achieving a peak permeability of around 1.8 x10^{-8} mol H_2 m^{-1} $Pa^{-1/2}$ s^{-1}. What is also of interest is that the tests conducted here are at temperatures of up to around 370 °C, which suggests that at least some of the amorphous alloys are capable of operating at the lower end of the US DoE target range. Tests appear to have been conducted with only hydrogen, as selectivity data was not provided.

Nickel appears to be a popular material for use in amorphous membranes, where (Sarker *et al.*, 2016) give a review on developments in nickel-niobium-zirconium alloys. The reviewers report that permeabilities for variations of this ternary alloy range from 1 x 10^{-10} to 5 x 10^{-8} mol m^{-1} s^{-1}, these values are comparable to those of palladium and some of its alloys (Sarker *et al.*, 2016). It is also stated that these membranes are capable of operating in the 200 to 400 °C temperature range, which is towards the lower end of the temperature range of interest.

Annealing Time and Temperature

Several papers have included data on annealing time for alloys and for cold worked membranes. As the annealing conditions (heating rate, maximum temperature and cooling rate) have an impact on

the grain size and macro structure of the membrane it is expected that the annealing conditions have an effect on membrane performance.

As shown in (Heinze *et al.*, 1999) the grain size has an impact on the hydrogen permeability, along with the amount of micro-strain found in the grains themselves. Annealing was undertaken under a variety of conditions by the group, with two temperatures investigated (400 and 800 °C) along with a range of annealing times, from 0 hours (untreated) to 200 hours. What could be seen is that the apparent grain size increased with annealing time, with the grain size increasing over six-fold with 200 hours of treatment. The higher annealing temperature also produced a larger grain size, with the increase in grain size also occurring much quicker at higher temperatures; thus 15 hours of annealing at 800 °C produced grains comparable in size to 60 hours of annealing at 400 °C (both grain sizes 65 nm). As larger grain sizes typically produce a purer permeate it is expected that higher temperature annealing for longer times would be ideal for producing the most effective separation membranes.

Annealing at higher temperatures by (Cheng, Pena and Fierro, 2002) found that significantly higher permeate flux values were recorded, an increase from 500 °C to 700 °C in annealing temperature shows a minimum five-fold increase in flux values for all three membranes tested (alumina, zeolite [ZSM-5] and a palladium).

The ternary Pd-Ag-Cu membranes tested by (Tarditi, Braun and Cornaglia, 2011) were significantly affected by the annealing conditions. Due to the complex fcc/bcc structure of the alloy, because of the copper component, the annealing time changed the structure significantly. Longer annealing times saw an increase in the fraction of the membrane exhibiting a bcc structure, resulting in a lower permeation. This suggests that for complex membranes care must be taken to ensure that the optimal annealing conditions are found, to ensure the highest possible permeability is achieved.

Surface Composition

Surfaces will be discussed in more detail later in this section, due to their significant importance in hydrogen permeation. As is suggested, the surface of a membrane has a significant impact on permeation rates. To prevent repetition only one example will be given here, that of (Cheng, Pena and Fierro, 2002), where the amount of silver at the surface of a separation membrane is varied. The study looks at separation of hydrogen from the other components of town-gas (primarily CO and CO_2), and three palladium-based membranes are studied. A pure palladium membrane and then two membranes with varying bulk and surface amounts of silver were tested, the varying amount of bulk silver makes comparisons of the permeate flux rate difficult as the variance is significant (3.3 % to

16.5%) but the purity of the hydrogen permeate is of interest. A surface composition of 28.8% silver resulted in a hydrogen permeate purity of 99.5%, in comparison to 98.7% for pure palladium.

Gas Composition

Gas composition has a significant effect on the performance of membranes. In the most obvious instance the amount of hydrogen present in the feed will have a significant effect on performance theoretically as a higher feed partial pressure of hydrogen leads to a higher flux (provided the permeate pressure is kept constant). Other gas contaminants can also have a significant impact, as has been mentioned at various points throughout this review; for example the presence of sulphur-based contaminants such as H_2S can cause significant damage to membranes with the end result being complete failure of the membrane (Al-Mufachi, Rees and Steinberger-Wilkens, 2015)(Dolan, 2010)(Phair and Donelson, 2006)(Ockwig and Nenoff, 2007). The reviews listed above also mention how the presence of other gases such as H_2O, HCl and CO can have a negative impact, either through causing physical damage to the membranes or by blocking active sites, either passively (reducing the local H_2 concentration) or actively (occupying the active site). Palladium membranes have been shown to be inert to CO_2 (Burkhanov *et al.*, 2011), and this holds true for various other non-palladium containing alloys (Dolan, 2010). As mentioned previously, care has to be taken to ensure that the membrane does not act as a catalyst for unwanted reactions in the presence of CO, CH_4, H_2 (Albers, Pietsch and Parker, 2001)(Ockwig and Nenoff, 2007).

Impurity Species in the Membrane

The presence of impurities such as oxygen, nitrogen and carbon in the atomic structure of the membrane can result in the reduction of the workability and ductility of bcc lattice membranes (Dolan, 2010) where the impurities can occupy interstitial sites in the lattice. Dolan also suggests that whilst dissolved oxygen can increase the hydrogen solubility in niobium and vanadium it can result in an overall decrease in hydrogen permeability; as permeability is a product of the solubility and diffusivity it is expected that the filling of the interstitial sites will result in a reduction in the diffusivity. Other problems can occur in which hydrogen can interact with oxygen or carbon impurities to form high pressure steam or methane trapped within the membrane (Dolan, 2010), this can lead to significant damage to the membrane. This effect is most commonly observed in the group Vb metals.

2.4.5 Non-Palladium Based Metallic Membranes for Hydrogen Separation

As stated above, palladium is deemed too expensive and rare to use in bulk for membrane applications and as such, alternatives have been and continue to be explored. Efforts have focussed on the transition block of elements primarily, but even this leaves a wide range of materials that can be used alone or in alloys to produce membranes for hydrogen separation. This leaves researchers with a large number of options to explore and combinations of these alloys. The task is made even more daunting considering that it is not only the elements that are up for selection but also the number of metals used (some pure, binary, ternary and greater combinations have all been studied) and also the composition of any alloys. As the Pd-Ag, Pd-Cu and Pd-Y systems show, even slight variations in composition can signify a significant shift in performance.

With this wide range of materials and alloys in mind it becomes necessary to deduce which metals are the most feasible for use. Once again, the previously discussed DoE targets are useful, as they give a fair indication of the characteristics of a potentially economically feasible membrane. Foremost of interest is the required flux rate of 91.5 $m^3/h/m^2$, and such a high required flux will require a high permeability.

Permeability data for many metals is widely available, selected values taken from (Phair and Donelson, 2006) and (Dolan, 2010) are included in table 2.15.

Table 2.15 – Hydrogen permeability figures for various metals at selected temperatures

Metal	**Temperature (°C)**	**Permeability (mol m^{-1} s^{-1} $Pa^{-0.5}$)**	**Source**
Niobium	500	1.6×10^{-6}	(Phair and Donelson, 2006)
Tantalum	500	1.3×10^{-7}	(Phair and Donelson, 2006)
Vanadium	500	1.9×10^{-7}	(Phair and Donelson, 2006)
Iron	500	1.8×10^{-10}	(Phair and Donelson, 2006)
Copper	500	4.9×10^{-12}	(Phair and Donelson, 2006)
Nickel	500	7.8×10^{-11}	(Phair and Donelson, 2006)
Niobium	400	3×10^{-6}	(Dolan, 2010)
Tantalum	400	2×10^{-7}	(Dolan, 2010)
Vanadium	400	3×10^{-7}	(Dolan, 2010)

The most striking figures are the permeabilities of the group Vb metals: niobium, tantalum and vanadium. The figures given for the group Vb metals are higher than those of palladium referenced in

both sources, the difference is significant as the increase in hydrogen permeation is in the order of 10 to 100 greater dependent on material. This makes the group Vb metals very attractive as a basis for membranes as the permeabilities listed would be more than capable of delivering the required flux. Iron, copper and nickel have significantly lower permeabilities which limits interest in using them as the bulk metal however they may be of use in alloys. Other metals of interest in terms of alloys are the group IVb metals, titanium, zirconium and hafnium; however, little is reported for the permeability of the pure metals (Dolan, 2010)(Ockwig and Nenoff, 2007); some data can be found for titanium coatings used as membranes (Kurdyumov, Lyasnikov and Shvachkina, 1983) which does not indicate much promise for use as a bulk membrane material.

As expected, a majority of research has been focused on group Vb metal containing membranes, suggesting this would be the most prudent area to review in detail. Whilst the group V metals show the most promise there are significant problems with their use for membranes as pure metals:

1. **Lack of hydrogen dissociation and re-association**: A significant issue that the group Vb metals face is their lack of catalytic ability for hydrogen dissociation. Unlike palladium, the group Vb metals have slow rates and high activation energies for dissociation (Dolan *et al.*, 2013), this limits their observed permeability significantly and requires the use of a catalytic surface dopant. Typically, this dopant is palladium, although alternatives continue to be explored. This is potentially problematic as the membrane still relies on palladium however the amount is significantly less – this reduced amount will be more economically viable.
2. **The formation of surface oxides**: The group Vb metals have been shown to form oxides on their surfaces that can inhibit the dissociation of hydrogen and prevent its subsequent absorption into the bulk (Ockwig and Nenoff, 2007)(Dolan, 2010)(Phair and Donelson, 2006). These oxides are deemed to be very stable (Ockwig and Nenoff, 2007) and coupled with the already low dissociation rate on clean group Vb metals the problem is only exasperated.
3. **Ready formation of hydrides**: The group Vb metals all have negative enthalpies of formation for hydrides (Phair and Donelson, 2006)(Ockwig and Nenoff, 2007), this can result in hydrides being readily formed leading to an increased risk of embrittlement and blistering of the membrane at certain operating temperatures and pressures.

The problems highlighted above give insight into why palladium has been of significantly more use than the group Vb metals for small-scale industrial applications, however through the use of alloys (and coatings) progress is being made in the design of viable membranes. The remainder of this section will focus on the group V metals, with a detailed review on the current state of the art.

Vanadium

Vanadium is the smallest (in terms of mass and atomic radius) of the group Vb metals, and as with the other members of the group it exhibits a bcc crystal structure. It offers permeability in the region of 10 times greater than palladium at 500°C. Vanadium forms a number of oxides readily in the II (VO), III (V_2O_3), IV (VO_2) and V (V_2O_5) valency states; with the V_2O_5 oxide being particularly problematic (Dolan, 2010) due to its ready formation at high temperatures.

The vanadium-hydrogen pressure, concentration and temperature (PCT) system has been studied extensively for a relatively long period of time, and studies by (Veleckis and Edwards, 1969)(Chang and Wert, 1973)(Griffiths, Pryde and Righini-Brand, 1972) are cited in modern reviews such as (Dolan, 2010). The phase diagram provided in (Griffiths, Pryde and Righini-Brand, 1972), shows that the critical temperature for V-H systems is at around 170 °C, which is significantly lower than that of palladium, thus giving an interesting increase in the range for potential operating temperatures alongside a lower chance of hydride damage from multiphase operation and phase transformations during heating and cooling cycles.

Hydrogen solubility in vanadium is highly temperature dependent. (Veleckis and Edwards, 1969) report a series of isotherms showing that, at increasing temperatures, solubility at a given pressure decreases significantly. This is likely to lead to the development of membranes with a maximum useful temperature, however the solubility in the temperature range specified by the DoE is still very high. This high solubility in itself could lead to problems of hydride embrittlement as mentioned above, so an increased operating temperature may actually be somewhat favourable. At room temperature the H/V ratio is given as 0.05 by (Phair and Donelson, 2006), a value greater than that of 0.03 given for palladium in the same work.

Alongside solubility, the hydrogen diffusivity of vanadium is significantly higher than most metals. A diffusion coefficient at 400 °C of 1.2 $x10^{-8}$ m^2 s^{-1} is given by (Dolan, 2010); in comparison the value for palladium given by the same source is 5.5 $x10^{-9}$ m^2 s^{-1} or around half of that given for vanadium. A key factor in this is the low activation energy for bulk interstitial diffusion, which is significantly lower than the vast majority of metals (Völkl and Alefeld, 1978)(Pokhmurs'kyi, Sokolovs'kyi and Fedorov, 1995). This high diffusivity is a potentially useful trait as it will allow for a consistently high permeability even at the lower hydrogen solubilities achieved through the creation of alloys.

A broad range of vanadium alloys have been investigated for use as membranes; reviews by (Dolan, 2010)(Dolan *et al.*, 2013)(Phair and Donelson, 2006) cover many variations in great detail and selected membranes will be discussed here. Widely studied secondary and tertiary alloying elements

investigated for use with vanadium include nickel, aluminium and titanium; with studies also carried out on cobalt, iron and chromium alloys to a lesser extent (Phair and Donelson, 2006)(Dolan, 2010).

Vanadium – nickel alloys are of great interest due to the reduction of hydrogen solubility, allowing for the development of a more stable membrane; V-Ni has a lower solubility than any other period 4 binary vanadium alloy (Dolan, 2010), Dolan shows that the H/M ratio in the 85V-15Ni alloy is relatively similar to that of palladium at temperatures in the range 340-400 °C. Whilst nickel typically produces an fcc crystal, at nickel contents of 15% or lower the bcc structure of vanadium is maintained for V-Ni alloys; resulting in alloys containing up to 15% nickel being of most interest for permeation studies ([85+] V/ [15-] Ni). (Kim, Shim and Lee, 2012) finds that the hydrogen solubility for the 90V-10Ni alloy is comparable to that of the 85V-15Ni alloy, this could be of interest as a higher diffusivity may be achievable with a decreased amount of nickel present. This idea is supported by (Shim *et al.*, 2013) where a lower diffusivity coefficient is found for alloys containing increasing amounts of nickel. The permeability of the 85V-15Ni membrane is also widely reported, with (Nishimura *et al.*, 2002)(Nishimura, Komaki and Amano, 1991) reporting permeabilities in the 3 – 4 $x10^{-8}$ mol m^{-1} s^{-1} $Pa^{-1/2}$ range for temperatures in the 200 to 450 °C range. A higher permeability of 5 $x10^{-7}$ mol m^{-1} s^{-1} $Pa^{-1/2}$ at a temperature of 350 °C was reported by (Ozaki *et al.*, 2003b) for the 85V-15Ni membrane; this is somewhat expected due to the higher hydrogen solubility of vanadium at lower temperatures. Ozaki et al also found cracks forming in the membrane at 200 °C suggesting lower temperature operation may be of limited use; but considering the temperatures of SMR and gasification syngas this shouldn't be a problem.

A wider range of vanadium-aluminium alloys have been tested, as they form the preferred bcc structure and show good hydrogen diffusivity (Dolan *et al.*, 2013); others have tested V-Al alloys on the basis of its use in the production of pure vanadium in commercial uses (Zhang *et al.*, 2002). Both (Zhang *et al.*, 2002) and (Dolan *et al.*, 2013) find that an increasing aluminium content leads to a decrease in diffusivity (and permeability); with Zhang et al finding that an increase from 20% to 30% aluminium content leads to a drop in permeability by a factor of around 150. (Dolan *et al.*, 2013) goes even further suggesting that aluminium alloys offer greater hydrogen diffusivities than nickel alloys thus reducing the need for a very high hydrogen pressure, which will result in lower H/M ratios likely to lead to less hydrogen embrittlement. Research continues into V-Al membranes, where (Suzuki *et al.*, 2016) have run tests on V-Al membranes to compare hydrogen solubility with Pd-Ag membranes; suggesting that normalised flux values for the vanadium membrane is over four times greater.

Before discussing other binary alloys, it is worthwhile mentioning that ternary membranes of vanadium, nickel and aluminium in varying concentrations have also been studied. It is suspected that

this is done in an attempt to retain the higher diffusivity of V-Al membranes alongside the increased mechanical strength of the V-Ni membranes. Studies on various alloys were conducted by (Ozaki *et al.*, 2003a) in a similar manner to their studies on V-Ni alloys; they found that the hydrogen diffusivity was only weakly dependent on the aluminium content. They report several results, but the best performing membrane was deemed to be the 85V-10.5Ni-4.5Al membrane, where the hydrogen permeability at 350 °C was reported as 6.29 $x10^{-8}$ mol m^{-1} s^{-1} $Pa^{-1/2}$, a value that is a factor of two larger than that of the 85V-15Ni membrane. Over longer tests the permeability of this membrane decreased by around 40% after 102 hours of operation but the permeability was fully restored through use of a "baking treatment" in air. This is a somewhat interesting development and would suggest that the membrane is reusable but that excessive exposure to hydrogen must have an effect on the surface (possibly the catalytic palladium over-layer). Other permeability values for V-Ni-Al membranes are reported by (Dolan, 2010) and (Phair and Donelson, 2006).

Titanium has also been alloyed rather extensively, both in binary and tertiary alloys. Binary alloys are reported in (Phair and Donelson, 2006) and (Dolan, 2010), titanium binary alloys provide the highest hydrogen solubility of all period 4 transition metals. Whilst this can lead to embrittlement of the membrane, the advantage of this is higher hydrogen permeability if conditions can be controlled; this can be seen in the reviews stated above that show higher permeabilities for V-Ti membranes than for V-Ni. V-Ni-Ti alloys are of interest for use as membranes, as they reportedly have excellent resistance to embrittlement (Dolan *et al.*, 2015)(Evtimova, Drioli and De Luca, 2016). A 89V-6Cr-5Ti alloy has also been investigated by (Romanenko *et al.*, 1996), however the measured permeability suggests that this alloy is not of much interest as it is in the order of 100 times lower than the V-Al membranes.

As mentioned previously, other membranes have also been investigated to varying degrees, vanadium-chromium (V-Cr) membranes have been investigated alongside the V-Al tests recorded in (Dolan *et al.*, 2013); where V-Cr membranes were shown to have higher diffusivities than V-Al and V-Ni membranes. V-Cr based membranes have also been tested with more than pure hydrogen feeds, with (Jeon and Park, 2013) testing a 89.8V-10Cr-0.2Y alloy in a mixture of gases produced from the water gas shift reaction: H_2, CO_2 and with small amounts of H_2S in some tests. The presence of CO_2 and H_2S are shown to reduce the flux achieved by the membrane, however the membrane is reported to be very stable in the CO_2 inclusive environments with no sign of damage after 7 days of operation. Vanadium cobalt alloys have also been investigated, with a relatively high permeability reported by (Phair and Donelson, 2006).

What can be summarised is that vanadium membranes vary greatly in composition, many promising alloys have been found but problems still exist with hydrides and the need for a palladium catalyst

present on the surface. The high diffusivity of vanadium-based membranes ensures however, that they remain an area of great interest for use as membranes.

Niobium

Niobium is the second group Vb metal, it is larger in size than vanadium and is typically alloyed with different metals. Niobium forms oxides most commonly in the V state (Nb_2O_5), with the IV (NbO_2) and III states (Nb_2O_3) states also being relatively common and the II state (NbO) being the rarest similar to vanadium. Once again, these oxides cause significant problems in reducing surface catalysis and activity.

The PCT diagram of niobium, along with the pressure isotherms, shows that (similar to vanadium) hydrogen solubility drops significantly as temperature increases (Veleckis and Edwards, 1969). The PCT diagram shows a miscibility gap, like palladium and vanadium, with a critical temperature of 171 °C for phase change, a value similar to that of vanadium. Whilst the similarities with vanadium so far have been striking (yet somewhat expected) a more significant divergence can be seen in comparing the permeabilities. The permeability of niobium from various sources has been included in table 2.16, what can be seen is that there is a significant amount of variance some of which is expected due to the varying temperatures but some of which is harder to explain.

Table 2.16 - Permeability of niobium measured at varying temperatures

Temperature (°C)	**Permeability (mol m^{-1} s^{-1} $Pa^{-1/2}$)**	**Source**
400	3 $x10^{-6}$	(Dolan, 2010)
420	3.6 $x10^{-7}$	(Buxbaum and Marker, 1993)
500	1.6 $x10^{-6}$	(Phair and Donelson, 2006)

The significant variations in permeability may be explained through the use of different surface catalyst compositions and thicknesses, which will have an effect on the measured value. The higher measured values of permeability are of most interest – these values are far and above any other pure metal reported widely.

This high permeability must be explained by the high hydrogen solubility of the metal, as the diffusion coefficient of niobium is somewhat comparable in size to that of vanadium. Several values are reported for 400 °C in (Dolan, 2010), ranging from 3 x 10^{-9} to 6.4 $x10^{-7}$ m^2 s^{-1} and a modal value of 1 $x10^{-8}$ m^2 s^{-1} with the data taken from (Cantelli, Mazzolai and Nuovo, 1969)(Schaumann, Völkl and

Alefeld, 1970); whilst there is some ambiguity it is clear to see that the diffusivity of hydrogen for niobium is of a similar scale to that of vanadium, as can be seen in (Pokhmurs'kyi, Sokolovs'kyi and Fedorov, 1995). This implies that the hydrogen solubility of niobium must be significantly higher than that of vanadium, this can be verified to some extent by studying the isotherms given by (Veleckis and Edwards, 1969) which clearly show at the same temperature the H/M ratio in niobium is significantly higher than in vanadium. This high solubility means that alloying is once again preferential to limit potential damaging of the membrane through high and low temperature cycles.

Efforts to alloy niobium with other metals are extensive and appear to be rather varied, including heavier elements than those seen typically alloyed with vanadium. Two examples of binary niobium alloys can be found in (Zhang *et al.*, 2010); where niobium, niobium-ruthenium (Nb-Ru) and niobium-tungsten (Nb-W) membranes were tested for their hydrogen permeation. The study found that at a temperature of 500 °C the diffusion coefficient of niobium was lower than the reported value, and that the addition of 5% of ruthenium or tungsten resulted in an increase in the diffusion coefficient as can be seen in table 2.17.

Table 2.17 – Hydrogen diffusion coefficient in various Nb alloys taken from (Zhang *et al.*, 2010)

Material	**Diffusion coefficient ($m^2\ s^{-1}$)**
Nb	2.97×10^{-9}
95Nb-5Ru	4.13×10^{-9}
95Nb-5W	4.06×10^{-9}

The paper also suggests an improved flux rate for the alloys, with the 95Nb-5Ru alloy providing the highest measured flux. This increase in diffusivity is explained by a decrease in the activation energy for diffusion, resulting in a change in the Arrhenius parameters that govern the process.

Multiple membranes were tested by (Suzuki *et al.*, 2015) including: Nb, 95Nb-5W, 95Nb-5Ru, 90Nb-5W-5Mo and 84Nb-8W-8Mo alloys; where the hydrogen permeability was recorded in terms of hydrogen chemical potential through the membrane instead of pure flux data. Data was also given for the activation energy and pre-exponential factors for diffusion, where it was found that the 84Nb-8W-8Mo alloy had the lowest activation energy resulting in the highest permeability recorded.

Some similarities to vanadium alloys can be seen, with tests on Nb-Ni-Ti membranes such as those studied in (Kishida *et al.*, 2008) A eutectic mixture between Nb and Ni/Ti (in various combinations) was investigated with a highest permeability recorded at 400 °C with a value of approximately $2 \times 10^{-}$

^{8} mol m^{-1} s^{-1} $Pa^{-1/2}$, which is similar in scale to that of pure palladium (at 500 °C). This is another promising development as this would probably produce a high enough flux rate to meet US DoE targets for viability.

Niobium also appears to be a popular choice for use in amorphous alloys, with Ni-Nb-Zr membranes emerging as an area of interest. (Sarker *et al.*, 2016) present a review of multiple amorphous alloys; the majority of these are nickel based but contain very high niobium content. Permeabilities of up to 1 x 10^{-7} mol m^{-1} s^{-1} $Pa^{-1/2}$ are reported. The high permeability of niobium and the stabilising behaviour of nickel drive interest in these membranes. An advantage over their crystalline counterparts is that an increased amount of nickel can be added. Nickel can act as a catalyst for dissociation of hydrogen, however as discussed for vanadium in crystalline alloys the nickel presence is capped at around 15% to maintain the bcc structure. These are very promising results but as the focus of this project is on crystalline materials little focus will be directed towards these.

Tantalum

As tantalum is not the focus of this research, this review will only provide a brief overview of the metal and its use as a membrane material. Tantalum is the largest of the group V metals widely reported for use as membranes. The isotherms in (Veleckis and Edwards, 1969) show that the behaviour of tantalum is similar to that of niobium and vanadium – the hydrogen solubility appears to be somewhere between that of vanadium and of niobium.

However, at low temperatures (Phair and Donelson, 2006) present data showing a H/M solid solubility ratio four times greater than that of niobium and vanadium. Another interesting factor to note is that the critical temperature for tantalum is stated as 10 °C (San-Martin and Manchester, 1991), although other figures suggest this temperature is around 47 °C (Mallett and Koehl, 1962). This low critical temperature is in a similar range to that of Pd-Ag membranes used commercially which are deemed stable enough for use.

One potential drawback is that the diffusion coefficient for tantalum is reported to be smaller than that of vanadium; at 4 x10^{-9} m^{2} s^{-1} this value is significantly smaller (Dolan, 2010). The permeability figures given in the same paper however are promising with permeabilities close in scale to that of the other group V metals.

The alloys of tantalum used are similar to those of the other metals in this review: a Ta-W membrane is reviewed very favourably by (Yukawa, Nambu and Matsumoto, 2011) where a high permeability is reported and a Pd-Ta membrane is reviewed by (Peachey, Snow and Dye, 1996).

It is important to note that other non-group V based membranes are also under research. As they fall out of the focus of the research undertaken as part of this project little emphasis will be put on them here. Membranes containing high amounts of group IV metals have been explored with, for example, (Hara *et al.*, 2003) and (Yamaura *et al.*, 2004) investigating membranes containing up to 40% bulk zirconium. The hydrogen permeation rates of some of these membranes are impressive but alloying with nickel and a group V metal (typically niobium) appears to be the norm.

In summary, it appears that several potential membranes offer viable alternatives to palladium-based ones. With significantly lower cost and good bulk diffusion/permeability properties the group V metals and their alloys have the potential to meet DoE targets for required flux, purity and cost. These are among the biggest barriers to usage of membrane technology and the wide range of potential membranes that can meet this bulk permeation rate is encouraging; ongoing research will continue on improving the permeability, sustainability and affordability of these membranes.

However, before these membranes can become economically and technologically feasible problems still persist. Hydride formation remains a concern that can be mitigated, the embrittlement of the membranes at high hydrogen concentrations also must be addressed. The key hurdle to application remains the dependence on palladium to provide a surface catalyst and a protective surface layer to prevent oxide formation.

2.4.6 The Impact of the Surface on Diffusion

As mentioned briefly in the summary in the section above, multiple group Vb alloys show potential to meet the DoE requirements for hydrogen flux, however concerns still persist over the surfaces of the membranes. It is widely reported that for most group Vb membranes a palladium coating layer is required, to protect against oxidation and to increase hydrogen dissociation catalysis; however the amount of palladium used is typically very small, with layers in the range of a couple of hundred nanometres thick, as shown in (Nishimura *et al.*, 2002)(Dolan *et al.*, 2015)(Wang *et al.*, 2013) amongst many others. The reduction in the mass of palladium required for these coatings edges membranes towards becoming more economically viable, but material scarcity may require even less palladium to be used – or potentially none at all. The practical problems of using pure palladium, highlighted in the section above, also persist.

Before considering alternative coatings to palladium it is worthwhile to consider the processes that are undertaken on the surface, albeit briefly before discussing in detail in chapter 3, which are covered by steps two and three of the seven step model discussed earlier. Hydrogen must be adsorbed to the

surface, dissociated and absorbed into the bulk, all these processes have associated activation energies that must be overcome in Arrhenius type reactions. On the permeate side these processes are reversed, so the energies of these reverse processes (re-association and desorption in particular) must also be considered.

Hydrogen adsorption on the surface is determined as an exothermic process for most transition metals, including the group Vb metals (Ferrin *et al.*, 2012), with the hydrogen sticking coefficients of tantalum and niobium investigated by (Pick, Greene and Strongin, 1980), the coefficient of niobium by (Hagen and Donaldson, 1974)(Pick, 1981) and of vanadium by (Romanenko *et al.*, 1996) and (Svedberg and Buckman, 1980). On a clean surface at elevated temperatures it appears that the hydrogen sticking coefficient is indeed sufficient for these metals, however it is shown that the hydrogen sticking coefficient is dependent heavily on the number of available surface sites; more adsorption of any gas molecules leads to less future adsorption due to the reduced availability.

As highlighted already a much more significant problem for the group Vb metals is the dissociation of molecular hydrogen into its atomic components. Catalytic coatings for dissociation are of major research interest; where a focus has been shifted to finding alternatives to pure palladium. Alloying palladium is a possibility, with Pd-Ag and Pd-Cu already proving suitable for use as membranes leading to the belief that they could potentially work as reasonable catalytic coatings.

Nickel has been suggested as an alternative coating, (Hara *et al.*, 2000) details a 36Zr-64Ni membrane that delivered a hydrogen flux of 1.9 [cm^3 H_2] cm^{-2} min^{-1} without a coating, at a temperature of 350 °C. This is due to nickel being a known hydrogen diffusion catalyst, the drawback is that in 85V-15Ni membranes the nickel concentration is not high enough to catalyse dissociation (Ozaki *et al.*, 2003b). Another amorphous nickel alloy (Ni-Nb-Ta-Zr-Co) was investigated in (Yamaura and Inoue, 2010), where comparisons between palladium and nickel coated membranes were made. The results show that, at any given temperature and pressure differential, the palladium coated membrane outperformed the nickel coated membrane by a factor of approximately 4. Whilst in terms of raw performance data this is unimpressive, the significant decrease in cost through the use of no palladium is important. At a temperature of 400 °C and a pressure differential of 2 bar, the hydrogen flux for the nickel coated membrane is approximately 2 [cm^3 H_2] cm^{-2} min^{-1} ; a value that is similar in scale to that reported by (Hara *et al.*, 2000) discussed at the beginning of this paragraph.

It is important to note that the tests discussed above used a feed of pure hydrogen, problems with using nickel as a coating occur when the other products of SMR and gasification are considered. Multiple sources stated that nickel is not resistant to H_2S, CO or moisture (Pokhmurs'kyi, Sokolovs'kyi

and Fedorov, 1995)(Dolan, 2010)(Phair and Donelson, 2006). (Leimert and Karl, 2016) discuss the addition of CO, N_2, CH_4 and H_2O to streams of hydrogen fed to nickel capillary tubes; where they found increasing amounts of CO reduced the hydrogen flux achieved. The study also considered the effect of H_2S, where damage was seen over long-term operation; this is significant, as DoE targets include a minimum longevity far beyond the test time. Other studies, such as (M. Wang *et al.*, 2016) however investigated nickel hollow fibre membranes and found the membranes to be "stable" in CO containing environments; but the selectivity of these membranes is significantly lower than that of the dense metal membranes discussed previously in this section (the H_2/CO_2 separation ratio is reported at a maximum of 100). Dolan states that nickel surfaces for hydrogen separation are likely to remain "a scientific curiosity with little scope for widespread implementation".

Other transitional metal catalytic coatings have been investigated including platinum, iridium, cobalt, iron, magnetite (Fe_3O_4), tungsten sulphide and molybdenum sulphide (Phair and Donelson, 2006)(Munschau, 2003). Some of these coatings have shown promise but currently there is no obvious choice to replace palladium, this point can be reinforced by viewing recent releases on the subject of hydrogen separation membranes: (Song *et al.*, 2015)(Abu El Hawa *et al.*, 2015)(Vigneault and Grace, 2015)(Lai, Yin and Laura Lind, 2015) all use palladium in the bulk or as a surface catalytic coating, confirming the belief that investigations need to continue in finding a viable alternative.

It is believed that the main requirement for the catalytic coating is that the reactive surface sites should be "sufficiently close and concentrated to assist the dissociative adsorption of hydrogen" (Phair and Donelson, 2006). These sites also need to not be blocked by CO, CO_2 or sulphur absorption (like nickel sites) or this will have a negative effect on the overall permeation.

Investigating Potential Surface Coatings

Computational studies continue to be useful in examining the potential of membrane permeability, with density functional theory (DFT) and molecular dynamics (MD) allowing researchers to generate large amounts of data (binding energies, activation energies and bond lengths for example) without the need for lengthy experimental work. Examples of these studies conducted for the calculation of hydrogen dissociation energies can be found with varying conditions; (German, Abir and Sheintuch, 2013) provide a model for activated hydrogen dissociation on metal surfaces. The paper details a "tunnelling model" where molecular hydrogen dissociation on the surfaces of metals such as Ni, Pd, Pt, Cu and Ag are considered; with activation energies used to calculate rate constants for the process of dissociation. The model suggests that silver and copper have the highest activation barriers for dissociation, which shows good agreement with experimental data. The model was also used to

predict the rate constants of hydrogen dissociation for a number of alloys including the favoured Pd-Ag alloy, along with an exploration of the effect of surface coverage on the surface hydrogen adsorption energy.

A similar study was conducted by (Gomez *et al.*, 2011), with the reactivity of transition metals towards the dissociation of molecular hydrogen studied. Included in the report is the activation energy for dissociation of hydrogen for numerous transition metals taken from numerous sources, this data has been reproduced in table 2.18 due to its relevance.

Table 2.18 – Dissociation energies for molecular hydrogen on various transition metal surfaces. Adapted from (Gomez *et al.*, 2011)

Surface	**Activation Energy (eV)**
Pd (001)	0.15
Pd (111)	0.002 – 0.02
Pt (001)	0.0
Pt (111)	0.0 – 0.33
Cu (001)	0.50 – 0.90
Cu (111)	0.48 – 0.73
Ag (001)	1.10 – 1.63
Ag (111)	0.74 – 1.11

As can be seen the ideal values are in the range of the platinum group metals, with silver and copper having a more significant barrier.

Other studies show the importance of another surface mechanism, the desorption from the active sites and into the bulk is also important in maintaining a high permeate flux. Studies by (Pozzo and Alfè, 2009) and (Wang *et al.*, 2014) investigate the dissociation of hydrogen and diffusion of hydrogen from the surface to the bulk (referred to in this report as the absorption, as referred to in the seven step model in this chapter) on transition metal doped magnesium surfaces. Whilst the data found in the paper is of limited use for pure transition metals, an interesting “volcano” plot is featured. The plot features three pieces of information for each transition metal: the dissociation activation energy, the absorption activation energy and the d-band centre energy (all in eV); as can be seen in figure 2.8.

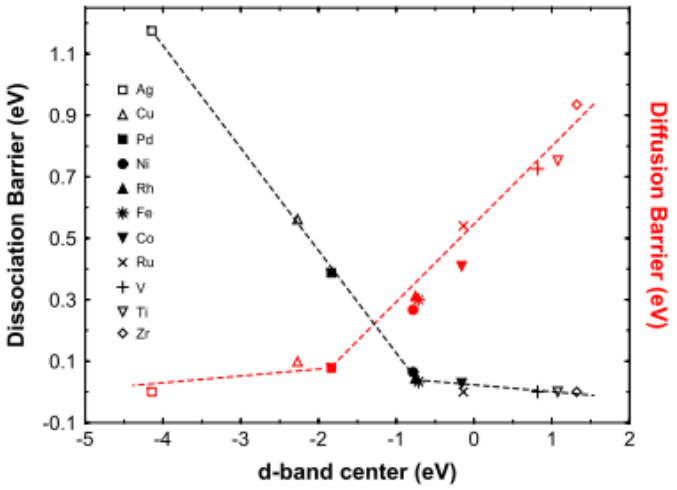

Figure 2.8 - Volcano plot of activation energies, taken from (Pozzo and Alfè, 2009)

As can be seen, a pattern emerges where those at either end of the d-band scale offers low activation energies for only one of the two processes, whilst those in the centre offer moderate values for both. Whilst there are no studies that have shown a similar plot for this type of behaviour at the surface of transition metals, it could be theorised to hold somewhat true due to the active surface dopants used in this study being transition metals. Platinum, as mentioned previously offers no diffusion barrier but its poor hydrogen solubility can be explained by poor absorption of atomic hydrogen. The opposite can be said of the group V metals and zirconium, although it is important to note that the V/Zr doped Mg studied by Pozzo et al appears to have the opposite problem due to the nature of the bond structure. Another interesting similarity is that both nickel and palladium are found towards the centre of the graph, along with iron, which suggests moderate activation energies for both processes making them the most suitable for use as a catalyst. The study is focused around suitability for use as catalysts for hydrogen storage in hydrides but the concept is somewhat similar in terms of the physical processes of dissociation and bulk absorption and it is significant to see a similar result found in a related field.

So far it has been clear that the use of pure silver is of limited use, multiple studies (Pozzo and Alfè, 2009)(Gomez *et al.*, 2011)(Mohammad *et al.*, 2007)(Sprunger and Plummer, 1993) show that clean, pure silver does not catalyse hydrogen dissociation. However, there are sources that suggest the activation energy for hydrogen dissociation can be reduced through oxidisation of silver, where the presence of sub-surface oxygen has been shown to reduce the activation energy (Xu, Greeley and Mavrikakis, 2005)(Mohammad *et al.*, 2007)(Mohammad *et al.*, 2008) significantly. (Mohammad *et al.*, 2007) reports that the addition of oxygen to the surface of silver makes “hydrogen dissociation kinetically feasible”, with advancements from the same group reporting that various surface and

subsurface oxygen species promote hydrogen dissociation on silver surfaces (Mohammad *et al.*, 2008). These related studies suggest the activation energy is lowered from approximately 125 kJ mol^{-1} to around 70 kJ mol^{-1}, the initial activation energy reported agrees with the value provided in table 2.18 above, adapted from (Gomez *et al.*, 2011).

A similar reduction in activation energy (to 71 kJ mol^{-1}) is reported by (Xu, Greeley and Mavrikakis, 2005), where it is stated comprehensively that "subsurface oxygen dramatically increases the reactivity of the silver surface". This change in reactivity is believed to be caused by an upshift in the centre of the d-band, this would show agreement with the volcano plot of (Pozzo and Alfè, 2009) where an upshift of the d-band would move silver more towards the centre of the graph and towards the better performing catalysts of palladium and nickel.

Experimental results have also suggested that the addition of oxygen to silver can improve its behaviour as a catalyst, although these results were obtained in a rather unrelated field. (Bron *et al.*, 2008) report the use of oxygen treated silver-silica catalysts for acrolein hydrogenation, where a key step in the reaction pathway is the dissociation of hydrogen. The report states, that surprisingly, the pre-treatment enhances the activity of silver; in reaction pressures of up to 10 bar, they report a two to three-fold increase in hydrogenation with the use of the oxygen pre-treatment catalyst.

It must be noted that the activation energy for dissociation on oxygen treated silver is still relatively high in comparison to palladium; however, silver does have other advantages that make it worthy of investigation. Unlike nickel, silver is more resistant to carbon monoxide blocking of surface sites; this can be seen by the metal-CO bond energies given in (Phair and Donelson, 2006). A high binding energy results in CO persisting and interfering with dissociation, silver has the lowest binding energy by far of the reported metals. However, there are suggestions that oxidised silver does display an increased metal-CO bond strength which may change this somewhat (Xu, Greeley and Mavrikakis, 2005).

Asymmetric Coatings

Asymmetric membranes have also been investigated, with efforts towards commercialisation made by Eltron (Evenson and Waters, 2011)(EERC, 2010) using an asymmetrically coated membrane. Asymmetric membranes are those where the surface conditions vary between the feed and permeate side, this can be from the application of a surface coating to one or both of the surfaces. Examples can be found in research too, (Yamaura and Inoue, 2010) investigated the use of palladium and nickel surface coatings, including asymmetric configurations using nickel as the feed or permeate coating and palladium for the reverse. They report the permeabilities for the amorphous membranes coated

and find that the permeability of the membrane with the nickel coated feed-side is higher than that of the palladium coated feed side by a factor of around 10.

An example of a crystalline asymmetrically layered membrane is given in (Viano *et al.*, 2015), where a vanadium membrane was coated with palladium on the feed side and varying levels of nickel on the permeate side. This has the advantage of using nickel in a suitable environment (containing no carbon or sulphur species) and the advantage of only using half as much palladium.

The paper suggests that the hydrogen flux increases as the nickel coat thickness decreases until a limiting thickness of 150 nm is reached. Beyond this point the flux decreases due to incomplete nickel coverage, the flux rate for the membrane peaked at 65% of the maximum value of a symmetrically palladium-coated vanadium membrane. The peak flux given is approximately 0.3 mol m^{-2} s^{-1} at a temperature of 425 °C. These results show that asymmetrical membranes may be preferable in the future, as the results show encouraging progress towards the DoE targets. The use of nickel is only somewhat limiting and, as mentioned before, the significant decrease in cost makes it the more economically viable choice.

2.4.7 Construction Methods for Metallic Membranes

A review on the use of metallic membranes would not be complete without at least a cursory overview of the potential methods of manufacture. The construction method of the membrane can have an effect on performance, with potential effects from the presence of surface (or bulk) contaminant species, the membrane material grain size and potential impacts on the longevity of the membrane through additional thermal r mechanical stressing of the metal. As the grain size can be reformed by annealing, the impact of this can be somewhat minimalised. Processes such as chemical vapour deposition, electroplating, sputtering and melt cooling typically increase the metals' grain size; whilst cold working methods like rolling, drawing, pressing, spinning, extruding and heating can decrease an alloy's grain size (Ockwig and Nenoff, 2007). Further details on the impacts of the processing methods used on membrane structure can be found in (Dolan *et al.*, 2013).

Thought must be given to the construction methods of membranes, especially if the intention is to increase use to larger scales as the method of manufacture is going to have a significant effect on the affordability of membranes, and the likelihood of meeting the US DoE target cost per unit area.

Bulk Material

The method of creating the bulk of the membrane is largely dependent on the thickness of the membrane. For ultrathin membranes, typically in the range of 10 µm or less, a support structure is required upon which the membrane can be deposited. In the case of ultrathin membranes care must be taken on selecting a support structure that is suitable. For thicker, free standing membranes a wider range of construction methods are available.

When designing ultrathin membranes one of the key aspects to consider is the support structure. Care must be taken to select a suitable structure, one that provides enough mechanical strength at the temperature of operation, one that does not have an active effect on altering the separation process and one that has a reasonable porosity so that hydrogen diffusion is only minimally impacted. This final part is of much interest to many researchers (Caravella, Barbieri and Drioli, 2008)(Nayebossadri *et al.*, 2016), as any form of obstruction to the surface of the membrane can potentially result in lower flux rates; either through changing flow patterns, restricting the escape of non-selected gas molecules, or through restriction of the surface area of the membrane.

Beyond this, the material of the support structure must be considered. Typically, the materials chosen exhibit good mechanical strength, good thermal stability and would ideally have minimal interaction with hydrogen to prevent embrittlement of the material. Favoured materials include stainless steel (Nayebossadri *et al.*, 2016)(Gade *et al.*, 2009)(Tarditi, Braun and Cornaglia, 2011), alumina (Al_2O_3) and other ceramics (Holladay *et al.*, 2009)(Lu *et al.*, 2007)(Amanipour *et al.*, 2012)(Nwogu, Anyanwu and Gobina, 2016) and glass (Uemiya *et al.*, 1991)(Lu *et al.*, 2007). Various designs have been implemented; both tubes and flat discs or plates have been used in various tests, as detailed in the sources above.

Application of the membrane to the support can be done using a number of techniques. Electroless plating is relatively common (Hatlevik *et al.*, 2010)(Lewis *et al.*, 2013) give details of processes. Hatlevik et al describes a process in which the support is seeded with palladium acetate in chloroform, followed by a calcination and reduction in a hydrazine solution. The membrane is then placed in a palladium electroless plating solution, where care must be taken to select a solvent that will not deposit carbon in the membrane bulk.

Electroless plating is conducted at moderate temperatures (50 °C) with a palladium deposition rate of 0.05 µm min^{-1} reported (Hatlevik *et al.*, 2010)(Lewis *et al.*, 2013). It is also shown in the same paper the same technique can be used for other metals (in this case gold, platinum and silver); or for the production of alloys where a binary species plating mixture is used. The related technology of

electroplating (where an electric current is applied to the plating bath) has also been used for membrane construction (Phair and Donelson, 2006).

Sol-gel processes have also been used, although these are typically found in the construction of ceramic membranes as detailed in (Nwogu, Anyanwu and Gobina, 2016), with wider use suggested by (Phair and Donelson, 2006).

Physical vapour deposition (PVD) is also widely used for the production of thin films and has thus been of great interest for the production of thin membranes. The technology is diverse, with methodologies such as electron beam evaporation and cathodic arc evaporation used (Lewis *et al.*, 2014)(Phair and Donelson, 2006)(Lu *et al.*, 2007)(Ockwig and Nenoff, 2007)(Yang *et al.*, 2015). This work utilised electron beam evaporation for deposition of silver. The basic principle is somewhat similar in most technologies, with the idea of turning the material to be coated into a vapour usually through the use of heating or sputtering in a low pressure (high vacuum) environment. Whilst the process is very energy intensive, it does allow for the deposition of layers of material in a uniform manner. Chemical vapour deposition (CVD) has also been used to create thin membranes layered onto the substrate, as referred to by (Amanipour *et al.*, 2012)(Lu *et al.*, 2007)(Adhikari and Fernando, 2006)(Gabitto and Tsouris, 2008).

Free-standing membranes have the advantage of not requiring a support layer, obviously as these membranes are thicker they do result in lower permeate fluxes in comparison to the equivalent ultrathin membranes. Construction methods vary but rolling techniques appear to be among the most popular.

Cold rolling is a popular “conventional” technique; (Kozhakhmetov *et al.*, 2015)(Dolan, 2010)(Tosti, Bettinali and Violante, 2000)(Burkhanov *et al.*, 2011)(Lewis *et al.*, 2013) all provide details of various rolling techniques. Typically ingots or lumps of the metal are rolled and annealed in multiple steps, intermediate annealing is required as many metals, including palladium, undergo work hardening when they are rolled. Annealing is typically conducted at very high temperatures for a few hours and thus can be rather energy intensive but the methodology is relatively simple and low tech in comparison to some alternatives. A hot rolling technique is mentioned in (Dolan, 2010), where the only real significant change is that the roller used is at an elevated temperature.

Alongside cold rolling, melt spinning has been used to produce membranes, where metal is heated and then cooled on a rotating wheel (roller). A rapid quenching roller technique is detailed in (Hara *et al.*, 2003), where an amorphous Zr-Ni-Hf was constructed by arc melting the three components in an argon atmosphere before crushing the pieces into sizes of around a few millimetres. The pieces were

then quenched before being melted via high frequency induction and sprayed onto a cooling rotating copper roller. The resultant membranes were 30-40 µm thick and amorphous in structure. Obviously this is useful if amorphous alloys are wanted, but (Dolan, 2010) states that other benefits exist even for crystalline membranes. The major advantages Dolan states is that the membranes are typically produced in a shape that is "ready for use" (a ribbon of variable width and variable thickness typically in the 40 – 100 µm range) and that the process is somewhat easy to scale, as the roller can be left running to produce a ribbon of any required length and width. The need to melt the metals twice in the method of Hara et al is however somewhat concerning, as this is likely to be rather energy intensive.

(Dolan, 2010) suggests that the most likely route to large scale fabrication of membranes is through the use of cold rolling, Dolan details a process of arc melting ingots of alloy, hot rolling, annealing and then finally cold rolling to a thickness of 40 µm. This is reasonable, as it is arguably the simplest method available for the production of the membrane bulk. It would also suggest that even though ultrathin membranes offer increased performance their increased fragility and pre-requisite support layer negates this, or at least in terms of current technology. One other possible reason for the use of thick membranes is their increased recyclability; where in instances it may be possible to melt the bulk material and re-use it for future membrane use.

Preparation of the surface

If it is deemed that a membrane needs a surface coating for any reason, a number of techniques can be used to apply this. Generally, the techniques used for surface coatings are similar to those listed above; with PVD and CVD amongst the most popular. These methods have been introduced above and will not be discussed again, however it is worthwhile to note that alternative coating methods have been explored such as the one detailed below. PVD deposited palladium has been used to coat group V membranes in previous studies (Dolan *et al.*, 2013)(Zhang *et al.*, 2002).

Electroplating has been attempted, with the drawback being that it is difficult to obtain a homogeneous palladium coating (Ozaki *et al.*, 2003b), the same paper found more success with the use of an electroless plating technique. The electroless plating method used involved the cleaning of the membrane surface through mechanical and then chemical polishing of the surface (using a hydrofluoric acid, nitric acid and lactic acid solution). Sensitising of the membrane was done with a tin chloride solution before plating in a palladium chloride solution where ethylene-diamine was used as a complexing agent, hydrazine ($N_2H_4.H_2O$) was used as a reducing agent, with the pH adjusted using hydrochloric acid and sodium hydroxide. This coating method is relatively complex and relies on

numerous chemicals that are relatively hazardous, this may make it rather difficult to complete on a larger than bench scale. The end result appears to be a stable and uniform palladium coating on the vanadium based membranes; however, it must be noted that other groups have also found success with electroplating, (Viano *et al.*, 2015) detail coating processes for palladium and nickel onto vanadium.

This would suggest that, similar to the production of the bulk membrane, some versatility is available in the methods of producing the surface layer. PVD is a reliable coating method but are much more energy intensive than electroplating and electroless plating however it offers the advantage of increased versatility without the need for the use of a wide range of chemicals and solvents and very high-purity and well adhered thin films.

2.5 A Summary of the Review and a Statement of Research Tasks

2.5.1 A Summary of the Review

This review has set out to make clear the need for an alternative energy vector due to the damaging effects of fossil fuel combustion on both human health and the environment; a suggestion for increased use of hydrogen is made. Hydrogen has numerous advantages, in being a clean combusting, easy to transport fuel that is versatile enough to be used in both fuel cells and conventional burners and does not produce sub-micron particulate matter which is generally deemed as unfilterable. Many forms of hydrogen production are available and are in varying states of technological readiness, it is generally accepted that the most "industry ready" technologies are steam methane reformation and gasification of coal and/or biomass. These processes typically produce a mixture of gases referred to as syngas, consisting primarily of carbon dioxide, hydrogen, carbon monoxide (with small amounts of methane and other gases).

Hydrogen needs to be separated from this mixture; a range of technologies are available for this, however current market ready technologies have drawbacks: they are expensive to operate, energy intensive or are not capable of producing hydrogen at the relevant purity for use in hydrogen fuel cells. This work suggests the use of membranes for hydrogen separation, in particular the use of metallic membranes. The advantages offered by metallic membranes are mainly determined by their ability to produce very high purity hydrogen with the use of a passive technology, allowing for significantly lower operating costs. However, current membrane technology is not ready for wide scale use; the US DoE have provided numerous targets for the pathway of development towards feasible membrane usage, yet designs that meet these targets are still limited in number.

Traditional palladium based membranes are capable of producing the required flux and purity, with alloys such as Pd-Ag, Pd-Y and Pd-Cu delivering excellent flux values. However, the dependence on palladium is not ideal due to its high cost (pushing the cost per m^2 above the DoE target), and its designation as a rare and strategic metal limit their wide-scale use. Alternatives based on group V metals are discussed in detail in this review, where they have been shown to produce permeated hydrogen flux rates above that of palladium based membranes. The current limitation to the use of group V membranes is the need for a catalytic surface coating that also protects against membrane oxidation and has a low susceptibility to carbon or sulphur "poisoning" of hydrogen dissociation active sites. The group V metals produce poor hydrogen dissociation when clean, and when surface oxides are formed this is only made worse. Currently most group V membranes are coated with palladium for test purposes but alternatives to this coating are being investigated.

As part of this work it is suggested to investigate the use of silver enriched with both surface and sub-surface oxygen, which is known to reduce the activation energy for hydrogen dissociation on silver. Silver has an added advantage of being more resistant to carbon monoxide and sulphur (H_2S) than nickel and is significantly cheaper and more abundant than palladium.

An alternative approach could be to limit the use of palladium in the catalytic coat by using a palladium alloy, with the obvious choices being Pd-Ag, Pd-Y or Pd-Cu. However, it remains to be seen if a large enough reduction in palladium use can be made to make the coating economically feasible.

2.5.2 An Overview of Tasks Completed as Part of This Project

At this point it is considered worthwhile to expand on the objectives laid out in the introduction chapter of this thesis. This section has been included to give an introduction into the research tasks undertaken as part of this Ph.D. programme:

1. **Review the literature to identify a suitable model for predicting membrane behaviour, in particular the membrane permeated flux.** Identifying a suitable model allows for greater study and understanding of the experimental results gathered based on the underpinning science, whilst allowing for the investigation of a wider range of process conditions and membrane designs.
2. **Design and construct a number of membranes suitable for testing.** After identifying suitable membranes through the use of literature studies and computational modelling, it is necessary to conduct experimental tests to validate the data collected and generated. A rigorous set of experiments was undertaken to investigate various membranes bulk and surface properties under a range of process conditions; with a focussed interest in the permeate flux and purity. Tests were designed to allow for the comparison of palladium with oxygen activated silver-coated group V metals and silver-palladium coated group V metals and alloys.
3. **Design and construct an experimental set up suitable for testing metallic membranes.** Alongside the design of the membranes it was necessary to design an experimental process to allow for testing under conditions that simulated (as far as reasonable) real process conditions. A focus was put on the key parameters of feasibility and affordability on an industrial scale.

2.6 Chapter Two Reference List

Abu El Hawa, H. W., Paglieri, S. N., Morris, C. C., Harale, A. and Douglas Way, J. (2015) 'Application of a Pd-Ru composite membrane to hydrogen production in a high temperature membrane reactor', *Separation and Purification Technology*. Elsevier B.V., 147, pp. 388–397. doi: 10.1016/j.seppur.2015.02.005.

Adhikari, S. and Fernando, S. (2006) 'Hydrogen Membrane Separation Techniques', *Industrial & Engineering Chemistry Research*, 45(3), pp. 875–881. doi: 10.1021/ie050644l.

Air Liquide (2008) *Hydrogen Key Dates*. Available at: http://www.uk.airliquide.com/en/solution-for-industry/innovative-hydrogen-solutions-for-clean-energy/hydrogen-key-dates.html (Accessed: 3 June 2016).

Air Liquide (2010) *MEDAL Membrane Separation*. Available at: http://www.medal.airliquide.com/en/hydrogen-membrane-gas-separation/hydrogen-membrane-technology.html (Accessed: 4 July 2016).

Air Liquide (2015) *Air Liquide starts up a large hydrogen production unit in Germany*, *AirLiquide.com*. Available at: https://www.airliquide.com/media/air-liquide-starts-large-hydrogen-production-unit-germany (Accessed: 3 June 2016).

Air Products (2012) *Air Products and Technip Hydrogen Alliance Working together to enhance refining industry productivity for over 20 years . Then & Now.* Available at: http://www.h2alliance.com/pdf/Final _H2Alliance_DS_1-22-13.pdf.

Air Products (2015a) *Hydrogen Pressure Swing Adsorption (PSA) Services and Solutions*. Available at: http://www.airproducts.com/~/media/final39128PSAServicesSolutionsDSHRpdf.pdf.

Air Products (2015b) *PRISM ® Membrane Systems For Oil Refinery Applications*. Available at: http://www.airproducts.com/~/media/Files/PDF/products/supply-options/prism-membrane/en-prism-process-gas-brochure.pdf?la=en.

Air Products (2016) *Air Products Holds Groundbreaking for World-Class SMR at Covestro in Texas*, *Airproducts.co.uk*. Available at: http://www.airproducts.co.uk/Company/news-center/2016/02/0225-air-products-holds-groundbreaking-for-world-class-smr-at-covestro-in-texas.aspx (Accessed: 3 June 2016).

Al-Mufachi, N. A., Rees, N. V. and Steinberger-Wilkens, R. (2015) 'Hydrogen selective membranes: A review of palladium-based dense metal membranes', *Renewable and Sustainable Energy Reviews*. Elsevier, 47, pp. 540–551. doi: 10.1016/j.rser.2015.03.026.

Albers, P., Pietsch, J. and Parker, S. F. (2001) 'Poisoning and deactivation of palladium catalysts', *Journal of Molecular Catalysis A: Chemical*, 173(1–2), pp. 275–286. doi: 10.1016/S1381-1169(01)00154-6.

Amanipour, M., Safekordi, A., Ganji Babakhani, E., Zamaniyan, A. and Heidari, M. (2012) 'Effect of synthesis conditions on performance of a hydrogen selective nano-composite ceramic membrane', *International Journal of Hydrogen Energy*. Elsevier Ltd, 37(20), pp. 15359–15366. doi: 10.1016/j.ijhydene.2012.07.085.

Andrew, P. L. and Haasz, a. a. (1992) 'Models for hydrogen permeation in metals', *Journal of Applied Physics*, 72(7), p. 2749. doi: 10.1063/1.351526.

Antonov, V. E., I. T. Belash, I. T., Malyshev, V. Y. and Ponyatovsky, E. G. (1984) 'Volume 28 Issue 4 The Solubility of Hydrogen in the Platinum Metals under High Pressure | Platinum Metals Review', *Platinum Metals Review*, (4), p. 158. doi: 10.1016/0360-3199(86)90083-2.

APMEX (2016) *Palladium Price Chart*. Available at: http://www.apmex.com/spotprices/palladium-price.

Araki, H., Nakamura, M., Harada, S., Obata, T., Mikhin, N., Syvokon, V. and Kubota, M. (2004) 'Phase diagram of hydrogen in palladium', *Journal of low …*, 134(June), pp. 363–421. Available at: http://linkinghub.elsevier.com/retrieve/pii/S0921452602018859%5Cnhttp://link.springer.com/article/10.1023/B:JOLT.0000016734.40467.28.

Baker, R. W. (2004) *Membrane Technology and Applications*. Chichester, UK: John Wiley & Sons, Ltd. doi: 10.1002/9781118359686.

Balachandran, U., Lee, T. H., Park, C. Y., Emerson, J. E., Picciolo, J. J. and Dorris, S. E. (2014) 'Dense cermet membranes for hydrogen separation', *Separation and Purification Technology*. Elsevier B.V., 121, pp. 54–59. doi: 10.1016/j.seppur.2013.10.001.

Bartels, J. R., Pate, M. B. and Olson, N. K. (2010) 'An economic survey of hydrogen production from conventional and alternative energy sources', *International Journal of Hydrogen Energy*. Elsevier Ltd, 35(16), pp. 8371–8384. doi: 10.1016/j.ijhydene.2010.04.035.

Bernardo, P., Drioli, E. and Golemme, G. (2009) 'Membrane Gas Separation: A Review/State of the

Art', *Industrial & Engineering Chemistry Research*, 48(10), pp. 4638–4663. doi: 10.1021/ie8019032.

BOC (2007) *ECOVAR – onsite gas generation solutions*. Available at: https://www.boconline.co.uk/internet.lg.lg.gbr/en/images/ecovar-onsite-gas-generation-solutions410_39656.pdf.

BOC (2013) *Safety Data Sheet: Natural Gas*, *BOC Safety Sheets*. Available at: https://www.boconline.co.uk/internet.lg.lg.gbr/en/images/natural_gas410_55840.pdf.

Bolez, C. and Pryor, J. (1967) 'United States Patent 3,359,744', *US Patent Office*. United States. Available at: https://docs.google.com/viewer?url=patentimages.storage.googleapis.com/pdfs/US3359744.pdf.

Bron, M., Teschner, D., Wild, U., Steinhauer, B., Knop-Gericke, A., Volckmar, C., Wootsch, A., Schlögl, R. and Claus, P. (2008) 'Oxygen-induced activation of silica supported silver in acrolein hydrogenation', *Applied Catalysis A: General*, 341(1–2), pp. 127–132. doi: 10.1016/j.apcata.2008.02.033.

Burkhanov, G. S., Gorina, N. B., Kolchugina, N. B., Roshan, N. R., Slovetsky, D. I. and Chistov, E. M. (2011) 'Palladium-based alloy membranes for separation of high purity hydrogen from hydrogen-containing gas mixtures', *Platinum Metals Review*, 55(1), pp. 3–12. doi: 10.1595/147106711X540346.

Buxbaum, R. and Marker, T. (1993) 'Hydrogen transport through non-porous membranes of palladium-coated niobium, tantalum and vanadium', *Journal of Membrane Science*, 85, pp. 29–38. Available at: http://www.sciencedirect.com/science/article/pii/037673889385004G (Accessed: 28 March 2014).

Cantelli, R., Mazzolai, F. M. and Nuovo, M. (1969) 'Internal Friction due to Long-Range Diffusion of Hydrogen in Niobium (Gorsky Effect)', *physica status solidi (b)*, 34(2), pp. 597–600. doi: 10.1002/pssb.19690340221.

Carapellucci, R. and Milazzo, A. (2003) 'Membrane systems for CO 2 capture and their integration with gas turbine plants', 217, pp. 505–517. doi: 10.1243/095765003322407557.

Caravella, A., Barbieri, G. and Drioli, E. (2008) 'Modelling and simulation of hydrogen permeation through supported Pd-alloy membranes with a multicomponent approach', *Chemical Engineering Science*, 63(8), pp. 2149–2160. doi: 10.1016/j.ces.2008.01.009.

Chang, H. . and Wert, C. . (1973) 'The solubility and trapping of hydrogen in vanadium', *Acta*

Metallurgica, 21. Available at: http://www.sciencedirect.com/science/article/pii/0001616073901648 (Accessed: 9 September 2014).

Cheng, Y. S., Pena, M. and Fierro, J. L. (2002) 'Performance of alumina, zeolite, palladium, Pd–Ag alloy membranes for hydrogen separation from Towngas mixture', *Journal of membrane …*, 204(1–2), pp. 329–340. doi: 10.1016/S0376-7388(02)00059-5.

CO2 Capture Project (2008) 'Three basic methods to separate gases', *CO2 Capture Project*, pp. 1–2. Available at: www.co2captureproject.com.

Decaux, C., Ngameni, R., Ranjbari, A., Grigoriev, S. A. and Millet, P. (2013) 'Dynamics of hydrogen permeation across metallic membranes', *International Journal of Hydrogen Energy*. Elsevier Ltd, 38(20), pp. 8584–8589. doi: 10.1016/j.ijhydene.2012.11.021.

Dolan, M. D. (2010) 'Non-Pd BCC alloy membranes for industrial hydrogen separation', *Journal of Membrane Science*. Elsevier B.V., 362(1–2), pp. 12–28. doi: 10.1016/j.memsci.2010.06.068.

Dolan, M. D., Kellam, M. E., McLennan, K. G., Liang, D. and Song, G. (2013) 'Hydrogen transport properties of several vanadium-based binary alloys', *International Journal of Hydrogen Energy*. Elsevier Ltd, 38(23), pp. 9794–9799. doi: 10.1016/j.ijhydene.2013.05.073.

Dolan, M. D., Kochanek, M. A., Munnings, C. N., McLennan, K. G. and Viano, D. M. (2015) 'Hydride phase equilibria in V-Ti-Ni alloy membranes', *Journal of Alloys and Compounds*. Elsevier B.V., 622, pp. 276–281. doi: 10.1016/j.jallcom.2014.10.081.

Doyle, B. M. L. and Harris, I. R. (1988) 'Palladium-Rare Earth Alloys', (3), pp. 130–140.

EERC (2010) 'Hydrogen separation membranes', *Advanced Membrane Technology and Applications*. EERC. Available at: http://www.undeerc.org/ncht/pdf/eercmh36028.pdf (Accessed: 20 November 2013).

Eltron R&D (2008) *Tech Brief A New Technology of Integrated Water-Gas Shift / Hydrogen Transport Membrane Eltron Research & Development*. Available at: http://www.eltronresearch.com/docs/Integrated_Water_Gas_Shift_Hydrogen_Transport_Membrane.pdf.

Emami Taba, L., Irfan, M. F., Wan Daud, W. A. M. and Chakrabarti, M. H. (2012) 'The effect of temperature on various parameters in coal, biomass and CO-gasification: A review', *Renewable and Sustainable Energy Reviews*. Elsevier, 16(8), pp. 5584–5596. doi: 10.1016/j.rser.2012.06.015.

Evard, E. A., Kurdumov, A. A., Berseneva, F. N. and Gabis, I. E. (2001) 'Permeation of hydrogen through amorphous ferrum membrane', *International Journal of Hydrogen Energy*, 26(5), pp. 457–460. doi: 10.1016/S0360-3199(00)00078-1.

Evenson, C. and Jack, D. (2009) 'II . D . 2 Scale Up of Hydrogen Transport Membranes for IGCC and FutureGen Plants', (L), pp. 66–68. Available at: https://www.hydrogen.energy.gov/pdfs/progress09/ii_d_2_jack.pdf.

Evenson, C. and Waters, D. (2011) *High Temperature, Hydrogen Separation: A Carbon Capture Process Technology*. Available at: http://www.eltronresearch.com/docs/Eltron_Membrane_Program_Overview_Feb_2011.pdf.

Evtimova, J., Drioli, E. and De Luca, G. (2016) 'A density functional theory study of hydrogen occupation in VNiTi alloys used for dense metal membranes', *Journal of Alloys and Compounds*. Elsevier B.V, 665, pp. 225–230. doi: 10.1016/j.jallcom.2016.01.037.

Farid, A., Gallarda, J., Mineur, B., Bradley, S., Ott, W. and Ibler, M. (2009) *Best available techniques for hydrogen production by steam methane reforming*, *IGC document*. Available at: http://scholar.google.com/scholar?hl=en&btnG=Search&q=intitle:BEST+AVAILABLE+TECHNIQUES+FOR+HYDROGEN+PRODUCTION+BY+STEAM+METHANE+REFORMING#0.

Ferrin, P., Kandoi, S., Nilekar, A. U. and Mavrikakis, M. (2012) 'Hydrogen adsorption, absorption and diffusion on and in transition metal surfaces: A DFT study', *Surface Science*. Elsevier B.V., 606(7–8), pp. 679–689. doi: 10.1016/j.susc.2011.12.017.

Fort, D., Farr, J. P. G. and Harris, I. R. (1975) 'A comparison of palladium-silver and palladium-yttrium alloys as hydrogen separation membranes', *Journal of The Less-Common Metals*, 39(2), pp. 293–308. doi: 10.1016/0022-5088(75)90204-0.

Fowler, R. H. and Smithells, C. J. (1937) 'A Theoretical Formula for the Solubility of Hydrogen in Metals', *Proceedings of the Royal Society A: Mathematical, Physical and Engineering Sciences*, 160(900), pp. 37–47. doi: 10.1098/rspa.1937.0093.

Fukada, S., Shimoshiraishi, R. and Katayama, K. (2014) 'Enhancement of hydrogen production rates in reformation process of methane using permeable Ni tube and chemical heat pump', *International Journal of Hydrogen Energy*. Elsevier Ltd, 39(35), pp. 20632–20638. doi: 10.1016/j.ijhydene.2014.07.008.

Gabitto, J. and Tsouris, C. (2008) 'Hydrogen transport in composite inorganic membranes', *Journal of*

Membrane Science, 312(1–2), pp. 132–142. doi: 10.1016/j.memsci.2007.12.061.

Gade, S. K., Keeling, M. K., Davidson, A. P., Hatlevik, O. and Way, J. D. (2009) 'Palladium-ruthenium membranes for hydrogen separation fabricated by electroless co-deposition', *International Journal of Hydrogen Energy*. Elsevier Ltd, 34(15), pp. 6484–6491. doi: 10.1016/j.ijhydene.2009.06.037.

German, E. D., Abir, H. and Sheintuch, M. (2013) 'A tunnel model for activated hydrogen dissociation on metal surfaces', *Journal of Physical Chemistry C*, 117(15), pp. 7475–7486. doi: 10.1021/jp309509c.

Gomez, T., Florez, E., Rodriguez, J. A. and Illas, F. (2011) 'Reactivity of transition metals (Pd, Pt, Cu, Ag, Au) toward molecular hydrogen dissociation: Extended surfaces versus particles supported on TiC(001) or small is not always better and large is not always bad', *Journal of Physical Chemistry C*, 115(23), pp. 11666–11672. doi: 10.1021/jp2024445.

Grashoff, G. J., Pilkington, C. E. and Corti, C. W. (1983) 'Purification of Hydrogen.', *Platinum Metals Review*, 27(4), pp. 157–169.

Griffiths, R., Pryde, J. A. and Righini-Brand, A. (1972) 'Phase diagram and thermodynamic data for the hydrogen/vanadium system', *Journal of the Chemical Society, Faraday Transactions 1: Physical Chemistry in Condensed Phases*, 68(1), p. 2344. doi: 10.1039/f19726802344.

Gross, A. (1998) 'Hydrogen dissociation on metal surfaces - a model system for reactions on surfaces', 635, p. 10. doi: 10.1007/s003390050834.

Hagen, D. I. and Donaldson, E. E. (1974) 'Interaction of hydrogen with a (100) niobium surface', *Surface Science*, 45(1), pp. 61–76. doi: 10.1016/0039-6028(74)90155-1.

Hara, S., Hatakeyama, N., Itoh, N., Kimura, H. M. and Inoue, A. (2003) 'Hydrogen permeation through amorphous-Zr36-xHfxNi64-alloy membranes', *Journal of Membrane Science*, 211(1), pp. 149–156. doi: 10.1016/S0376-7388(02)00416-7.

Hara, S., Sakaki, K., Itoh, N., Kimura, H.-M., Asami, K. and Inoue, a. (2000) 'An amorphous alloy membrane without noble metals for gaseous hydrogen separation', *Journal of Membrane Science*, 164(1–2), pp. 289–294. doi: 10.1016/S0376-7388(99)00192-1.

Hatlevik, Ø., Gade, S. K., Keeling, M. K., Thoen, P. M., Davidson, a. P. and Way, J. D. (2010) 'Palladium and palladium alloy membranes for hydrogen separation and production: History, fabrication strategies, and current performance', *Separation and Purification Technology*, 73(1), pp. 59–64. doi: 10.1016/j.seppur.2009.10.020.

Heinze, S., Vuillemin, B., Colson, J. ., Giroux, P. and Leterq, D. (1999) 'Relation between grain size and hydrogen diffusion coefficient in an industrial Pd–23% Ag alloy', *Solid State Ionics*, 122(1–4), pp. 51–57. doi: 10.1016/S0167-2738(99)00058-2.

Higman, C. and Van Der Burgt, M. (2008) 'Gasification Processes', in, pp. 91–191. doi: 10.1016/B978-0-7506-8528-3.00005-5.

Hinchliffe, A. B. and Porter, K. E. (2000) 'A Comparison of Membrane Separation and Distillation', *Chemical Engineering Research and Design*, 78(2), pp. 255–268. doi: 10.1205/026387600527121.

Holladay, J. D., Hu, J., King, D. L. and Wang, Y. (2009) 'An overview of hydrogen production technologies', *Catalysis Today*, 139(4), pp. 244–260. doi: 10.1016/j.cattod.2008.08.039.

van Holt, D., Forster, E., Ivanova, M. E., Meulenberg, W. a., Müller, M., Baumann, S. and Vaßen, R. (2014) 'Ceramic materials for H2 transport membranes applicable for gas separation under coal-gasification-related conditions', *Journal of the European Ceramic Society*. Elsevier Ltd, pp. 1–9. doi: 10.1016/j.jeurceramsoc.2014.03.001.

Honeywell UOP (2016) *50 Years of PSA Technology for H 2 Purification*. Available at: http://www.uop.com/?document=psa-50-paper&download=1.

Hosseini, S. S., Peng, N. and Chung, T. S. (2010) 'Gas separation membranes developed through integration of polymer blending and dual-layer hollow fiber spinning process for hydrogen and natural gas enrichments', *Journal of Membrane Science*, 349(1–2), pp. 156–166. doi: 10.1016/j.memsci.2009.11.043.

Huang, C. and T-Raissi, A. (2007a) 'Analyses of one-step liquid hydrogen production from methane and landfill gas', *Journal of Power Sources*, 173(2), pp. 950–958. doi: 10.1016/j.jpowsour.2007.08.018.

Huang, C. and T-Raissi, A. (2007b) 'Thermodynamic analyses of hydrogen production from sub-quality natural gas. Part II: Steam reforming and autothermal steam reforming', *Journal of Power Sources*, 163(2), pp. 637–644. doi: 10.1016/j.jpowsour.2006.02.082.

International Energy Agency (2006) *Hydrogen Production and Storage. R&D Priorities and Gaps*, *Hydrogen Implementing Agreement*. doi: 10.1016/0360-3199(88)90106-1.

Iwaoka, H. and Horita, Z. (2013) 'Hydrogen behavior in ultrafine-grained palladium processed by high-pressure torsion', *International Journal of Hydrogen Energy*. Elsevier Ltd, 38(34), pp. 14879–14886. doi: 10.1016/j.ijhydene.2013.08.098.

Jeon, S. Il and Park, J. H. (2013) 'Hydrogen permeation properties of Pd-coated V89.8Cr 10Y0.2 alloy membrane using WGS reaction gases', *International Journal of Hydrogen Energy*. Elsevier Ltd, 38(14), pp. 6085–6091. doi: 10.1016/j.ijhydene.2013.01.172.

Johnson, W. L. (2002) 'Bulk amorphous metal—An emerging engineering material', *JOM*, 54(3), pp. 40–43. doi: 10.1007/BF02822619.

Jones, J. M., Dupont, V. A., Brydson, R., Fullerton, D. J., Nasri, N. S., Ross, A. B. and Westwood, A. V. K. (2003) 'Sulphur poisoning and regeneration of precious metal catalysed methane combustion', *Catalysis Today*, 81(4), pp. 589–601. doi: 10.1016/S0920-5861(03)00157-3.

Joseck, F., Wang, M. and Wu, Y. (2008) 'Potential energy and greenhouse gas emission effects of hydrogen production from coke oven gas in U.S. steel mills', *International Journal of Hydrogen Energy*, 33(4), pp. 1445–1454. doi: 10.1016/j.ijhydene.2007.10.022.

Jüttke, Y., Richter, H., Voigt, I., Prasad, R. M. and Mahdi, S. (2013) 'Polymer Derived Ceramic Membranes for Gas Separation', 32, pp. 1891–1896. Available at: http://www.aidic.it/cet/13/32/316.pdf.

Keizer, K., Vuren, R. J. V. A. N. and Burggraaf, A. J. (1988) 'GAS SEPARATION MECHANISMS IN MICROPOROUS MODIFIED AL2O3 MEMBRANES', 39, pp. 285–300.

Kim, J.-H., Kang, Y.-M., Kim, B.-G., Lee, S.-H. and Hwang, K.-T. (2011) 'Preparation of dense composite membrane with Ba-cerate conducting oxide and rapidly solidified Zr-based alloy', *International Journal of Hydrogen Energy*. Elsevier Ltd, 36(16), pp. 10129–10135. doi: 10.1016/j.ijhydene.2011.02.145.

Kim, K.-H., Shim, J.-H. and Lee, B.-J. (2012) 'Effect of alloying elements (Al, Co, Fe, Ni) on the solubility of hydrogen in vanadium: A thermodynamic calculation', *International Journal of Hydrogen Energy*. Elsevier Ltd, 37(9), pp. 7836–7847. doi: 10.1016/j.ijhydene.2012.01.117.

Kishida, K., Yamaguchi, Y., Tanaka, K., Inui, H., Tokui, S., Ishikawa, K. and Aoki, K. (2008) 'Microstructures and hydrogen permeability of directionally solidified Nb-Ni-Ti alloys with the Nb-NiTi eutectic microstructure', *Intermetallics*, 16(1), pp. 88–95. doi: 10.1016/j.intermet.2007.08.001.

Knapton, A. (1977) 'Palladium alloys for hydrogen diffusion membranes', *Platinum Metals Review Rev*, (6), pp. 44–50. Available at: http://www.platinummetalsreview.com/pdf/pmr-v21-i2-044-050.pdf (Accessed: 5 February 2014).

Kostroski, K. P. and Wankat, P. C. (2009) 'Separation of concentrated binary gases by hybrid

pressure-swing adsorption/ simulated-moving bed processes', *Industrial and Engineering Chemistry Research*, 48(9), pp. 4445–4465. doi: 10.1021/ie801371t.

Kozhakhmetov, S., Sidorov, N., Piven, V., Sipatov, I., Gabis, I. and Arinov, B. (2015) 'Alloys based on Group 5 metals for hydrogen purification membranes', *Journal of Alloys and Compounds*. Elsevier B.V., 23, pp. 1–5. doi: 10.1016/j.jallcom.2015.01.242.

Kumar, A., Jones, D. D. and Hanna, M. A. (2009) 'Thermochemical biomass gasification: A review of the current status of the technology', *Energies*, 2(3), pp. 556–581. doi: 10.3390/en20300556.

Kurdyumov, A. A., Lyasnikov, V. N. and Shvachkina, T. A. (1983) 'Hydrogen permeability of plasma titanium coatings', *Soviet Materials Science*. Edited by Intergovernmental Panel on Climate Change. Cambridge: Cambridge University Press, 19(3), pp. 192–196. doi: 10.1007/BF00723381.

Lai, T., Yin, H. and Laura Lind, M. (2015) 'The hydrogen permeability of Cu-Zr binary amorphous metallic membranes and the importance of thermal stability', *Journal of Membrane Science*. Elsevier, 489, pp. 264–269. doi: 10.1016/j.memsci.2015.03.098.

Latge, A., Ribeiro-Teixeira, R. . and Iglesias, J. . (1984) 'Binding energy of a hydrogen impurity in an f.c.c. lattice', *Solid State Communications*, 52(2), pp. 87–91. doi: 10.1016/0038-1098(84)90602-1.

Lee, H. M. (1979) 'Electron density and hydrogen solubility in transition metals', *Journal of Materials Science*, 14(4), pp. 1002–1006. doi: 10.1007/BF00550737.

Leimert, J. M. and Karl, J. (2016) 'Nickel membranes for in-situ hydrogen separation in high-temperature fluidized bed gasification processes', *International Journal of Hydrogen Energy*, 1, pp. 1–12. doi: 10.1016/j.ijhydene.2016.04.073.

Lemier, C. and Weissmüller, J. (2007) 'Grain boundary segregation, stress and stretch: Effects on hydrogen absorption in nanocrystalline palladium', *Acta Materialia*, 55(4), pp. 1241–1254. doi: 10.1016/j.actamat.2006.09.030.

Lewis, A. E., Zhao, H., Syed, H., Wolden, C. A. and Way, J. D. (2014) 'PdAu and PdAuAg composite membranes for hydrogen separation from synthetic water-gas shift streams containing hydrogen sulfide', *Journal of Membrane Science*. Elsevier, 465, pp. 167–176. doi: 10.1016/j.memsci.2014.04.022.

Lewis, a. E., Kershner, D. C., Paglieri, S. N., Slepicka, M. J. and Way, J. D. (2013) 'Pd–Pt/YSZ composite membranes for hydrogen separation from synthetic water–gas shift streams', *Journal of Membrane Science*, 437, pp. 257–264. doi: 10.1016/j.memsci.2013.02.056.

Lewis, F. a. (1982) 'The Palladium-Hydrogen System A SURVEY OF HYDRIDE FORMATION AND THE EFFECTS', *Platinum Metals Review*, 26(1), pp. 20–27.

Lewis, F. a. (1990) 'Solubility of hydrogen in metals', *Pure and Applied Chemistry*, 62(11), pp. 2091–2096. doi: 10.1351/pac199062112091.

Linde Engineering (2014) *Cryogenic air separation .* Available at: http://www.linde-engineering.com/internet.global.lindeengineering.global/en/images/AS.B1EN 1113 - %26AA_History_.layout19_4353.pdf.

Linde Group (2013) 'Hydrogen Recovery by Pressure Swing Adsorption'. Available at: http://www.linde-engineering.com/internet.global.lindeengineering.global/en/images/HA_H_1_1_e_12_150dpi19_6130.pdf.

Liu, K., Song, C. and Subramani, V. (2010) *Hydrogen and syngas production and purification technologies*. Available at: http://onlinelibrary.wiley.com/doi/10.1002/9780470561256.fmatter/summary (Accessed: 4 February 2014).

Lopes, F. V. S., Grande, C. a. and Rodrigues, A. E. (2011) 'Activated carbon for hydrogen purification by pressure swing adsorption: Multicomponent breakthrough curves and PSA performance', *Chemical Engineering Science*, 66(3), pp. 303–317. doi: 10.1016/j.ces.2010.10.034.

Lu, G. Q., Diniz da Costa, J. C., Duke, M., Giessler, S., Socolow, R., Williams, R. H. and Kreutz, T. (2007) 'Inorganic membranes for hydrogen production and purification: a critical review and perspective.', *Journal of colloid and interface science*, 314(2), pp. 589–603. doi: 10.1016/j.jcis.2007.05.067.

Ludwig, J., Vlachos, D. G., Van Duin, A. C. T. and Goddard, W. A. (2006) 'Dynamics of the dissociation of hydrogen on stepped platinum surfaces using the ReaxFF reactive force field', *Journal of Physical Chemistry B*, 110(9), pp. 4274–4282. doi: 10.1021/jp0561064.

Mallett, M. W. and Koehl, B. G. (1962) 'Thermodynamic Functions for the Tantalum-Hydrogen System', *Journal of The Electrochemical Society*, 109(7), p. 611. doi: 10.1149/1.2425507.

McCool, B. and Lin, Y. (2001) 'Nanostructured thin palladium-silver membranes: effects of grain size on gas permeation properties', *Journal of materials science*, 6, pp. 3221–3227. Available at: http://link.springer.com/article/10.1023/A:1017938403725 (Accessed: 3 February 2014).

McLeod, L. S. (2008) 'HYDROGEN PERMEATION THROUGH MICROFABRICATED PALLADIUM-SILVER

ALLOY MEMBRANES HYDROGEN PERMEATION THROUGH MICROFABRICATED PALLADIUM-SILVER ALLOY MEMBRANES', (December).

Melchor-Hernández, C., Gómez-Cortés, A. and Díaz, G. (2013) 'Hydrogen production by steam reforming of ethanol over nickel supported on La-modified alumina catalysts prepared by sol-gel', *Fuel*, 107, pp. 828–835. doi: 10.1016/j.fuel.2013.01.047.

Mohammad, A. B., Hwa Lim, K., Yudanov, I. V., Neyman, K. M. and R?sch, N. (2007) 'A computational study of H2 dissociation on silver surfaces: The effect of oxygen in the added row structure of Ag(110)', *Physical Chemistry Chemical Physics*, 9(10), p. 1247. doi: 10.1039/b616675j.

Mohammad, A. B., Yudanov, I. V., Lim, K. H., Neyman, K. M. and Rösch, N. (2008) 'Hydrogen activation on silver: A computational study on surface and subsurface oxygen species', *Journal of Physical Chemistry C*, 112(5), pp. 1628–1635. doi: 10.1021/jp0765190.

Munschau, M. . (2003) 'Hydrogen transport membranes'. Available at: https://www.google.com/patents/US6899744.

Nayebossadri, S., Fletcher, S., Speight, J. D. and Book, D. (2016) 'Hydrogen permeation through porous stainless steel for palladium–based composite porous membranes', *Journal of Membrane Science*. Elsevier, 515, pp. 22–28. doi: 10.1016/j.memsci.2016.05.036.

NETL (2003) *CAPITAL AND OPERATING COST OF HYDROGEN PRODUCTION FROM COAL GASIFICATION*. Available at: https://www.netl.doe.gov/File Library/Research/Coal/energy systems/gasification/pubs/HydrogenFromCoalGasificationFinalReport.pdf.

Nexant Inc. (2006) *Equipment Design and Cost Estimation for Small Modular Biomass Systems , Synthesis Gas Cleanup , and Oxygen Separation Equipment. Task 1: Cost Estimates of Small Modular Systems*, *Subcontract Report NREL/SR-510-39943*. Available at: http://www.nrel.gov/docs/fy06osti/39943.pdf.

Nishimura, C., Komaki, M. and Amano, M. (1991) 'Hydrogen Permeation Characteristics of Vanadium-Nickel Alloys', *Materials Transactions, JIM*, 32(5), pp. 501–507. doi: 10.2320/matertrans1989.32.501.

Nishimura, C., Komaki, M., Hwang, S. and Amano, M. (2002) 'V–Ni alloy membranes for hydrogen purification', *Journal of Alloys and Compounds*, 330–332, pp. 902–906. doi: 10.1016/S0925-8388(01)01648-6.

Norby, T. and Haugsrud, R. (2006) *Dense Ceramic Membranes for Hydrogen Separation*.

Nwogu, N. C., Anyanwu, E. E. and Gobina, E. (2016) 'An initial investigation of a nano-composite silica ceramic membrane for hydrogen gas separation and purification', *International Journal of Hydrogen Energy*. Elsevier Ltd, 41(19), pp. 8228–8235. doi: 10.1016/j.ijhydene.2015.11.162.

Nwogu, N. C., Kajama, M. and Gobina, E. (2015) 'A study of gas diffusion characteristics on a micro porous composite silica ceramic membrane', *Composite Structures*. Elsevier Ltd, 134, pp. 1044–1050. doi: 10.1016/j.compstruct.2015.07.121.

Oates, W. A. (1979) 'Solubility and Diffusion of Hydrogen in Solid Metals.', *Metals Forum*, 2(3), pp. 138–148. doi: 0.1238/Physica.Topical.094a00043.

Ockwig, N. W. and Nenoff, T. M. (2007) 'Membranes for hydrogen separation.', *Chemical reviews*, 107(10), pp. 4078–110. doi: 10.1021/cr0501792.

Opalka, S. M., Huang, W., Wang, D., Flanagan, T. B., L??vvik, O. M., Emerson, S. C., She, Y. and Vanderspurt, T. H. (2007) 'Hydrogen interactions with the PdCu ordered B2 alloy', *Journal of Alloys and Compounds*, 446–447, pp. 583–587. doi: 10.1016/j.jallcom.2007.01.130.

Opalka, S. M., Løvvik, O. M., Emerson, S. C., She, Y. and Vanderspurt, T. H. (2011) 'Electronic origins for sulfur interactions with palladium alloys for hydrogen-selective membranes', *Journal of Membrane Science*. Elsevier B.V., 375(1–2), pp. 96–103. doi: 10.1016/j.memsci.2011.03.018.

Ozaki, T., Zhang, Y., Komaki, M. and Nishimura, C. (2003a) 'Hydrogen permeation characteristics of V-Ni-Al alloys', *International Journal of Hydrogen Energy*, 28(11), pp. 1229–1235. doi: 10.1016/S0360-3199(02)00251-3.

Ozaki, T., Zhang, Y., Komaki, M. and Nishimura, C. (2003b) 'Preparation of palladium-coated V and V-15Ni membranes for hydrogen purification by electroless plating technique', *International Journal of Hydrogen Energy*, 28(3), pp. 297–302. doi: 10.1016/S0360-3199(02)00065-4.

Peachey, N. M., Snow, R. C. and Dye, R. C. (1996) 'Composite Pd/Ta metal membranes for hydrogen separation', *Journal of Membrane Science*, 111(1), pp. 123–133. doi: 10.1016/0376-7388(95)00298-7.

Phair, J. W. and Badwal, S. P. S. (2006) 'Materials for separation membranes in hydrogen and oxygen production and future power generation', *Science and Technology of Advanced Materials*, 7(8), pp. 792–805. doi: 10.1016/j.stam.2006.11.005.

Phair, J. W. and Donelson, R. (2006) 'Developments and design of novel (non-palladium-based) metal membranes for hydrogen separation', *Industrial and Engineering Chemistry Research*, pp. 5657–

5674. doi: 10.1021/ie051333d.

Phillips, J. (2006) 'Different types of gasifiers and their integration with gas turbines', in *The Gas Turbine Handbook*, pp. 67–77. Available at: http://netldev.netl.doe.gov/File Library/Research/Coal/gasification/gasifipedia/1-2-1.pdf (Accessed: 12 November 2013).

Pick, M. A. (1981) 'Kinetics of hydrogen absorption-desorption by niobium', *Physical Review B*, 24(8), pp. 4287–4294. doi: 10.1103/PhysRevB.24.4287.

Pick, M. A., Greene, M. G. and Strongin, M. (1980) 'International Symposium on the Properties and Applications of Metal Hydrides, 7-11 April 1980', *Journal of the Less-Common Metals*, 73(1), pp. 89–95. Available at: http://dx.doi.org/10.1016/0022-5088(80)90346-X%5Cnpapers2://publication/uuid/9DF251B0-A26B-4E9D-BFA1-9D176C033F03.

Pokhmurs'kyi, V. I., Sokolovs'kyi, O. R. and Fedorov, V. V. (1995) 'High-temperature hydrogen permeability of vanadium and niobium', *Materials Science*, 30(4), pp. 410–418. doi: 10.1007/BF00558832.

Porter, K. E., Hinchliffe, A. B. and Tighe, B. J. (1997) 'Gas Separation Using Membranes. 2. Developing a New Membrane for the Separation of Hydrogen and Carbon Monoxide Using the Targeting Approach', *Industrial & Engineering Chemistry Research*, 36(3), pp. 830–837. doi: 10.1021/ie960328u.

Pozzo, M. and Alfè, D. (2009) 'Hydrogen dissociation and diffusion on transition metal (= Ti, Zr, V, Fe, Ru, Co, Rh, Ni, Pd, Cu, Ag)-doped Mg(0001) surfaces', *International Journal of Hydrogen Energy*. Elsevier Ltd, 34(4), pp. 1922–1930. doi: 10.1016/j.ijhydene.2008.11.109.

Qiu, G., Zeng, W., Shi, Z., Fang, M. and Luo, Z. (2010) 'The physical and chemical properties of fly ash from coal gasification and study on its recycling utilization', *Proceedings - 2010 International Conference on Digital Manufacturing and Automation, ICDMA 2010*, 2, pp. 738–741. doi: 10.1109/ICDMA.2010.309.

Radtke, K. (2011) 'ThyssenKrupp Uhde's PRENFLO ® and HTW ™ Gasification Technologies Global Update on Technology and Projects'. Available at: https://www.netl.doe.gov/File Library/research/coal/energy systems/gasification/gasifipedia/16RADTKE.pdf.

Rahimpour, M. R., Ghaemi, M., Jokar, S. M., Dehghani, O., Jafari, M., Amiri, S. and Raeissi, S. (2013) 'The enhancement of hydrogen recovery in PSA unit of domestic petrochemical plant', *Chemical Engineering Journal*. Elsevier B.V., 226, pp. 444–459. doi: 10.1016/j.cej.2013.04.029.

Rath, L. K. (2010) *Assessment of Hydrogen Production with CO 2 Capture Volume 1 : Baseline State-of- the-Art Plants*, *Doe/Netl-2010/1434*.

Renzenbrink, W., Wischnewski, R. and Engelhard, J. (1998) *High Temperature Winkler (HTW) Coal Gasification Development State of the HTW Process*.

Robeson, L. M. (1991) 'Correlation of separation factor versus permeability for polymeric membranes', *Journal of Membrane Science*, 62(2), pp. 165–185. doi: 10.1016/0376-7388(91)80060-J.

Robeson, L. M. (2008) 'The upper bound revisited', *Journal of Membrane Science*, 320(1–2), pp. 390–400. doi: 10.1016/j.memsci.2008.04.030.

Romanenko, O. G., Tazhibaeva, I. L., Shestakov, V. P., Klepikov, A. K., Chikhray, Y. V., Golossanov, A. V. and Kolbasov, B. N. (1996) 'Hydrogen gas driven permeation through vanadium alloy VCr6Ti5', *Journal of Nuclear Materials*, 233–237(PART 1), pp. 376–380. doi: 10.1016/S0022-3115(96)00034-7.

Roos, C. J. (2010) 'Clean Heat and Power Using Biomass Gasification for Industrial and Agricultural Projects', 3165(February), pp. 1–58.

Rostrup-Nielsen, J. R. and Rostrup-Nielsen, T. (2002) 'Large-scale hydrogen production', *Cattech*, 6(4), pp. 150–159. doi: 10.1023/A:1020163012266.

San-Martin, A. and Manchester, F. D. (1991) 'The H-Ta (hydrogen-tantalum) system', *Journal of Phase Equilibria*, 12(3), pp. 332–343. doi: 10.1007/BF02649922.

Sanders, D. F., Smith, Z. P., Guo, R., Robeson, L. M., McGrath, J. E., Paul, D. R. and Freeman, B. D. (2013) 'Energy-efficient polymeric gas separation membranes for a sustainable future: A review', *Polymer (United Kingdom)*, 54(18), pp. 4729–4761. doi: 10.1016/j.polymer.2013.05.075.

Sarker, S., Chandra, D., Hirscher, M., Dolan, M., Isheim, D., Wermer, J., Viano, D., Baricco, M., Udovic, T. J., Grant, D., Palumbo, O., Paolone, A. and Cantelli, R. (2016) 'Developments in the Ni–Nb–Zr amorphous alloy membranes: A review', *Applied Physics A: Materials Science and Processing*. Springer Berlin Heidelberg, 122(3), pp. 1–9. doi: 10.1007/s00339-016-9650-5.

Saxena, S., Kumar, S. and Drozd, V. (2011) 'A modified steam-methane-reformation reaction for hydrogen production', *International Journal of Hydrogen Energy*. Elsevier Ltd, 36(7), pp. 4366–4369. doi: 10.1016/j.ijhydene.2010.12.133.

Schaefter, A. E. (1981) 'United States Patent 4,242,875'. United States. Available at: https://docs.google.com/viewer?url=patentimages.storage.googleapis.com/pdfs/US4242875.pdf.

Schaumann, G., Völkl, J. and Alefeld, G. (1970) 'The diffusion coefficient of hydrogen and deuterium in vanadium, niobium and tantalum by Gorsky-effect measurements.', *Phys. Stat. Sol.*, 42(1), pp. 401–413. doi: 10.1016/0042-207X(71)92620-0.

Shao, L., Lau, C.-H. and Chung, T.-S. (2009) 'A novel strategy for surface modification of polyimide membranes by vapor-phase ethylenediamine (EDA) for hydrogen purification', *International Journal of Hydrogen Energy*. Elsevier Ltd, 34(20), pp. 8716–8722. doi: 10.1016/j.ijhydene.2009.07.115.

Shim, J. H., Ko, W. S., Kim, K. H., Lee, H. S., Lee, Y. S., Suh, J. Y., Cho, Y. W. and Lee, B. J. (2013) 'Prediction of hydrogen permeability in V-Al and V-Ni alloys', *Journal of Membrane Science*. Elsevier, 430, pp. 234–241. doi: 10.1016/j.memsci.2012.12.019.

Shu, J., Grandjean, B. P. A., Neste, A. Van and Kaliaguine, S. (1991) 'Catalytic palladium-based membrane reactors: A review', *The Canadian Journal of Chemical Engineering*, 69(5), pp. 1036–1060. doi: 10.1002/cjce.5450690503.

Sinnott, R. (1996) 'Coulson & Richardson's chemical engineering'. Available at: http://scholar.google.com/scholar?hl=en&btnG=Search&q=intitle:Coulson+&+Richardson's+Chemical+Engineering+Volume+2#1 (Accessed: 6 November 2013).

Sircar, S. (2002) 'Pressure Swing Adsorption', pp. 1389–1392.

Song, J., Meng, B., Tan, X. and Liu, S. (2015) 'Surface-modified proton conducting perovskite hollow fibre membranes by Pd-coating for enhanced hydrogen permeation', *International Journal of Hydrogen Energy*. Elsevier Ltd, 40(18), pp. 6118–6127. doi: 10.1016/j.ijhydene.2015.03.057.

Spaeth, J. (2012) 'Main reactions during biomass gasification primary devolatilization primary tar', *IEA Bioenergy*, p. 14. Available at: http://www.ieatask33.org/app/webroot/files/file/various/Main reactions during biomass gasification.pdf.

Sprunger, P. T. and Plummer, E. W. (1993) 'Interaction of hydrogen with the Ag(110) surface', *Physical Review B*, 48(19), pp. 14436–14446. doi: 10.1103/PhysRevB.48.14436.

Sreenivasulu, B., Gayatri, D. V., Sreedhar, I. and Raghavan, K. V. (2015) 'A journey into the process and engineering aspects of carbon capture technologies', *Renewable and Sustainable Energy Reviews*. Elsevier, 41, pp. 1324–1350. doi: 10.1016/j.rser.2014.09.029.

Strezov, V. and Evans, T. J. (2014) *Biomass Processing Technologies*. Illustrate. CRC Press. Available at: https://books.google.co.uk/books?id=9TfcBQAAQBAJ&pg=PA99&lpg=PA99&dq=warnecke+advantag

es+and+disadvantages+of+gasification+types&source=bl&ots=mYDAx5mx2p&sig=8wYLZciFdATXzBm5Jp3Olwf7OIo&hl=en&sa=X&ved=0ahUKEwjR4NbBgJ7NAhWKJcAKHUKhD-wQ6AEIJTAB#v=onepage&q=.

Sunarso, J., Baumann, S., Serra, J. M., Meulenberg, W. a., Liu, S., Lin, Y. S. and Diniz da Costa, J. C. (2008) 'Mixed ionic–electronic conducting (MIEC) ceramic-based membranes for oxygen separation', *Journal of Membrane Science*, 320(1–2), pp. 13–41. doi: 10.1016/j.memsci.2008.03.074.

Suzuki, A., Yukawa, H., Nambu, T., Matsumoto, Y. and Murata, Y. (2015) 'Analysis of hydrogen mobility in Nb-based alloy membranes in view of new description of hydrogen permeability based on hydrogen chemical potential', *Journal of Alloys and Compounds*. Elsevier B.V., 645(S1), pp. S107–S111. doi: 10.1016/j.jallcom.2014.12.265.

Suzuki, A., Yukawa, H., Nambu, T., Matsumoto, Y. and Murata, Y. (2016) 'Analysis of pressure-composition-isotherms for design of non-Pd-based alloy membranes with high hydrogen permeability and strong resistance to hydrogen embrittlement', *Journal of Membrane Science*. Elsevier, 503, pp. 110–115. doi: 10.1016/j.memsci.2015.12.030.

Svedberg, R. C. and Buckman, R. W. (1980) 'Gas-metal reactions in vanadium and vanadium-base alloys', *International Metals Reviews*, 25(1), pp. 223–231. doi: 10.1179/imtr.1980.25.1.223.

Tao, Z., Yan, L., Qiao, J., Wang, B., Zhang, L. and Zhang, J. (2015) 'A review of advanced proton-conducting materials for hydrogen separation', *Progress in Materials Science*. Elsevier Ltd, 74, pp. 1–50. doi: 10.1016/j.pmatsci.2015.04.002.

Tarditi, A. M., Braun, F. and Cornaglia, L. M. (2011) 'Novel PdAgCu ternary alloy: Hydrogen permeation and surface properties', *Applied Surface Science*. Elsevier B.V., 257(15), pp. 6626–6635. doi: 10.1016/j.apsusc.2011.02.089.

Tarditi, A. M. and Cornaglia, L. M. (2011) 'Novel PdAgCu ternary alloy as promising materials for hydrogen separation membranes: Synthesis and characterization', *Surface Science*. Elsevier B.V., 605(1–2), pp. 62–71. doi: 10.1016/j.susc.2010.10.001.

Tavan, Y., Hosseini, S. H. and Olazar, M. (2015) 'A Note on an Integrated Process of Methane Steam Reforming in Junction with Pressure-Swing Adsorption to Produce Pure Hydrogen: Mathematical Modeling', *Industrial and Engineering Chemistry Research*, 54(51), pp. 12937–12947. doi: 10.1021/acs.iecr.5b01477.

Tennant, J. and Evenson, C. (2011) *Project FACTS Gasification Technologies & Hydrogen and Clean*

Fuels Scale-Up of Hydrogen Transport Membranes. Available at: https://www.netl.doe.gov/File Library/Factsheets/Project/NT42469.pdf.

Terrien, P., Lockwood, F., Granados, L. and Morel, T. (2014) 'CO2 capture from H2 plants: Implementation for EOR', *Energy Procedia*. Elsevier B.V., 63, pp. 7861–7866. doi: 10.1016/j.egypro.2014.11.821.

Thind, H. S., Yadvinder-Singh, Bijay-Singh, Varinderpal-Singh, Sharma, S., Vashistha, M. and Singh, G. (2012) 'Land application of rice husk ash, bagasse ash and coal fly ash: Effects on crop productivity and nutrient uptake in rice-wheat system on an alkaline loamy sand', *Field Crops Research*. Elsevier B.V., 135, pp. 137–144. doi: 10.1016/j.fcr.2012.07.012.

Tierney, H. L., Baber, A. E., Kitchin, J. R. and Sykes, E. C. H. (2009) 'Hydrogen dissociation and spillover on individual isolated palladium atoms', *Physical Review Letters*, 103(24), pp. 1–4. doi: 10.1103/PhysRevLett.103.246102.

Tosti, S., Bettinali, L. and Violante, V. (2000) 'Rolled thin Pd and Pd–Ag membranes for hydrogen separation and production', *International Journal of Hydrogen Energy*, 25. Available at: http://www.sciencedirect.com/science/article/pii/S0360319999000440 (Accessed: 10 February 2014).

Tsai, Y. C., Lin, C. C., Lin, W. L., Wang, J. H., Chen, S. Y., Lin, P. and Wu, P. W. (2015) 'Palladium based cermet composite for hydrogen separation at elevated temperature', *Journal of Power Sources*. Elsevier B.V, 274, pp. 965–970. doi: 10.1016/j.jpowsour.2014.10.085.

Turnock, P. H. and Robert H. Kadlec (1971) 'Separation of nitrogen and methane via periodic adsorption', *AiChE Journal*, 17(2), pp. 335–342. Available at: http://dx.doi.org/10.1002/aic.690170219.

U.S Department of Energy (2010) *Hydrogen Production*, *Fuel Cell Technologies Program*. Available at: http://www.afdc.energy.gov/fuels/hydrogen_production.html.

Uemiya, S., Sato, N., Ando, H., Kude, Y., Matsuda, T. and Kikuchi, E. (1991) 'Separation of hydrogen through palladium thin film supported on a porous glass tube', *Journal of Membrane Science*, 56(3), pp. 303–313. doi: 10.1016/S0376-7388(00)83040-9.

UK H2Mobility (2013) 'Phase 1 Results', (April). Available at: https://www.gov.uk/government/uploads/system/uploads/attachment_data/file/192440/13-799-uk-h2-mobility-phase-1-results.pdf.

US Department of Energy (2013) 'Report of the Hydrogen Production Expert Panel : A Subcommittee of the Hydrogen & Fuel Cell Technical Advisory Committee', *DoE Fuel Cell Technologies Office*, (October 2012).

US OEERE (2016) *Hydrogen Production Pathways*. Available at: http://energy.gov/eere/fuelcells/hydrogen-production-pathways (Accessed: 20 May 2016).

Vassilev, S. V., Baxter, D., Andersen, L. K. and Vassileva, C. G. (2010) 'An overview of the chemical composition of biomass', *Fuel*. Elsevier Ltd, 89(5), pp. 913–933. doi: 10.1016/j.fuel.2009.10.022.

Veleckis, E. and Edwards, R. (1969) 'Thermodynamic properties in the systems vanadium-hydrogen, niobium-hydrogen, and tantalum-hydrogen', *The Journal of Physical Chemistry*, 7(9). Available at: http://pubs.acs.org/doi/abs/10.1021/j100723a033 (Accessed: 10 September 2014).

Verma, A., Olateju, B., Kumar, A. and Gupta, R. (2015) 'Development of a process simulation model for energy analysis of hydrogen production from underground coal gasification (UCG)', *International Journal of Hydrogen Energy*. Elsevier Ltd, 40(34), pp. 10705–10719. doi: 10.1016/j.ijhydene.2015.06.149.

Viano, D. M., Dolan, M. D., Weiss, F. and Adibhatla, A. (2015) 'Asymmetric layered vanadium membranes for hydrogen separation', *Journal of Membrane Science*. Elsevier, 487, pp. 83–89. doi: 10.1016/j.memsci.2015.03.048.

Vigneault, A. and Grace, J. R. (2015) 'Hydrogen production in multi-channel membrane reactor via steam methane reforming and methane catalytic combustion', *International Journal of Hydrogen Energy*. Elsevier Ltd, 40(1), pp. 233–243. doi: 10.1016/j.ijhydene.2014.10.040.

Voldsund, M., Jordal, K. and Anantharaman, R. (2016) 'Hydrogen production with CO2 capture', *International Journal of Hydrogen Energy*. Elsevier Ltd, 41(9), pp. 4969–4992. doi: 10.1016/j.ijhydene.2016.01.009.

Völkl, J. and Alefeld, G. (1978) 'Diffusion of hydrogen in metals', in *Hydrogen in metals 1*, pp. 321–348. doi: 10.1007/3540087052_51.

Wang, M., Song, J., Wu, X., Tan, X., Meng, B. and Liu, S. (2016) 'Metallic nickel hollow fiber membranes for hydrogen separation at high temperatures', *Journal of Membrane Science*. Elsevier, 509, pp. 156–163. doi: 10.1016/j.memsci.2016.02.025.

Wang, T., Zhang, H., Meng, B., Wang, X., Sunarso, J., Tan, X. and Liu, S. (2016) 'SrCe 0.95 Y 0.05 O 3−δ –ZnO dual-phase membranes for hydrogen permeation', *RSC Advances*. Royal Society of Chemistry,

6(43), pp. 36786–36793. doi: 10.1039/C6RA02921C.

Wang, Y. I., Suh, J. Y., Lee, Y. S., Shim, J. H., Fleury, E., Cho, Y. W. and Koh, S. U. (2013) 'Direct measurement of hydrogen diffusivity through Pd-coated Ni-based amorphous metallic membranes', *Journal of Membrane Science*. Elsevier, 436, pp. 195–201. doi: 10.1016/j.memsci.2013.02.040.

Wang, Z., Guo, X., Wu, M., Sun, Q. and Jia, Y. (2014) 'First-principles study of hydrogen dissociation and diffusion on transition metal-doped Mg(0 0 0 1) surfaces', *Applied Surface Science*. Elsevier B.V., 305, pp. 40–45. doi: 10.1016/j.apsusc.2014.02.153.

Ward, T. and Dao, T. (1999) 'Model of hydrogen permeation behavior in palladium membranes', *Journal of Membrane Science*, 153(January 1998), pp. 211–231. Available at: http://www.sciencedirect.com/science/article/pii/S0376738898002567 (Accessed: 18 February 2014).

Wei, L., Xu, S., Zhang, L., Liu, C., Zhu, H. and Liu, S. (2007) 'Steam gasification of biomass for hydrogen-rich gas in a free-fall reactor', *International Journal of Hydrogen Energy*, 32(1), pp. 24–31. doi: 10.1016/j.ijhydene.2006.06.002.

Wiheeb, A. D., Helwani, Z., Kim, J. and Othman, M. R. (2016) 'Pressure Swing Adsorption Technologies for Carbon Dioxide Capture', *Separation & Purification Reviews*, 45(2), pp. 108–121. doi: 10.1080/15422119.2015.1047958.

Xiao, J., Peng, Y., Bénard, P. and Chahine, R. (2015) 'Thermal effects on breakthrough curves of pressure swing adsorption for hydrogen purification', *International Journal of Hydrogen Energy*, 1, pp. 2–11. doi: 10.1016/j.ijhydene.2015.11.126.

Xu, G., Li, L., Yang, Y., Tian, L., Liu, T. and Zhang, K. (2012) 'A novel CO2 cryogenic liquefaction and separation system', *Energy*, 42(1), pp. 522–529. doi: 10.1016/j.energy.2012.02.048.

Xu, Y., Greeley, J. and Mavrikakis, M. (2005) 'Effect of subsurface oxygen on the reactivity of the Ag(111) surface', *Journal of the American Chemical Society*, 127(37), pp. 12823–12827. doi: 10.1021/ja043727m.

Yaman, S. (2004) 'Pyrolysis of biomass to produce fuels and chemical feedstocks', *Energy Conversion and Management*, 45(5), pp. 651–671. doi: 10.1016/S0196-8904(03)00177-8.

Yamaura, S. I., Shimpo, Y., Okouchi, H., Nishida, M., Kajita, O., Kimura, H. and Inoue, A. (2004) 'Hydrogen permeation characteristics of melt-spun Ni-Nb-Zr amorphous alloy membranes', *Nippon Kinzoku Gakkaishi/Journal of the Japan Institute of Metals*, 68(11), pp. 952–957. doi:

10.4028/www.scientific.net/JMNM.24-25.315.

Yamaura, S. ichi and Inoue, A. (2010) 'Effect of surface coating element on hydrogen permeability of melt-spun Ni40Nb20Ta5Zr30Co5 amorphous alloy', *Journal of Membrane Science*, 349(1–2), pp. 138–144. doi: 10.1016/j.memsci.2009.11.037.

Yang, S.-I., Choi, D.-Y., Jang, S.-C., Kim, S.-H. and Choi, D.-K. (2008) 'Hydrogen separation by multi-bed pressure swing adsorption of synthesis gas', *Adsorption*, 14(4–5), pp. 583–590. doi: 10.1007/s10450-008-9133-x.

Yang, S.-M., Chen, Y.-C., Chen, C.-H., Huang, W.-P. and Lin, D.-Y. (2015) 'Microstructural characterization of δ/γ/σ/γ2/χ phases in silver-doped 2205 duplex stainless steel under 800°C aging', *Journal of Alloys and Compounds*. Elsevier B.V., 633, pp. 48–53. doi: 10.1016/j.jallcom.2015.01.165.

Yeboah, N. N. N., Shearer, C. R., Burns, S. E. and Kurtis, K. E. (2014) 'Characterization of biomass and high carbon content coal ash for productive reuse applications', *Fuel*. Elsevier Ltd, 116(X), pp. 438–447. doi: 10.1016/j.fuel.2013.08.030.

Yoshihara, M., Pharr, G. M. and McLellan, R. B. (1987) 'The structure of Pd-Y solid solutions', *Scripta Metallurgica*. Edited by Intergovernmental Panel on Climate Change. Cambridge: Cambridge University Press, 21(3), pp. 393–396. doi: 10.1016/0036-9748(87)90235-3.

Yukawa, H., Nambu, T. and Matsumoto, Y. (2011) 'Ta-W Alloy for Hydrogen Permeable Membranes', *Materials Transactions*, 52(4), pp. 610–613. doi: 10.2320/matertrans.MA201007.

Zaginaichenko, S. Y., Matysina, Z. A., Schur, D. V., Teslenko, L. O. and Veziroglu, A. (2011) 'The structural vacancies in palladium hydride. Phase diagram', *International Journal of Hydrogen Energy*. Elsevier Ltd, 36(1), pp. 1152–1158. doi: 10.1016/j.ijhydene.2010.06.088.

Zhang, G. X., Yukawa, H., Nambu, T., Matsumoto, Y. and Morinaga, M. (2010) 'Alloying effects of Ru and W on hydrogen diffusivity during hydrogen permeation through Nb-based hydrogen permeable membranes', *International Journal of Hydrogen Energy*. Elsevier Ltd, 35(3), pp. 1245–1249. doi: 10.1016/j.ijhydene.2009.11.066.

Zhang, W., Gaggl, M., Gluth, G. J. G. and Behrendt, F. (2014) 'Gas separation using porous cement membrane', *Journal of Environmental Sciences*. The Research Centre for Eco-Environmental Sciences, Chinese Academy of Sciences, 26(1), pp. 140–146. doi: 10.1016/S1001-0742(13)60389-7.

Zhang, Y., Ozaki, T., Komaki, M. and Nishimura, C. (2002) 'Hydrogen permeation characteristics of vanadium-aluminium alloys', *Scripta Materialia*, 47(9), pp. 601–606. doi: 10.1016/S1359-

6462(02)00218-X.

Zhu, L., Li, L. and Fan, J. (2015) 'A modified process for overcoming the drawbacks of conventional steam methane reforming for hydrogen production: Thermodynamic investigation', *Chemical Engineering Research and Design*. Institution of Chemical Engineers, 104, pp. 792–806. doi: 10.1016/j.cherd.2015.10.022.

Zhu, Z., Hou, J., He, W. and Liu, W. (2016) 'High-performance Ba(Zr0.1Ce0.7Y0.2)O3-?? asymmetrical ceramic membrane with external short circuit for hydrogen separation', *Journal of Alloys and Compounds*. Elsevier B.V, 660, pp. 231–234. doi: 10.1016/j.jallcom.2015.11.065.

3 The Theory of Hydrogen Permeation

3.1 The Richardson Equation & Other Early Models

Before discussing the more advanced models for predicting hydrogen permeation later in this chapter it is worthwhile to cover some of the relevant historic studies and relationships discovered.

Multiple attempts have been made to explain and model the behaviour of hydrogen permeation through metals, one of the earliest examples of note was that of O.W Richardson in 1904. Richardson studied the relationship between hydrogen flux (J) ([mol H] m^{-2} s^{-1}) and permeability (Φ) ([mol H_2] m^{-2} s^{-1} Pa $^{-1}$), by considering the steady-state diffusion of hydrogen atoms through metals. The development of what became known as Richardson's equation is laid out in (Andrew and Haasz, 1992) and summarised below.

Consider the concentration of hydrogen atoms in the membrane as c_f (mol m^{-3}) for upstream/feed side of the membrane, and as c_d for downstream/permeate side. If c_u equals c and c_d is negligibly small, then the permeated flux is governed by Fick's law for diffusion:

$$J = \frac{D}{t}\, c \qquad \text{(Equation 3.1)}$$

Where D is the diffusion coefficient (m^2 s^{-1}), (previously discussed in chapter 2.4) and t is the membrane thickness (m). Assuming that the hydrogen concentration, c_u, is in equilibrium with the hydrogen gas concentration upstream of the membrane (determined by its partial pressure) then Sieverts law can be applied:

$$c = K_S\sqrt{P} \qquad \text{(Equation 3.2)}$$

Where K_S is the Sievert constant (dimensionless) for hydrogen and P refers to the pressure (Pa); applying Sieverts law to this instance results in c_u being governed by S and P_u, the upstream pressure. For consistency, if c_d is to be negligible it must be that the hydrogen pressure downstream is also low. The diatomic nature of hydrogen is responsible for the presence of the root function, as two atoms are produced from each molecule. Combining both equations allows for the elimination of c and gives Richardson's equation (Andrew and Haasz, 1992):

$$J = DK_S\left(\frac{\sqrt{P}}{t}\right) \qquad \text{(Equation 3.3)}$$

As has previously been discussed, the diffusion and Sievert constants multiplied together equal the permeability. Richardson's equation is of limited use in the form above, and is typically displayed as (Kozhakhmetov *et al.*, 2015)(Ockwig and Nenoff, 2007):

$$J = DK_S \frac{\sqrt{P_u} - \sqrt{P_d}}{t} \qquad \text{(Equation 3.4)}$$

This result is derived in the same manner, but just with the consideration of c_d being non-zero, resulting in the presence of a downstream pressure term, P_d.

An alternate form for this equation is given in (Smithells and Ransley, 1935) and later in (McLeod, 2008):

$$J = \frac{k_{ri}}{t} T^{0.5} e^{-\frac{b}{T}} (P_u^{0.5} - P_d^{0.5}) \qquad \text{(Equation 3.5)}$$

Where b (dimensionless) is a constant for the gas-metal system, k_{ri} is a rate constant and all other components have been previously described.

This equation is deemed to be reliable in the most part, as it was determined that in most instances permeation wasn't limited by reactions at the surface (Andrew and Haasz, 1992). However, real behaviour diverges from predicted behaviour at low pressures as discussed by (Smithells and Ransley, 1935). This work built on the early work of Richardson and noted that whilst the effect of temperature is satisfactorily represented in equation 3.5, the effect of pressure is only approximate and at low pressures notable deviations between real and predicted behaviour can be measured. It was generally accepted that the relationship between the generated flux and the pressure differential could be defined as:

$$J = k_{ri} \sqrt{\Delta P} \qquad \text{(Equation 3.6)}$$

Smithells and Ransley collected experimental data produced and published by others and plotted the hydrogen flux against the square root of the pressure differential, before extrapolating the data back to the x axis (pressure differential) using the first-order Richardson equation. It was found that extrapolating using the Richardson equation resulted in a non-zero intercept, suggesting a threshold pressure differential (ΔP_{THR}) was required to be met. This threshold, whilst very small in scale is problematic as it renders the Richardson equation incorrect under these conditions, as any ΔP of hydrogen should result in some hydrogen flux. The occurrence of a minimum value led to the conclusion that diffusion or solution of a gas in a metal must be proceeded by adsorption onto the surface of the material (Smithells and Ransley, 1935).

Figure 3.1 shows a non-specific example of what is described above, the red dotted line represents behaviour predicted by the Richardson equation and the blue line represents the amendment made suggested by Smithells and Ransley to validate the model at low pressures.

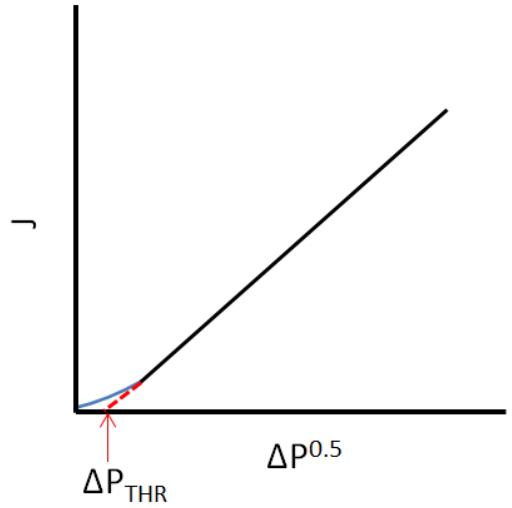

Figure 3.1 – Diagram displaying the limitations of the unadjusted Richardson equation

The equation was amended by allowing for the fraction of the surface covered by absorbed gas, by introducing the Langmuir isotherm resulting in the addition of a term to equation 3.6:

$$J = k_{ri}\sqrt{\Delta P}\left(\frac{a\Delta P}{1+a\Delta P}\right) \qquad \text{(Equation 3.7)}$$

The consideration of the surface processes was a significant development, as until this point only bulk diffusion had been considered as important to determining flux. However, it must be noted in most circumstances the bulk diffusion is the rate limiting step (Ward and Dao, 1999)(Ockwig and Nenoff, 2007)(McLeod, 2008); with surface processes having an increased effect when pressures remain low (vacuum) or when membranes are so thin that the reaction rates of the surfaces have to be considered as the diffusive rate is high. For palladium membranes, the key thickness is 10 µm (Ward and Dao, 1999)(Caravella, Barbieri and Drioli, 2008), where membranes thinner then this are considered "ultrathin".

An alternative way of expressing equation 3.7 is given in (McLeod, 2008):

$$J = \frac{k_{ri}e^{\frac{-b}{T}}(P_u^{0.5}-P_d^{0.5})}{t}\theta_{eq} \qquad \text{(Equation 3.8)}$$

Where the term Θ_{eq} (dimensionless) represents the surface component and can be defined as:

$$\theta_{\mathrm{eq}} = \frac{\sqrt{\frac{k_{ads}}{k_{des}}}\,P^{0.5}}{1+\sqrt{\frac{k_{ads}}{k_{des}}}\,P^{0.5}} \qquad \text{(Equation 3.9)}$$

Where k_{ads} and k_{des} are the rate constants for adsorption and desorption of hydrogen onto/from the metal respectively ($m^2\ mol^{-1}\ s^{-1}$). These amendments to the Richardson equation allow for rather accurate if somewhat limited predictions of gas permeation in metals, as it's empirical nature fits measured behaviour for bulk-diffusion limited processes.

Before moving onto more involved models, it is worthwhile to explore how permeability can be derived with the utilisation of thermodynamic data. Both the diffusion coefficient and the Sievert constant can be displayed as Arrhenius processes:

$$\mathrm{D} = \mathrm{D_0 e^{-E_{dif}/RT}} \qquad \text{(Equation 3.10)}$$

$$\ln \mathrm{K_s} = \frac{\Delta \mathrm{S^0}}{\mathrm{R}} - \frac{\Delta \mathrm{H^0}}{\mathrm{RT}} \qquad \text{(Equation 3.11)}$$

Where D_0 is the pre-exponential factor for diffusion, E_{dif} is the activation energy for diffusion, R is the gas constant ΔS^0 is the standard molar entropy of solution and ΔH^0 is the molar enthalpy of solution (both in the limit of infinite dilution). Thus permeability can be displayed as a product of the two:

$$\Phi = \mathrm{D_0}\,(\mathrm{e}^{\frac{\Delta \mathrm{S}}{\mathrm{R}}})(\mathrm{e}^{-\frac{\Delta \mathrm{H^0 + E_{dif}}}{\mathrm{RT}}}) \qquad \text{(Equation 3.12)}$$

This expression is a useful one, as it allows for the consideration of potential membrane materials through the use of thermodynamic data, an alternative to the direct methods of determining permeability through the measurement of permeate flows through a membrane or the use of electrochemical methods such as the one discussed in (Akamatsu *et al.*, 2005).

Data on diffusion and solubility for hydrogen in transition metals can be gathered from a number of sources, with much of the thermodynamic properties and diffusion coefficients described in detail in literature (Oates and Flanagan, 1981)(Wipf, 2001)(Völkl and Alefeld, 1978) are all deemed reputable and values reported here are still used in recent simulations. A more detailed review of the mechanisms of solubility and diffusivity will be covered later in this chapter.

3.2 The Wang Model of Hydrogen Permeation

Whilst the work of Richardson and Smithells & Ransley is useful for the determining flux rate of hydrogen, it is somewhat limited in giving an understanding of the mechanism of diffusion. Whilst the work previously discussed was empirically derived, efforts have been made to develop models that are more mechanistically sound (Andrew and Haasz, 1992).

The first model of note was developed by Wang in 1936; where over the course of two papers a one-dimensional model for hydrogen permeation was laid out (Andrew and Haasz, 1992). Wang's model contains elements for gas-surface, surface-bulk and bulk transport processes. The model developed was successful in predicting behaviour in permeate-side low-pressure/vacuum states where the permeation rate is directly proportional to the upstream pressure.

A detailed summary of Wang's model is given by (Andrew and Haasz, 1992) and key components of this are included within this work. Wang's model consists of five flux reactions:

1. Adsorption of the hydrogen molecule (Dissociative chemisorption)
2. Absorption of hydrogen ions into the bulk
3. Bulk diffusion of hydrogen ions
4. Desorption of hydrogen ions from the bulk to the surface
5. Re-association of the hydrogen molecule and desorption from the surface

Whilst expanded upon and altered somewhat these five steps form the basis of most hydrogen permeation models, including the model developed by Ward and Dao to be discussed later. The model developed by Ward and Dao in 1999 is still referenced heavily in current studies into membrane separators (Faizal *et al.*, 2015)(Lai, Yin and Laura Lind, 2015)(Tsai *et al.*, 2015)(Dolan, 2010).

Each of the five steps described above can also be described mathematically in terms of a flux rate equation. Each step is reversible, with the reverse of adsorption (step one) being desorption from the surface (step five). Bulk absorption (step two) and bulk desorption (step four) are also the reverse of each other with bulk diffusion governed by Fick's law. By taking mass balances at each of the five interfaces of the membrane a net flux can be determined; in steady state this net flux is equal to the permeated hydrogen flux. The five interfaces are defined as:

1. **Feed-side/upstream surface:** Adsorption (reaction 1) – Desorption (reaction 5)
2. **Surface to bulk:** Absorption (reaction 2) – Desorption onto surface (reaction 4)
3. **Bulk diffusion:** Diffusion (reaction 3)

4. **Bulk to surface**: Desorption onto surface (reaction 4) – absorption (reaction 2)
5. **Permeate-side/downstream surface:** Desorption (reaction 5) – Adsorption

By reducing the permeate-side hydrogen pressure to zero (typically done using a vacuum), the fifth balance can be reduced to the desorption only term as was done by Wang in the original model.

The first step in the mechanism is dissociative chemisorption of gaseous hydrogen into metal, this requires two adjacent and vacant surface sites for adsorption and dissociation and so a key component is the surface coverage, Θ. The surface coverage is given as a value between 0 (no coverage) to 1 (full surface occupation). Other factors that affect the flux are the adsorption probability (α_m) and a kinetic factor (μ).

$$J_{ads} = 2\alpha_m(1-\Theta)^2\mu P \qquad \text{(Equation 3.13)}$$

$$\mu = (2\pi m_h k_b T)^{-0.5} \qquad \text{(Equation 3.14)}$$

Where k_b is the Boltzmann constant and m_h is the molecular mass of hydrogen.

The second step is the absorption stage, where the surface coverage once again plays a key role in the flux generated. Here ϒ is the proportionality constant.

$$J_{abs} = \Upsilon\Theta \qquad \text{(Equation 3.15)}$$

The bulk diffusion is governed by Fick's law for diffusion, as discussed in previous models.

$$J_{dif} = -D\frac{dc}{dx} \qquad \text{(Equation 3.16)}$$

Diffusion from the bulk is dependent on another proportionality constant (ω), the concentration of the gas and the fraction of un-occupied surface sites. For the surface coverage term in this equation there is no squared factor as diffusion to the surface is conducted on a singular ion basis.

$$J_{dsb} = \omega(1-\Theta)c \qquad \text{(Equation 3.17)}$$

The final process is that of desorption from the surface, as expected the surface coverage factors into the flux alongside a rate constant for desorption (δ). The surface coverage is once again raised to a power of two, as for re-association a pair of occupied neighbour sites is required.

$$J_{des} = 2\delta\Theta^2 \qquad \text{(Equation 3.18)}$$

An overall expression in terms of permeability (equating to pressure) for Wang's model is given in (Andrew and Haasz, 1992), this expression is referred to as Wang's equation. The general form of this is given as follows:

$$P = \frac{\delta}{\alpha_m \mu} \frac{J}{(2\delta+J)}\{1 + [1 + \frac{(2\delta+J)}{(\Upsilon-J)}\left(\frac{t\omega}{D\sqrt{2\delta}} + \frac{2(2\delta+\Upsilon)}{(\sqrt{2\delta}-\sqrt{J})(2\delta+J)}\right)J^{0.5}]^2\} \qquad \text{(Equation 3.19)}$$

As can be seen, Wang's equation in its full form is unwieldy. The application of various assumptions can be used to simplify the equation for various case studies.

If the condition of permeated flux (J) approaches 0 is applied at which point Wang's equation can be expressed as:

$$P_u = (\frac{\delta}{\alpha_m \mu})(\frac{J}{2\delta})(1+1) \qquad \text{(Equation 3.20)}$$

or

$$J = \alpha_m \mu P_u \qquad \text{(Equation 3.21)}$$

This special case allows for the development of an understanding of the relationship in Wang's model between hydrogen pressure and the permeated flux. What this shows is that if the surface is clean (Θ approaching 0), then equation 3.21 suggests that half of the adsorbed flux is being desorbed on either surface (upstream and downstream). This suggests that desorption is a slower process than bulk diffusion in this case, as the flux (and hence the surface coverage) is small (Andrew and Haasz, 1992).

A second special case that can be considered is one of very large fluxes, where the right hand side of Wang's equation becomes infinite as the flux (J) approaches the terms 2δ or ϒ. As stated by (Andrew and Haasz, 1992), this means that as the pressure differential becomes infinite the flux saturates to the smaller value of either 2δ or ϒ. If ϒ is the limiting factor, this represents the physical limitation of atoms on the feed side only being able to enter the bulk at a finite rate. If 2δ is the limiting factor desorption of hydrogen from the permeate surface is limited as surface coverage (Θ_d) approaches unity (complete coverage).

The final case to consider from Wang's model is for intermediate fluxes, these are more typical of real life behaviour for most membrane operations. In these instances, the conditions state that the permeated flux is much smaller than the terms 2δ or ϒ, this allows for a reduction in the number of terms in Wang's equation. Under these conditions, if the membrane is sufficiently thick diffusion across the whole membrane will be slower than the single jump between bulk and surface sites (represented by the aforementioned terms). (Andrew and Haasz, 1992) shows that this manifests in a

further of simplification of Wang's equation, as the surface to bulk and bulk to surface terms approach unity. This results in Wang's equation becoming:

$$J = \frac{D}{t}\frac{\gamma}{\omega}\left(\frac{\alpha_m \mu}{\delta}\right)^{0.5} P_u^{0.5} \qquad \text{(Equation 3.22)}$$

This expression predicts the dependence of the permeated flux (J) on the thickness of the membrane (t) and the pressure differential (if the permeate side is not held at vacuum) or the feed side pressure (if the permeate side is kept in vacuum), this dependence is the same as predicted by Richardson's equation.

These case studies help demonstrate what Wang's model/equation is; fundamentally, the equation is the general form for a permeation isotherm. Initial criticism of the equation came from Wang himself, as the model predicts a pressure-independent regime at sufficiently high pressures - the saturation of the flux. At the time of the models development, this had not been observed at pressures as high as 113 bar (Wang and Roberts, 1936a) leading Wang to believe that this was not the case. This led to Wang developing two new processes for direct hydrogen transfer between the metal bulk and the gas phase, which has been utilised by multiple later works.

Whilst modifications have been made to Wang's original model/equation the fundamental concepts discussed have not been replaced, with newer models built on the relationships discussed (Andrew and Haasz, 1992).

3.3 Modifications of the Wang Model

Whilst multiple changes have been made to the Wang Model only a limited number will be discussed within this section, as the work of Ward and Dao discussed in the next chapter incorporates many of these changes whilst drawing heavily from the work of Wang also.

Ash & Barrer, who themselves are significant contributors to the development of membrane technology, developed the model of Wang further through several studies. (Barrer, 1939) is an early work in which Barrer identifies that Wang's model overlooks that there are a limited number of sites available in the bulk, where the maximum bulk concentration feasible is expected to be in the order of the metal atom density, or a H/M ratio of 1. Under most conditions the hydrogen concentration (c) is significantly lower than the atom density (N); however, as discussed below, experiments have shown that H/M ratios approaching 1 are possible to achieve.

(Ash and Barrer, 1959) is an update of the earlier paper by Barrer in which an expression for this case is evolved including four additional processes added by Wang. This expression has not been included here due to the later work of Andrew & Haasz superseding the expression and removing the need for Wang's additional processes.

(Andrew and Haasz, 1992) returns to the earlier criticism of Wang's model by Wang himself. Wang based his criticism of his model on the work of Smithells and Ransley who, as previously mentioned in this chapter, conducted permeation experiments on a range of metals. Wang cited data published in their work, where permeation tests on 0.35 mm thick nickel showed no sign of saturation even at upstream pressures of 113 bar, where observations of pressure dependence were still made. Wang believed that this dependence on pressure even at such high upstream pressures invalidated the idea of a simple dissociative chemisorption model, like the one he had developed (Wang and Roberts, 1936b). As stated previously, this led Wang to develop mechanisms of direct movement of hydrogen atoms from the gas phase to the bulk of the membrane, without any interaction with the surface.

Wang's argument and his model alterations can be viewed in detail in the second paper he published (Wang and Roberts, 1936b) on the matter, a year later. However, the work of Andrew & Haasz concludes that the "saturation dilemma" at the centre of Wang's criticism does not exist and that it is possible to reconcile the pressure dependence at pressures above those deemed to saturate the surface with hydrogen with use of the original model/equation (Andrew and Haasz, 1992).

This reconciliation draws heavily on the work of (Pick and Sonnenberg, 1985), who developed an estimation for the proportionality constant ω in terms of metal density (N) and an attempt frequency for jumps between interstitial lattice sites for hydrogen (Γ_j):

$$\omega = \Gamma_j N^{-1/3} \exp^{\frac{-E_{bs}}{kT}} \qquad \text{(Equation 3.23)}$$

Where E_{bs} is the activation energy for a hydrogen atom moving from a bulk to surface site.

The same publication provides a similar estimation for the diffusion coefficient:

$$D = \Gamma_j N^{-2/3} \exp^{\frac{-E_{dif}}{kT}} \qquad \text{(Equation 3.24)}$$

Where E_{dif} is the activation energy for hydrogen diffusion in the bulk.

Equation 3.24 provides good numerical agreement with literature values of the diffusion coefficient for reasonable values of Γ_j (given in the approximate range of 10^{13} s^{-1}). If E_{bs} and E_{dif} are taken to be similar in value, then equations 3.23 and 3.24 can be combined to give:

$$\frac{D}{\omega} \sim N^{-1/3} \qquad \text{(Equation 3.25)}$$

(Pick and Sonnenberg, 1985) and (Andrew and Haasz, 1992) state that $N^{-1/3}$ is approximately equal to the diameter of a metal atom, then multiplying the D/ω term by t (membrane thickness) the thickness can be given in metal atom diameters.

Taking the developments of (Pick and Sonnenberg, 1985), (Andrew and Haasz, 1992) then applied this to a specific case derived from the Wang model. Working on a basis that the permeating flux saturates due to processes on the upstream surface and also assuming that $\Upsilon << 2\delta$, Andrew & Haasz investigated the effect of the permeating flux (J) on surface coverage. This was done by considering the three mass balances at interfaces 2, 3 and 4 discussed previously, by combining the three balance equations the terms c_u and c_d can be eliminated, and provided the membrane is symmetrical (i.e. $\omega_u = \omega_d = \omega$ and $\Upsilon_u = \Upsilon_d = \Upsilon$) the following expression can be obtained:

$$\frac{J}{\Upsilon} = \frac{\theta_u - \theta_d\left[\frac{(1-\theta_u}{1-\theta_d}\right]}{1+\left(\frac{\omega t}{D}\right)+(1-\theta_u)+\left(\frac{1-\theta_u}{1-\theta_d}\right)} \qquad \text{(Equation 3.26)}$$

As can be seen the equation presents the flux in terms of the upstream and downstream surface coverage, by multiplying the numerator and denominator by the term $(1-\theta_d)$ the expression above becomes:

$$\frac{J}{\Upsilon} = \frac{\theta_u - \theta_d}{(1-\theta_u)+(1-\theta_d)+[\left(\frac{\omega t}{D}\right)(1-\theta_u)(1-\theta_d)]} \qquad \text{(Equation 3.27)}$$

As J ≤ Υ and the assumption that Υ << 2δ has been made, then it can be shown that J << 2δ. Applying these conditions to the mass balance at interface five (simplified in vacuum conditions to equation 3.18 applied to the downstream surface) then it can be seen that Θ_d << 1, to allow for a small flux and a large value for the term 2δ. This small value then represents an almost bare downstream surface, regardless of the upstream conditions.

If Θ_u approaches one (complete coverage) along with the application of the conditions discussed above, then equation 3.27 can be reduced to:

$$\frac{J}{\Upsilon} = \frac{\theta_u}{1+\left(\frac{\omega t}{D}\right)(1-\theta_u)} \qquad \text{(Equation 3.28)}$$

It can be seen clearly that if Θ_u equals 1, then J must equal Υ, meaning that the permeating flux is saturated. However, as stated above, the surface coverage only approaches complete coverage asymptotically (the downstream surface is not in the same condition) and for J to be comparable to Υ then it is required that the term [1+(1-Θ_u)(ωt/D)] must not be much larger than unity.

What can also be reasoned is that if ωt/D >> 1, it is possible that the flux saturates only when the term (1-Θ_u) << 1, or at a complete or near complete surface coverage (Θ_u ≈ 1). Figure 3.1 shows J/Υ plotted against upper surface coverage (Θ_u) for varying values of the term ωt/D.

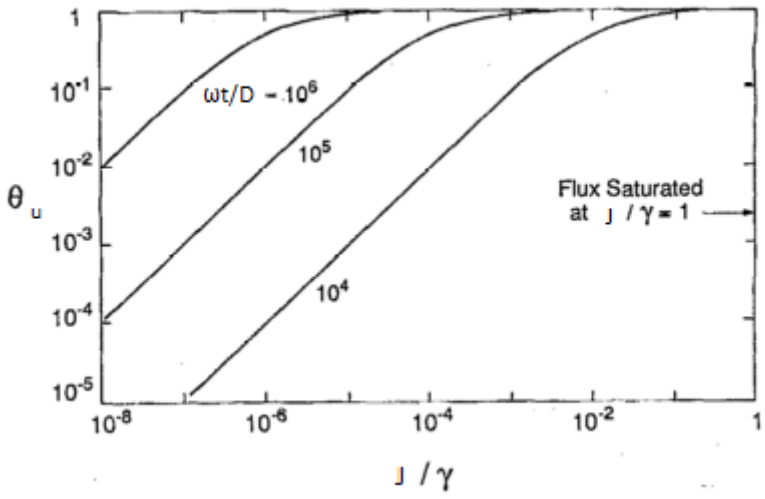

Figure 3.2 - Upstream surface coverage vs. J/Υ for varying values of ωt/D, adapted from (Andrew and Haasz, 1992)

Looking at figure 3.2, it can be seen for larger values of the ωt/D term, saturation of the surface occurs significantly quicker, the value of J/Υ was determined through use of equation 3.28. Assuming that D

and ω remain constant (i.e. constant temperature) then it can be seen that the thickness (t) has a significant effect.

As shown in equation 3.25 and stated by Pick and Sonnenberg, the term ωt/D can be interpreted as given in the order of the membrane thickness in metal atom diameters. Andrew & Haasz drew the conclusion that "the pressure at which the permeating flux will start to saturate exceeds the pressure at which the upstream surface coverage begins to saturate by a factor of order $tN^{1/3}$". Applying this to Wang's model, it can be seen why Wang felt the model needed amending, as at a feed pressure of 113 bar Smithells and Ransley were likely seeing complete coverage. However, as Andrew and Haasz highlight the tests conducted by Smithells and Ransley were done on nickel membranes of 0.35 mm thickness, approximately 10^6 atoms thick resulting in a factor ($tN^{1/3}$) in the order of 10^6.

Andrew and Haasz used this to demonstrate that, for this specific membrane, the work done by Smithells and Ransley did not reach the required upstream/feed pressure to demonstrate a saturation of the permeating flux (the pressure independent phase predicted by Wang) thus removing the need for the amendments of Wang, whilst providing validation for his original work. In (Andrew and Haasz, 1992), and replicated in figure 3.3 below, alongside a plot of the upstream and downstream coverage at the same pressure.

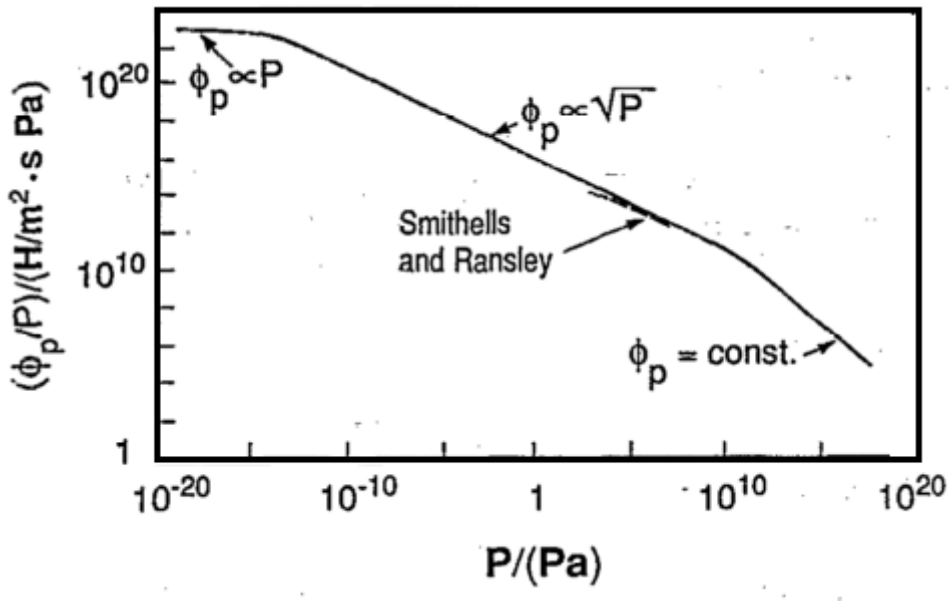

Figure 3.3 – Relationship between upstream pressure and permeating flux for a Nickel membrane, adapted from (Andrew and Haasz, 1992)

What can be seen is that when the pressure independent/saturated flux phase takes hold, a significant increase in downstream coverage can be seen, and as pressure continues to increase this reaches an

asymptotic value. No immediate explanation is given by the authors (although they study two further cases that may provide context) but it could be predicted that at these ultra-high upstream pressures the bulk material reaches saturation long before the downstream surface does.

As mentioned, Andrew and Haasz identify two other cases which will mathematically lead to a saturation of the flux. The first of which being a physical limit to the bulk concentration of hydrogen, represented by:

$$J = \frac{D\, c_s}{t} \qquad \text{(Equation 3.29)}$$

Where c_s is the saturation concentration of hydrogen in the metal, it is also important to note that at concentrations this high the diffusion coefficient itself may be a function of concentration (Andrew and Haasz, 1992). This conclusion has been somewhat superseded in more modern works with the use of chemical potential instead of concentration.

This upper limit is deemed to be "exceedingly" high if determined through the use of equation 3.29, as the saturation concentration will be in the order of the metal density. Saturation will require the filling of a large number of interstitial sites and this becomes increasingly difficult, to achieve saturation in a conventional system the feed pressure would have to be gigantic for most metals as hydrogen is absorbed into the bulk as an endothermic process (Andrew and Haasz, 1992)(San Marchi, Somerday and Robinson, 2007)(Kim, Shim and Lee, 2012).

An exception to this rule is palladium, where hydrogen is absorbed exothermically and as such even at lower pressures a large amount of hydrogen can be absorbed by the metal. As discussed in chapter 2, this solubility for palladium is even higher at moderate temperatures – this is logical as a lower temperature favours the exothermic reaction of hydride formation. (Barrer, 1940) utilises an electrochemical supply of hydrogen to achieve hydrogen saturation of palladium, with other electrochemical methods used in (Czerwiński *et al.*, 1999) on pure palladium and in (Hubkowska, Łukaszewski and Czerwiński, 2010) on palladium alloys.

The near-surface hydrogen concentration determined by Barrer was about half that of the metal concentration (H/M ratio of 0.5), however the more modern works listed suggest a H/M ratio of almost 0.9 achieved. If all interstitial sites could be filled the concentration would be significantly higher than these values, however there is no evidence to suggest this is possible. The likelihood of achieving these conditions in a more conventional, practical membrane application is rather low, especially when using group V metals.

The final case that can lead to saturation of the permeating flux is through the downstream desorption limit. The downstream surface limit is reached before complete coverage of the downstream surface (i.e. Θ_d in this case does not equal 1) as for this limit to be applied then $2\delta < \Upsilon$. This limit is proven mathematically in (Pick and Sonnenberg, 1985), however it has been difficult to observe experimentally.

The work of (Causey and Baskes, 1987) suggest if this effect exists it would affect plasma driven permeation measurements, it could also affect the electrochemical methods listed in the previous case study due to the high H/M ratios developed. (Causey and Baskes, 1987) suggest that when hydrogen is implanted into metal at high rates, the concentration of hydrogen found in the bulk will be controlled by the rate of re-emission out of the downstream surface.

If the re-emission rate reaches saturation, then “anomalously large” hydrogen concentrations can be found just below the surface. Causey and Baskes include calculations using the Wang model showing that the rate of desorption predicted by the model was significantly lower than the rate measured experimentally.

Whilst this may initially appear to be problematic this difference can be explained by discrepancies in the desorption activation energy used. The value used by Causey and Baskes was for a small surface coverage; however, at higher surface coverage it has been shown that the activation energy decreases. (Christmann *et al.*, 1974) shows a step decrease in the activation energy for desorption at medium surface coverage on nickel surfaces. This decrease of activation energy has also been demonstrated for other metals, such as platinum (Gudmundsdóttir *et al.*, 2013) and iron (Wang, 2015). By adjusting the calculations to include this lower activation energy, the Arrhenius nature of the model allows for an increase in the desorbed flux predicted by the Wang model; with the new flux being in line with the measured data (Andrew and Haasz, 1992)(Causey and Baskes, 1987).

As briefly mentioned above, the limit testing conducted by Andrew and Haasz and others has limited practical use, especially for typical membrane applications. The purpose of these studies is to give evidence of the robustness of the models, and to give a greater understanding of the underlying processes. What can clearly be seen from the case studies is that a number of physical factors have a profound effect on membrane behaviour, with the membrane thickness, upstream and downstream pressures (concentrations) and the temperature being controllable variables. It is also demonstrated that by varying these parameters it is possible to change the rate determining process for the overall hydrogen flux.

The conditions of interest, and those that will be modelled are significantly more moderate in pressure (and thus hydrogen concentration) and temperature than those required to reach a saturated flux. However, the permeation model utilised in this thesis is not that of Wang but one developed by Ward and Dao which is discussed in detail below.

3.4 The Ward and Dao Hydrogen Permeation Model for Palladium

The model created by Ward and Dao is conceptually similar to the initial model developed by Wang; however, as research interests in the area have intensified a greater understanding of hydrogen permeation has been developed. The model of Ward and Dao leans heavily on this increased understanding by bringing together several elements of other researchers and can generally be viewed as an update or expansion of the Wang model. Whilst the model itself will be referred to as the Ward and Dao permeation model, within this work it is important to stress the contributions of others intertwined by Ward and Dao, as they do themselves within their publication.

Ward and Dao developed this model for use with palladium, however with minor adaption the model is suitable for use with any transition metal, including those found in group Vb. It is stated within the models initial publication (Ward and Dao, 1999) that membrane research has expanded beyond interest in pure palladium alone, with much interest in palladium alloys and group V metals/alloys. Ward and Dao state that diffusion and solubility data is readily available for many of these alloys, but at the time of writing one of the major limitations for using their model was the lack of data on sticking and desorption parameters, and surface-bulk activation barriers (Ward and Dao, 1999). This problem has been mitigated somewhat recently with intensification of research in the area and the increased development of computer simulations, such as density functional theory (DFT) and molecular dynamics simulation (MDS), capable of providing accurate data for desorption, surface-bulk processes and sticking coefficients.

The workings of the model were set out in a 1999 paper entitled "*Model of hydrogen permeation behaviour in palladium membranes*" which has been used as the primary source for this section. The model itself is semi-empirical, with a structure similar to Wang's model complete with the addition of two external mass transfer steps to give seven steps for hydrogen permeation in total:

1. The raw gas (in this case syngas a mixture of hydrogen and the undesired carbon oxides) moves randomly in the vicinity of the membrane.
2. The gas contacts the membrane, with the hydrogen gas dissociating into hydrogen ions and electrons due to the presence of the surface catalyst. Other gases present are not split as readily.
3. The hydrogen ions are adsorbed into the bulk of the membrane material.
4. The hydrogen ions and free electrons diffuse through the membrane bulk.
5. The hydrogen ions are desorbed to the surface of the membrane on the product side.

6. The hydrogen ions and free electrons re-associate into hydrogen molecules.
7. The hydrogen molecules are diffused from the surface of the membrane.

Figure 3.4 below shows the seven-step model in diagram form.

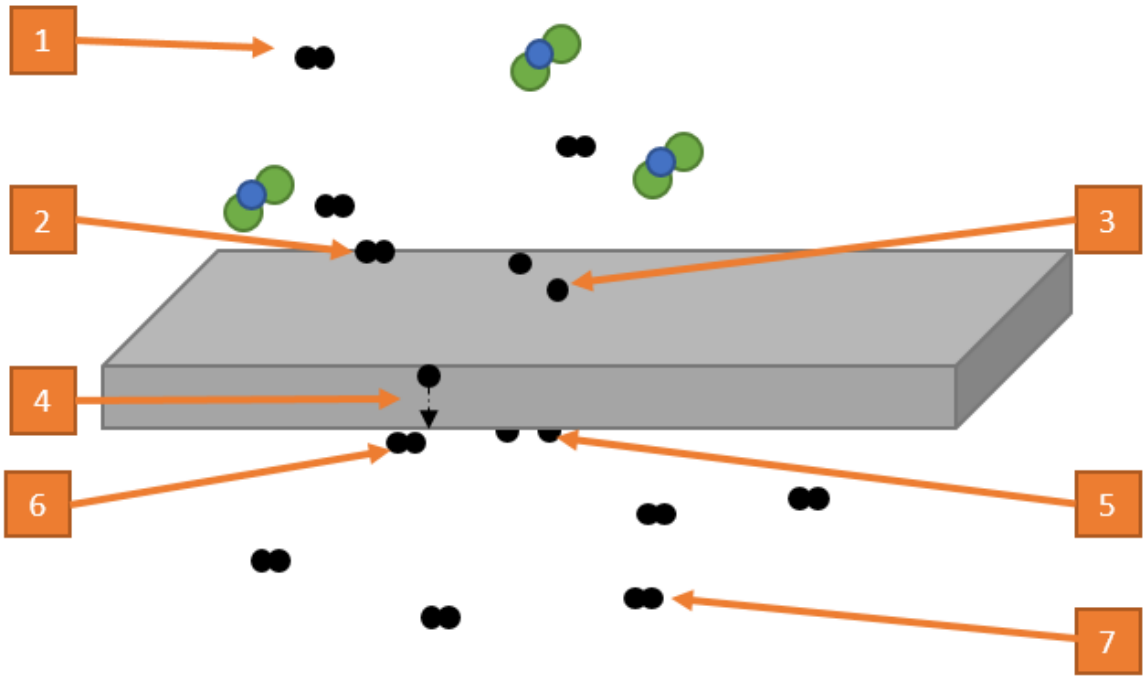

Figure 3.4 – Diagram of the seven-step model for hydrogen diffusion through metal membranes

With the seven steps referred to in later reviews, as discussed previously, including (Ockwig and Nenoff, 2007)(Al-Mufachi, Rees and Steinberger-Wilkens, 2015)(Phair and Badwal, 2006). Once again, like Wang, these seven steps can be utilised to form a number of mass balances at various points throughout the membrane.

The mass balances consist of forward and reverse reactions, where the overall hydrogen permeation rate may be limited by one or multiple of these steps. Figure 3.2 contains a diagram originally found in (Ward and Dao, 1999) and is a schematic representation of the energy levels used to model hydrogen permeation in palladium.

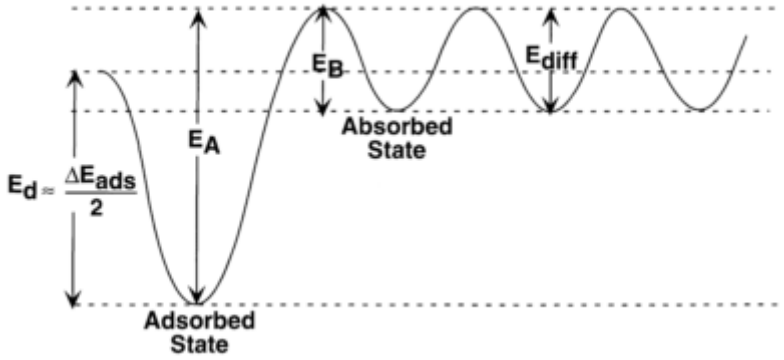

Figure 3.5 – Energy level schematic for hydrogen permeation through palladium, taken from (Ward and Dao, 1999)

The diagram in figure 3.5 shows the activation energy of each process, with E_d being the activation energy for dissociative adsorption, E_A being the activation energy for surface to bulk transition (kJ mol^{-1}), E_B being the activation energy for bulk to surface transition (kJ mol^{-1}) and E_{dif} is the activation energy for diffusion (kJ mol^{-1}). Alongside the references to activation energy included is the heat of adsorption (kJ mol^{-1}), E_d is half the value due to the diatomic nature of the gas. This schematic of the Pd-H system is similar to that of others, (Pick and Sonnenberg, 1985)(Behm, Christmann and Ertl, 1980) and more recently (Gross, 1998) and it shows the activation energies required for each Arrhenius- type step of the Ward and Dao model.

It is worthwhile noting some sources, including (Behm, Christmann and Ertl, 1980), suggest through the use of desorption data that crystalline palladium may possess multiple absorbed surface states for atomic hydrogen. Ward and Dao noted that the inclusion of this would significantly complicate the model for surface to bulk transition, but state that this added complexity would not likely be valuable due to a lack of data for these states. Due to this the model incorporates only a single surface-state approach; this approach appears to be viable due to the accuracy of the model over the temperature range of particular interest to the membrane separations of interest within this work.

Steps One and Seven: Mass Transfer from the Bulk to the Surface

For each stage of the seven-step diffusion model there is an applicable rate equation collated by Ward and Dao. Steps one and seven are responsible external mass transfer, from the bulk of the gas to the surface of the metal. In many instances this step of the model is ignored, so as to focus on the effects of surface versus bulk processes but it has been included here for comprehensiveness.

$$J = 2h(C - C_s) \qquad \text{(Equation 3.30)}$$

Where J is the hydrogen flux ([mol H] m^{-2} s^{-1}); h is a mass transfer coefficient (m s^{-1}) and C/C_s refer to the concentration of hydrogen in the bulk and near to the surface respectively ([mol H] m^{-3}).

When ignoring the external mass transfer steps, it is taken that C and C_s are equal (Ward and Dao, 1999). External mass transfer is not a problem in single gas systems, however in binary (or greater) gas systems poor gas mixing may lead to near surface hydrogen depletion (as a result of hydrogen permeating and other gases being rejected) creating a significant concentration difference from the bulk value.

Step Two: Dissociative Adsorption onto the Metal Surface

The atomic adsorption rate ([mol H] m^{-2} s^{-1}) is given by the following equation:

$$\text{Adsorption rate} = 2S(\Theta)\Gamma \qquad \text{(Equation 3.31)}$$

Where S(Θ) is a coverage dependant sticking coefficient (dimensionless) and Γ is the bombardment rate ([mol H] m^{-2} s^{-1}), with adsorption rate being a product of the two. Logically, a higher rate of bombardment and a lower surface coverage will provide a higher rate of surface adsorption. The factor of two is included due to the need for two surface sites for diatomic adsorption, and S(θ) is dependent on the surface coverage, θ. The bombardment rate is calculated as follows:

$$\Gamma = C_s\left(\frac{RT}{2\pi M_{H2}}\right)^{0.5} \qquad \text{(Equation 3.32)}$$

Where R is the ideal gas constant (J K^{-1} mol^{-1}), T is the temperature (K) and M_{H2} is the molar mass of hydrogen (g mol^{-1}); the bombardment rate is essentially a collision incidence rate and is determined by a combination of kinetic movement factors and the concentration. An increase in gas molecules present (through a higher concentration) or an increase in gas kinetic energy will lead to an increase in bombardment rate ultimately increasing adsorption onto the surface.

The sticking coefficient is somewhat more complex in its nature; with the surface coverage playing an important role in determining the value of S(θ). At low coverage, approaching zero, Langmuir adsorption kinetics can be assumed (Ward and Dao, 1999)(Pick and Sonnenberg, 1985); leading to the expression:

$$\left(\frac{S(\theta)}{S_0}\right)_L = (1-\theta)^2 \qquad \text{(Equation 3.33)}$$

Where S_0 is the initial sticking coefficient at zero coverage (dimensionless), and the $(1-\theta)^2$ term accounts for the need for two adjacent sites to be available for dissociative adsorption. Whilst this term has been utilised in some models, such as the work of Wang, (Andrew and Haasz, 1992) and (Pick and Sonnenberg, 1985) it is of limited use for higher surface coverage. At higher surface coverage, interaction between adsorbed species can impart structural order and this may affect the sticking probability (Behm, Christmann and Ertl, 1980). To deal with this a modified Langmuir adsorption model has been suggested, where the possibility of physisorbed molecules hopping on the surface to find a pair of empty sites to allow for chemisorption has been accounted for (Ward and Dao, 1999). The expression is as follows:

$$\left(\frac{S(\theta)}{S_0}\right) = [1 + K\left(\frac{1}{\theta_{00}} - 1\right)]^{-1} = G(\theta) \qquad \text{(Equation 3.34)}$$

Where K is a constant that is dependent on the probability of adsorption and desorption over empty and occupied sites (dimensionless). The expression G(θ) is an alternative way of displaying the term $S(\theta)/S_0$ utilised later within the model.

Multiple sources place the value of S_0 for clean palladium at near unity (S_0 =1) (Shu *et al.*, 1991)(Pick and Sonnenberg, 1985)(Behm, Christmann and Ertl, 1980); however this may not necessarily be applicable to other metals or alloys.

The term θ_{00} is included as a modification of the surface coverage, with the consideration that two adjacent empty sites are required. The term is calculated based on the quasi-chemical equilibrium approximation (Ward and Dao, 1999), given as:

$$\theta_{00} = 1 - \theta - \frac{2\theta(1-\theta)}{[1-4\theta(1-\theta)\left(1-e^{\frac{-w}{RT}}\right)]^{0.5}+1} \qquad \text{(Equation 3.35)}$$

Where w is the pair-wise interaction energy (kJ mol^{-1}), as described by (Behm, Christmann and Ertl, 1980) and (King and Wells, 1974a). This approximation describes the distribution of surface site concentrations through the equilibrium constant for 2OA → OO + AA, where OO, AA and OA represent pairs of occupied sites, empty sites and occupied-empty sites respectively (King and Wells, 1974b). The site transformation equilibrium can be displayed as:

$$\frac{4N_{OO}N_{AA}}{N_{OA}^2} = e^{(\frac{-w}{RT})} \qquad \text{(Equation 3.36)}$$

Where N_{xx} represents the number of OO, AA and OA pair sites available (mol pairs m^{-2}).

As mentioned above equations 3.34 and 3.35 feed into a modified Langmuir adsorption expression, the expression can be simplified back to the original Langmuir version in the limit K = 1 and w = 0. This limit assumes no interaction between atoms on the surface, hence the reduction of the pair-wise interaction to zero. As smaller values of K correspond to an increased likelihood of hydrogen molecules migrating over the surface to find two adjacent empty sites, a unity value for K suggests a severely limited amount migration by hydrogen across sites.

By varying the K and w values various profiles for the term S/S_0 have been determined by (King and Wells, 1974b), Ward and Dao used values of K = 0.05 and w = 0.5 kcal mol^{-1} (2.09 kJ mol^{-1}) within their publication, citing that (Behm, Christmann and Ertl, 1980) found a good fit experimentally for the sticking coefficients at 170 K, up to a value of θ = 0.6. As is apparent, the temperature used by Behm et al is significantly lower than that of typical membrane operations, including the ones detailed in this thesis. Whilst Ward and Dao note that the appropriate parameter values for the temperature range of interest are likely to be different, it can be seen from the accuracy of their results (in comparison to experimental data) that the values are a close enough approximation for use (Ward and Dao, 1999). Applying these parameter values and comparing the sticking coefficient for palladium calculated against the values predicted using the Langmuir model a significant difference in behaviours can be seen, as shown in figure 3.6.

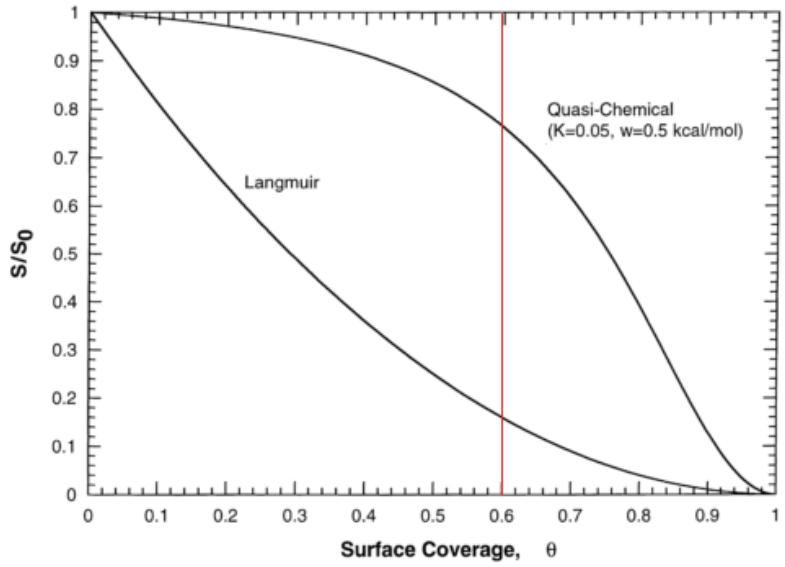

Figure 3.6 – Comparison of calculating sticking coefficients for H_2 on Pd using the Langmuir model and the quasi-chemical method, adapted from (Ward and Dao, 1999)

The red line added to the original plot is included as a visual aid to indicate where agreement between the model predictions and measured values drops off, according to (Behm, Christmann and Ertl, 1980). As S_0 is generally taken as unity both models have the same y-intercept, but it can be clearly seen that

the quasi-chemical plot predicts the retention of a higher S value for increasing coverage. This is due to the surface interactions represented by K and w; by accounting for the migration of hydrogen across the surface it can be seen that the chances of hydrogen sticking to the surface are increased due to the chance for migration to a pair of empty sites. As the Langmuir method simplifies this with no surface interaction at increased coverage, where the chances of instantaneously finding a pair of empty sites are lower, the predicted sticking coefficient is obviously lower.

(Behm, Christmann and Ertl, 1980), the source for the K and w values used by Ward and Dao also provides an alternative calculation for S, which can be written as:

$$\frac{S}{S_0} = \frac{(1-\Theta)}{(1-K\Theta)} \qquad \text{(Equation 3.37)}$$

Equation 3.37 is a first order equation and under the conditions specified (T = 170 K), with a K value of 0.75; the model is accurate up to Θ = 1. This K value is significantly higher than the one used by Ward and Dao, and would suggest a very high likelihood of surface migration by hydrogen. The reason for this additional suggested mechanism is due to the variance from second order behaviour at high concentrations; where equation 3.34 under-represents the term S/S_0.

Figure 3.7 below shows plots for both the pseudo first order model (equation 3.37) and the second order model (equations 3.34 and 3.35).

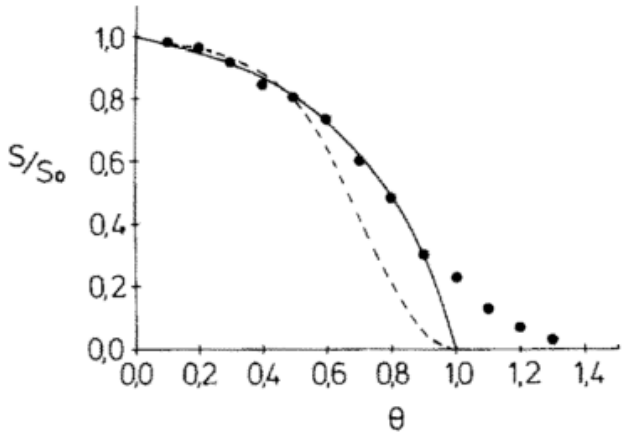

Figure 3.7 – S values for H_2 on Pd at T = 170 K. Experimental data (dots) plotted against first order (solid line) and second order (dashed line) precursor models. Taken from (Behm, Christmann and Ertl, 1980)

Ward and Dao state that their use of the second order model is due to "the solid theoretical basis under variable coverage" (Ward and Dao, 1999). Therefore, it could be assumed that the pseudo-first order case may only be applicable in the specific conditions tested by Behm et al, whilst the second

order model gives a more accurate prediction of higher temperature behaviour. As the methodology of Ward and Dao appears to hold true the second order mechanics have been used within this work.

Behm et al also explain that for even higher coverage ($\Theta > 1$), the adsorption energy decreases strongly and that the derived sticking coefficients are already affected by transfer from the surface (either into the bulk or desorption) to the point that no further modelling was possible. This behaviour may be explainable by considering the work of Wang and then of (Andrew and Haasz, 1992); where in extreme conditions hydrogen can be instantaneously absorbed into the bulk.

It is also worthwhile to note that this model assumes no activation energy for the sticking of hydrogen to the surface, as there is no activation energy term included in the sticking term expression (and as displayed in figure 3.2). This holds true to the predictions of many sources (Ward and Dao, 1999)(Pick and Sonnenberg, 1985)(Behm, Christmann and Ertl, 1980), but may not be applicable to non-palladium based membranes or surface catalysts.

Step Three: Surface-to-Bulk Metal Transition

Upon adsorption to the surface of the membrane, hydrogen can either be desorbed back to the gaseous state or be absorbed into the bulk. The transition rate of hydrogen from the surface to bulk ([mol H] m^{-2} s^{-1}) is given as follows:

$$\mathrm{S-B\ rate} = \mathrm{N_s N_b \nu_d \Theta (1 - X_s)} \qquad \text{(Equation 3.38)}$$

Where N_s is the metal surface atom concentration ([mol Pd] m^{-2}), N_b is the bulk metal atom concentration ([mol Pd] m^{-3}), ν_d is the rate constant for surface to bulk transfer (m^3 [mol H]$^{-1}$ s^{-1}) and X_s is the hydrogen-metal atomic ratio in the bulk metal (dimensionless).

Each factor of the surface-to-bulk rate equation is logical and the equation can be split into three broader factors. The first factor is surface dependent, by including the surface coverage and multiplying by the total number of surface sites (θ . N_s) thus giving a value for the actual surface coverage. The second factor is bulk dependent, by including the total number of bulk sites and multiplying by the factor currently unoccupied (N_b . [1 – X_s]) thus giving the availability of sites for a surface hydrogen atom to jump to the bulk. The final factor is the rate constant governing the process, where the rate constant (ν_d) is calculated through the use of an Arrhenius-type equation:

$$\nu_d = \nu_0 e^{\frac{-E_A}{RT}} \qquad \text{(Equation 3.39)}$$

Where v_0 is the pre-exponential factor (m^3 [mol H]$^{-1}$ s^{-1}) and E_A is the activation energy for surface to bulk transfer (kJ [mol H]$^{-1}$). The activation energy E_A can be estimated through the use of the following equation:

$$E_A - E_B = \frac{\Delta E_{ad} - \Delta E_{ab}}{2} \qquad \text{(Equation 3.40)}$$

Where E_B is the activation energy for bulk-to-surface transition (kJ [mol H]$^{-1}$), ΔE_{ad} is the heat of adsorption (kJ [mol H]$^{-1}$) and ΔE_{ab} is the heat of absorption (dissolution) (kJ [mol H]$^{-1}$). Equation 3.40 is used by (Ward and Dao, 1999), this would suggest a lack of experimentally determined values for E_A but the approximation appears to hold true. Ward and Dao used values for ΔE_{ad} and ΔE_{ab} published in (Behm, Christmann and Ertl, 1980).

It is interesting to note that equation 3.40 predicts that E_A will always be greater than E_B by a factor determined by surface processes; with both dissociation and adsorptive processes having an impact. Obviously, in the instance of bulk-to-surface transition hydrogen is already dissociated and absorbed therefore this factor is not applied. E_B is given the same value as E_{diff}, the activation energy for bulk diffusion; this is logical as in theory there is no difference between hydrogen jumping from a bulk site to another bulk site or to a surface site.

From this it could be determined that:

$$E_B = E_D = E_A + \frac{\Delta E_{ad} - \Delta E_{ab}}{2} \qquad \text{(Equation 3.41)}$$

Whilst this is not explicitly given by Ward and Dao, the relationship between the activation energies is simple to infer from the equations and from figure 3.2. The impact of surface interactions is made clear through equation 3.41, where it can be seen that by reducing the energy required for adsorption and dissociative absorption the value for E_A can be reduced towards the level of E_D and E_B, the diffusive processes. It is important to note however, that this does not necessarily mean that the permeated hydrogen flux is limited through adsorption as will be discussed later.

The values for N_B and N_S are entirely dependent on the metal used for the membrane and/or the surface catalyst, Ward and Dao used the following equations for determining N_S and N_B for palladium.

$$N_b = \frac{\rho_m}{M_m} \qquad \text{(Equation 3.42)}$$

$$N_s = N_b^{\frac{2}{3}} / N_{av}^{\frac{1}{3}} \qquad \text{(Equation 3.43)}$$

Where ρ_m is the membrane metal density (g m^{-3}) and M_m is the membrane metal atomic mass (g mol^{-1}), with palladium being the metal used by Ward and Dao. For calculating N_s the Avogadro number is used to determine the number of surface sites available. This expression is valid for any two-dimensional plane within the metal lattice (McLeod, 2008), however it is of most interest for calculating surface conditions.

Equations 3.42 and 3.43 show how the membrane material can have an impact on interaction rates; an increased density and a decreased molar mass will result in an increase in bulk sites, alongside an increase in surface sites. The impact of varying this will be discussed later within this report, upon completion of the model outline.

Step Four: Bulk Diffusion

The fourth step in the model is the atomic diffusion of hydrogen through the bulk of the membrane material. Ward and Dao model the diffusive flux/rate ([mol H] m^{-2} s^{-1}) with the use of a one-dimensional expression derived from Fick's first law:

$$\text{Diffusion flux} = \frac{DN_b(X_1 - X_2)}{t} \qquad \text{(Equation 3.44)}$$

Where D and t are the diffusion coefficient (m^2 s^{-1}) and membrane thickness (m) as previously described when discussing the Wang model. X_1 and X_2 are used by Ward and Dao to differentiate the hydrogen-metal ratio adjacent to the high and low pressure surfaces (upstream and downstream respectively), this notation is interchangeable with the notation X_u and X_d used within this thesis.

The diffusion coefficient used is determined through the use of an Arrhenius-type equation:

$$D = D_0 e^{\frac{-E_{diff}}{RT}} \qquad \text{(Equation 3.45)}$$

Where E_{diff} has been previously described and D_0 is the pre-exponential factor for bulk diffusion (m^2 s^{-1}). Data for hydrogen diffusion has been reported widely for various metals including palladium (Shu *et al.*, 1991)(McLeod, 2008)(Lewis *et al.*, 2013) and group V metals (Rogan and Lagos, 1999)(Ozaki *et al.*, 2003). These sources provide a multitude of values for D_0, E_{diff} and D, with reasonable consistency. Ward and Dao utilised data that was collected at temperatures in the correct range for membrane operation (260 – 640 °C) (Ward and Dao, 1999).

Studying the diffusion rate equation, several factors can appear to have an effect on hydrogen permeation rate. Immediately obvious is the impact of the membrane thickness, as a thicker

membrane will reduce the permeated flux; assuming that all other factors are kept constant the change in membrane thickness follows a reciprocal pattern, if plotted graphically the relationship is displayed as a rectangular hyperbola. As expected, a thinner membrane will produce a larger diffusive flux with this typically resulting in a larger overall permeating flux due to bulk diffusion being the rate limiting step in most typical "thick" membrane operations.

As with all the Arrhenius-type relationships discussed within this section the temperature can be seen to have an impact on the rate constant and thus the rate itself, along with the upstream and downstream pressure due to their involvement in the determination of the values X_1 and X_2. The bulk metal atom concentration is also present in equation 3.44; conceptually this makes sense as the number of sites available for diffusion will have an impact on the overall rate of diffusion.

Step Five: Bulk Metal-to-Surface Transition

After diffusing across the bulk, hydrogen atoms will diffuse to the surface. Ward and Dao modelled the bulk-to-surface transition rate with the following equation:

$$\mathrm{B-S\ rate} = \mathrm{N_s N_b X_s}(1-\Theta)\beta_\mathrm{d} \qquad \text{(Equation 3.46)}$$

Where β_d is the bulk-to-surface rate constant (m^3 [mol H]$^{-1}$ s^{-1}), calculated through the following Arrhenius-type equation:

$$\beta_d = \beta_0 e^{\frac{-E_B}{RT}} \qquad \text{(Equation 3.47)}$$

Where E_B is the previously defined activation energy for bulk-to-surface transfer and β_0 (m^3 [mol H]$^{-1}$ s^{-1}) is the pre-exponential factor for bulk-to-surface transfer. As previously mentioned, E_B is assumed to be equal to E_{diff} by Ward and Dao, with this assumption also used in this work; this is based on an assumption that the activation barrier to the surface should not be substantially different than the bulk diffusion activation barrier (Ward and Dao, 1999). As no evidence of kinetic limitations in the bulk-to-surface transfer have been found in desorption studies this assumption appears to hold true.

As one might expect, Equation 3.46 shares symmetry with equation 3.38, the surface-to-bulk transfer rate. However, two key differences can be highlighted the first of which being the different rate constant (β_d in place of ν_d) and the second being the switching of X_s and θ. This switching of the bulk (X_s) and surface (θ) ratio factors is due to the fact that this process is obviously the physical reverse of step three. In this step, the hydrogen trapped in the bulk near the surface (represented by the factor

N_bX_s) requires a vacant surface site for transition (with the vacant site availability determined by the factor $N_s[1-\theta]$).

Ward and Dao state that the pre-exponential factors β_0 and ν_0 can be seen as being related to the jump attempt frequencies of hydrogen for the surface-bulk-surface transitions (Ward and Dao, 1999). The relationship between β_0 and ν_0 will be discussed later within this section, but first a method for estimating the value of β_0 is to be detailed.

A reasonable value for β_0 can be attained analogous to solid-state diffusion theory; here the diffusion coefficient (D) can be expressed as:

$$D = \alpha_c a^2 \Gamma_j \qquad \text{(Equation 3.48)}$$

This is discussed in greater detail by (Borg and Dienes, 1988). The diffusion coefficient is given in terms of α_c, which is a coefficient determined by the geometric relationship between interstitial sites (dimensionless); a, which is the lattice parameter (m) and Γ_j the diffusive jump frequency (s^{-1}). The terms α and a are geometrical in nature dependent on the membrane material, whilst the diffusive jump frequency gives detail on the kinetic activity of hydrogen within the membrane. The jump frequency can be represented through an Arrhenius-type relationship:

$$\Gamma_j = \Gamma_{j0} e^{\frac{-E_j}{RT}} \qquad \text{(Equation 3.49)}$$

Where Γ_{j0} is the pre-exponential factor (s^{-1}) and E_j is the activation energy for a jump (kJ mol^{-1}), Ward and Dao show a relationship in which the pre-exponential factors Γ_{j0} and D_0 can be related:

$$\Gamma_{j0} = \frac{12 D_0}{a^2} \qquad \text{(Equation 3.50)}$$

Equation 3.50 can be solved with data readily available for most pure metals and many alloys of interest for membrane separation. From this, it can be expected that the jump frequency from the bulk to the surface will be similar to that for inter-bulk diffusion; as the hydrogen atom is jumping from a bulk interstitial site in both instances. For diffusion between planes, it is reasonable to assume that one third of jumps will be into the next plane; with one third of jumps being to other sites within the same plane and the final third being in the opposite direction to that desired.

Thus, in the bulk plane adjacent to the surface the bulk diffusive jump (BDJ) rate for jumps to the surface can be given as:

$$\text{BDJ rate} = \frac{1}{3} N_s X_s \Gamma_j \qquad \text{(Equation 3.51)}$$

Where the area concentration of hydrogen atoms in the bulk adjacent to the surface (N_sX_s) can be equated to equation 3.46 to give:

$$\frac{1}{3}\Gamma_{j0} = N_b(1-\Theta)\beta_0 \qquad \text{(Equation 3.52)}$$

If θ << 1, the surface coverage does not inhibit the bulk-to-surface transition allowing for the solving of the equation to give a value for β_0 (Ward and Dao, 1999).

Step Six: Re-combinative Desorption from the Metal Surface

Upon reaching the surface hydrogen atoms are reformed into molecules before being expelled from the membrane. Before the work of Ward and Dao several groups (Pick and Sonnenberg, 1985)(Pick, 1981)(Ash and Barrer, 1959) had described the desorption rate as follows:

$$\text{desorption rate} = 2k_d N_s^2 \Theta^2 \qquad \text{(Equation 3.53)}$$

Where k_d is the activated rate constant (m^2 mol^{-1} s^{-1}); the inclusion of the factor of two is due to the need for two hydrogen atoms to be available for desorption and the θ^2 factor is the product of the need for two adjacent sites to be occupied for recombination.

The value for k_d is determined through the use of an Arrhenius type equation:

$$k_d = k_0 e^{\frac{-2E_d}{RT}} \qquad \text{(Equation 3.54)}$$

Where k_0 is the pre-exponential factor for the desorption rate (m^2 [mol H]$^{-1}$ s^{-1}) and E_d is the activation energy for desorption (kJ mol^{-1}), once again the factor of two is included due to the diatomic nature of desorption.

Ward and Dao state that the second order rate equation given above is limited to use with only small values of θ (i.e. little surface coverage), with greater coverage being better described by the pseudo-first order model of (Behm, Christmann and Ertl, 1980). A more general term for the desorption rate is given as (Ward and Dao, 1999):

$$\text{desorption rate} = 2k_d'' N_{AA} \qquad \text{(Equation 3.55)}$$

Where k_d" is the modified rate constant (s^{-1}) and N_{AA} is the concentration of occupied nearest neighbour sites (mol pairs m^{-2}) as discussed above and by (Behm, Christmann and Ertl, 1980). The modified rate constant can be related to the original constant:

$$k_d^{"} = \frac{k_d N_s}{2} \qquad \text{(Equation 3.56)}$$

This relationship is governed by the need for equation 3.55 to reduce to equation 3.53 as the system approaches the limit of θ = 0 (or w = 0) (Ward and Dao, 1999).

A figure for N_{AA} can be calculated through the use of the following expression:

$$N_{AA} = \frac{zN_s\Theta}{2}F(\Theta) \qquad \text{(Equation 3.57)}$$

With N_s and θ previously described, z is the number of nearest neighbour sites on the surface and F(θ) is the coverage factor calculated as follows:

$$F(\Theta) = (1 - \frac{2-2\Theta}{[1-4\Theta(1-\Theta)\left(1-e^{\frac{-w}{RT}}\right)]^{0.5}+1}) \qquad \text{(Equation 3.58)}$$

Whilst not discussed by Ward and Dao, the factor $N_s\theta$ gives an indication of the quantity of hydrogen present on the surface; with z providing an indication on the geometrical layout of the sites; a larger value for z would indicate more interstitial connectivity of surface sites. The factor F(θ) is similar to the factor G(θ) or S/S_0 for adsorption and gives an indication of the interaction between hydrogen atoms on the surface. Once again the pair-wise interaction energy (w) is a factor to be considered, with a larger interaction energy resulting in a reduced coverage factor and thus a reduced number of pairs of occupied active sites.

Figure 3.2 suggests that the activation energy for desorption (E_d) is approximately equal to the heat of adsorption (Ward and Dao, 1999); reported figures for this energy vary somewhat dependent on the crystal facet. Values for the heat of adsorption can be found in (Behm, Christmann and Ertl, 1980) amongst others and are found to vary between 83 - 112 kJ $[mol\ H_2]^{-1}$ however some sources suggest a weaker adsorption energy of 29 – 41 kJ $[mol\ H_2]^{-1}$ for models possessing two surface energy levels. Ward and Dao modelled using only a single level model and thus utilised a value for E_d equal to half of the energy of adsorption to account for hydrogen desorbing as a single atom; however, as the calculation for k_d contains a factor of $2E_d$ due to the need for recombination this appears to be of purely academic in nature.

The Relationship Between the Pre-Exponential Factors ν_0 and β_0

There is no well-defined relationship between the bulk diffusional jump frequency and the surface-to-bulk metal transition frequency, this is due to the vibrational state of a hydrogen atom on the surface being different to that in the bulk metal (Ward and Dao, 1999).

Ward and Dao overcame this problem by comparing H/Pd solubility data, gathered from literature sources, to theoretical equilibrium relationships to estimate a value for the ratio of β_0/ν_0. By employing this approach, the model calculations are reduced to empirically observed Sievert's law behaviour within the limit of diffusion-limited permeation (Ward and Dao, 1999). The principles utilised by Ward and Dao relate kinetic parameters to equilibrium solubility results; where at equilibrium, the adsorption and desorption rates (equations 3.31 and 3.55) are equal. Alongside this, the surface-bulk-surface transition rates (equations 3.38 and 3.46) are also taken to be equal, equating and combining these expressions (whilst applying the ideal gas law) gives the following relationship:

$$\frac{1-X}{X}P^{0.5} = \frac{\beta_0 k_0 N_s (2\pi M_H RT)^{0.25}}{\nu_0 S_0^{0.5}} \left(\frac{F(\Theta)(1-\Theta)^2}{G(\Theta)\Theta}\right)^{0.5} e^{\frac{E_A - E_B - E_d}{RT}} \qquad \text{(Equation 3.59)}$$

The elements of Sievert's law can be spotted within equation 3.59 ($P^{0.5}$), with the hydrogen concentration in the metal and the hydrogen partial pressure replaced with the relevant terms for the conditions assumed.

This can be compared with the thermodynamic relationship for equilibrium in hydrogen dissolution and absorption into the membrane. Where $0.5H_2$ (gas) $\leftrightarrow$ H (absorbed), this can be expressed thermodynamically as follows:

$$RT \ln P_{H_2}^{0.5} = \Delta\overline{G_H} \qquad \text{(Equation 3.60)}$$

Where $\Delta\overline{G_H}$ is the relative partial Gibbs free energy of dissolution (kJ [mol H]$^{-1}$); this can be written as:

$$\Delta\overline{G_H} = \Delta\overline{H_H^0} - T\Delta\bar{S}_H^0 + RT\ln\left(\frac{X}{1-X}\right) + 2XW_{HH} \qquad \text{(Equation 3.61)}$$

Where $\Delta\bar{S}_H^0$ (kJ [mol H]$^{-1}$) and $\Delta\overline{H_H^0}$ (kJ [mol H]$^{-1}$) are the relative partial molar entropy and enthalpy respectively at infinite dilution. W_{HH} is a term that accounts for hydrogen interactions in the solid (kJ [mol H]$^{-1}$), which causes deviation from the ideal Gibbs energy value (somewhat similar to the parameter w for surface hydrogen). Combining equations 3.60 and 3.61 gives:

$$RT \ln\left(P_{H_2}^{0.5}\frac{X}{1-X}\right) = \Delta\overline{H_H^0} - T\Delta\bar{S}_H^0 + RT\ln\left(\frac{X}{1-X}\right) + 2XW_{HH} \qquad \text{(Equation 3.62)}$$

For X<< 1, which is a reasonable approximation for many membrane permeation conditions the interaction term is negligible and the left hand side simplifies to $RT\ln(P^{0.5}/X)$ (Ward and Dao, 1999). This can be written as Sieverts constant, which is essentially the rate constant for the absorption of hydrogen into the metallic membrane. Thus K_s can be expressed as:

$$K_s = \frac{P_{H_2}^{0.5}}{X} \qquad \text{(Equation 3.63)}$$

The Sievert constant can also be defined as the inverse of the above equation, so for values of X << 1, K_s can also be expressed as:

$$K_s = e^{\left(\frac{\overline{\Delta H_H^0}}{RT} - \frac{\Delta \bar{S}_H^0}{R}\right)} \qquad \text{(Equation 3.64)}$$

At this point Ward and Dao equate the right hand side of equation 3.64 with the earlier developed equation 3.59 to give:

$$\frac{\beta_0 k_0^{0.5} N_s (2\pi MRT)^{0.25}}{\nu_0 S_0^{0.5}} \left(\frac{F(\Theta)(1-\Theta)^2}{G(\Theta)\Theta}\right)^{0.5} e^{\frac{E_A - E_B - E_d}{RT}} = e^{\left(\frac{\overline{\Delta H_H^0}}{RT} - \frac{\Delta \bar{S}_H^0}{R}\right)} \qquad \text{(Equation 3.65)}$$

Provided that X << 1; the activation energies from both sides of the equation are deemed to be equal, allowing for a simpler expression for the β_0/ν_0 ratio to be given:

$$\frac{\beta_0}{\nu_0} = \frac{Q}{T^{0.25}} \left(\frac{G(\Theta)\Theta}{F(\Theta)(1-\Theta)^2}\right)^{0.5} \qquad \text{(Equation 3.65)}$$

Where Q is used to represent the constant parameters:

$$Q = \frac{S_0^{0.5}}{k_0^{0.5} N_s (2\pi M_H R)^{0.25}} \qquad \text{(Equation 3.66)}$$

This expression is not given by Ward and Dao, as they model only for palladium where they give Q = 10.154. Ward and Dao also state that by substituting in the value for β_0 into equation 3.65 they find the β_0/ν_0 ratio to vary between 2 to 7.5 for the conditions modelled.

Utilising the Model to Produce Flux Data

As described in the description of the Wang model, and briefly mentioned at the beginning of this section the flux is determined through the use of a number of mass balance equations, the locations of the mass balances are shown on figure 3.8.

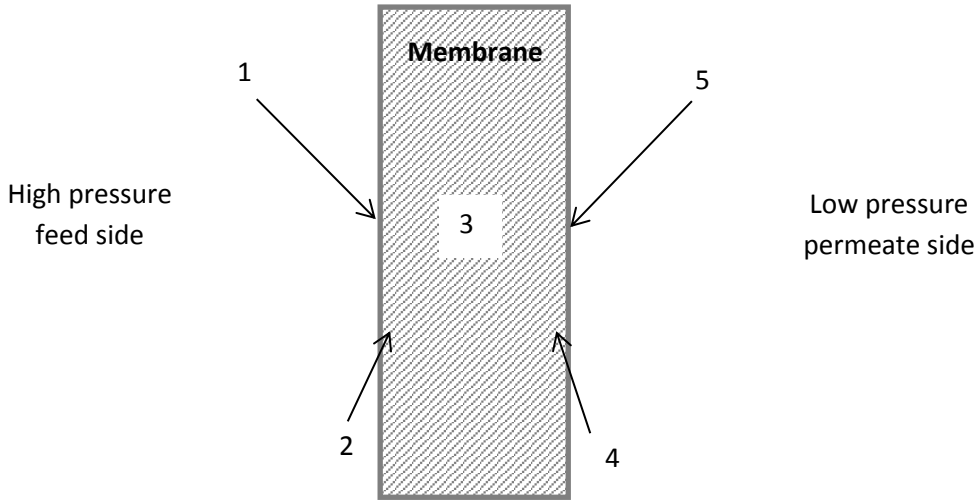

Figure 3.8 – Diagram showing locations of the five mass balances utilised for flux prediction

The mass balances at each of these points are given as follows:

$$1)\ J = 2S_H(\Theta_H)\Gamma_H - 2k_d^{''}N_{AA(H)} \qquad \text{(Equation 3.67)}$$

$$2)\ J = N_s N_b \nu_d \Theta_H (1 - X_H) - N_s N_b X_H (1 - \Theta_H)\beta_d \qquad \text{(Equation 3.68)}$$

$$3)\ J = \frac{DN_b(X_1 - X_2)}{\Delta z} \qquad \text{(Equation 3.69)}$$

$$4)\ J = N_s N_b X_L (1 - \Theta_L)\beta_d - N_s N_b \nu_d \Theta_L (1 - X_L) \qquad \text{(Equation 3.70)}$$

$$5)\ J = 2k_d^{''}N_{AA(L)} - 2S_L(\Theta_L)\Gamma_L \qquad \text{(Equation 3.71)}$$

A more detailed methodology for solving the model will be given later in chapter five, but in brief Ward and Dao state that the model is to be solved in sequential steps using an iterative method. By selecting a partial pressure (P_u) for hydrogen, iterative steps can be taken to calculate a desired downstream hydrogen partial pressure (P_d). In sequence, P_u is used to calculate C_u/C_{us} leading to calculating Θ_u, X_u, X_d, Θ_d, C_{ds}/C_d and finally P_d through the use of approximating the flux in each of the five mass equations. For steady state flow, the flux calculated in equations 3.67 to 3.71 must be equal. If the calculated downstream pressure does not match the target value, adjust the estimated flux appropriately and run the simulation again.

Accuracy of the Model

Ward and Dao provide a plot containing the diffusion-limited flux data calculated using the model for various thicknesses of palladium membranes, overlaid onto this chart is experimental data for various

membrane thicknesses, collected from other publications. The chart has been included as figure 3.9 below.

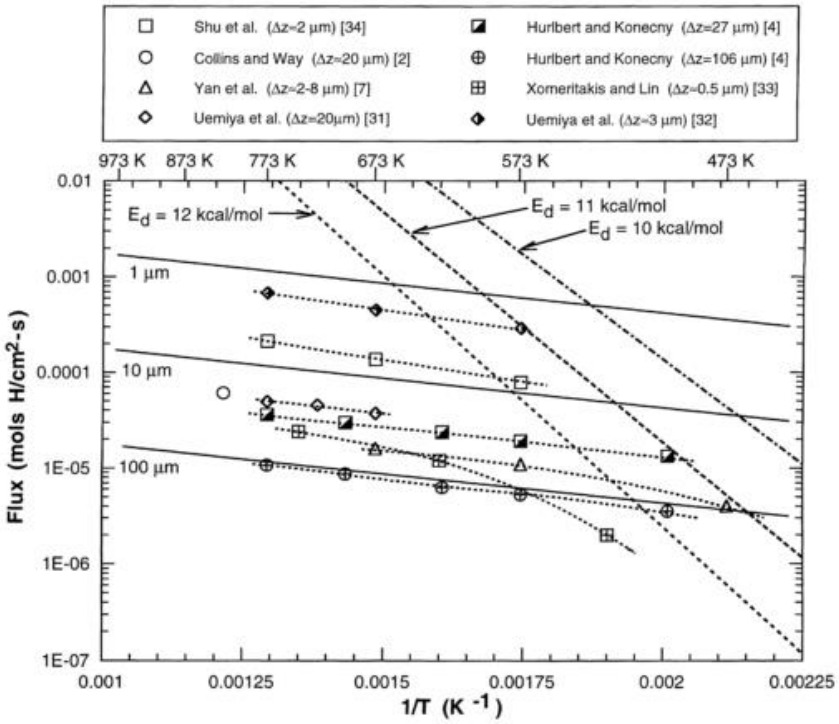

Figure 3.9 – Diffusion limited fluxes for various membrane thicknesses; values predicted using the Ward-Dao model are (solid lines) are compared to experimental fluxes (dashed lines and data points). Sourced from (Ward and Dao, 1999)

As can be seen a reasonable consensus is present between predicted fluxes and the experimental data points available, although in some instances it is hard to compare the data accurately as only 1, 10 and 100 μm models are included. The palladium membranes tested as part of this thesis are of 100 μm thickness, it can be seen that the model is accurate over the temperature range tested (300 – 600 °C) due to the similarity of flux when compared to a 106 μm thick experimentally tested membrane, used in (Hurlbert and Konecny, 1961).

The accuracy of the model predictions can also be attested due to its continued use by other researchers, including (McLeod, 2008)(Gabitto and Tsouris, 2008)(Caravella, Barbieri and Drioli, 2008)(Boon *et al.*, 2015), alongside references to the work in (Hulme *et al.*, 2011)(Dunbar, 2015)(Dolan, McLennan and Way, 2012)(Tsai *et al.*, 2015) amongst other sources.

3.5 Adjustments to the Ward and Dao Model

As mentioned above, adjustments and advancements have been made to the model presented by Ward and Dao.

The work of (McLeod, 2008) draws heavily from the work of Ward and Dao; where the model forms a central tenant of the thesis presented. Whilst not explicitly stated by McLeod, some of the functions within the model are presented differently from the original publication.

McLeod presents an alternative method for calculating the bulk-to-surface transition rate, giving the following rate equation:

$$\mathrm{B-S\ rate} = \frac{1}{3} N_S \Gamma_j X \qquad \text{(Equation 3.72)}$$

Where Γ_j is the jump frequency (s^{-1}), this rate equation is derived from the same thinking utilised by Ward and Dao where solid-state diffusion theory is employed to derive a relationship. Before discussing the equation given, it is worthwhile to give McLeod's derivation of the jump frequency:

$$D = \frac{\Gamma_j a^2}{12} \rightarrow \Gamma_j = \frac{12D}{a^2} \qquad \text{(Equation 3.73)}$$

With the factor β_0 (for calculation of ν_0) being equated as follows:

$$\beta_0 = \frac{4D_0}{a^2} \qquad \text{(Equation 3.74)}$$

Where equation 3.74 is derived from combining the reaction rate derived by McLeod and the original rate equation given by Ward and Dao; the result is a value for β_0 that varies by a factor of 10, with units of s^{-1} instead of (cm^3 [mol H]$^{-1}$ s^{-1}).

Returning to equation 3.72, McLeod suggests through the use of solid-state theory that the likelihood of a jump into the next plane is 1/3 in the same manner as Ward and Dao did. However, McLeod appears to give no consideration to current surface coverage (1-θ) or the density of available sites in the bulk (N_b). The expulsion of the N_b term would suggest that McLeod assumes that the jump frequency (and its dependence on the diffusion coefficient and lattice parameter) is sufficiently membrane and condition specific to combine with X to give an indication of the total amount of hydrogen present attempting to diffuse to the surface. For the removal of the (1-θ) term from the equation, this would suggest that McLeod assumes that surface coverage is significantly low enough to not be a factor; this assumption could be made if modelling the downstream side as a vacuum or

near vacuum. It must be noted that the results McLeod present for Pd and Pd-Ag membranes suggest reasonable agreement with available experimental data, validating the assumptions made to a degree.

Whilst McLeod makes seemingly minor changes to the model; others such as (Gabitto and Tsouris, 2008) and (Caravella, Barbieri and Drioli, 2008) make significant changes to factor in porous support layers and binary gas feed mixtures.

Beginning with (Gabitto and Tsouris, 2008), the work outlines a combination of the Ward and Dao model with the work of (Burggraaf and Cot, 1996); where an expression is proposed to combine the effects of Knudsen flow, viscous flow and transition through porous media. As this thesis is primarily concerned with thick, unsupported membranes only a cursory overview of the work of (Burggraaf and Cot, 1996) is included. By combining the aforementioned porous diffusion models Burggraaf developed the following flux expression:

$$\mathrm{J} = -\frac{\varepsilon}{\tau}(\mathrm{Ar}^2\mathrm{P_m} + \mathrm{B\ r})\frac{\Delta \mathrm{P}}{\mathrm{t_p}} \qquad \text{(Equation 3.75)}$$

Where ε is the support porosity, τ is the tortuosity, r is the characteristic pore diameter (m), t_p is the porous layer thickness (m), P_m is the mean pressure (average of P_u and P_d) (Pa), and finally A and B are defined as the following:

$$A = \frac{1}{8\mu RT} \qquad \text{(Equation 3.76)}$$

$$B = \left(\frac{2}{3\theta_k}\right)\sqrt{\frac{8}{\pi RTM_{H2}}} \qquad \text{(Equation 3.77)}$$

Where θ_k is the Knudsen surface coverage and μ is the gas viscosity (mPa s^{-1}); the flux derived here can then be used to generate a value for c_u (or c_{su}) in the Ward and Dao model. No obvious deviations from the Ward and Dao model can be observed in terms of calculating the permeating flux.

The model is set up in a near identical way to the original model by Ward and Dao, where a number of mass balances are used to derive a flux through iteration. The effect of the support layer can be seen clearly from the results published, with a lower hydrogen flux developed for a thicker porous support layer.

(Caravella, Barbieri and Drioli, 2008) also builds on the work of Ward and Dao, claiming to improve the original model by considering “several elementary steps of the permeation process” for self supported membranes. Beyond this, the model is also modified to deal with multi-component gases utilising the Stefan-Maxwell equations to generate external mass transfer data, with adjustments made for the modelling of supported membranes also.

The development of the Ward and Dao model in (Caravella, Barbieri and Drioli, 2008) is extensive; however as highlighted by the authors the model uses the same mechanisms for adsorption and desorption and surface-bulk-surface transitions as Ward and Dao. There are however some noticeable differences presented in the model, arguably the most radical of which being the change in calculation for the rate of diffusion. Ward and Dao model diffusion through the use of a concentration gradient, whilst Caravella et al model diffusion with the use of a chemical potential gradient.

(Caravella, Barbieri and Drioli, 2008) give the diffusion of hydrogen through the bulk as:

$$J = -N_b D \psi_H \frac{\partial X}{\partial t} \qquad \text{(Equation 3.78)}$$

Where the factor ψ_H is a thermodynamic factor, calculated as follows:

$$\psi_H = 1 + X\frac{\partial \ln \gamma_H}{\partial X} = \frac{X}{RT}\frac{\partial \mu_h}{\partial X} \qquad \text{(Equation 3.79)}$$

Where γ_H is an activity coefficient (dimensionless) and is related to the hydrogen chemical potential (μ_H, kJ mol^{-1}) through the expression given in equation 3.79. The chemical potential is calculated using the following equation:

$$\mu_H = \mu_H^0 + RT \ln\left(\frac{X}{1-X}\right) + 2XW_{HH} - \overline{V_H}\,\sigma \qquad \text{(Equation 3.80)}$$

The term μ_H^0 is the chemical potential at infinite dilution (i.e. X → 0) (kJ mol^{-1}), and the last term of the equation (σ, Pa) accounts for crystalline deformation due to the stress caused by atomic hydrogen diffusion, also referred to as the hydrostatic pressure of hydrogen in the metal lattice.

This elastic deformation becomes stronger as hydrogen concentration increases with the term being negligible for dilute systems (Caravella, Barbieri and Drioli, 2008). The value of σ can be calculated using equation 3.81, this term (not included by Ward and Dao in the original model) is useful as it provides inclusion of the observed physical phenomenon of hydrogen damage. The damage caused at high hydrogen solubilities can result in operational failure, as discussed in chapter two.

$$\frac{\partial \sigma}{\partial t} = -\frac{2Y\overline{V_H}\,N_b}{3}\frac{\partial X}{\partial t} \qquad \text{(Equation 3.81)}$$

Where Y is the stress parameter (Pa). A full derivation of the final flux terms can be found in (Caravella, Barbieri and Drioli, 2008), with the end result being as follows:

$$J = \frac{N_b D}{t}\left[\ln\left(\frac{1-X_1}{1-X_2}\right) + \left(\frac{W_{HH}}{RT} + \frac{N_b Y \overline{V_H^2}}{3RT}\right)(X_1^2 - X_2^2)\right] \qquad \text{(Equation 3.82)}$$

Equation 3.82 is an extension of equation 3.78, showing the factors that affect the parameter ψ_H. The equation would suggest the bulk diffusive rate is dependent on the concentration gradient (analogous to Ward and Dao) but also includes metal-lattice factors to account for distortion. This distortion will ultimately have an effect on the evolved flux at high hydrogen concentration, as distortion will lead to changes in the lattice structure and changes to the available interstitial sites. These changes are likely to lead to a retardation of the evolved flux as represented in the above equation.

For dilute systems (X << 1) equation 3.82 can be simplified as ψ_H approaches unity, with the result becoming:

$$J = \frac{-DN_b(X_1 - X_2)}{t} \qquad \text{(Equation 3.83)}$$

As can be seen, this final equation is equal to the flux calculation given by Ward and Dao and is also similar to equation 3.78 given at the start of this section. As Ward and Dao focussed primarily on low surface coverage, low hydrogen bulk concentration systems equation 3.83 (and its equivalent in the Ward and Dao derivation) is sufficient. The addition of the chemical potential model allows for the investigation of a wider range of conditions provided the required data can be sourced.

Another development covered in (Caravella, Barbieri and Drioli, 2008) is the addition of multi-component feed gases, not discussed by Ward and Dao in their original paper. In the case of binary gas mixtures the following expression, first given by (Bird, Stewart and Lightfoot, 1960), can be used to relate the partial pressure of a gas at a solid interface to its flux:

$$J_g = \frac{1}{RT} Kc\left(P_g^{bulk} - P_g^{surface}\right) + \frac{J_{tot}}{P_{tot}} P_g^{surface} \qquad \text{(Equation 3.84)}$$

Where the subscript g is used to denote the gas species, with the quantities of the other components known by subtracting the difference as the total pressure is constant.

Caravella et al utilised film theory to model mass transfer, treating the near surface as a fluid film and this appears to be a reasonable assumption with regard to observed conditions. Using film theory, a relationship between the transfer film thickness and diffusivity can be written as follows:

$$Sh = \frac{K_c t_f}{D_{gb}} = g(Re)Sc^q \qquad \text{(Equation 3.85)}$$

Where Sh is the Sherwood number (dimensionless), K_c is the film mass transfer coefficient (m s^{-1}), t_f is the film thickness (m), D_{gb} is the binary gas diffusivity (m^2 s^{-1}) g(Re) is a function of the Reynolds number (dimensionless), Sc is the Schmidt number and q is a real number.

For multi-component gases equation 3.85 is transformed into a more complex approach, with the scalar dimensionless groups transformed into dimensionless matrices to account for the varying behaviour (Caravella, Barbieri and Drioli, 2008). The Stefan-Maxwell transport theory is used to transform the scalar products, a more detailed review of the methodology can be found in (Taylor and Krishna, 1993), but for now the flux in a multi-component mixture can be given as:

$$\vec{J} = \frac{1}{RT}\{Kc\}\{Z\}\left(\overrightarrow{P^{bulk}} - \overrightarrow{P^{surface}}\right) + \frac{J_{tot}}{P_{tot}}\overrightarrow{P^{surface}} \qquad \text{(Equation 3.86)}$$

Where all vectors (noted →) and matrices (noted "{}") have dimensions of (n-1) and $(n-1)^2$ respectively, as the profile of one of the components can be calculated by the others. $\{K_c\}$ is the matrix of the mass transfer coefficients and {Z} is the matrix of the correction factors used to account for the high transfer rates. Definitions and further derivations of each of the matrices can be found in (Caravella, Barbieri and Drioli, 2008), (Taylor and Krishna, 1993).

To find the partial pressures of all the components a trial value of the film thickness is used for an initial iteration, with the Newton-Raphson method [$x_1 = x_0 - (f(x_0)/f'(x_0)$] used to solve the following equation:

$$f = \vec{P}_{SMdiff}^{Surface} - \vec{P}_{SMmass}^{surface} = 0 \qquad \text{(Equation 3.87)}$$

Where the subscripts refer to the Stefan-Maxwell differential equations and multi-component mass transfer respectively (Caravella, Barbieri and Drioli, 2008). The differential equations referred to in equation 3.87 are the vectors of each partial pressure calculated by integrating the Stefan-Maxwell equations along the mass transfer thickness.

Whilst the full methodology has been included within this thesis for posterity, only binary component mixtures have been considered and studied in chapter five and thus equations 3.84 and 3.85 have been utilised instead of equation 3.87. As expected the evolved flux is highly dependent on the partial pressure of hydrogen present in the transfer film, alongside this the kinetic behaviour of hydrogen (and other gases) also has an impact.

3.6 Chapter Summary

This chapter includes a detailed review of the various models used for hydrogen permeation through metallic membranes.

- The Richardson equation is the earliest development of a model for hydrogen permeation, but it's application is limited due to its lack of a surface parameter.
- The chapter gives details on the development of more detailed permeation models, with the work of Wang and Pick & Sonnenberg being of particular interest. These works expanded on the work of Richardson to consider surface interactions between metals and hydrogen.
- The model developed by Ward and Dao for modelling hydrogen permeation through palladium incorporates the developments of various earlier models discussed in this chapter and acts as a "composite" of these, capable of accurately predicting hydrogen flux rates for palladium membranes of various thicknesses operating at a range of temperatures and pressures. It is speculated that this model could be applied to other membranes operating under similar conditions, with this idea tested and developed further in chapter five.
- Advancements have been made on the Ward and Dao model, with the work of (Caravella, Barbieri and Drioli, 2008) being one such example of this. The main developments include the implementation of chemical potential in place of a concentration as the driving force for diffusion, the development of a model for a binary gas system and the inclusion of additional mass balances to account for supported membranes.
- The work of Ward and Dao & Caravella et al utilise the same mass balance-based concept for predicting flux. This allows for the identification of several key relationships, those initially identified in the seven-step model for diffusion. As such, it should be considered that the rate equations for adsorption, surface-bulk transport, bulk diffusion, bulk-surface transport and desorption are the key relationships/equations for the prediction of membrane flux. The impact of varying values for components of each of these rate equations is explored in chapter five.

3.7 Chapter Three Reference List

Akamatsu, T., Kume, Y., Komiya, K., Yukawa, H., Morinaga, M. and Yamaguchi, S. (2005) 'Electrochemical method for measuring hydrogen permeability through metals', *Journal of Alloys and Compounds*, 393(1–2), pp. 302–306. doi: 10.1016/j.jallcom.2004.10.007.

Al-Mufachi, N. A., Rees, N. V. and Steinberger-Wilkens, R. (2015) 'Hydrogen selective membranes: A review of palladium-based dense metal membranes', *Renewable and Sustainable Energy Reviews*. Elsevier, 47, pp. 540–551. doi: 10.1016/j.rser.2015.03.026.

Andrew, P. L. and Haasz, a. a. (1992) 'Models for hydrogen permeation in metals', *Journal of Applied Physics*, 72(7), p. 2749. doi: 10.1063/1.351526.

Ash, R. and Barrer, R. M. (1959) 'Permeation of hydrogen through metals', *Philosphical Magazine*, 4(47), pp. 1197–1206. doi: 10.1080/14786435908235823.

Barrer, R. M. (1939) 'The Permeability of Metal Membranes to Diatomic Gases', *The London, Edinburgh, and Dublin Philosophical Magazine and Journal of Science*, 28(188), pp. 353–358. doi: http://dx.doi.org/10.1080/14786443908521189.

Barrer, R. M. (1940) 'Stationary and non-stationary states of flow of hydrogen in palladium and iron', *Transactions of the Faraday Society*, 36, pp. 1235–1248. Available at: http://pubs.rsc.org/en/content/articlepdf/1940/tf/tf9403601235.

Behm, R. J., Christmann, K. and Ertl, G. (1980) 'Adsorption of hydrogen on Pd(100)', *Surface Science*, 99(2), pp. 320–340. doi: http://dx.doi.org/10.1016/0039-6028(80)90396-9.

Bird, R. ., Stewart, W. . and Lightfoot, E. . (1960) *Transport Phenomena*. 1st edn. Wiley.

Boon, J., Pieterse, J. A. Z., van Berkel, F. P. F., van Delft, Y. C. and van Sint Annaland, M. (2015) 'Hydrogen permeation through palladium membranes and inhibition by carbon monoxide, carbon dioxide, and steam', *Journal of Membrane Science*. Elsevier, 496, pp. 344–358. doi: 10.1016/j.memsci.2015.08.061.

Borg, R. . and Dienes, G. . (1988) *An Introduction to Solid State Diffusion*. San Diego: Academic Press. Available at: http://www.sciencedirect.com/science/book/9780121184254.

Burggraaf, A. J. and Cot, L. (1996) 'Chapter 9 Transport and separation properties of membranes with gases and vapours', in *Fundamentals of inorganic membrane science and technology*, pp. 331–433. doi: http://dx.doi.org/10.1016/S0927-5193(96)80012-X.

Caravella, A., Barbieri, G. and Drioli, E. (2008) 'Modelling and simulation of hydrogen permeation through supported Pd-alloy membranes with a multicomponent approach', *Chemical Engineering Science*, 63(8), pp. 2149–2160. doi: 10.1016/j.ces.2008.01.009.

Causey, R. A. and Baskes, M. I. (1987) 'Plasma-driven permeation of deuterium in nickel', *Journal of Nuclear Materials*, 145–147(C), pp. 284–287. doi: 10.1016/0022-3115(87)90344-8.

Christmann, K., Schober, O., Ertl, G. and Neumann, M. (1974) 'Adsorption of hydrogen on nickel single crystal surfaces', *The Journal of Chemical Physics*, 60(11), p. 4528. doi: 10.1063/1.1680935.

Czerwiński, A., Kiersztyn, I., Grdeń, M. and Czapla, J. (1999) 'The study of hydrogen sorption in palladium limited volume electrodes (Pd-LVE)I. Acidic solutions', *Journal of Electroanalytical*

Chemistry, 471(2), pp. 190–195. doi: 10.1016/S0022-0728(99)00276-4.

Dolan, M. D. (2010) 'Non-Pd BCC alloy membranes for industrial hydrogen separation', *Journal of Membrane Science*. Elsevier B.V., 362(1–2), pp. 12–28. doi: 10.1016/j.memsci.2010.06.068.

Dolan, M. D., McLennan, K. G. and Way, J. D. (2012) 'Diffusion of atomic hydrogen through V-Ni alloy membranes under nondilute conditions', *Journal of Physical Chemistry C*, 116(1), pp. 1512–1518. doi: 10.1021/jp208691x.

Dunbar, Z. W. (2015) 'Hydrogen purification of synthetic water gas shift gases using microstructured palladium membranes', *Journal of Power Sources*. Elsevier B.V, 297, pp. 525–533. doi: 10.1016/j.jpowsour.2015.08.015.

Faizal, H. M., Kawasaki, Y., Yokomori, T. and Ueda, T. (2015) 'Experimental and theoretical investigation on hydrogen permeation with flat sheet Pd/Ag membrane for hydrogen mixture with various inlet H2 mole fractions and species', *Separation and Purification Technology*. Elsevier B.V., 149, pp. 208–215. doi: 10.1016/j.seppur.2015.05.003.

Gabitto, J. and Tsouris, C. (2008) 'Hydrogen transport in composite inorganic membranes', *Journal of Membrane Science*, 312(1–2), pp. 132–142. doi: 10.1016/j.memsci.2007.12.061.

Gross, A. (1998) 'Hydrogen dissociation on metal surfaces - a model system for reactions on surfaces', 635, p. 10. doi: 10.1007/s003390050834.

Gudmundsdóttir, S., Skúlason, E., Weststrate, K.-J., Juurlink, L. and Jónsson, H. (2013) 'Hydrogen adsorption and desorption at the Pt(110)-(1×2) surface: experimental and theoretical study.', *Physical chemistry chemical physics : PCCP*, 15(17), pp. 6323–32. doi: 10.1039/c3cp44503h.

Hubkowska, K., Łukaszewski, M. and Czerwiński, A. (2010) 'Influence of temperature on hydrogen electrosorption into palladium-noble metal alloys. Part 1: Palladium-gold alloys', *Electrochimica Acta*, 56(1), pp. 235–242. doi: 10.1016/j.electacta.2010.08.093.

Hulme, J., Komaki, M., Nishimura, C. and Gwak, J. (2011) 'The effects of gas mixtures on hydrogen permeation through Pd–Ag/V–Ni alloy composite membrane', *Current Applied Physics*. Elsevier B.V, 11(4), pp. 972–975. doi: 10.1016/j.cap.2010.12.024.

Hurlbert, R. C. and Konecny, J. O. (1961) 'Diffusion of Hydrogen through Palladium', *The Journal of Chemical Physics*, 34(2), p. 655. doi: 10.1063/1.1701003.

Kim, K.-H., Shim, J.-H. and Lee, B.-J. (2012) 'Effect of alloying elements (Al, Co, Fe, Ni) on the solubility of hydrogen in vanadium: A thermodynamic calculation', *International Journal of Hydrogen Energy*. Elsevier Ltd, 37(9), pp. 7836–7847. doi: 10.1016/j.ijhydene.2012.01.117.

King, D. A. and Wells, M. G. (1974a) 'Reaction Mechanism in Chemisorption Kinetics: Nitrogen on the Plane of Tungsten', *Proceedings of the Royal Society A: Mathematical, Physical and Engineering Sciences*, 339(1617), pp. 245–269. doi: 10.1098/rspa.1974.0120.

King, D. A. and Wells, M. G. (1974b) 'Reaction Mechanism in Chemisorption Kinetics: Nitrogen on the Plane of Tungsten', *Proceedings of the Royal Society A: Mathematical, Physical and Engineering Sciences*, 339(1617), pp. 245–269. doi: 10.1098/rspa.1974.0120.

Kozhakhmetov, S., Sidorov, N., Piven, V., Sipatov, I., Gabis, I. and Arinov, B. (2015) 'Alloys based on Group 5 metals for hydrogen purification membranes', *Journal of Alloys and Compounds*. Elsevier B.V., 23, pp. 1–5. doi: 10.1016/j.jallcom.2015.01.242.

Lai, T., Yin, H. and Laura Lind, M. (2015) 'The hydrogen permeability of Cu-Zr binary amorphous metallic membranes and the importance of thermal stability', *Journal of Membrane Science*. Elsevier, 489, pp. 264–269. doi: 10.1016/j.memsci.2015.03.098.

Lewis, a. E., Kershner, D. C., Paglieri, S. N., Slepicka, M. J. and Way, J. D. (2013) 'Pd–Pt/YSZ composite membranes for hydrogen separation from synthetic water–gas shift streams', *Journal of Membrane Science*, 437, pp. 257–264. doi: 10.1016/j.memsci.2013.02.056.

McLeod, L. S. (2008) 'HYDROGEN PERMEATION THROUGH MICROFABRICATED PALLADIUM-SILVER ALLOY MEMBRANES HYDROGEN PERMEATION THROUGH MICROFABRICATED PALLADIUM-SILVER ALLOY MEMBRANES', (December).

Oates, W. a and Flanagan, T. B. (1981) 'the Solubility of Hydrogen in Transition-Metals and Their Alloys', *Progress in Solid State Chemistry*, 13(3), pp. 193–283. doi: 10.1016/0079-6786(81)90002-9.

Ockwig, N. W. and Nenoff, T. M. (2007) 'Membranes for hydrogen separation.', *Chemical reviews*, 107(10), pp. 4078–110. doi: 10.1021/cr0501792.

Ozaki, T., Zhang, Y., Komaki, M. and Nishimura, C. (2003) 'Preparation of palladium-coated V and V-15Ni membranes for hydrogen purification by electroless plating technique', *International Journal of Hydrogen Energy*, 28(3), pp. 297–302. doi: 10.1016/S0360-3199(02)00065-4.

Phair, J. W. and Badwal, S. P. S. (2006) 'Materials for separation membranes in hydrogen and oxygen production and future power generation', *Science and Technology of Advanced Materials*, 7(8), pp. 792–805. doi: 10.1016/j.stam.2006.11.005.

Pick, M. A. (1981) 'Kinetics of hydrogen absorption-desorption by niobium', *Physical Review B*, 24(8), pp. 4287–4294. doi: 10.1103/PhysRevB.24.4287.

Pick, M. a. and Sonnenberg, K. (1985) 'A model for atomic hydrogen-metal interactions — application to recycling, recombination and permeation', *Journal of Nuclear Materials*, 131(2–3), pp. 208–220. doi: 10.1016/0022-3115(85)90459-3.

Rogan, J. and Lagos, M. (1999) 'Quantum diffusion in FCC metals', *Journal of Physics: Condensed Matter*, 2(25), pp. 5627–5632. doi: 10.1088/0953-8984/2/25/015.

San Marchi, C., Somerday, B. and Robinson, S. (2007) 'Permeability, solubility and diffusivity of hydrogen isotopes in stainless steels at high gas pressures', *International Journal of Hydrogen Energy*, 32(1), pp. 100–116. doi: 10.1016/j.ijhydene.2006.05.008.

Shu, J., Grandjean, B. P. A., Neste, A. Van and Kaliaguine, S. (1991) 'Catalytic palladium-based membrane reactors: A review', *The Canadian Journal of Chemical Engineering*, 69(5), pp. 1036–1060. doi: 10.1002/cjce.5450690503.

Smithells, C. . and Ransley, C. . (1935) 'The Diffusion of Gases through Metals', 150(869), pp. 172–197. Available at: http://www.jstor.org/stable/96330.

Taylor, R. and Krishna, R. (1993) *Multi-Component Mass Transfer*. New York: Wiley.

Tsai, Y. C., Lin, C. C., Lin, W. L., Wang, J. H., Chen, S. Y., Lin, P. and Wu, P. W. (2015) 'Palladium based cermet composite for hydrogen separation at elevated temperature', *Journal of Power Sources*. Elsevier B.V, 274, pp. 965–970. doi: 10.1016/j.jpowsour.2014.10.085.

Völkl, J. and Alefeld, G. (1978) 'Diffusion of hydrogen in metals', in *Hydrogen in metals 1*, pp. 321–348. doi: 10.1007/3540087052_51.

Wang, J.-S. and Roberts, J. K. (1936a) ‘On the diffusion of gases through metals’, *Mathematical Proceedings of the Cambridge Philosophical Society*. University of Sheffield Library, 32(4), p. 657. doi: 10.1017/S030500410001940X.

Wang, J.-S. and Roberts, J. K. (1936b) ‘On the diffusion of gases through metals’, *Mathematical Proceedings of the Cambridge Philosophical Society*. University of Sheffield Library, 32(4), p. 657. doi: 10.1017/S030500410001940X.

Wang, T. (2015) ‘About CO and H2 Activation Mechanisms on Fe and Mo2C Catalysts on the Basis of Densitiy Functional Theory Computation and Ab Initio Atomistic Thermodynamics’.

Ward, T. and Dao, T. (1999) ‘Model of hydrogen permeation behavior in palladium membranes’, *Journal of Membrane Science*, 153(January 1998), pp. 211–231. Available at: http://www.sciencedirect.com/science/article/pii/S0376738898002567 (Accessed: 18 February 2014).

Wipf, H. (2001) ‘Solubility and diffusion of hydrogen in pure metals and alloys’, *Physica Scripta*, 43, pp. 138–148. Available at: http://iopscience.iop.org/article/10.1238/Physica.Topical.094a00043/meta.

4 Experimental Apparatus, Techniques and Methods

4.1 Overview

As detailed in chapter one of this thesis, the aim of this project was to test and analyse the viability of a number of membranes and potential catalytic coatings with a focus on the targets set by the US DoE (given in chapter two) that need to be achieved for technological maturity. Whilst chapter three introduces the theory behind hydrogen permeation and its associated computational models; chapter four provides an introduction to the experimental apparatus, techniques and methods that have been used within this project. “Techniques” has been used a broad catch-all term here for processes used in the preparation of the membranes and for the analytical techniques used for analysis of the membrane and the permeated gas.

Chapter two highlighted the need for a surface coating for group V based membranes, and this aspect has been central to the experimental investigation undertaken as part of this thesis. The coatings investigated can be split into two groups: silver/oxidised silver and palladium-silver alloys.

Oxidised silver was investigated for reasons given in chapter two, whilst silver itself does not act as a catalyst for hydrogen dissociation the presence of surface and sub-surface oxygen, it shifts the centre of the metals d-band reducing the required activation energy to allow for dissociation.

Various palladium-silver alloys were investigated due to the effectiveness of palladium as a catalytic coating; with it currently holding the role as the standard catalytic coating for testing non-palladium or nickel-based membranes. As highlighted in chapter two there are doubts about the feasibility of this for wider scale utilisation, largely due to the high cost and relative scarcity of palladium. Alternative coatings do exist, and as part of this work it was decided to investigate the use of a palladium-silver coat; primarily due to the industrial success of palladium-silver membranes.

Palladium-silver membranes produce higher hydrogen permeation rates than pure palladium; thus it was believed that a palladium-silver catalytic coating should give no reduction in membrane permeability whilst providing a reduction in the amount of palladium used for the same thickness of surface coating. Other advantages for the addition of silver to palladium membranes are detailed in chapter two, including increased resistivity to surface poisoning, with this potentially being a secondary benefit to a Pd-Ag coating. Other alternatives to limiting palladium usage, such as coating the permeate side with nickel instead are discussed in chapter seven.

Alongside the catalytic coatings tested a number of bulk membrane materials were tested. Niobium and vanadium were chosen as a bulk material for testing the coatings mentioned above; this was done primarily for two reasons. One was the relative low-cost in comparison with the majority of Group-V alloys commercially available and more importantly a vast amount of permeability data is available for comparison with other catalytic coatings such as palladium and nickel. Tests were also conducted on vanadium-nickel and vanadium-nickel-aluminium alloys. As discussed in chapter two, these are more feasible for commercial use due to their decreased susceptibility to hydride damage whilst offering good levels of hydrogen permeability. Numerous tests were also conducted on palladium membranes, initially to test the validity of the experimental set up utilised within this thesis (as direct comparisons to literature sources were easy to find) and also to serve as a "yardstick" to measure other tested membranes performance.

As discussed in chapters two and three, membranes can be described as either thick or thin in nature. All of the membranes tested within this work are of the thick type, with thicknesses ranging from 100 to 250 µm. Thick membranes were tested due to their ease of use (as no support layer is required) and thick membranes also produce a higher purity hydrogen permeate as permeation of non-desirable gases through grain boundaries/deficiencies is virtually non-existent. One potential drawback to the use of thick membranes is the lower permeation rate, therefore steps must be taken to ensure that any thick membranes utilised are not too thick, the range of thicknesses investigated here is similar to that of other many publications. Cost is also a factor of concern for membrane design and was considered as part of the selection process of the membranes tested. An analysis focussed on costing and the selection of membrane thickness can be found in chapter seven.

As highlighted in chapters two, three and five there a number of variable parameters that can have an impact on membrane performance; membrane thickness and composition have been discussed previously, however alongside this upstream and downstream pressure and the operational temperature could all be controlled and varied. More attention is given to the process conditions utilised within the relevant subsections of this chapter, however it was the intention of the project to meet DoE targets were possible. Operational temperatures, where possible, were in the range of 300 – 550 °C, incorporating the range set by the DoE, however safety restrictions on available equipment limited upstream pressure to 10 bar, somewhat below the DoE target mentioned in chapter two. Whilst this is a limitation it is assumed that trends established at the lower pressures tested should give an indication on membrane performance.

A focus was placed on developing a low cost, easy to use membrane enclosure; this was done successfully. One DoE target is based on a desired level of hydrogen recovery from the feed gas; the

enclosure designed as part of this project did not facilitate this as it was decided to focus primarily on achieving the hydrogen flux and permeate purity targets whilst keeping in mind the cost target. Alternative enclosure designs to allow for high hydrogen recovery rates are discussed in chapter seven; however, this was deemed beyond the scope of this project and has not been addressed physically.

The majority of the work discussed within this chapter was undertaken at the University of Sheffield's Buxton Test Facility, this was done as it provided the necessary space and features to conduct the experiments in a safe and controlled manner. As highlighted above All permeation experiments were conducted here, alongside the majority of the membrane preparation (except the PVD coating) and gas compositional analysis was also undertaken on site. SEM studies were conducted in the Department of Chemical and Biological Engineering at the University of Sheffield main campus.

4.2 Overview and Diagram of Membrane Permeation Test Apparatus

Figure 4.1 shows a diagram of the permeation test apparatus, the main aspects of this will be discussed here before a more detailed apparatus list will be given in section 6.4.

As the diagram shows, the membrane test enclosure sits within an electrically powered furnace. The membrane enclosure was fed gas through a flexible nylon pipe, with the gas supply provided from pressurised gas bottles. A gas regulator was used to regulate the pressure in the membrane enclosure and the feed-side of the enclosure, with a flash back arrestor present as a safety measure to reduce the risk of possible explosions. A flow meter was also present on the feed line; however, this was not used to control flow, merely to observe flow conditions and identify leaks (as described in section 6.5: experimental procedures).

The feed side also had an outlet/vent pipe to remove rejected CO_2 and prevent over-pressurisation of the enclosure. Due to the high temperature of the outlet gas, the enclosure outlet was connected to a length of stainless steel pipe prior to connection with the nylon outlet pipe. A needle valve was used to restrict and control the feed side flow rate and a non-return valve was also installed as an additional safety precaution to prevent flammable hydrogen-oxygen mixtures forming at low pressures.

The permeate side of the enclosure has a single outlet, where the enclosure is connected to nylon pipe and a non-return valve. The permeate side is flushed with argon before use to minimise oxygen exposure. Typically, the permeate outlet was connected to a rotameter to allow measurement of the flux and the volume collected, with the rotameter then feeding into a gas sampling bag to allow for collection before gas chromatograph analysis. On occasion, as discussed later in this chapter, the rotameter and gas bag were disconnected and the outlet was placed within a large beaker of water, with the gas used to displace water in a measuring tube (for more accurate measurement of low permeation rate membranes).

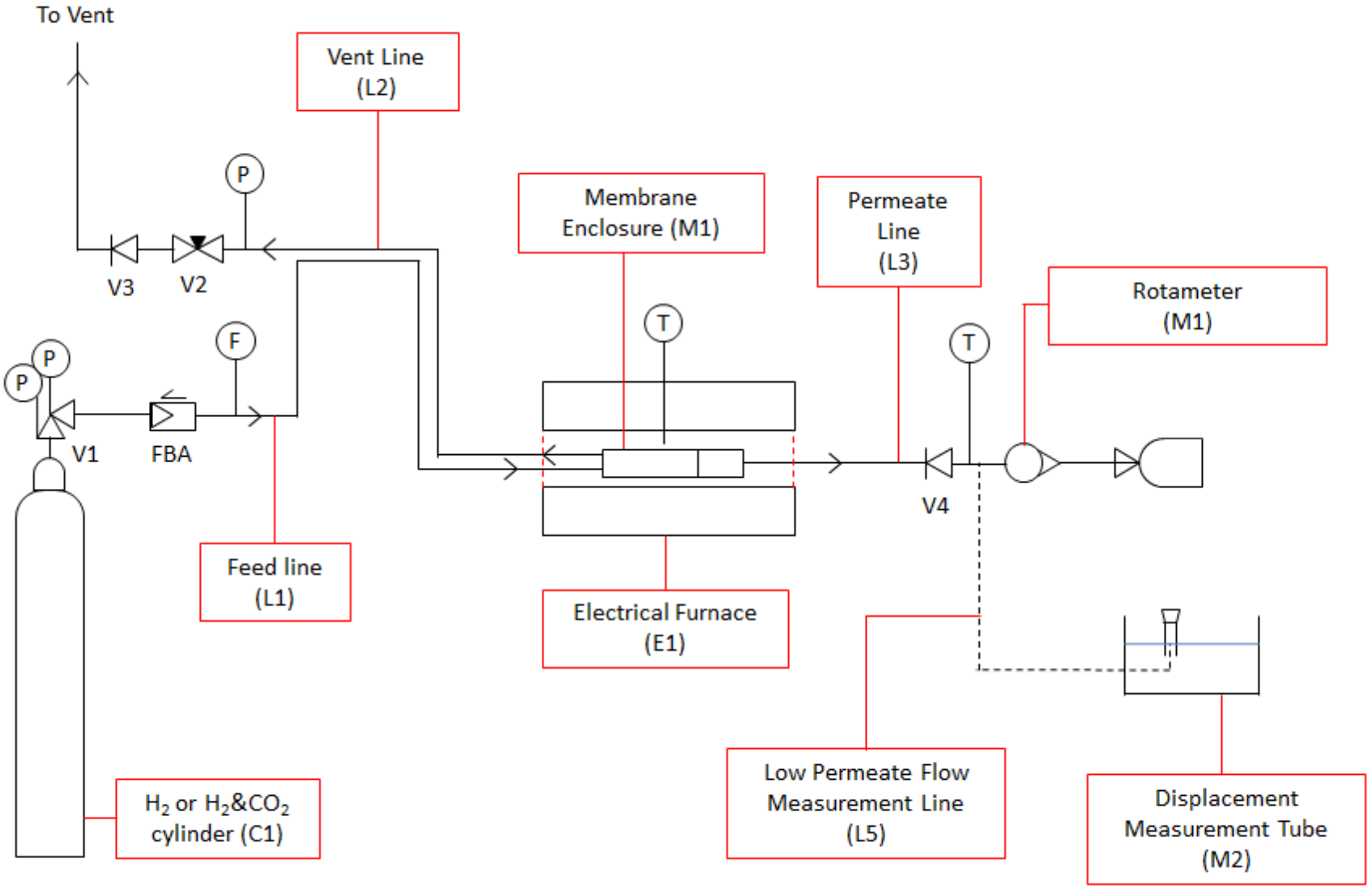

Figure 4.1 – Process flow diagram for the hydrogen permeation tests

4.3 Membrane Enclosure Design Specification

As already noted in this chapter the main aim of this work was to investigate the suitability of various membranes for large-scale hydrogen separation and, as mentioned previously, the suitability of a membrane is defined by the likelihood of it meeting specific targets outlined by the US DoE. It was decided that, of these targets, the experimental work in this thesis would focus around the permeate purity and required flux targets; with consideration also given to the cost target. This was done consciously, and in this work these are seen as the primary targets of focus for two main reasons.

The first is the belief that these are the key hurdles to overcome at this level of technological readiness with promising materials required to show good performance first and foremost; with material cost being an important indication of the feasibility of increasing the scale. If the cost is impractical, alternative cheaper materials with similar properties can be investigated or lower-cost alloys could be formed that may perform even better – as is the case with the palladium-silver system.

Secondly, whilst the longevity of the membrane and hydrogen recovery rate (as a percentage of the hydrogen in the feed) is important, conducting tests focussed around these goals was deemed unfeasible for this thesis. Longevity tests lasting numerous months were not feasible and are of questionable use until the short-term performance of a membrane is of a suitable level. A similar argument can be made for the hydrogen recovery rate target; where until a membrane has proven capable of meeting flux targets the recovery rate is somewhat immaterial; as the membrane permeate flux rate will ultimately form a key aspect of the design of any high recovery enclosure.

Therefore, with a focus established towards testing the flux rate and hydrogen purity of the permeated gas, a membrane enclosure was designed and constructed to allow for appropriate experimental testing.

Whilst the membrane enclosure is a bespoke design, developed as part of this thesis, attention was paid to the work of others to provide guidance on typical designs. The publications of (Dolan, McLennan and Way, 2012) and (Dolan *et al.*, 2013) give details on the methodology used by a group prominent in current metallic membrane research, where details are given of a “custom module manufactured from Inconel” with copper gaskets used to seal planar membranes compressively. Whilst no images of the module are provided, it would be reasonable to recognise some similarity with the enclosure/module developed as part of this work.

The work of (Romanenko *et al.*, 1996) also gives details of the permeation equipment used, however there are some significant differences; as instead of using copper gaskets and pressure to form a seal

the tested membranes were welded to a titanium flange in a relatively exotic set up shown in the publication. The welded membranes are still trapped in a tubular unit with “sealing O rings” similar to this work and the work of Dolan et al above.

Figure 4.6 contains the schematic of the membrane enclosure, with the schematic including drawings of the side view and views of both permeate and feed ends. As shown in the figure, the membrane enclosure splits into two halves to allow for placement of the membrane for testing.

The body of the enclosure has an internal diameter of 21 mm, with a wall thickness of 2 mm – giving a total body diameter of 25 mm. The overall diameter of the enclosure is increased by the presence of the coupling flanges. Including the flanges, the diameter of the enclosure is 55 mm.

The feed side of the enclosure is larger than the permeate side; the total length of the main chamber of the enclosure is 325 mm; with the feed side being 225 mm of this total, and the permeate side being 100 mm.

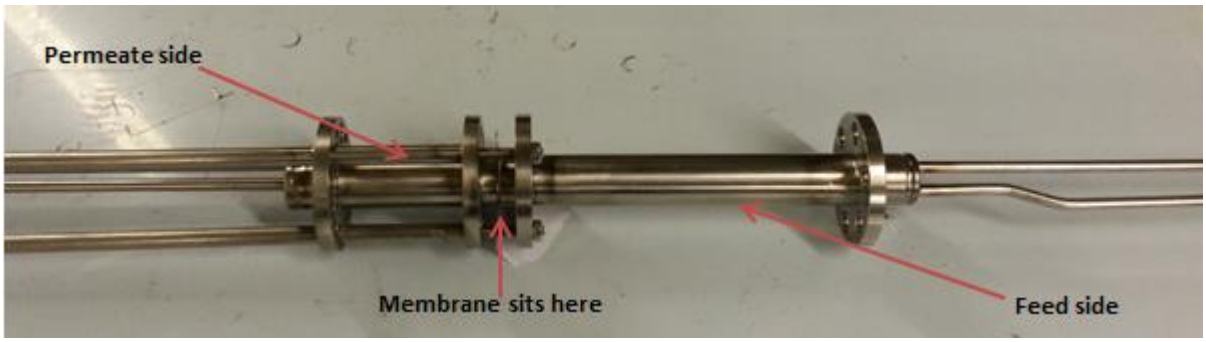

Figure 4.2 – Annotated photograph of the assembled enclosure highlighting the feed and permeate sides

The two halves of the enclosure are held together using six M6 screws nuts and washers, three of which are shown in figure 4.3 to be located close to the split (these are the primary couplings) and three of which are located on the support rods at the permeate end (these are the secondary couplings). The secondary couplings are also shown to have springs in place; these springs were fastened under tension and were included to allow for thermal expansion of the enclosure if required.

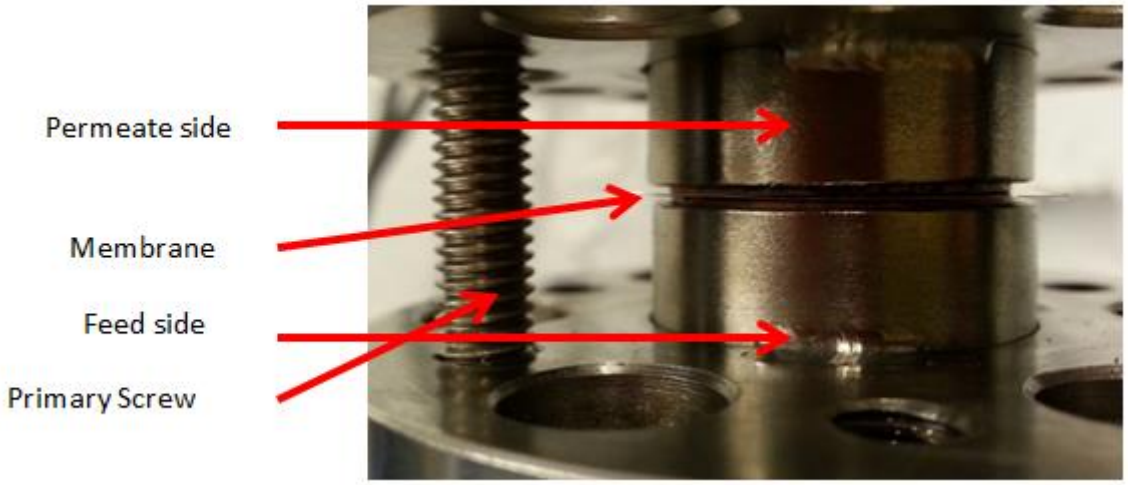

Figure 4.3 – Annotated photograph of the membrane fastened into the enclosure

As mentioned previously the enclosure has three pipes welded in place; on the feed side a supply pipe and an outlet/rejected gas vent are present. The inlet pipe is longer internally as this allows for agitation of gas near the surface of the membrane to prevent polarisation/CO_2 build up. On the permeate side, a singular permeate outlet can be found. All three pipes have the same 3 mm outer diameter (with a wall thickness of 0.25 mm) and all three are connected to the nylon pipe work through the use of pipe fittings purchased from FTI.

Examples of the pipe fittings can be seen in figure 4.4, compatible fittings were vital to ensure no leakage of potentially dangerous hydrogen and carbon dioxide gases.

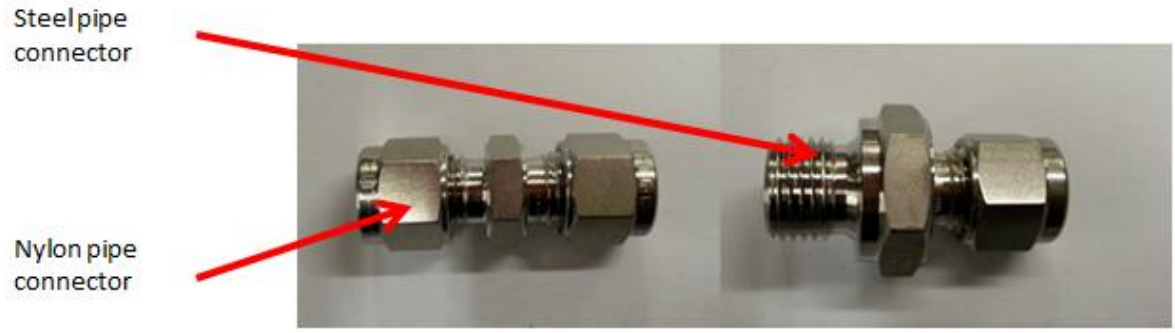

Figure 4.4 – Images of the FTI pipe fittings used to connect metal and nylon piping without gas leakage

When opened and examined at the membrane housing, both halves of the enclosure can be seen to have a 1 mm wide x 1 mm deep offset/groove, in this groove sits a copper gasket of 23 mm outer diameter and an internal diameter of 17 mm. These gaskets are annealed and used to form an air tight seal with the membrane when compressed, as shown in figure 4.5.

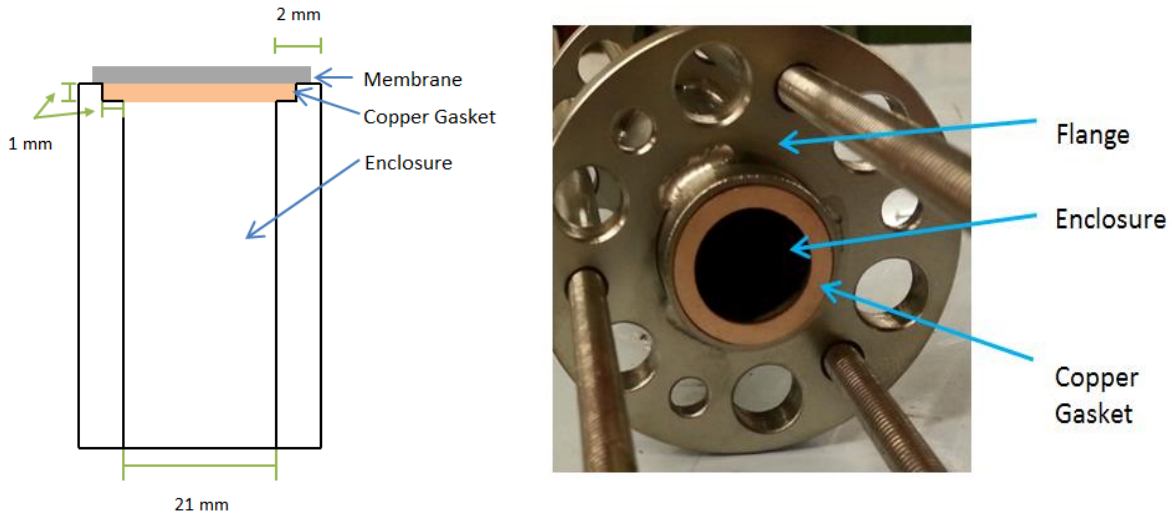

Figure 4.5 – Simplified schematic and photograph showing placement of the gasket and membrane within enclosure (left) and photograph of the gasket and enclosure (right)

The enclosure body and feed/vent/permeate pipes are constructed of type 316 stainless steel; type 316 was chosen as it is widely available and demonstrates good corrosion-resistance in comparison to most other commonly available steel grades. Hydrogen embrittlement is also a cause for concern, as repeated exposure to hydrogen-rich environments could result in damage to the enclosure. (Michler and Naumann, 2008) gives details on hydrogen embrittlement of stainless steels at low temperatures, where it is stated that alloys with 10+ % of nickel content are more resistant to low temperature embrittlement.

The purchased screws and nuts; and the manufactured springs and washers were all constructed from type 304 stainless steel due to the low cost and ease of replacement in case of damage.

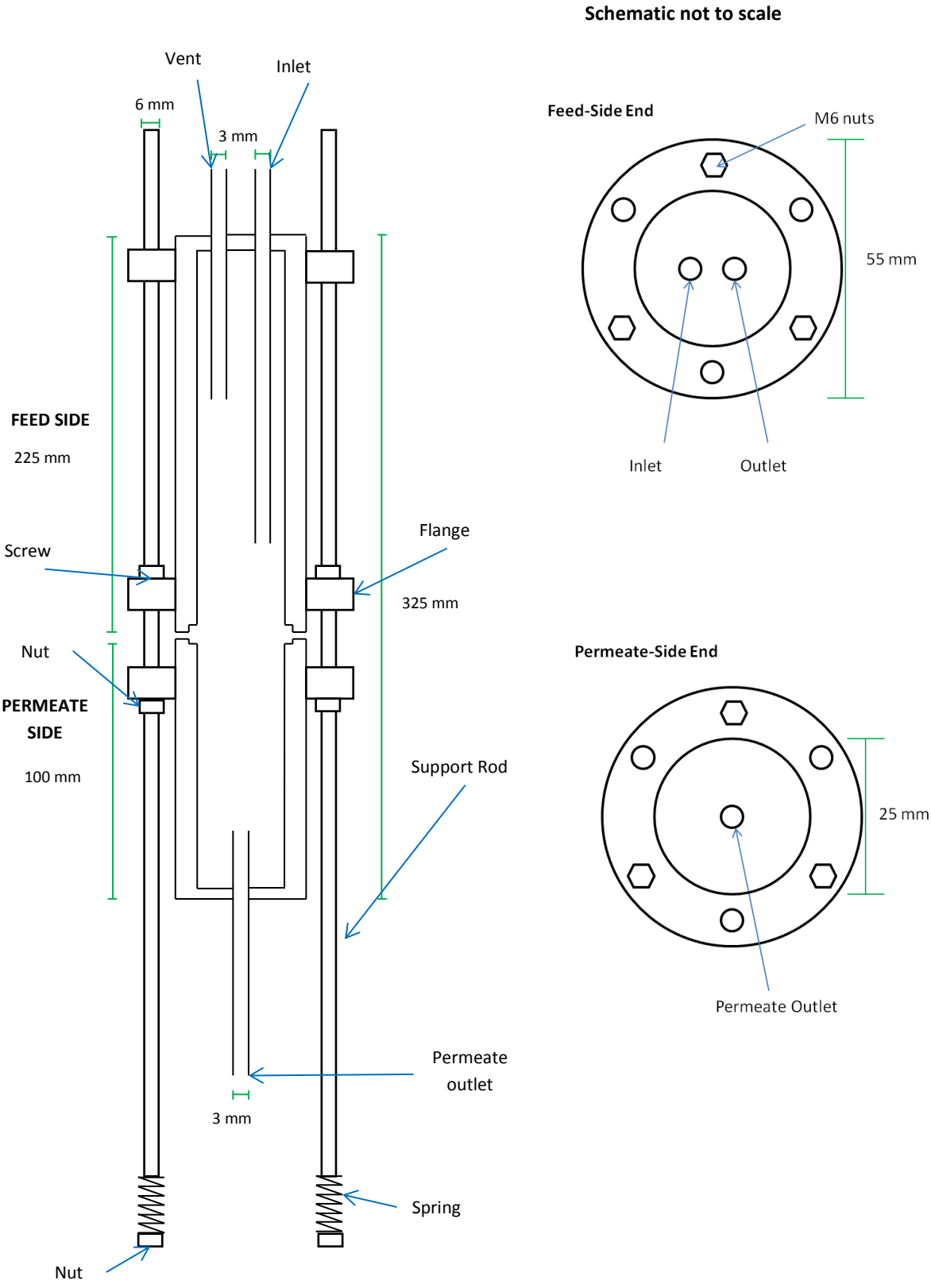

Figure 4.6 – Schematic of the membrane separation enclosure design, side and end views included

4.4 Overview of the Experimental Techniques Utilised

4.4.1 Physical Vapour Deposition (PVD)

PVD was briefly mentioned in chapter two, when discussing construction methods for membranes and coating techniques. PVD is a frequently used technique for multiple reasons; controlling the thickness of the membrane coating is relatively simple, the coating is typically uniform in thickness and the range of materials PVD is compatible with is diverse. A number of techniques fall within the umbrella term of PVD and this section will only focus on those relevant to this thesis.

Coating of silver onto the membranes was done through the use of electron beam physical vapour deposition (EBPVD). EBPVD is a well-established process, and there are multiple sources that given great detail on the process with (Sree Harsha, 2006) providing a comprehensive introduction to the subject matter, and multiple sources providing details on PVD for various coatings including silver (Levenets *et al.*, 2006)(Ra *et al.*, 2016)(Ewald *et al.*, 2006).

The EBPVD provides a coating by bombarding a target anode (in this case a silver ingot) with an electron beam in a vacuum; the electron beam excites the anode material, resulting in the material transforming into a vapour. After vaporisation the excited atoms begin to precipitate back into solid form, coating everything within “line of sight” of the electron beam and ingot (Sree Harsha, 2006).

A strong vacuum is necessary for successful coating to prevent unwanted interactions between the electron beam and gas molecules as this would prevent vaporisation of the metal ingot; (Sree Harsha, 2006) states that the reaction chamber must be evacuated to a pressure below 10^{-2} Pa for successful operation.

The electron beam required for vaporisation is provided through the use of an electron gun, with thermionic emission and field electron emission common methods of producing the required electrons. The electron beam is accelerated until the electrons have a high kinetic energy and the beam is directed at the material to be evaporated with the electrons losing the energy rapidly upon striking the material (George, 1992). The kinetic energy transferred from the striking electrons is partially converted to thermal energy in the target atoms, resulting in the heating and eventual evaporation of the metal. If the vacuum and temperature are high enough, the metal vapour produced will coat everything within “line of sight” of the target/sputter (George, 1992).

To ensure the coating will adhere to the surface, and to remove any unwanted contaminants, cleaning of the substrate (in this case the membrane) is required before the PVD process can begin. Typically

this is done ultrasonically in an alkaline solution for many transition metals (Ewald *et al.*, 2006)(Cassar, Matthews and Leyland, 2012), as this process has been shown to cause little damage to the material.

The advantages of EBPVD over alternate coating methods are numerous, the primary of these is mentioned above – typically coatings are of uniform thickness. This is of importance in this work, as the catalytic layer thickness needs to be controlled to prevent limitation of the bulk flux. Another considerable advantage is the efficiency in the use of coating materials over alternatives such as electroless plating; where the system loses the ability to coat before the use of most of the raw materials. This increased efficiency and controlled, uniform deposition rate (Sree Harsha, 2006) are among the main reasons that EBPVD was used as a coating method within this body of work. Alongside this EBPVD offers the advantage of dense coatings applied with good adhesion.

There are limitations that must also be considered, the requirement for "line of sight" exposure means that complex geometries are more difficult to coat thoroughly. For this work this is not a problem, but future membrane designs may not be so simple and thus this limitation should be considered; other coating methods such as electroless plating discussed below can overcome this problem. The need for a high vacuum for successful coating could also be seen as problematic for anything beyond batch production; but once again this a problem for consideration in a scope wider than that of this thesis.

4.4.2 Electroless Plating

The second coating technique to be discussed within this chapter is electroless plating; this technique was used for producing the palladium-silver coating used on the niobium and vanadium alloy membranes discussed in chapter six.

Electroless plating is a non-galvanic method of chemical deposition, where a compound or element in an aqueous solution can be deposited onto a substrate through the completion of a number of simultaneous chemical reactions. Parallels can be drawn to electro-deposition, where the main difference is the need for external electrical power to drive the reaction. There are numerous advantages to using electroless plating over the galvanic process; the most obvious of which being the lack of a need for a power supply which is a minor simplification of the process. Beyond this, it is reported that electroless plating gives a more uniform coating than electroplating (Ohno, 2010) (Okinaka and Wolowodiuk, 1990), this is of particular importance when coating membranes where the thickness has a significant impact on the rate of hydrogen permeation. A secondary note can be made about the thickness of the surface layer also, as a surface catalytic layer that is too thick will act independently as a membrane itself; for the purpose of this thesis a coating that is considered "thick"

(i.e. an independent membrane) is one in which the surface processes dominate the overall hydrogen permeation under conditions where the flux is predicted to be diffusion limited.

Electroless plating has been used to coat both palladium and silver successfully on to various substrates, with many examples available in published literature, with (Tarditi and Cornaglia, 2011)(Lin and Rei, 2001)(Alimov *et al.*, 2015)(Vaitsi *et al.*, 2011)(Zhao *et al.*, 2011) and (Ozaki *et al.*, 2003) giving details of electroless plating techniques used in the preparation of membranes. Detailed overviews of palladium (Okinaka and Wolowodiuk, 1990) and silver (Koura and Kubota, 1990) electroless plating techniques are included in the book "*Electroless Plating: Fundamentals and Applications*" with this section being only a brief summary of the technique. Ozaki et al is of particular interest to this thesis, as the process outlined details the deposition of palladium onto vanadium and vanadium-nickel giving evidence that the process is indeed feasible for membrane construction.

(Ohno, 2010) and (Okinaka and Wolowodiuk, 1990) both give descriptions of the various baths which can be used to provide an electroless coating for palladium with (Koura and Kubota, 1990) providing a similar overview for silver. Electroless plating baths are classified based on the reducing agent used; typical baths use either hydrazine or hypophosphite for palladium deposition (Ohno, 2010)(Okinaka and Wolowodiuk, 1990) but alternatives have been investigated with details given on hydroxylamine (Ohno, 2010), amine borane and formaldehyde (Okinaka and Wolowodiuk, 1990) baths used. The palladium bath used in this thesis are the hypophosphite type, as sodium hypophosphite is less hazardous to handle than hydrazine. The efficiency of deposition via the hypophosphite method is also higher, with a 100% efficiency possible; whilst hydrazine-type efficiency is given in the range of 28-86% (Van Den Meerakker, 1981).

The compositions of the baths used within this thesis are given in chapter six; however, the plating theory is discussed as part of this chapter. The palladium coating bath used in this work is detailed by both (Ohno, 2010) and (Okinaka and Wolowodiuk, 1990); the bath is characterised by using ammonia as the complexing agent for the coating process.

Palladium is present in the bath as palladium-amine complex; this complex is formed by dissolving $PdCl_2$ into 1M HCl, which is then diluted with de-ionised water:

$$PdCl_2 + 2\,HCl \rightarrow H_2[PdCl_4] \qquad \text{(Equation 4.1)}$$

To this NH_4OH (ammonium hydroxide) is added to form the palladium ligand:

$$H_2[PdCl_4] + 4\,NH_4OH \rightarrow Pd[(NH_3)]_4Cl_2 + H_2O + HCl \qquad \text{(Equation 4.2)}$$

This solution was then allowed to stand at room temperature for 24 hours before usage. The addition of ammonium chloride stabilises the bath but lowers deposition rate (Okinaka and Wolowodiuk, 1990); sodium hypophosphite is added last as this is the active reducing agent. Before coating the membrane is placed in tin (IV) chloride to seed the surface for 30 seconds to reduce the initial incubation period and allow for precise control of the thickness of the deposited coating.

The reaction pathway for palladium deposition is taken from (Cheng and Yeung, 2001), the half-cell equations are as follows:

$$\mathrm{Pd[N}H_3]_4^{2+} + \ 2e^- \ \rightarrow \mathrm{Pd} + 4\mathrm{N}H_3 \qquad \text{(Equation 4.3)}$$

$$2\mathrm{H_2PO_2^-} + 2\mathrm{H_2O^-} \rightarrow 2\mathrm{HPO_3^{2-}} + 4\mathrm{H^+} + \mathrm{H_2} + 2e^- \qquad \text{(Equation 4.4)}$$

Combining equations 4.3 and 4.4 above give the overall palladium deposition reaction:

$$\mathrm{Pd[N}H_3]_4^{2+} + \ 2\mathrm{H_2PO_2^-} + 2\mathrm{H_2O^-} \ \rightarrow \mathrm{Pd} + 4\mathrm{NH_3} + \ 2\mathrm{HPO_3^{2-}} + 4\mathrm{H^+} + \mathrm{H_2} \qquad \text{(Equation 4.5)}$$

Deposition is conducted at 50 °C, with a coating thickness of 2.5 µm/hour (Okinaka and Wolowodiuk, 1990); the coating rate for this bath varies from that discussed in chapter two due to the use of a different reducing agent. The coating thickness can be estimated reasonably accurately from the coating time and the deposition rate.

For silver deposition the silver complex is formed via a two-step reaction as follows:

$$2\mathrm{AgNO_3} + 2\mathrm{NH_4OH} \ \rightarrow \ \mathrm{Ag_2O} + 2\mathrm{NH_4NO_3} + \mathrm{H_2O} \qquad \text{(Equation 4.6)}$$

$$\mathrm{Ag_2O} + 4\mathrm{NH_4OH} \ \rightarrow \ 2[\mathrm{Ag(NH_3)_2}]\mathrm{OH} + 3\mathrm{H_2O} \qquad \text{(Equation 4.7)}$$

For silver, hypophosphite is not used as the reducing agent as a stronger reducing agent is required; hydrazine was used instead. Whilst hydrazine can also be used as the reducing agent in the for palladium it was decided to limit the use of hydrazine where possible as a safety precaution. The bath utilised in this work was taken from (Tarditi, Braun and Cornaglia, 2011); where hydrazine is used as the reducing agent after complexing of the silver ion with NH_4OH. The reducing reaction is suggested by (Chen and Lim, 2002) and (Cheng and Yeung, 1999) as follows:

$$4\mathrm{Ag[N}H_3]^+ + \ N_2H_2 + 4\mathrm{OH^-} \ \rightarrow 4\mathrm{Ag} + 4\mathrm{NH_3} + \mathrm{N_2} + 4\mathrm{H_2O} \qquad \text{(Equation 4.8)}$$

It must also be noted that the silver bath typically lacks long term stability, the stability of the bath used here is improved by the addition of Na_2EDTA salt. The need for free hydroxyl groups

demonstrates the need for this reaction to be conducted in alkaline conditions; (Tarditi, Braun and Cornaglia, 2011) uses a bath with a pH of 10.

For the formation of the Pd-Ag alloy coating, the methodology of (Tarditi, Braun and Cornaglia, 2011) was followed where a ternary Pd-Ag-Cu membrane was constructed by compiling three layers of pure metal (Pd followed by Ag and finally Cu) onto a porous steel support. Upon completion of the layering, the membranes were heated to 500 °C and held for varying periods of time between 48 and 162 hours to allow for the formation of homologous alloys through thermal diffusion. In the case of the Pd-Ag-Cu alloy discussed in the publication the annealing stage is complicated by the presence of both FCC (the pure metals) and BCC (the ternary alloy) structures, thus varying annealing times were used to investigate the impact on the crystal structure. In the case of the Pd-Ag coatings used in this work, both metals exhibit FCC structures and so annealing times on the shorter end of the range given by Tarditi et al were used.

To ensure that the sequential layers diffused to form a single coating analysis of the surface is important. As discussed in section 4.6 scanning electron microscopy (SEM) and energy dispersive x-ray analysis spectroscopy (EDS) were used to analyse the surface, this is consistent with the surface analysis conducted by (Tarditi and Cornaglia, 2011).

4.4.3 Oxidation of the Silver Layer

After coating the membranes with silver, and completion of the annealing stage (to allow for intermetallic diffusion at the V-Ag interface), a number of silver coated membranes were oxidised to allow for testing of a Ag-O coating.

Silver is relatively unreactive as a metal; its electron configuration is [Kr] $4d^{10}$ $5s^{1}$. It's unreactive nature can be explained through its filled 4d shell, as this shell is not very effective in shielding the electrostatic forces of attraction from the nucleus to the 5s electron (Greenwood and Earnshaw, 1997).

This un-reactivity means that silver is not readily oxidised in air, even if heated to high enough temperatures to make the metal glow (Greenwood and Earnshaw, 1997) and thus oxidisation of silver needs to be achieved chemically.

Oxidation of silver can be conducted in numerous ways, with the practice being common for the production of jewellery. The methodologies used vary greatly, however for this work it was decided that a controllable reliable methodology should be employed.

One commonly reported method for producing silver oxide is detailed in (Bjelkhagen, 1995), where silver nitrate solution is reacted with a base solution:

$$2\ AgNO_3 + 2\ OH^- \rightarrow\ Ag_2O + H_2O + 2\ NO_3^-$$ (Equation 4.9)

This methodology however, requires the precursor state of silver nitrate which cannot be utilised here. Instead an alternative must be found, with it being suggested that pure silver can be oxidised readily through the use of a strong oxidisation agent (Greenwood and Earnshaw, 1997). Silver is attacked by strong oxidising reagents such as potassium permanganate ($KMnO_4$), and potassium dichromate ($K_2Cr_2O_7$) (Greenwood and Earnshaw, 1997)(Bjelkhagen, 1995). However, in this work it was decided to use sodium hypochlorite where as an oxidant hypochlorite decomposes to:

$$NaOCl\ \rightarrow NaCl + [O]$$ (Equation 4.10)

Heterogeneous reactions of metals with sodium hypochlorite are detailed in (OxyChem, 2014) and (Powell Fabrication & Manufacturing, 2009); metals are shown to be oxidised, with an example of zinc given in the texts above:

$$NaOCl + Zn\ \rightarrow ZnO + NaCl$$ (Equation 4.11)

(Yuan *et al.*, 2013) gives details of a similar process for silver nanoparticles, where sodium hypochlorite was amongst a number of oxidising agents reacted with a colloidal suspension of silver. Yuan et al state that hypochlorite oxidises silver rapidly, and thus the silver coating was exposed to the hypochlorite/peroxide solution for only short periods of time. Silver oxide is described in the above sources as having a dark colour, and thus it was decided to remove the membranes from the solution when a noticeable colour change had occurred. Whilst this method is not ideal, little other information on silver oxidation kinetics is available.

Due to the amount of free chlorine available in hypochlorite, concerns persisted that silver will react to produce Ag-Cl on the membrane surface. Ag-Cl can be reacted with NaOH (sodium hydroxide) to produce Ag-O:

$$AgCl + NaOH\ \rightarrow AgO + NaCl + \frac{1}{2}H_2$$ (Equation 4.12)

Therefore, after treatment with NaOCl the membrane was washed and then treated with NaOH to ensure only Ag-O was found in the silver layer, before washing the membrane again before use.

4.4.4 Permeate Analysis: Gas Chromatography

After conclusion of the permeation tests, the collected permeate required analysis of its composition. This is a standard procedure in the running of membrane permeation tests, as without analysis no reliable result can be ascertained. Chapter two references several permeation tests, and what can be found to be almost unanimous regardless of alternate varying factors (porous/non-porous, membrane material type and composition, pressures, temperatures) is the use of gas chromatography analysis (GC) in the analysis of the permeate.

This thesis includes only a brief summary of GC analysis, focussing primarily on the set-ups used within this work. A detailed and wider review of GC can be found in (Grob and Barry, 2004), with the following sources also providing comprehensive details: (Higson, 2004), (Engel *et al.*, 2006). GC analysis is a chemical analysis; one in which the unknown composition of a mixture of known gaseous or liquid species can be identified through separation of the mixture and subsequent species detection (Grob and Barry, 2004). A GC analyser typically consists of an inlet, a sample injector, a separation column and an outlet upon which a detector is mounted, the column is also mounted within an oven due to the elevated operating temperatures used. The temperature of the column is important; as a higher temperature will result in a quicker test but a reduced interaction of the mobile phase with the stationary phase can result in less separation of the species. A brief overview of the gas chromatograph used can be found in chapter six, or in the sales manual produced by the manufacturer (ABB, 2002).

Multiple inlet types are available, with details given about varying designs in (Grob and Barry, 2004)(Higson, 2004). A separation column in a GC analyser consists of two phases; a mobile phase consisting of a carrier gas and the fluid to be analysed, in this case a gas, and a stationary phase. Each component of the mobile phase interacts with the stationary phase at differing rates; resulting in different retention times for each of the gases. A suitable column length and stationary phase must be selected to ensure good separation of species for accurate concentration measurement.

At the outlet of the column a number of detector types are available, once again details on various detectors can be found widely, with (Higson, 2004)(Engel *et al.*, 2006)(Grob and Barry, 2004) providing a detailed overview of various designs. As the variety available is extensive, the focus within this section will be the thermal conductivity detector (TCD) as this was the detector used within this work. The TCD detector is seen as a versatile, general-purpose detector capable of use with most gases (Higson, 2004).

The TCD detects changes in the thermal conductivity of the mobile phase; changes in conductivity are detected by a filament through which an electrical current is passed. A common filament material is tungsten-rhenium alloy (Harris, 2007), it is also worthwhile to note that the detector sensitivity is proportional to the current passed through the filament and inversely proportional to the temperature of the detector and the flowrate of the mobile phase (Harris, 2007).

The TCD detects changes in conductivity via a Wheatstone bridge; this circuit allows for the measurement of an unknown electrical resistance through the balance of two parallel legs of a circuit (Ekelof, 2001). In the case of a gas chromatograph the pure carrier gas is known, and thus its conductivity/resistivity is known, the change in this value is then caused by the unknown component. As the change is measured, it is important to ensure that the carrier gas is calibrated precisely to ensure an accurate analysis of the sample – in this case the permeated gas. Calibration was undertaken with the carrier gas and known sample compositions to ensure accuracy throughout this work.

Typical carrier gases used with TCD detectors are helium and nitrogen, as they have a high thermal conductivity which helps to cool the filament and keep uniform resistivity along the filament (Higson, 2004)(Harris, 2007) – for the gas chromatograph used in this work carrier gases consisting of helium and nitrogen were used. The use of nitrogen is of particular importance when testing for the hydrogen, as helium and hydrogen have relatively similar conductivities (Harris, 2007)(Higson, 2004).

When a sample is added to the carrier gas changes in the thermal conductivity are monitored and recorded. The recorded data is used to produce a chromatogram of detector response plotted against retention time; with this utilised to identify the gas species and concentration. The identification of the gas species is conducted through comparing the expected retention time of a given species within the analyser column.

4.4.5 Membrane Surface Analysis: SEM

Alongside analysis of the gas, it is also deemed important to analyse the membrane; of particular interest is the surface where the composition of the coating is of interest alongside any signs of obvious damage due to hydride formation or undue stresses – such as cracks forming that could result in a drop in performance or the failure of the membrane. Studies of the surface topography can provide insight into other properties too; one example being the real surface area (per unit of superficial surface area) – an increased surface area (achieved through varying the membrane coating method or membrane manufacture method for example).

Scanning electron microscopy (SEM) is widely used in imaging analysis of membranes for the reasons mentioned above, and a large number of publications that provide permeation data contain electron micrographs of the membrane surfaces (Tarditi, Braun and Cornaglia, 2011)(Ozaki *et al.*, 2003)(Dolan *et al.*, 2013)(Hatlevik *et al.*, 2010). The vast majority of micrographs are provided through the use of SEM or transmission electron microscopy (TEM), although alternative imaging technique are occasionally used. Reviews, such as (Ockwig and Nenoff, 2007)(Al-Mufachi, Rees and Steinberger-Wilkens, 2015) also contain images collected from SEM and give further details on potential alternates. Due to the technology available to this project, it was decided to use SEM and thus these alternatives will not be discussed here.

Similar to the section on chromatography above, this section will provide a brief overview of SEM due to its use within this thesis; more detailed reviews can be found elsewhere if required. This section provides an introduction to the technical aspects of imaging and its limitations in regards to this project. A detailed review of the early history of the SEM can be found in (Oatley, 1982), where Professor C.W Oatley a pioneer in the field gives a detailed overview of the fundamentals of SEM, Oatley is responsible for countless other relevant publications with examples such as (Oatley, 1981) providing a detailed review of the electron detector technology – although it must be noted that this is relatively dated in terms of modern work.

A concise introduction to SEM is given by (FEI, 2012), with FEI being a major supplier of electron microscopes. The SEM is a form of electron microscope that produces images of a surface by scanning it with a focussed beam of electrons. This beam of electrons interacts with the surface, producing signals that contain information about the surface topography of the scanned sample, in this case the membrane surface (McMullan, 1995).

The main components of a SEM are an electron optical column, a vacuum system, the specimen chamber, various electronic components and analytical software (FEI, 2012). The column consists of several components; at the top of the column is an electron gun which produces a beam of electrons via the use of a tungsten filament in a thermionic process. Further down the column condenser lenses and apertures are used to focus the electron beam; towards the bottom of the column the beam passes through a number of deflection coils/plates and a final lens and aperture. The deflection coils are used to form a rectangular raster pattern of electrons for scanning (FEI, 2012), the electrons then interact with the surface producing data.

Beam electrons are referred to as primary electrons, interaction with the sample causes these electrons to lose energy through repeated random scattering. The interaction varies significantly with

the electrons landing energy and the atomic number of the specimen (also, the specimen density). Interaction of the beam with the species can provide backscattered electrons (primary electrons not absorbed by the sample), secondary electrons (electrons displaced by primary electrons) and electromagnetic radiation such as x-rays (McMullan, 1995) – with each of these available for analysis with the relevant detector. The interactions of the beam are analysed and stored by the software; allowing for the construction of images by mapping the stored values as variation in brightness (FEI, 2012). The SEM micrographs produced in this work were done so through the use of secondary electron detection.

The most commonly used signal is the secondary electron signal, as the electron energy is dependent on the depth with this producing images accurately reflecting the topography: where edges are bright and recesses are dark (FEI, 2012). As secondary electrons are low energy species, they typically originate from within a few nanometres of the sample surface (McMullan, 1995). Collection of the secondary electrons is a multi-step process; first they are attracted to an electrically-biased grid before being accelerated to a sufficient level through the use of a scintillator. When energised to the correct level the electrons cause the scintillator to emit light. These light flashes are conducted to a photomultiplier outside of the column, where the signal emitted from the photomultiplier is displayed as a two-dimensional (x and y) intensity distribution which as previously mentioned is related to the topography (McMullan, 1995)(Oatley, 1981).

A major advantage of SEM over alternatives such as TEM is the fine point focussed beam, instead of the broad static beam of TEM; this allows for accurate readings of topography down to spots as small as 1nm in diameter (FEI, 2012). A second advantage is that there are no restrictions on specimen dimensions (bar the size of the vacuum chamber).

4.4.6 Membrane Surface Analysis: EDX

Many SEM instruments provide a housing for auxiliary components/detectors that may garner additional useful information. In the case of the SEM utilised in this work energy dispersive x-ray spectroscopy (EDX) was available through auxiliary detectors in the SEM.

EDS is described as an analytical technique capable of elemental analysis and chemical characterisation (Goldstein, 2003), where analysis relies on interaction between an x-ray source and a sample.

Characterisation of the sample is based on the principle that each element has a unique atomic structure allowing for a unique set of peaks on its associated electromagnetic spectrum (Goldstein, 2003).

Characteristic x-rays are produced from a sample through bombardment of charged particles, in this case electrons. This bombardment then excites the atomic electrons above their ground state; if an incident electron excites an inner shell electron an electron hole can be formed. This hole is then filled by an electron from a higher energy outer shell, with the result energy difference between the states emitted as an X-ray. The quantity of X-rays and their energies can be measured via EDX (Goldstein, 2003); with the count giving an indication of atom frequency and the energy of the characteristic x-rays used to identify the species.

There are four main components of an EDX setup: the excitation source (in this case the electron beam), the x-ray detector, the pulse processor and the analyser (Goldstein, 2003). The detector is used to convert X-ray energy into voltage signals; this voltage signal is then sent to the pulse processor where the signals are measured before sent to the analyser for analysis.

The EDX system used within this report is capable of detecting all atoms larger than helium, allowing for accurate spectra of the membrane surface and near-surface to be drawn. One obvious drawback is the inability to detect hydrides as hydrogen will not be found by the detector; however obvious hydride formation should be visible on SEM micrographs through the presence of cracks and distortions of the membrane.

Concerns have also persisted over the accuracy of EDX especially for species that have overlapping peaks (Hodoroaba and Procop, 2014); however it is also stated in the same paper that advancements in modern EDX technologies have contributed to “superior performance”. Improvements appear to focus on improved manufacturing of the detector devices with silicon drift detectors (SDD) replacing older designs resulting in increases in the active detector area and higher energy resolution (Hodoroaba and Procop, 2014), with other advancements including the development of pulse processing techniques resulting in improved performance characterising parameters in EDX.

The SDD is a high-resistivity silicon chip, electrons in the chip are driven to a small collecting anode with a low capacitance. This allows for many advantages including shorter processing times which allow for higher count rates and higher resolution than traditional chips, as mentioned above.

The JEOL SEM (model JSM-6010LA) used in this is known to have the SDD technology described above.

4.5 Experimental Apparatus and Reagents

Alongside the cell membrane enclosure, a range of other components were used throughout this project. This section has been included to give details of the other equipment, reagents and materials.

4.5.1 Bulk Membrane Materials

All bulk membrane materials were purchased from Goodfellow.

Palladium was purchased with a thickness of 0.1 mm, in two pieces measuring 50 mm x 50 mm. The purity of the metal was given as a minimum of 99.95 %. At the thickness supplied Goodfellow state a ±10 % error, however a thickness of 0.098 mm was measured with a micrometer eliminating this error. The material provided was prepared through cold-rolling of an ingot of material and therefore required annealing before use to reshape the metal grains. Figure 4.7 below contains an image of one 50 mm x 50 mm membrane; it must be noted however that these membranes were cut to 25 mm x 25 mm before usage.

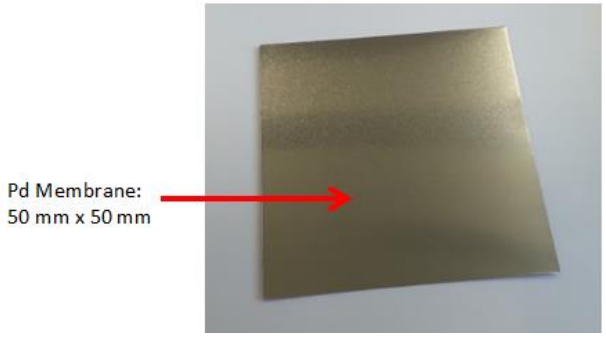

Figure 4.7 – Annotated photograph of palladium membrane

Vanadium was purchased with a thickness of 0.125 mm, in one piece measuring 100 mm x 100 mm. The purity of the metal was given as a minimum of 99.8 %. The thickness was reduced to 0.101 mm through filing/sanding of the material to allow for a more direct comparison with the palladium membranes. The material provided was prepared through cold-rolling of an ingot of material and therefore required annealing before use to reshape the metal grains. Vanadium membranes were also coated with silver by the use of electron beam physical vapour deposition (EBPVD).

Niobium was purchased with a thickness of 0.1 mm, in one piece measuring 100 mm x 100 mm. The purity of the metal was given as a minimum of 99.9 %. At the thickness supplied Goodfellow state a ±10 % error, a thickness of 0.1 mm exactly was measured using a micrometer. The material provided

was prepared through cold-rolling of an ingot of material and therefore required annealing before use to reshape the metal grains. Niobium membranes were also coated with silver by the use of EBPVD, and were also coated with silver and palladium by the use of an electroless plating bath.

Vanadium-nickel (V-Ni) alloy was purchased with a thickness of 0.25 mm; two discs were purchased with a diameter of 25 mm. The V-Ni alloy used was not a standard Goodfellow product and thus an exact specification was provided for alloy content: the alloy contained 85% vanadium and 15% nickel by weight, with an error of ±0.2 %. The alloy was produced through sputter deposition, the alloy was annealed to maximise uniform composition and grain size. The V-Ni alloy was coated with silver and palladium through the use of an electroless plating bath.

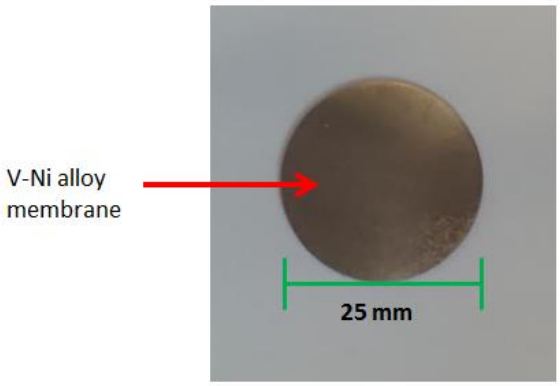

Figure 4.8 – Annotated photograph of a V-NI membrane

Vanadium-nickel-aluminium (V-Ni-Al) alloy was purchased with a thickness of 0.25 mm; two discs were purchased with a diameter of 25 mm. The V-Ni alloy used was not a standard Goodfellow product and thus an exact specification was provided for alloy content: the alloy contained 85% vanadium; 10% nickel and 5% aluminium by weight, with an error of ±0.4 %. The alloy was produced through sputter deposition, the alloy was annealed to maximise uniform composition and grain size. The V-Ni-Al alloy was coated with silver and palladium through the use of an electroless plating bath.

Figure 4.9 below shows an image a palladium membrane after use, the image clearly shows the deformation of the membrane; only palladium membranes showed this level of deformation. Also shown is the fusion of the copper sealing gasket to the membrane, this was found to happen primarily to palladium membranes and the PVD coated membranes. Whilst this showed no performance problems during permeation tests (even when disassembled and reassembled), it did make the copper seals a sacrificial part that needed replacement.

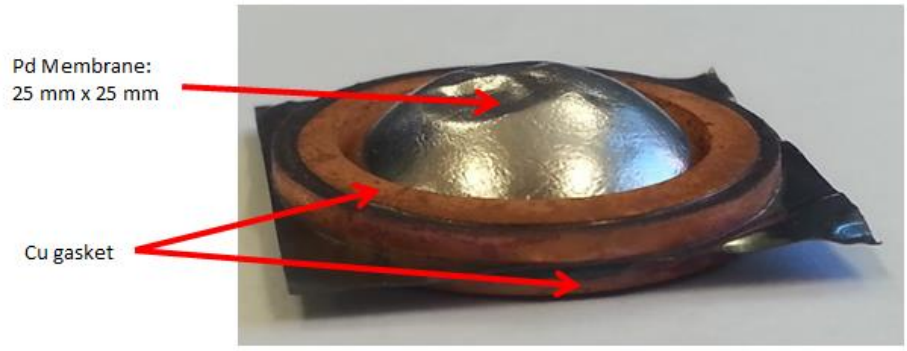

Figure 4.9 – Annotated photograph showing a used palladium membrane and copper gasket

As discussed, a number of membranes tested in this section were silver coated using EBPVD; with the PVD coating provided from one of two sources. Early, auxiliary tests that yielded negative results on titanium coated vanadium membranes were PVD coated by the author using the PVD coating machine provided by the university.

The silver PVD coated membranes discussed within this chapter were coated by Wallwork HT in Cambridge. The methodology described in chapter four accurately represents the coating methodology used by Wallwork and in the earlier application of titanium on vanadium. The methodology can be summarised as:

- The membranes were cleaned ultrasonically in an alkaline solution for six hours
- The membranes were hung within the PVD chamber to allow for complete and uniform coverage
- A silver ingot was placed in line with the electron gun, the chamber was closed.
- The pre-requisite temperature and vacuum for coating were reached within the chamber before coating could start.
- An argon splutter pre-clean treatment was undertaken before coating.
- A coating of 200 nm of silver was deposited on the membrane surface before coating was stopped.
- The chamber was allowed to cool before evacuation and testing of the surface coating through ball crater analysis.

4.5.2 Electroless Plating and Oxidisation Reagents

The Electroless plating methodology followed is primarily that of (Ohno, 2010), with (Tarditi and Cornaglia, 2011)(Koura and Kubota, 1990)(Okinaka and Wolowodiuk, 1990) providing further details,

where the work of Koura & Kubota provided information on the process for the plating of silver. The reagents used in the process are detailed below.

The following reagents were all purchased from Sigma-Aldrich:

- Palladium chloride [$PdCl_2$] powder (5 g); 99 % assay – reagent grade.
- Silver nitrate [$AgNO_3$] powder (10 g); 99 % assay – reagent grade.
- Ammonium hydroxide [NH_4OH] (2 L); 30 % weight NH_3 in H_2O, 99.999% trace metal basis.
- Ammonium chloride [NH_4Cl] (50 g); 99.998 % assay – reagent grade.
- Sodium hypophosphite monohydrate [$NaPO_2H_2.H_2O$] (25 g); >99% assay – reagent grade.
- Tin chloride [$SnCl_2$] (10 g); 99.995 % assay – reagent grade.
- Hydrochloric acid [HCl] (100 mL); 37 % weight HCl in H_2O.
- Hydrazine solution [N_2H_4] (100 g); 35% weight N_2H_4 in H_2O.
- Sodium-EDTA dihydrate [$Na_2C_{10}H_{14}N_2O_8.2H_2O$]; minimum 99% - reagent grade.

The electroless plating bath itself consisted of a 5 L glass beaker; the temperature was maintained and controlled through the use of an oven. Details of the preparation of the bath and the coating of the membranes can be found in the experimental method, in section 6.5.

For oxidisation of the silver layer, sodium hypochlorite solution (reagent grade) and sodium hydroxide (50% in H_2O) were purchased from Sigma Aldrich.

4.5.3 Annealing Chamber

A custom-made annealing chamber was constructed from type 304 stainless steel. The purpose of this chamber was to provide a suitable vessel and environment for the annealing of the membranes when required. Annealing was conducted at elevated temperatures, typically of 300 °C or 500 °C (dependent on the membrane), and was conducted in a pressurised (10 bar) inert argon atmosphere to minimise oxygen and nitrogen exposure of the membrane surfaces at high temperatures.

These operational specifications were used to design a simple pressure chamber, of which a schematic is included in figure 4.11 below. The schematic shows that the annealing chamber consists of two main components: the body of the chamber and a lid. The internal diameter of the body is 30 mm, with a wall thickness of 10 mm giving an external diameter of 50 mm. A flange was welded to the top of the body to allow secure fastening of the lid; M8 screws and nuts are used to form an airtight seal and within the flange a groove for a copper sealing gasket was custom-made.

The diameter of the lid and of the flange is 70 mm; attached to the lid are two lengths of type 304 stainless steel pipe that act as an inlet and a vent. The gas feed and vent pipes are of 3mm external diameter (0.25 mm wall thickness) and of the same specification as the gas feed and vent pipe found on the membrane enclosure, to allow for connection to the same pipe network. Pipe fittings purchased from FTI, identical to those used on the membrane enclosure were attached, to accommodate the nylon pipe work.

Figure 4.10 below contains an image showing the main features of the disassembled chamber.

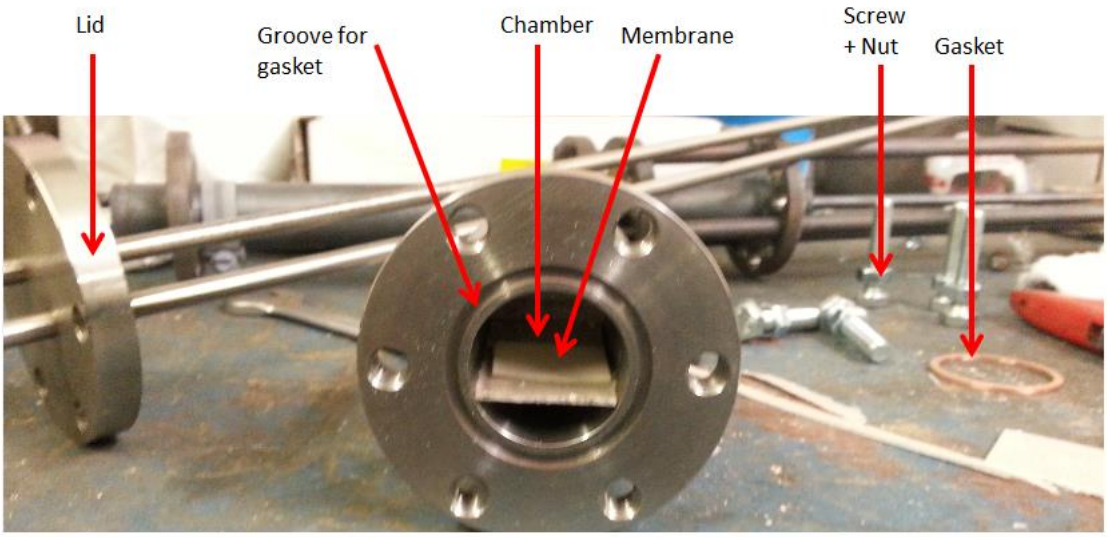

Figure 4.10 – Annotated photograph of the disassembled annealing chamber

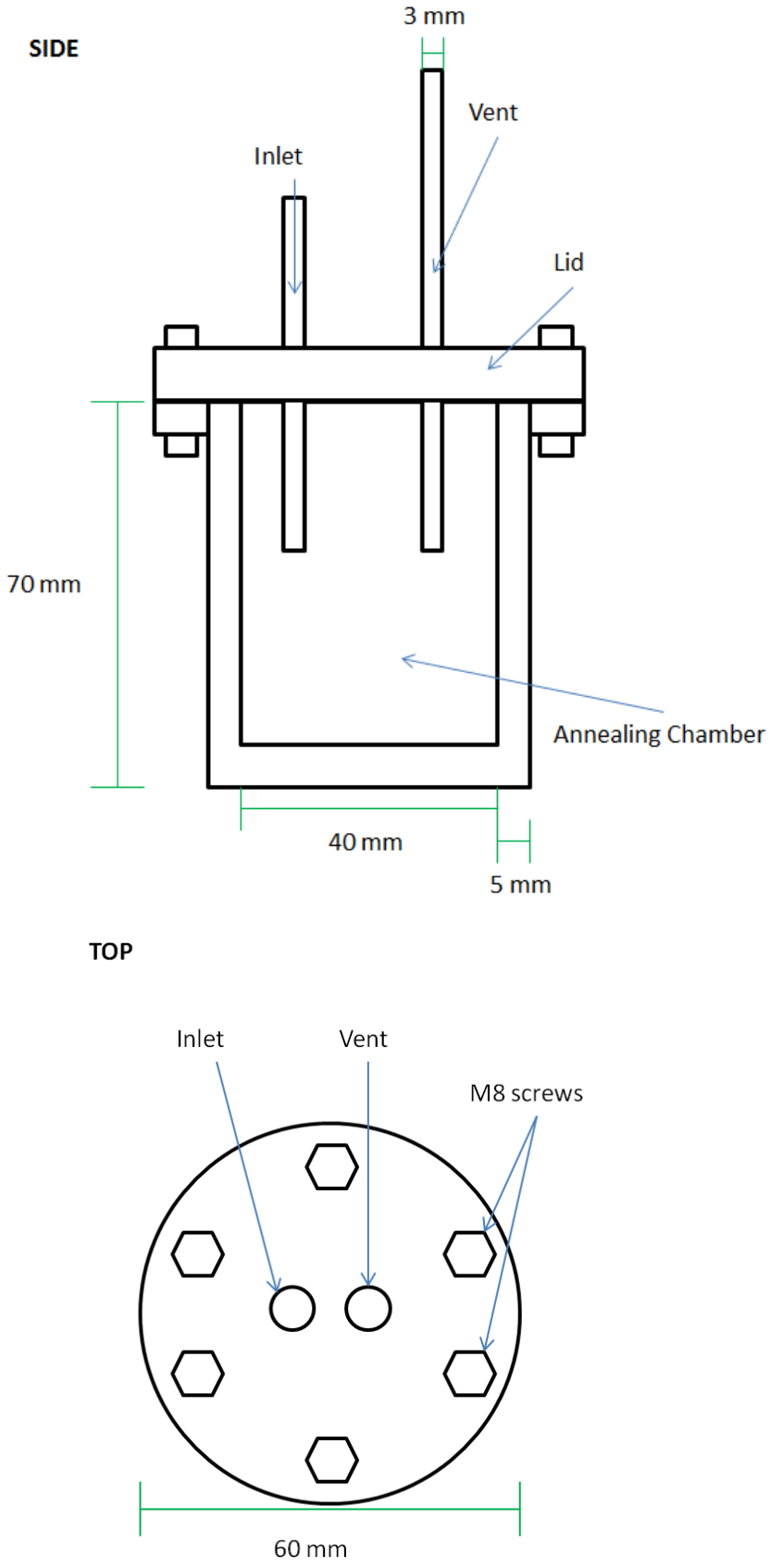

Figure 4.11 – Schematic showing dissected side view and top view of annealing chamber

4.5.4 Gas Chromatography

The gas chromatograph system utilised in this work to analyse the permeate gas stream was manufactured by ABB; the specific model of GC is the PGC2000. Detection and identification of the gases is done through the use of a thermal conductivity detector (TCD), with details on how this detector works given earlier in this chapter. A manual for the specific GC used is referenced within this text, (ABB, 2006), and details of an online version (.pdf download) can be found in the relevant bibliography entry.

Carrier gases are required for transport of the permeate sample, the GC used the following gases, all supplied from BOC:

- Nitrogen (N 5.2 grade, 99.9992% purity). GC supply pressure: 3.41 bar (g).
- Helium (N 5.0 grade, 99.999% purity). GC supply pressure: 6.07 bar (g).
- Hydrogen (N5.0 grade, 99.999% purity). GC supply pressure: 3.96 bar (g).

The supply pressures were set to the value given in the GC operating manual. The GC has two method tables programmed into its software that run on a master and slave loop (named tables one and two respectively on the instrument); with each table responsible for collecting information on different gases. Details of which gas was recorded on each method table can be found in table 4.1; all components capable of detection and analysis by the GC are listed however many of these components are not applicable to this project. The analysis time refers to the expected time required by the GC for the species to travel through the column and pass through the detector for analysis.

Before use the GC required calibration. For this project a gas mixture of 98% hydrogen 2% carbon dioxide was used for calibration, with an accuracy of ±0.5%, limiting accuracy of the GC permeate composition measurements to this same margin. Details on how to run a calibration model on the GC can be found in section 3.1 of the GC manual (ABB, 2006). The calibration gas was supplied by BOC via a custom order.

Table 4.1 – Table containing calibration data for GC used in the analysis of the permeate

Method Table	Component	Concentration in Calibration Gas (%)	Analysis Time (s)
1	Hydrogen	98	92
1	Oxygen	0	N/A
1	Nitrogen	0	N/A
1	Methane	0	N/A

Method Table	Component	Concentration in Calibration Gas (%)	Analysis Time (s)
1	Carbon Monoxide	0	N/A
2	Carbon Dioxide	2	185
2	Propane	0	N/A

As can be seen in table 4.1, significantly different retention times are found for hydrogen and carbon dioxide within the column. Whilst not highlighted on the method table, argon is deemed safe to pump through the GC without risk of damage (ABB, 2006). Details of the analysis method are given in the manual, in section 4: "Technical Description" in source (ABB, 2006). The manual indicates that five internal valves are responsible for controlling flow of the sample gas into ten columns, with valves one to four (and the preceding columns) providing data for the master loop and the fifth valve (and preceding columns) providing data for the slave loop.

The opening and closing time for each valve have been included for reference in table 4.2; each valve and column(s) set up is responsible for analysis of a different gas as shown in the table.

Table 4.2 – Open and close time for internal control valves in GC

Valve	Open (s)	Close (s)	Gases Analysed
1	5	90	Hydrogen
2	35	111	Oxygen, Methane
3	390	520	Carbon Monoxide
4	35	285	Methane
5	5	310	Carbon Dioxide, Propane

Figure 4.12 below shows the inside of the GC oven, complete with internal workings including various columns and valves.

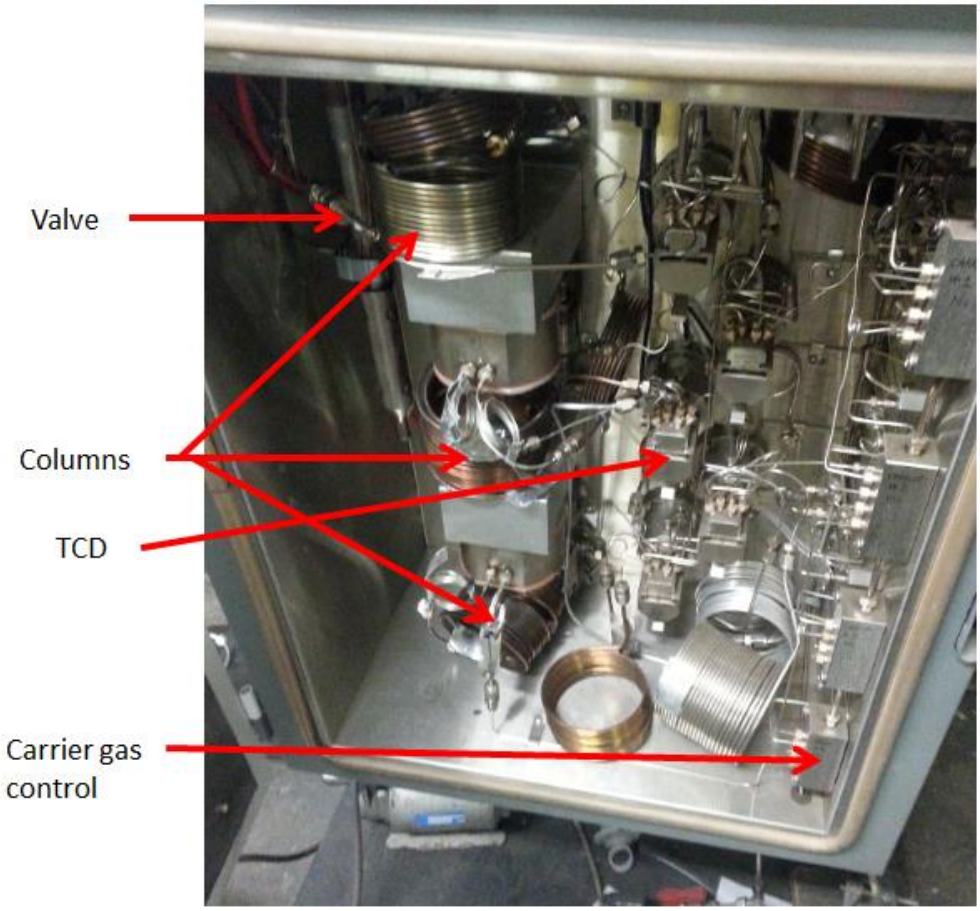

Figure 4.12 – Internal workings of the GC column used for permeate analysis

All gas mixtures/samples were fed into the GC via the gas bag used to collect the samples in the experiment; if the sample needed more gas volume for analysis argon was used to provide bulk without causing any change to the H_2/CO_2 ratio.

4.5.5 Scanning Electron Microscope

As discussed in chapter four, analysis of the membrane was undertaken using a SEM. The SEM used is manufactured by JEOL; with the exact model being the JEOL JSM 6010LA. The SEM is capable of operating in both high and low vacuum modes, however only high vacuum mode was used to generate images for increased clarity.

The SEM is capable of producing images at magnifications between 8x and 300,000x; with the image point-to-point resolution in high vacuum mode reported as 3 nm (JEOL, 2012). Further details on detectors, lenses and other key features can be found in (JEOL, 2012).

EDX is utilised to gather information about topography and surface composition, the EDX detector is of the silicon drift detector (SDD) type. As discussed in chapter four this detector type offers increased accuracy and reliability over older detector types.

The SEM is connected to a computer running “Intouch Scope”; the proprietary software provided by the SEM supplier. The software allowed for the processing of data provided from the SEM and provided outputs in terms of secondary electron micrographs and data on surface composition collected from the backscattered electron detector.

EDX spectra were produced at a range of magnifications, with the magnification given on each micrograph used in this thesis. A range of magnifications were investigated to allow for analysis of the surface, with spectra taken at several spots over the membrane to ensure that any image was reflective of the whole surface.

Data from the EDX can be collected and collated into either surface compositional maps or into energy/intensity spectra. The program also gave the mass and atom percentage of each species present at the surface in tabular form to allow for exact reading ensuring a reliable result was collected.

4.5.6 Measuring Equipment

The feed flowmeter was a volumetric flow meter calibrated for use with hydrogen and then for use with hydrogen/carbon dioxide feed mix. The flow meter was manufactured by CT Platon; the flow meter is part of the NG series. The maximum measurable flow rate is 250 cm^3 min^{-1}; with a minimum measureable flow rate of 50 cm^3 min^{-1}. Incremental measurements of 10 cm^3 min^{-1} were displayed on the flow meter, and the error percentage is given as ± 1.25 % of the full scale, or ± 3.125 mL in this instance.

Two measurement systems were used when recording the permeate flow rate, with the preferred method dependent on the flow rate scale. For larger permeate flows, the rotameter was taken to be the primary measuring tool. The rotameter used was manufactured by Alexander Wright/G.H Zeal Ltd; the model number is specified as DM3 A. The rotameter consists of an analogue face that measures 250 cm^3 of flow per rotation, with a digital face to record the total number of revolutions. The error is given as ± 5 % of the full scale, or ± 12.5 mL in this instance.

Also used was a 10 cm^3 Pyrex measuring tube, manufactured by Cole-Parmer. The accuracy of the tube was given as ±0.2 cm^3 over any range with the scale calibrated for room temperature gas; the

permeate measured in the tube was deemed to be at room temperature as it was bubbled through cool water during collection. The measuring tube method was used to verify the results of the rotameter as well as to measure flow rate for membranes in which the permeate flux was lower.

The measuring tube and the rotameter used collected data on volume only, to calculate a permeate flow rate time it was also important to accurately record the amount of time taken to collect said volume. For this, a digital stopwatch was purchased from RS components; the specific model purchased was the "RS Pro Digital Stopwatch". The datasheet states an accuracy of 0.5 seconds over a 10-hour period, interpolating this gives an assumed error equal to 0.05 seconds per 3600 seconds (1 hour) giving an accuracy approaching 100 %. As the stop watch was operated manually an error of ±0.2 seconds to represent reaction time has been assumed, with the time collected on the stop watch taken to the nearest tenth of a second recorded alongside the permeate volume (and its respective error).

System pressure at the needle valve was measured using an analogue pressure gauge purchased from RS components and manufactured by Wika (model number: 7075741). The maximum pressure readable was 16 bar, with incremental steps of 0.5 bar, from 0 bar (gauge) to the maximum value. This pressure gauge was used to confirm that there was no significant pressure loss on the feed side of the enclosure, as a significant pressure drop from the supply to the vent would suggest a gas leak.

Measurement of the gas outlet temperature was done by inserting a k-type thermocouple into the gas outlet tube. The thermocouple was connected to a data logger with a digital display showing the temperature. The k-type thermocouple was calibrated to an appropriate low temperature range and the temperature measured was recorded to the nearest whole degree.

4.5.7 Miscellaneous and Consumable Items

This brief section has been included to give details on any item deemed necessary for operation of the membrane enclosure or for sample preparation that has not been discussed in the above sections.

The annealing gas and the permeation test feed gases were purchased from BOC; details of each are:

- Hydrogen (N5.0 grade, 99.999 % purity)
- Hydrogen and carbon dioxide mixture (40% vol. hydrogen and 60% vol. carbon dioxide)
- Argon, Pureshield (99.998 % purity)

Gas regulators were used to control the feed side pressure of the membrane enclosure. Two gas regulators were required, one for argon and a second for the flammable gas mixtures. Both of the regulators used were manufactured by gas arc (and purchased through FTI), with identical specifications. The bottle side of the regulator included a pressure gauge to allow for reading of the amount of gas remaining (maximum of 300 bar) and the feed side of the regulator included a pressure gauge used to control system pressure (maximum of 10 bar). The pressure gauges used were manufactured by Wika Instruments.

As stated in the apparatus overview in section 4.2 (and shown in figure 4.1) a tubular-type furnace was used throughout this project in both permeation tests and in the annealing of membranes. The furnace was manufactured by Lenton furnaces; the year of manufacture is 1996.

The furnace is electrically powered, with a maximum power rating of 7.7 kW and an average power use of 3.5 kW. Power was supplied from a mains connection via a phase one socket. The maximum operating temperature of the furnace is 1600 °C, however the maximum temperature used within this body of work was 800 °C.

Temperature was controllable in increments of 1 °C through the use of a digital control located on the front panel of the furnace, with a digital display of both instantaneous and target temperatures of the furnace. The temperature of the furnace was measured through the use of two k-type thermocouples within the furnace wall; the furnace thermocouples were calibrated with the temperature measured within the enclosure before permeation experiments were conducted. Figure 4.13 shows the furnace thermocouple position (blue arrow) and the inlet tube from the furnace circuitry (red arrow).

The furnace tube was measured to be 600 mm long, with an internal diameter of 76 mm; thus providing a maximum size for the membrane enclosure during the design phase. As shown in figure 4.13, the furnace is open ended and thus requires packing to maintain a stable temperature, for this Rockwool thermal insulation wool was used due to its fire-resistance and stability at the operating temperatures utilised. The inside of the furnace is shown to consist of a high-temperature stable ceramic lining.

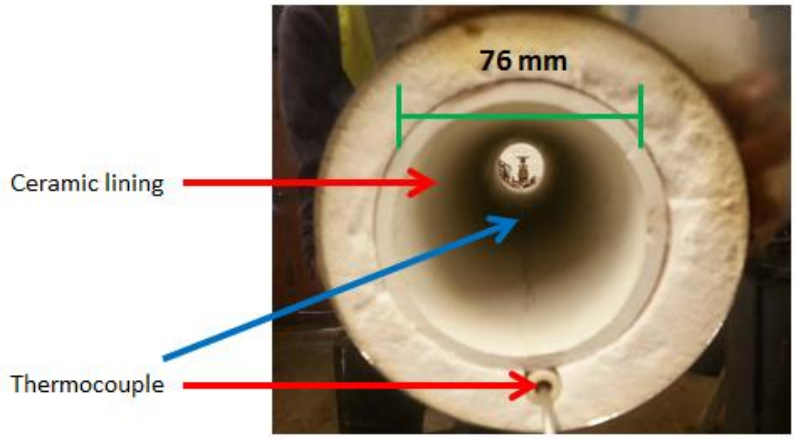

Figure 4.13 – Annotated photograph of the furnace tube

The oven used in the electroless plating step was manufactured by VWR, the model was the "DRY-Line". The oven was of the natural convection (not fan assisted) type, and offered temperature control in increments of 1 °C up to 220 °C, via the use of a digital control on the front door. When the oven door was closed during operation ventilation of off-gas was conducted via the use of the exhaust duct at the rear. Figure 4.14 shows the internals of the oven along with a electroless plating bath post-use.

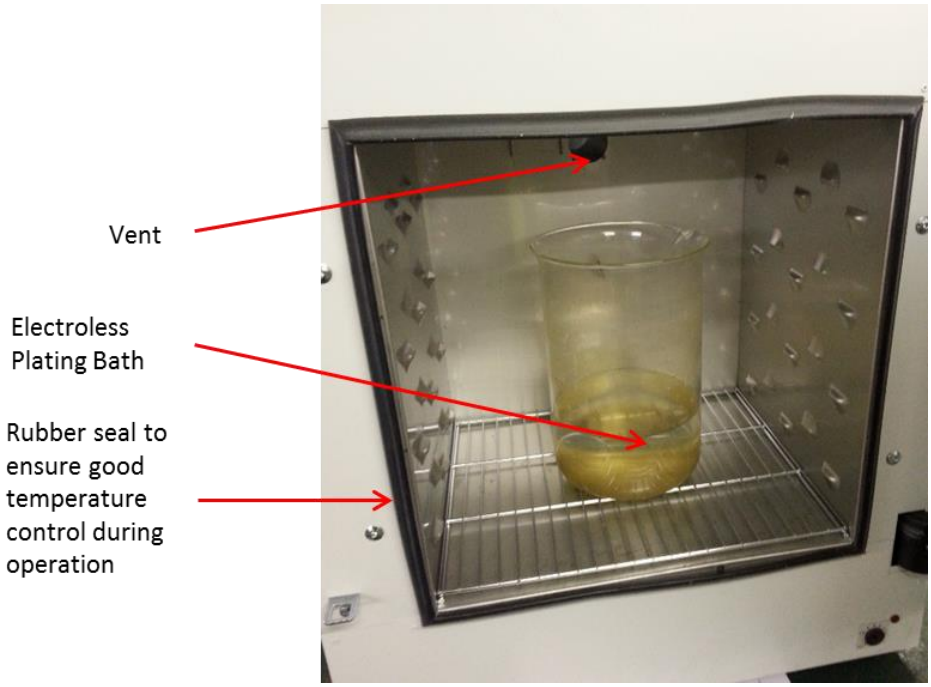

Figure 4.14 – Annotated photograph of the oven internals and electroless plating bath

Gas bags were purchased from Sigma Aldrich to capture samples for analysis; the bags purchased were the Supel-Inert Foil gas sampling bags (with a capacity of 2 L). The bags are manufactured from multiple layers of aluminium and polyethylene layered onto 60-gauge nylon. The bags have a

maximum operating temperature of 87 °C and care was taken to not overheat the bags. Loss of permeate from the bags was not deemed a problem, the bags are stated to lose a maximum of 0.00005 cm^3 of CO_2/day. As the bags were only used over a maximum of six hours it has been assumed that no permeated gas was lost.

The needle valve used to control flow on the feed side was purchased from RS components, a needle valve was selected to allow for precise control of the feed flowrate to prevent CO_2 build up in the membrane enclosure. The configuration of the valve included a pressure gauge to manage leakage (as described in the experimental method in section 4.6); where the pressure gauge and the outlet/vent line are connected via the use of a T-junction pipe connector.

4.5.8 Safety Equipment

Before any experimental work was undertaken a thorough analysis of any potential hazards was undertaken, including the completion of the relevant COSHH forms and a detailed risk assessment. This assessment was used to identify vital pieces of safety equipment, some of which have been detailed in this section.

A ventilation system was constructed and was utilised during annealing, permeation testing and during the electroless plating of the membranes. In the case of permeation testing, the ventilation system was utilised to remove any gases from any leak from the membrane enclosure or annealing chamber and prevent a potentially explosive or asphyxiating environment forming during testing. For the electroless plating undertaken, the ventilation system was used to remove any potentially hazardous gases given off during coating. The ventilation system consisted of an ATEX-safe extractor fan and two 6 metre lengths of flexible ducting, with any gas collected and vented to atmosphere in a controlled and safe manner.

A mobile gas leak detector was purchased from RS components, the detector was manufactured by Kane International and the model used purchased was the CD100A/RS detector. The detector is located on the end of an extendable, flexible hose and is capable of detecting hydrogen and light hydrocarbon gases in concentrations as low as 50 ppm. When a leak is detected an audible alarm and flashing LED are activated.

A flashback arrestor manufactured by BOC was attached to the feed line to prevent any potential flash backs. The model used was the BOC standard in line flashback arrestor, which meets the relevant

British standard (BS EN730-1). The arrestor consisted of a non-return valve and a flame-arresting sintered element.

Suitable PPE was worn when handling chemicals deemed hazardous to health; such as those used in the preparation of the electroless plating bath and for the oxidisation of silver. PPE consisted of heavy-duty neoprene gloves, safety glasses and a protective overcoat. A respirator (with a P1 filter) was used for added precaution when handling the electroless plating baths. When handling any equipment that had been placed in the furnace (membrane enclosure and annealing chamber) heavy-duty heat resistant gloves were worn to limit burn risks.

4.6 Experimental Methods

4.6.1 Method for Electroless Plating of the Permeation Membranes

Due to the potential for the formation of small amounts of dangerous off-gas, other personnel on site were made aware of the process that was about to take place. The electroless plating was conducted in a well ventilated area and with the ventilation system (described in section 4.5.8 above) running.

Palladium

The method utilised here is based on that given by (Ohno, 2010) and (Okinaka and Wolowodiuk, 1990):

1. $PdCL_2$ (2 g) was added to 4 mL of 1M HCl solution, when dissolved this was added to 150 mL of NH_4OH and 10 mL H_2O allowed to stand for 20 hours. The gas extraction fan was turned on to remove any off-gas produced during this period.
2. The oven was turned on and set to a temperature to 50 °C to allow for the electroless plating to take place under optimal conditions.
3. The gas extraction fan was placed at the oven vent on to remove any off-gas produced during the plating reaction. The gas detector was placed above the gas ventilation ducting inlet to alert if any produced off-gas was not immediately vented.
4. The membranes were placed in a 1 M solution of HCl for 30 seconds to chemically clean the surface of the membranes, before being rinsed with deionised water and dried using compressed argon.
5. 100 grade emery paper was used to mechanically clean the membrane surface and provide roughness to allow for better adhesion of the coating.
6. The membrane surfaces were activated by dipping them initially in a tin chloride solution before being rinsed with deionised water and dipped in palladium chloride and 1M HCl solution and rinsed again in deionised water. This process was repeated eight times.
7. The electroless plating was conducted in a 5 L glass beaker. To the beaker the following chemicals were added: 27 g of NH_4Cl and 10 g of $NaH_2PO_2.H_2O$. H_2O is added until the bath is 1L in volume
8. The plating bath was placed in the oven and allowed to reach 50 °C. When the temperature was reached the membranes to be coated were added
9. The length of time for exposure to the bath for each membrane was determined by the deposition rates stated in the sources mentioned above. The deposition rate is stated as 2.5 µm/hr in the above sources; plating times were approximately 15 – 30 minutes.

10. Upon completion of the electroless plating step, the membranes were removed and washed with deionised water to prevent further reaction. The membranes were then dried with compressed air.
11. Membranes that were only to be coated with palladium were then placed in storage before annealing and reduction.
12. The spent reagents in the bath were disposed of in a safe manner in accordance to guidelines.

Silver

The method utilised here is taken from (Tarditi, Braun and Cornaglia, 2011) and (Koura and Kubota, 1990). Silver was always layered onto palladium and was never used as the primary electroless process.

1. The oven was turned on and set to a temperature to 50 °C to allow for the electroless plating to take place under optimal conditions.
2. The gas extraction fan was placed at the oven vent on to remove any off-gas produced during the plating reaction. The gas detector was placed above the gas ventilation ducting inlet to alert if any produced off-gas was not immediately vented.
3. 0.5 g of $AgNO_3$ was added to a solution of 650 mL of NH_4OH and mL of H_2O. To stabilise the bath 67g of $Na_2EDTA.H_2O$ was added to the bath.
4. The membranes were placed in a 1 M solution of HCl for 10 seconds to chemically clean the surface of the membranes, before being rinsed with deionised water and dried using compressed argon.
5. The membrane surfaces were activated by dipping them initially in a tin chloride solution before being rinsed with deionised water. This process was repeated five times.
6. The reducing agent, 10 mL of 1M N_2H_4 was added to the bath, along with enough H_2O to take the total bath volume to 1L.
7. The membranes were placed in the plating bath, with plating time approximately between 6 – 15 minutes.
8. Upon completion of the electroless plating step, the membranes were removed and washed with deionised water to prevent further reaction. The membranes were then dried with compressed air.
9. Membranes were then placed in storage before annealing and reduction.
10. The spent reagents in the bath were disposed of in a safe manner in accordance to guidelines.

4.6.2 Method for Annealing the Permeation Membranes

Annealing of the membranes was done for numerous reasons; all cold rolled membranes needed reshaping of the material grains and all coated membranes needed annealing to either form surface alloys (Pd-Ag coated alloys described above) or for the elimination of any boundary between the surface layer and the bulk of the membrane.

1. The furnace was turned on and the temperature set to 300/500 °C (temperature dependent on membrane to be annealed, lower temperature used for group V Pd-Ag coated membranes) and allowed to warm up.
2. The gas extraction system/fan was turned on.
3. The membrane was cut to a size of 50 mm x 25 mm to fit within the preparation vessel.
4. The membrane was placed within the vessel, along with a support to prevent damage from excessive contact with the vessel wall.
5. The copper gasket was annealed and quenched, before being placed into the O groove on the vessel body.
6. The vessel lid was attached to the vessel, with M8 screws and nuts used to secure its position.
7. Argon was connected to the pipe network; hydrogen/air was flushed from the piping with argon for 20 seconds at a flow rate of 5 L min^{-1}.
8. The vessel was connected to the pipe network via 0.25-inch pipe fittings; the air in the vessel was then flushed with argon for 20 seconds at a flow rate of 5 L min^{-1}.
9. The system was then pressurised to a pressure of 10 bar.
10. To test for leaks the argon storage tank was closed along with the feed side flue valve. If the system pressure remained constant the preparation could continue, if not steps 5 – 8 were repeated.
11. The vessel was placed in the furnace.
12. <u>For membranes coated using electroless deposition only</u>: Hydrogen was connected to the pipe network in place of argon. The argon was flushed from the system and replaced by hydrogen at 3 bar for 5 minutes. This was done to reduce and remove any surface contaminants as done in (Tarditi, Braun and Cornaglia, 2011) albeit with a shorter time span. After 5 minutes, hydrogen was replaced with argon as stated below and the test was carried out with no further variation.
13. The argon storage tank was re-opened but the flue valve was kept closed, thus by monitoring the Argon feed flow rate any leakage could be monitored. Any flow rate reading above zero would suggest a leak had developed and the argon storage tank would be closed.

14. The vessel was left in the furnace for 12-72 hours. Regular checks of the gas alarm were made to ensure no leakage of argon.
15. After 12-72 hours, the furnace was turned off.
16. The vessel was left pressurised with argon until the temperature of the furnace and vessel had fallen to 50 °C.
17. When at 50 °C the argon storage tank was closed and the outlet needle valve opened to allow for de-pressurisation.
18. The gas extraction fan was turned off.
19. The vessel was removed from the furnace and disconnected from the pipe network.
20. The vessel lid was removed, along with the membrane.
21. The membrane was then placed in storage until usage or until the oxidisation process was utilised.

4.6.3 Method for Oxidising Silver Coated Membranes

1. In a 500 mL glass beaker 200 mL of sodium hypochlorite solution (15% free chlorine basis) was added.
2. The membranes were added to the beaker.
3. The membranes were removed from the beaker when the membranes began to discolour; total exposure time was approximately 30 minutes on average.
4. Upon removal of the membranes they were washed with deionised water before being dried with compressed air.
5. Membranes were then placed in the NaOH solution for a total of 15 minutes to remove any surface chloride.
6. Upon removal of the membranes they were washed with deionised water before being dried with compressed air.

4.6.4 Method for Permeation Testing of Membranes

The permeation tests were carried out upon various membranes; however, the methodology utilised was consistent. Variables such as temperature and pressure were kept as consistent as possible for all membranes tested; details on specific conditions used are included in each relevant results section.

1. The gas chromatograph was turned on and allowed to warm up for later use.
2. The furnace was turned on and set to the first test temperature.

3. In case of a gas leak, the gas extraction fan was turned on to prevent any possible gas build up. The gas detector was placed in position near the furnace to detect any potential leaks
4. Two copper gaskets were annealed and quenched. The gaskets were then fitted to the cell enclosure (one on the permeate side and one on the feed side), as shown in figure 6.5.
5. The membrane was placed between the two gaskets, with care taken not to touch the surface, to prevent damage or dirt building up that may limit permeation.
6. Checks were made to ensure that the membrane was placed in the correct position to ensure a complete seal of the pressurised feed side. Checks consisted of visually inspecting the placement of the membrane.
7. The membrane enclosure was sealed through the tightening of the six M6 nuts and screws, with three primary screws located near the feed/permeate interface and three secondary screws located near the expansion springs, as described in section 6.3.
8. After assembly, the enclosure was placed within the furnace and fastened to the nylon pipe-work via 0.25 inch fittings. Air was flushed from the system (feed and permeate side) using an argon purge. The argon purge was also used to identify any leaks in the pipe work or membrane enclosure by monitoring inlet and outlet pressure as detailed previously. Checks were undertaken with a gas leakage monitor and by checking for pressure loss when the gas supply is closed (whilst the vent needle valve is closed) were undertaken.
9. When it was assured that no leaks were present the membrane enclosure was left in the furnace for 20 minutes to ensure that the temperature of the enclosure was equal to the value set in the furnace.
10. Upon equalisation of the temperature the gas feed (H_2 or H_2/CO_2) was turned on, with the argon flushed from the feed-side of the system. The feed pressure was set to the required value using the gas regulators. A feed flow rate of 50 cm^3 min^{-1} was maintained to ensure mixing near the membrane surface when the H_2/CO_2 feed was used. The feed flow rate was controlled through monitoring of the feed flowmeter and opening the vent needle valve.
11. The permeated gas flow rate was recorded through the use of a rotary flow meter and through the displacement of water in a 10 mL measuring cylinder for small flow rates. Recordings of volumes were taken alongside recordings of times for calculation of flow rate; the digital stopwatch was used to record times. A k-type thermocouple was used to determine the gas temperature at the outlet.
12. Flow rate tests were typically repeated five times for each feed pressure (range 1 to 10 bar) at every temperature investigated. Upon completing the five tests a gas bag was attached to the outlet to allow for collection of the permeated gas.

13. Upon completion of each test at a given temperature, the temperature was increased to the next value of interest, typically in increments of 25 to 50 °C – unless stated otherwise in the results.
14. When the temperature of the furnace and enclosure reached the next test temperature, the gas bag was sealed and disconnected to allow for flow rate recording.
15. Steps 11 to 14 were repeated until the final test temperature was reached. Upon completion of the final set of flow rate tests the gas bag was re-attached and left in place until a sufficient amount of permeated gas had been collected for testing.
16. This final gas stage collection was limited to 4 hours as a maximum, upon which if more gas volume was required to run a GC test argon was added to the collected permeate.
17. When a sufficient volume of gas had been collected the gas bag was sealed for later analysis and the feed gas flow was switched off. The vent non-return needle valve was opened fully to de-pressurise the feed side and the furnace was switched off. The gas extraction fan was then turned off.
18. The membrane and the membrane enclosure were left to cool in the furnace overnight, with the membrane recovered the following day for SEM and EBS analysis.
19. After shutdown of the furnace, the permeated sample was fed from the gas bag into the GC. Each GC run consisted of approximately seven minutes of analysis, with the gas composition given in vol. %. The reported data was recorded alongside the collected flow rate data and stored for later analysis.
20. Upon completion of analysis the GC was turned off and allowed to cool.

4.6.5 Emergency Procedures

A gas leak resulting in the formation of a potentially flammable or explosive atmosphere was identified as the major risk during permeation testing. The presence of CO_2 in the feed for various permeation tests also raised the possibility of the formation of an asphyxiating atmosphere.

If for any reason an emergency shutdown of the permeation test was required, the following procedure was to be followed:

1. Raise the alarm and use the Buxton site radio system to inform others on site of the potential hazard.
2. Close the gas bottle regulator to limit the amount of H_2/CO_2 released.
3. Fully open the vent needle valve to depressurise the membrane enclosure and allow for safe ventilation of the H_2/CO_2 present.

4. Leave the testing area via the main door to outside. Leave the door open wide to allow for natural ventilation of the room.
5. Head to the emergency assembly point and continue to make other personnel aware of the situation.
6. Do not re-enter the testing area until given permission to do so by the relevant safety officer or authority.
7. Report and record the incident for further investigation.

Electroless plating involved the use of several chemicals requiring the consideration of relevant COSHH procedures. The major risk identified was a chemical spill or the formation of an off-gas build up.

In the case of an off-gas build up:

1. If the gas alarm starts to sound, raise the site alarm and use the sites radio system to inform others on site of the potential hazard.
2. Leave the testing area via the main door to outside. Leave the door open wide to allow for natural ventilation of the room.
3. Head to the emergency assembly point and continue to make other personnel aware of the situation.
4. Do not enter the testing area until given permission to do so by the relevant safety officer or authority.
5. Report and record the incident for further investigation.

In the case of a chemical spillage:

1. If the spillage requires evacuation of the area raise the alarm and use the site radio to inform others of the hazard.
2. If evacuation is required, leave the testing area via the main door to outside. Leave the door open wide to allow for ventilation to limit any potential vapour build up.
3. If the spillage can be managed safely, inform the relevant site personnel of how the spillage should be safely cleaned.
4. If the spillage is to be cleaned, wearing suitable PPE and using suitable materials clean the spillage.
5. Report and record the incident for further investigation.

4.6.6 Method for Surface Analysis Through the Use of SEM and EDX

1. Membranes to be analysed were cleaned of surface grease using an ethanol spray and with light wiping with a suitable laboratory solvent cleansing wipe. Gloves were worn for every stage of handling the membrane.
2. The membrane was attached to a stainless steel 32 mm sample stub using carbon black adhesive tape.
3. After attachment the stub was fastened into the sample holder and placed within the SEM body.
4. The correct system operating conditions were set (metal, conducting sample, EDX enabled) as the SEM was pumped down to near vacuum using the control system to allow for image collecting.
5. When operating pressure was achieved, the filament lamp was turned on and the microscope began relaying images via the client on the computer system.
6. Images were taken at various magnifications, typically between 200x to 10,000x. At each magnification care was taken to ensure that the stigmatism and brightness was tuned to the correct level.
7. When the required numbers of SEM images were collected the magnification was reduced back to 200x before switching to the EDX sensor to allow for collection of surface data.
8. EDS data was collected both graphically for larger areas and mapped for smaller areas to allow for gathering of surface composition.
9. When all of the EDX data/images and SEM images had been collected the magnification was reduced to less than 100x and the filament was turned off, as per protocol for the SEM.
10. The SEM chamber was vented back to atmospheric pressure before opening; the sample holder was then removed before pumping the SEM chamber back down to near vacuum conditions.
11. The membrane was then removed from the sample holder, with acetone used to dissolve the carbon black adhesive type and remove the membrane without damage.

4.7 Chapter Four Reference List

ABB (2002) *PGC2000 Series Gas Chromatograph Sales Manual*. Available at: www.generaldetectors.com/v2/descargar.php?f=CROMAT~1.pdf.

ABB (2006) 'Operation and Service Manual Process Gas Chromatograph: PGC2000'. Available at: http://instrumentationandcontrol.net/2016/06/14/abb-2006-operation-and-service-manual-process-gas-chromatograph-pgc2000/.

Al-Mufachi, N. A., Rees, N. V. and Steinberger-Wilkens, R. (2015) 'Hydrogen selective membranes: A review of palladium-based dense metal membranes', *Renewable and Sustainable Energy Reviews*. Elsevier, 47, pp. 540–551. doi: 10.1016/j.rser.2015.03.026.

Alimov, V. N., Busnyuk, A. O., Notkin, M. E., Peredistov, E. Y. and Livshits, A. I. (2015) 'Hydrogen transport through V-Pd alloy membranes: Hydrogen solution, permeation and diffusion', *Journal of Membrane Science*. Elsevier, 481, pp. 54–62. doi: 10.1016/j.memsci.2015.01.058.

Bjelkhagen, H. I. (1995) *Silver-Halide Recording Materials*. Berlin, Heidelberg: Springer Berlin Heidelberg (Springer Series in Optical Sciences). doi: 10.1007/978-3-540-70756-1.

Cassar, G., Matthews, A. and Leyland, A. (2012) 'Triode plasma diffusion treatment of titanium alloys', *Surface and Coatings Technology, 212, pp. 20-31*. Available at: http://www.sciencedirect.com/science/article/pii/S0257897212008754 (Accessed: 7 November 2014).

Chen, J. P. and Lim, L. L. (2002) 'Key factors in chemical reduction by hydrazine for recovery of precious metals', *Chemosphere*, 49(4), pp. 363–370. doi: 10.1016/S0045-6535(02)00305-3.

Cheng, Y. S. and Yeung, K. L. (1999) 'Palladium-silver composite membranes by electroless plating technique', *Journal of Membrane Science*, 158(1–2), pp. 127–141. doi: 10.1016/S0376-7388(99)00009-5.

Cheng, Y. S. and Yeung, K. L. (2001) 'Effects of electroless plating chemistry on the synthesis of palladium membranes', *Journal of Membrane Science*, 182(1–2), pp. 195–203. doi: 10.1016/S0376-7388(00)00563-9.

Dolan, M. D., Kellam, M. E., McLennan, K. G., Liang, D. and Song, G. (2013) 'Hydrogen transport properties of several vanadium-based binary alloys', *International Journal of Hydrogen Energy*. Elsevier Ltd, 38(23), pp. 9794–9799. doi: 10.1016/j.ijhydene.2013.05.073.

Dolan, M. D., McLennan, K. G. and Way, J. D. (2012) 'Diffusion of atomic hydrogen through V-Ni alloy membranes under nondilute conditions', *Journal of Physical Chemistry C*, 116(1), pp. 1512–1518. doi: 10.1021/jp208691x.

Ekelof, S. (2001) 'The genesis of the Wheatstone bridge', *Engineering Science and Education Journal*, 10(1), p. 37. doi: 10.1049/esej:20010106.

Engel, R., Pavia, D., Lampman, G. and Kriz, G. (2006) *Introduction To Organic Laboratory Techniques: A Microscale Approach*. 4th edn. Brooks/Cole.

Ewald, A., Glückermann, S. K., Thull, R., Gbureck, U. and Lew, D. (2006) 'Antimicrobial titanium/silver PVD coatings on titanium', *BioMedical Engineering OnLine*, 5(1), p. 22. doi: 10.1186/1475-925X-5-22.

FEI (2012) *An Introduction to Electron Microscopy: The Scanning Electron Microscope*. Available at:

https://www.fei.com/introduction-to-electron-microscopy/sem/.

George, J. (1992) *Preparation of Thin Films*. CRC Press. ISBN: 9780849306518.

Goldstein, J. (2003) *Scanning Electron Microscopy and X-ray Microanalysis*. 3rd edn. Plenum. Available at: https://books.google.co.uk/books?id=ruF9DQxCDLQC&redir_esc=y.

Greenwood, N. . and Earnshaw, A. (1997) *Chemistry of the Elements*. 2nd editio. Butterworth-Heinemann.

Grob, R. . and Barry, E. . (2004) *Modern Practice of Gas Chromatography*. 4th edn. Wiley.

Harris, D. c (2007) *Quantitative Chemical Analysis*, *New York*. doi: 10.1016/j.micron.2011.01.004.

Hatlevik, Ø., Gade, S. K., Keeling, M. K., Thoen, P. M., Davidson, a. P. and Way, J. D. (2010) 'Palladium and palladium alloy membranes for hydrogen separation and production: History, fabrication strategies, and current performance', *Separation and Purification Technology*, 73(1), pp. 59–64. doi: 10.1016/j.seppur.2009.10.020.

Higson, S. (2004) *Analytical Chemistry*. Oxford University Press.

Hodoroaba, V.-D. and Procop, M. (2014) 'A Method to Test the Performance of an Energy-Dispersive X-Ray Spectrometer (EDS)', *Microscopy and Microanalysis*, 20(5), pp. 1556–1564. doi: 10.1017/S1431927614001652.

JEOL (2012) *JSM-6510 series*.

Koura, N. and Kubota, A. (1990) 'Electroless plating of silver.', in *Electroless Plating: Fundamentals and Applications*. William Andrew, pp. 441–463.

Levenets, V. V., Amaya, R. E., Tarr, N. G. and Smy, T. J. (2006) 'Application of PVD silver for integrated microwave passives in silicon technology', *Solid-State Electronics*, 50(7–8), pp. 1389–1394. doi: 10.1016/j.sse.2006.06.014.

Lin, Y. M. and Rei, M. H. (2001) 'Separation of hydrogen from the gas mixture out of catalytic reformer by using supported palladium membrane', *Separation and Purification Technology*, 25(1–3), pp. 87–95. doi: 10.1016/S1383-5866(01)00094-6.

McMullan, D. (1995) 'Scanning electron microscopy 1928–1965', *Scanning*, 17(3), pp. 175–185. doi: 10.1002/sca.4950170309.

Van Den Meerakker, J. E. A. M. (1981) 'On the mechanism of electroless plating. II. One mechanism for different reductants', *Journal of Applied Electrochemistry*, 11(3), pp. 395–400. doi: 10.1007/BF00613960.

Michler, T. and Naumann, J. (2008) 'Hydrogen environment embrittlement of austenitic stainless steels at low temperatures', *International Journal of Hydrogen Energy*, 33(8), pp. 2111–2122. doi: 10.1016/j.ijhydene.2008.02.021.

Oatley, C. W. (1981) 'Detectors for the scanning electron microscope', *Journal of Physics E: Scientific Instruments*, 14(8), pp. 971–976. doi: 10.1088/0022-3735/14/8/019.

Oatley, C. W. (1982) 'The early history of the scanning electron microscope', *Journal of Applied Physics*, 53(2). doi: 10.1063/1.331666.

Ockwig, N. W. and Nenoff, T. M. (2007) 'Membranes for hydrogen separation.', *Chemical reviews*,

107(10), pp. 4078–110. doi: 10.1021/cr0501792.

Ohno, I. (2010) 'Electroless Deposition of Palladium and Platinum', *Modern Electroplating*, pp. 477–482. doi: 10.1002/9780470602638.ch20.

Okinaka, Y. and Wolowodiuk, C. (1990) 'Electroless Plating Of Platinum Group Metals', in *Electroless Plating: Fundamentals and Applications*. William Andrew, pp. 421–440.

OxyChem (2014) *Sodium Hypochlorite Handbook*.

Ozaki, T., Zhang, Y., Komaki, M. and Nishimura, C. (2003) 'Preparation of palladium-coated V and V-15Ni membranes for hydrogen purification by electroless plating technique', *International Journal of Hydrogen Energy*, 28(3), pp. 297–302. doi: 10.1016/S0360-3199(02)00065-4.

Powell Fabrication & Manufacturing (2009) *Sodium Hypochlorite General Information Handbook*, *Industrial*. doi: 10.1021/ie50164a029.

Ra, A. R., Bushroa, A. R., Nasiri-tabrizi, B., Vadivelu, J. and Basirun, W. J. (2016) 'Surface & Coatings Technology Silver / silver oxide nanorod arrays from physical vapor deposition and subsequent anodization processes', 302, pp. 275–283. doi: 10.1016/j.surfcoat.2016.06.006.

Romanenko, O. G., Tazhibaeva, I. L., Shestakov, V. P., Klepikov, A. K., Chikhray, Y. V., Golossanov, A. V. and Kolbasov, B. N. (1996) 'Hydrogen gas driven permeation through vanadium alloy VCr6Ti5', *Journal of Nuclear Materials*, 233–237(PART 1), pp. 376–380. doi: 10.1016/S0022-3115(96)00034-7.

Sree Harsha, K. . (2006) *Principles of Vapor Deposition of Thin Films*. Elsevier Science Publishers B.V. Available at: https://www.dawsonera.com/abstract/9780080480312.

Tarditi, A. M., Braun, F. and Cornaglia, L. M. (2011) 'Novel PdAgCu ternary alloy: Hydrogen permeation and surface properties', *Applied Surface Science*. Elsevier B.V., 257(15), pp. 6626–6635. doi: 10.1016/j.apsusc.2011.02.089.

Tarditi, A. M. and Cornaglia, L. M. (2011) 'Novel PdAgCu ternary alloy as promising materials for hydrogen separation membranes: Synthesis and characterization', *Surface Science*. Elsevier B.V., 605(1–2), pp. 62–71. doi: 10.1016/j.susc.2010.10.001.

Vaitsi, S. T., Salmas, C. E., Tsapekis, O. G., Katsoulidis, A. P. and Androutsopoulos, G. P. (2011) 'Evaluation of hydrogen permselective separation from "synthesis gas" components based on single gas permeability measurements on anodic alumina membranes', *Fuel Processing Technology*. Elsevier B.V., 92(12), pp. 2375–2388. doi: 10.1016/j.fuproc.2011.07.024.

Yuan, Z., Chen, Y., Li, T. and Yu, C. P. (2013) 'Reaction of silver nanoparticles in the disinfection process', *Chemosphere*. Elsevier Ltd, 93(4), pp. 619–625. doi: 10.1016/j.chemosphere.2013.06.010.

Zhao, R., Ding, R., Yuan, S., Jiang, W. and Liang, B. (2011) 'Palladium membrane on TiO2 nanotube arrays-covered titanium surface by combination of photocatalytic deposition and modified electroless plating processes and its hydrogen permeability', *International Journal of Hydrogen Energy*. Elsevier Ltd, 36(1), pp. 1066–1073. doi: 10.1016/j.ijhydene.2010.09.085.

5 The Modelling of Membrane Permeation

The prediction of membrane behaviour through the use of accurate models is a useful and important tool in most branches of engineering research, and the development of separation membranes is no different.

By identifying the factors and parameters that result in improved membrane performance designs of future membranes can be improved via the study of the key principles of successful operation. Alongside this, the use of models allows for efficient use of finances and time; allowing for the consideration of a large number of highly specialised and varied membranes without the need for expensive procurement.

As shown in chapter three, attempts to model permeation behaviour have been ongoing for a significant period of time due to its well-established importance. Chapter three also gave details of a number of models that can be utilised (and modified) to predict permeation behaviour, with a single and important caveat. This caveat being that the vast majority of detailed permeation models require the compiling and collection of thermodynamic data, much of which is hard to compile or measure or predict.

A range of data has been used in this work, from a variety of sources; some of this data is empirical with measured values being more “traditionally” used and reported in models. However, this has its limitations (as discussed previously in chapter three) and the increased availability of high-powered computing (HPC) networks has resulted in large amounts of model-predicted thermodynamic data becoming available for physical processes that previously had little thermodynamic data available. This is particularly useful when attempting to model non-palladium-based membranes; where empirical data is typically difficult to collate.

This chapter contains work based primarily on the models discussed in chapter three; where the framework provided by others is utilised to build and investigate alternative membranes to those initially considered. Considered initially is the work of Richardson (Barrer, 1939) and its modification for more accurate prediction of membrane behaviour.

Efforts are made to identify key operational properties and parameters that can be controlled and altered to improve the performance of membrane separation systems. These parameters are varied in nature, ranging from inherent membrane properties (hydrogen diffusivity, solubility) to operational parameters such as operating pressures and temperatures.

The Ward and Dao model (Ward and Dao, 1999) (and its advancements/modifications) discussed at length in chapter three has been used in an attempt to model for non-palladium-based membranes. The hypothesis that the model can be used to predict non-palladium-based membranes permeation behaviour is tested; with concerns raised over the increased hydrogen solubility in group Vb metals and how this may result in deviation from predicted behaviour.

5.1 The Prediction of the Bulk Membrane Permeate Flux

5.1.1 Introduction to Bulk Limited Calculations

It has been well established in the literature and in this report that membranes can be seen to be either “bulk limited” or “surface limited”. As a reminder, bulk limited membranes are those where the permeation rate is limited by the bulk transport of hydrogen and surface limited being the membranes where the surface processes (chemisorption or desorption) limit the permeate flux.

Whilst thin membranes (<10 μm) are typically surface limited the case for thick membranes is more involved. Thick membranes can be largely split into two categories: those that dissociate hydrogen molecules and those that do not; obviously the membranes that do not promote dissociation without coating are by definition surface limited (as chemisorption cannot take place) and those that do promote dissociation are typically dominated by the bulk resistance to diffusion.

To overcome the lack of hydrogen dissociation for various membranes, such as those based on group V metals, a catalytic coating can be applied to the surface allowing for the transition of the membrane from being surface-limited to bulk limited. Practically, no membranes that do not promote hydrogen dissociation exist (as they provide no permeate) and thus these will not be considered further. Thus, it is assumed in this work that any membrane that requires a catalytic surface coating for operation (such as the group V metals and alloys) has the relevant coating. It is also assumed within section 5.1 that this coating is of a thickness that does not affect bulk-membrane limitation; i.e. the coating is thin (no bulk diffusion resistance) and the surface chemisorption is fast enough that the permeate flux remains limited by bulk diffusion.

By allowing for these assumptions it is possible to use the bulk permeation model first developed by Richardson to calculate the permeate flux for a range of membranes relatively simply. The simplest form of the Richardson equation was given previously as equation 3.4:

$$J = DK_S \frac{P_u^{0.5} - P_d^{0.5}}{t} \qquad \text{(Equation 3.4)}$$

With the molar flux (J) being the product of the diffusion coefficient (D), Sievert constant (K_s), membrane thickness (t) and the upstream and downstream pressures (P_u and P_d respectively). The above expression requires Sievert’s law to be upheld to ensure accuracy, however operating conditions may result in a deviation from conditions where Sievert’s law is applicable. Thus a more general expression can also be considered; this is arrived at by using another expression established in chapter three and chapter two.

The general definition of permeability used throughout this work is as follows:

Permeability (ϕ) = Gas diffusivity (D) x Gas solubility (K)

This expression still assumes that the (partial) pressure of the gas, in this case hydrogen, is related to the concentration of the gas in the metal through the constant K, so the general form of equation 3.4 can be retained. Evidently, in conditions where Sievert's law is valid K would be equal to K_s. Deviation from Sievert's law can be evidenced by plotting hydrogen partial pressure against the hydrogen concentration measured in the metal and comparing with the idealised Sievert values – any difference in K means idealised behaviour is not applicable. Experimentally, this can be done by weighing a piece of metal, exposing it to a source of pure hydrogen for a set period of time and then weighing the metal again to measure the mass of hydrogen absorbed. Temperature data should also be collected to allow for the calculation of density. This is typically using Sieverts' technique for measuring hydrogen solubility**.** Examples (and more details of the technique) can be found in (Dolan et al 2012). Such tests were not conducted experimentally in this work, as only the apparent permeability was investigated experimentally.

It must also be noted that the square root factor present in equation 3.4 is also not universal; a more general expression is given with the power expressed as *n*. Thus giving a general expression of:

$$J = \phi \frac{P_u^n - P_d^n}{t} \qquad \text{(Equation 5.1)}$$

Whilst differing in appearance to equation 3.4 somewhat the relationship displayed is the same as initially described by Richardson and is therefore still considered as the "Richardson Equation" in this body of work.

Whilst the consideration of differing values of *n* is included within this chapter calculations assuming Sievert's law holds are discussed first.

5.1.2 Utilising the Richardson Equation to Predict Permeate Flux Values

In this section the general form of the Richardson equation (equation 5.1) has been used, with n set equal to 0.5 as is common for many investigations (Phair and Donelson, 2006)(Morreale *et al.*, 2003)(Dolan, 2010). In table 5.1 below the hydrogen molar flux for various transition metals is displayed.

The permeability data used is taken from (Phair and Donelson, 2006) with the same values as stated in (Al-Mufachi, Rees and Steinberger-Wilkens, 2015); for completeness the permeability data is included in table 5.1.

Table 5.1 – Reported permeability values for various metals at 500 °C and calculated flux values using the Richardson equation

Metal	Permeability at 500 °C (mol m^{-1} s^{-1} $Pa^{-0.5}$)	Calculated Molar Flux (Mol H_2) m^{-2} s^{-1}	Calculated Vol. Flux (cm^3 H_2) cm^{-2} min^{-1}
Niobium (Nb)	1.60E-06	7.164	1016
Tantalum (Ta)	1.30E-07	0.582	82.6
Vanadium (V)	1.90E-07	0.851	121
Iron (Fe)	1.80E-10	8.06E-04	0.114
Copper (Cu)	4.90E-12	2.19E-05	0.003
Nickel (Ni)	7.80E-11	3.49E-04	0.050
Palladium (Pd)	1.90E-08	8.51E-02	12.1
Platinum (Pt)	2.00E-12	8.95E-06	0.001

The calculated molar flux was produced assuming a pure hydrogen feed; an upstream/feed-side pressure of 3 bar; a permeate/downstream pressure of 0.1 bar and a membrane thickness of 0.1 mm. These conditions have been used purely for demonstrative purposes to illustrate the variation in flux values.

As can be seen in the table the values vary greatly, the high calculated flux values for the group Vb metals illustrate perfectly the attraction of the metals for bulk membrane purposes, as discussed in chapter two.

The final column in table 5.1 includes the volume of the hydrogen flux for the corresponding molar flux. The volume calculated assumes a gas temperature of 15 °C and a hydrogen compressibility factor of 1.0006. The figures in table 5.1 have not been included for comparisons with experimental data, but purely to illustrate in real terms the difference in permeate volume evolved.

5.1.3 Investigating the Validity of Sievert's Law

However, concerns can immediately be raised about the validity of the data due to the assumption that Sievert's law holds. For Sievert's law to hold it is generally reported that the H/M ratio must be

significantly lower than 1 (H/M << 1) (Ward and Dao, 1999)(Phair and Donelson, 2006). The validity of this assumption can be tested by calculating the ratio; this was done using the following method.

If permeability is assumed to be equal to the Sievert constant (K_s) multiplied by the diffusivity; it can be seen that the value of K_s for each system described in table 5.1 can be calculated from the reported permeability and through calculating the diffusivity. As shown in chapter three, the diffusivity is described by an Arrhenius type relationship:

$$D = D_0 e^{\frac{-E_{diff}}{RT}} \qquad \text{(Equation 3.45)}$$

The values for E_{diff} and D_0 are reported for many materials, (Völkl and Alefeld, 1978) provides data for many metals and specific values for palladium (Ward and Dao, 1999) and the group V metals (Suzuki and Takata, 1993) can be found in the sources listed – values in all sources show good conformity. The activation energies are more frequently reported than the pre-exponential factors, with (Ockwig and Nenoff, 2007)(Al-Mufachi, Rees and Steinberger-Wilkens, 2015) and (Phair and Donelson, 2006) all providing E_{diff} values. For the calculated diffusivity values in table 5.2 all metals bar copper and platinum were calculated using data from (Völkl and Alefeld, 1978), data for hydrogen diffusivity in platinum (Katsuta and McLellan, 1979) and copper (Lloyd, Kress and Tatarchuk, 1997) was taken from the referenced sources.

The diffusivity for each of the metals in table 5.1 at 500°C is shown in table 5.2 along with the related calculated Sievert constant. The concentration of hydrogen in the metal can then be calculated through the use of Sievert's law; where $C_{HM} = P^{0.5} K_s$. In table 5.2 the concentration values are those that would be expected under the conditions described in section 5.1.2.

Table 5.2 – Calculated values for diffusivity, Sievert constant and hydrogen concentration in the membrane

Metal	**Permeability at 500 °C ([mol H_2] m^{-1} s^{-1} $Pa^{-0.5}$)**	**Diffusivity (m^2/s)**	**Sievert Constant ([mol H_2] m^{-3} $Pa^{0.5}$)**	**Conc^n H in Metal ([mol H] m^{-3})**
Niobium (Nb)	1.60E-06	1.02E-08	156.5	85701
Tantalum (Ta)	1.30E-07	4.61E-09	28.21	15449
Vanadium (V)	1.90E-07	1.30E-08	14.65	8023
Iron (Fe)	1.80E-10	8.17E-08	0.0022	1.2
Copper (Cu)	4.90E-12	1.72E-09	0.0029	1.6
Nickel (Ni)	7.80E-11	1.37E-09	0.057	31.3
Palladium (Pd)	1.90E-08	6.93E-09	2.743	1502
Platinum (Pt)	2.00E-12	1.39E-08	0.0001	0.1

The data in table 5.2 can be used to test whether Sievert's law holds true for each of the metals under the conditions specified. By calculating the molar density (mol/m^3) of each metal the H/M ratio can be found. The molar density was calculated using molecular mass and density data taken from (Perry, Green and Maloney, 2008) and the resultant values can be found in table 5.3.

Table 5.3 – Table containing the calculated H/M ratios

Metal	**Conc^n H in Metal ([mol H] m^{-3})**	**Metal Molar Density (mol m^{-3})**	**Hydrogen/Metal Atom Ratio**
Niobium (Nb)	85701.7	0.092	0.93
Tantalum (Ta)	15449.3	0.092	0.17
Vanadium (V)	8023.8	0.118	0.07
Iron (Fe)	1.2	0.141	8.56E-06
Copper (Cu)	1.6	0.141	1.11E-05
Nickel (Ni)	31.3	0.152	2.06E-04
Palladium (Pd)	1502.3	0.113	0.01
Platinum (Pt)	0.1	0.110	7.19E-07

If for Sievert's law H/M<<1, then it can be seen that under the specified conditions Sievert's law holds for iron, copper, nickel and platinum without question. It can also be seen that deviation from Sievert's law behaviour is likely in both tantalum and niobium. If the assumption made in (Ward and Dao, 1999) is assumed to be correct, palladium under the specified conditions is likely to exhibit Sievert's law behaviour but it is less clear for vanadium. Whilst vanadium may follow Sievert's law in the example discussed here it must be noted that the feed side pressure is relatively low and the higher pressures utilised in the experimental testing conducted as part of this work could lead to deviation from Sievert behaviour. It must also be noted that other sources suggest vanadium does not exhibit ideal, Sievert behaviour.

5.1.4 A Brief Analysis and Discussion of Permeability

The diffusivity and Sievert constants displayed in table 5.2 are interesting for reasons extending beyond the trivial example used here to illustrate the model. For diffusion-limited membranes the permeability is one of the key intrinsic properties, with the two constituent components giving an

indication on how the permeate flux is generated. As the permeability is a composite property it is worthwhile to consider both aspects of it, hydrogen diffusivity and solubility.

Hydrogen diffusivity, represented by the diffusion coefficient D, can be seen as the proportionality constant between molecular diffusion and the concentration gradient. This relationship is instantly recognisable as Fick's first law of diffusion, used in chapter three during the derivation of the Richardson equation.

$$J = D \frac{dC}{dt} \qquad \text{(Equation 3.1)}$$

In its simplest form, it can be shown from Fick's law that if two hypothetical systems were to have an identical driving force (in this case concentration gradient across the membrane) then the system with the largest diffusivity will produce the highest flux. Therefore, it is immediately apparent why a higher diffusivity is considered a positive attribute for a membrane to have.

The values for permeability in table 5.2 show the highest diffusivities for iron, platinum vanadium, niobium and palladium. Three of these metals are instantly recognisable as metals widely considered for the construction of hydrogen separation membranes as discussed in chapter two which is unsurprising. However, the presence of iron as having the highest and platinum as the second highest diffusivity is certainly more surprising.

The diffusivity of iron is reduced if the figures for iron solubility and permeability from (Marchi and Somerday, 2012) are used to calculate the value, with the diffusivity halved from $8x10^{-8}$ to $4x10^{-8}$, however this is still higher than any other value for the metals presented in table 5.2. Whilst the high diffusivity of iron (and its cheap bulk cost) has led to much research into iron-alloy separation membranes, few of these membranes can boast the high flux rates delivered by the group V metal alternatives.

The high diffusivity but low permeability of iron and platinum highlight the need to consider the second component of Fick's law – the driving force provided by the concentration gradient.

The dependence on hydrogen solubility in the metal to form the driving force for separation is what adds complexity to the designing of high-performance membranes, with the required longevity to make the technology competitive. The ideal membrane needs to have good hydrogen solubility to allow for the generation of the permeate flux, but this solubility must be below the level at which the solute hydrogen begins to cause detrimental effects to membrane performance and longevity.

Thus, the ideal membrane would combine the highest possible diffusivity with reasonable hydrogen solubility at the required operating temperatures (between 300 to 500 °C ideally). Arguably the most prudent starting place for the selection of a membrane material would be to study the diffusivities for the most promising membrane materials covered above and in chapter two.

The D0 and E_{diff} values used to calculate the diffusivities in table 5.2 above have been used to calculate the diffusion coefficients for selected metals under varying temperatures as shown in figure 5.1.

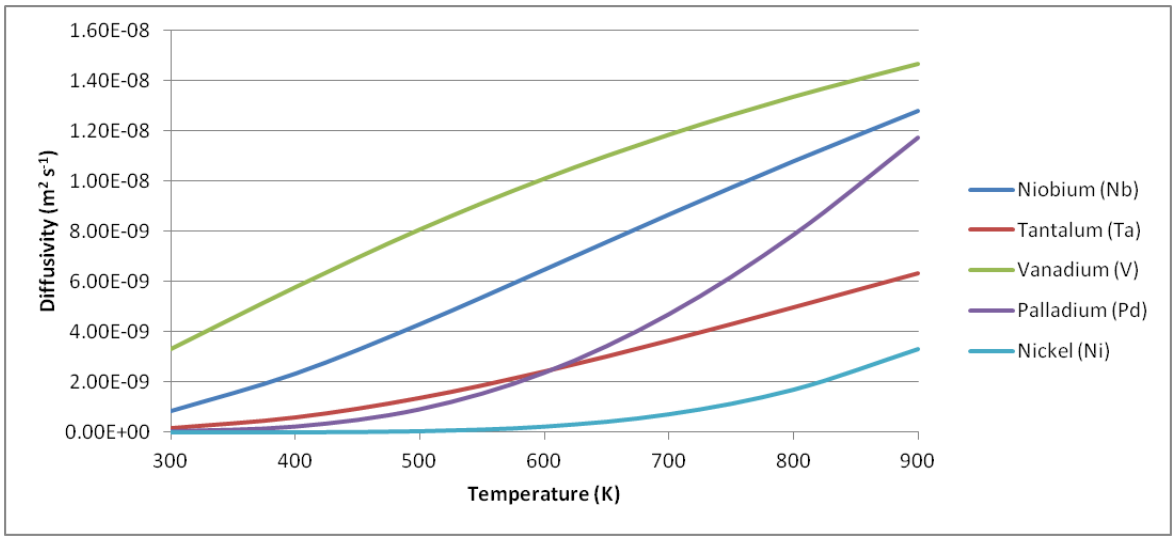

Figure 5.1 – Diffusivities of selected metals over the temperature range of 300 to 900 K

Figure 5.1 shows clearly that for all the metals considered the diffusivity increases as temperature increases. This is not surprising and can be explained somewhat by considering an alternative approach to calculating diffusivity, an alternative expression for the diffusivity/diffusion coefficient is provided in (Ward and Dao, 1999), where an analogy to solid-state diffusion gives rise to:

$$D = \alpha_c a^2 \Gamma_j \qquad \text{(Equation 3.48)}$$

Where the jump frequency itself can be described with an Arrhenius type relationship (equation 3.49), thus leading to an explanation of the temperature dependence of the diffusivity – an increase in temperature corresponds to an increase in the number of interstitial lattice jumps made resulting in an increase in diffusivity.

Figure 5.1 also shows that the relationship between diffusivity and temperature varies between each metal; evidenced by the differing values for D_0 and E_{diff} for each metal. The importance of the activation energy and the pre-exponential constant in each of these relationships is explained by the Arrhenius relationship. D_0 provides an upper asymptote for the diffusivity at an infinite temperature; it can be seen as an absolute diffusivity limit. E_{diff}, the activation energy, provides an indication of the

temperature dependency of diffusivity which sets the gradient for the predicted diffusivity values in figure 5.1. The D_0 and E_{diff} values used have been included in table 5.4, with the sources stated previously in section 5.1.3 used once again.

Table 5.4 – D_0 and E_{diff} values used for various transition metals

Metal	**D_0 (m^2 s^{-1})**	**E_{diff} (kJ mol^{-1})**
Niobium (Nb)	5.000E-08	10.2
Tantalum (Ta)	4.400E-08	14.5
Vanadium (V)	3.100E-08	5.6
Nickel (Ni)	6.900E-07	40
Palladium (Pd)	2.900E-07	24

Utilising the above relationships it can actually be seen from the D_0 values in table 5.4 that the D_0 values for the group V metals are significantly smaller than those of nickel and palladium. However, the low activation energies are of much more importance as this leads to a higher diffusivity in the temperature range used for membrane separation.

It is now possible to expand upon the conclusion reached earlier in this section where it was assumed that a higher diffusivity would be beneficial for membrane performance. As the US DoE targets for marketability demand an operating temperature of 250 – 500 °C (523 – 773 K), the ideal membrane would have a high diffusivity potential (D_0) and a low activation energy (E_{diff}) alongside a moderate hydrogen solubility for increased membrane stability.

It is for these reasons that the experimental work undertaken as part of this thesis has included the investigation of bulk vanadium alloy membranes, with 85V-15Ni and 85V-10Ni-5Al membranes tested to investigate their permeability under varying conditions.

As covered in chapter two these membranes are shown to have good diffusivity and suppressed hydrogen solubility (in comparison to pure vanadium)(Dolan, 2010). Data from various sources (Dolan *et al.*, 2013), (Ozaki *et al.*, 2003a) and(Ozaki *et al.*, 2003b) have been used later in this chapter to predict bulk permeation flux data for these membranes.

5.1.5 Operational Parameters and Their Effect on the Predicted Permeate Flux

After considering the impact of the intrinsic properties of the membrane material, this section has been included to briefly investigate the effect of the main operational parameters (pressure,

membrane thickness and temperature) on the permeate flux. The general form of the Richardson equation (equation 5.1) allows for the making of simple predictions in this regard.

$$J = \phi \frac{P_u^n - P_d^n}{t} \qquad \text{(Equation 5.2)}$$

Once again, for investigation of the trends of each parameter n is set to equal 0.5 and Sievert's law is assumed to hold true. The flux values suggested by this method are likely to be higher than those achieved in real operation.

The relationship between the permeate flux and the membrane thickness can be represented graphically as a hyperbolic curve (with the form of $f(x) = c/x$), an example of this is included in figure 5.2 where the molar flux of a vanadium membrane is predicted. As discussed in chapter two, many membranes undergoing research are designed to be as thin as possible – the attraction to this is obvious as the improvement to the flux evolved grows exponentially with decreasing thickness. It must be noted that there are potential downsides to decreasing membrane thickness; a thinner membrane may require a support layer that can negatively affect mass transfer and reduce the effective membrane surface area or can result in a lower purity of hydrogen permeate.

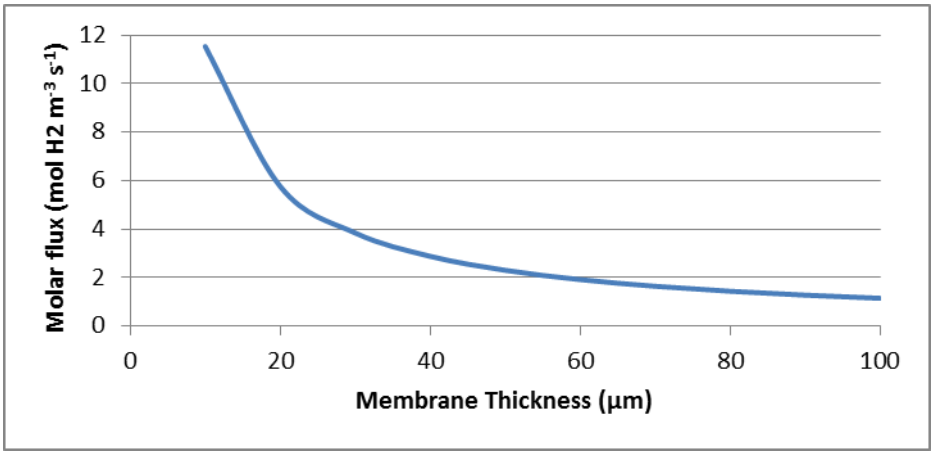

Figure 5.2 – Predicted permeate molar flux for a vanadium membrane with varying thickness, at a temperature of 773 K and with an upstream pressure of 5 bar and a downstream pressure of 0.1 bar.

The relationship between flux and pressure is also rather simple to predict, provided that Sievert's law is observed. Figure 5.3 shows the predicted flux for a vanadium membrane with varying upstream pressure. A similar graph could be drawn by changing downstream pressure as it is the difference between the two values that results in a change of the driving force (the concentration gradient of hydrogen across the membrane). The relationship between the pressure and flux is best described as a function with the form of $f(x) = \sqrt{x}$, thus increasing the pressure has diminishing returns in terms of

increasing the permeate flux. If Sievert's law is assumed not to hold this function is expected to be altered, but follow the same graphical form, $f(x) = x^n$.

This is important to note in operational terms, as during real operations the feed-side/upstream pressure is likely to be set by the operating pressure of the gasifier or the reformer (typically 10 – 30 bar minimum); figure 5.3 suggests increasing this further would have limited benefits in comparison to the required energy for compression due to the diminishing returns.

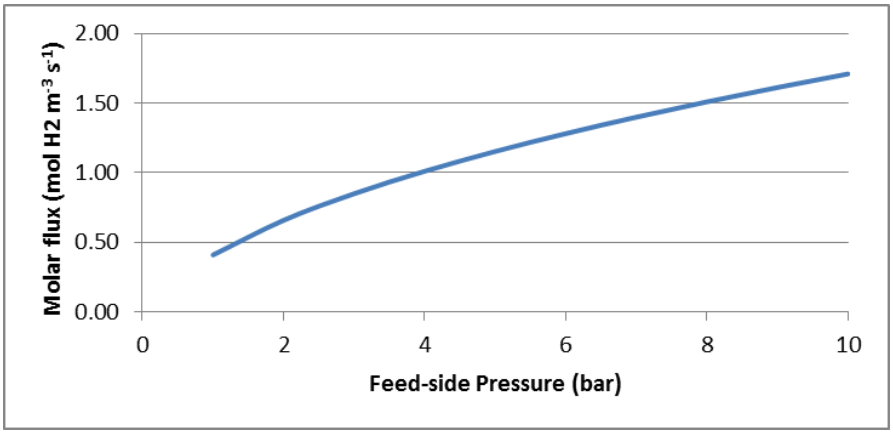

Figure 5.3 – Predicted molar permeate flux (y-axis) for a vanadium membrane (100 µm thick) with varying upstream pressure, at a temperature of 773 K and with a downstream pressure of 0.1 bar.

The final operating parameter to consider is the operating temperature. Unlike the operational pressures (feed and permeate side) or the membrane thickness, the relationship between temperature and the permeate flux is more dependent on the membrane material.

The diffusivity of various metals was discussed at length in section 5.1.4, however the solubility of hydrogen in metals also varies with temperature and this relationship does not offer the same uniform outcome as diffusivity. Two differing examples have been included in this work to highlight this feature, with figure 5.4 showing the calculated flux for a vanadium membrane and figure 5.5 showing the calculated flux for a palladium membrane at varying temperatures. Permeability data for vanadium and palladium was taken from (Steward, 1983).

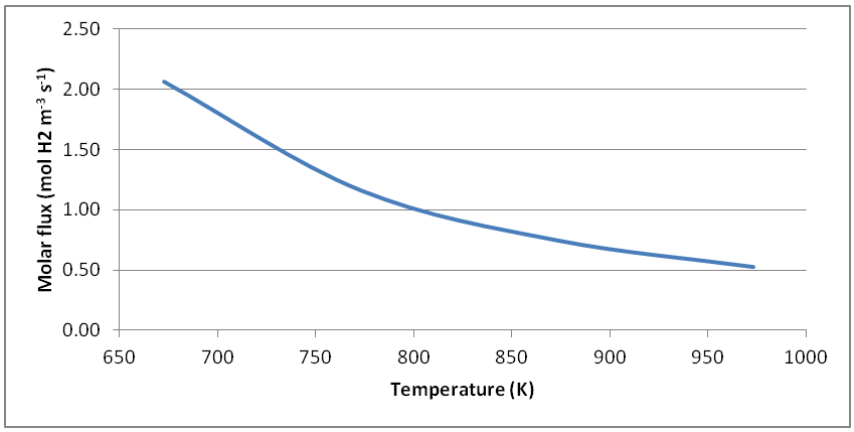

Figure 5.4 – Predicted molar permeate flux for a vanadium membrane (100 µm thick) with a feed side pressure of 5 bar and a permeate side pressure of 0.1 bar at varying temperatures

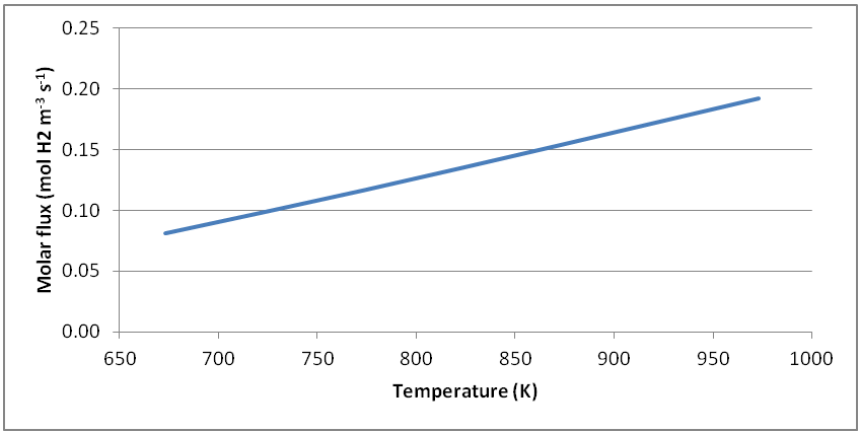

Figure 5.5 - Predicted molar permeate flux for a palladium membrane (100 µm thick) with a feed side pressure of 5 bar and a permeate side pressure of 0.1 bar at varying temperatures

Figure 5.4 and 5.5 show very different behaviour with regards to increasing temperature. Whilst it is known that the diffusivity for both metals increases, the resultant loss of hydrogen solubility for vanadium leads to a significant drop off in generated molar flux.

Whilst increasing the pressure differential and decreasing the membrane thickness are shown to increase the permeate flux, nevertheless care must be taken when deciding an ideal operating temperature to ensure that the maximum flux is reached for any given membrane in the operational (250 – 500 °C) range.

As the conclusions in this section are determined for thick membranes it is assumed that they are applicable to the physical membranes studied in chapter six of this thesis. A more precise model is required to give accurate prediction of the membrane flux but the effect of changing the operational parameters should be considered universal.

5.2 Deviations from Sievert's Law and the Effect on Permeation Modelling

So far all of the models considered above have assumed Sievert's law to be valid; however under the conditions utilised for membrane separation (high temperature, high pressure) the application of Sievert's law can potentially lead to inaccuracy in predicting the membrane flux.

This assumption was useful for investigating the impact of operational parameters and intrinsic membrane properties (utilising reported permeability and diffusivity data) in a general sense to give trends but may lead to inaccuracy for real membrane operations.

Sievert's law models ideal behaviour, one of the assumptions of this ideal behaviour is that the absorbed hydrogen molecules do not interact with each other. Evidently as the saturation of hydrogen in the membrane/metal increases hydrogen atoms begin to interact and distort the idealised relationship.

The assumption of H/M << 1 validating Sievert's law has been made in (Ward and Dao, 1999) and in (Phair and Donelson, 2006). In instances where the hydrogen solubility exceeds this, the model proposed by Ward and Dao discussed in chapter three requires alteration.

Deviations from Sievert's law can be investigated for any given system by plotting the square root of the pressure ($Pa^{0.5}$) against the H/M ratio to give isotherms. If Sievert's law is observed then the isotherms drawn will be linear (Dolan *et al.*, 2013) and would represent a constant value for K for any given temperature.

The data required for this plot of hydrogen isotherms can be gathered through hydrogen absorption measurements; this is carried out using Sievert's technique (experimentally) as is done in (Dolan, McLennan and Way, 2012) or can be predicted using thermodynamic models as is done by (Shim *et al.*, 2013) and (Kim, Shim and Lee, 2012). The thermodynamic models can either be semi-empirical, as is the case for (Shim *et al.*, 2013) or based on atomic models as is done in (Kim, Shim and Lee, 2012).

Alternatively, if the relationship between the H/M ratio and the pressure deviates from linearity then Sievert's law is not applicable. This ultimately leads to the breakdown of the Ward and Dao model and the Richardson equation (where n=0.5) and thus requires adjustment.

This adjustment comes in the form of a shift in defining the driving force of permeation, from concentration gradient to the difference in chemical potential.

This idea is well established in the literature, with (Caravella, Barbieri and Drioli, 2008)(Dolan, McLennan and Way, 2012)(Suzuki *et al.*, 2016) and (Flanagan, Wang and Shanahan, 2007) all discussing models based on chemical potential in place of concentration gradient.

Using the chemical potential as the driving force allows for the modelling of permeation in conditions where the diffusivity/diffusion coefficient varies with the hydrogen concentration. This can be seen in non-idealised behaviour where diffusivity is a function of both temperature and pressure.

Whilst caution must be exercised when considering "classical" diffusion theory in these instances (Dolan, McLennan and Way, 2012)(Flanagan, Wang and Shanahan, 2007) it is possible to compare measurable solubility and steady-state permeability data in order to estimate the diffusion coefficient; examples of such studies can be found for various materials including niobium (Zhang *et al.*, 2008) and vanadium alloys (Suzuki *et al.*, 2014)(Dolan *et al.*, 2013). As permeability is still considered to be a composite of the solubility and the diffusivity of the membrane, it can be seen that this increased solubility essentially leads to a decrease in diffusivity (in comparison to the values estimated with Sievert's law valid).

This can be attributed to the interactions between hydrogen atoms in the bulk material as mentioned earlier. It is posited that this increased interaction leads to an increase in the activation energy for diffusion (Zhang *et al.*, 2008).

The consideration of the chemical potential in place of the concentration gradient does not invalidate Sievert's law, as it can be seen that Sievert's law is a special subset of the more general term. The conditions of this subset being that hydrogen concentration is low enough to ensure limited interaction between the dissolved atoms in the matrix resulting in minimal change to the barrier of diffusivity, leading to only a temperature dependence for this term. The hydrogen concentration at which each metal deviates from the idealised behaviour varies; hence as vanadium-alloy membranes are modelled in this chapter a brief summary of the vanadium-hydrogen system is included below in section 5.2.1.

The limitations of the Ward and Dao model were highlighted in chapter three, with an alternate bulk diffusion rate equation taken from (Caravella, Barbieri and Drioli, 2008); where the remaining rate equations (dissociative adsorption, re-combinative desorption, surface-bulk and bulk-surface) remain unchanged. Thus it is assumed that any model that accurately describes bulk permeation can be substituted in place of the one utilised by Ward and Dao.

It is worthwhile to note that (Caravella, Barbieri and Drioli, 2008) presents calculated flux values that are identical to those presented by Ward and Dao for a 100 μm thick membrane under a range of

temperatures and hydrogen pressures of 1 atm on the feed side and a high vacuum (modelled as 0 atm in the model) on the permeate side. Evidently this would suggest that under the conditions specified, a palladium membrane would act with ideal behaviour.

Comparison between the ideal flux values and the measured flux values can be used to give some indication of deviation from idealised behaviour. Taking both predicted and measured flux data it should be possible to refine the model by following the method of (Flanagan, Wang and Shanahan, 2007) or (Suzuki *et al.*, 2014) to improve future models. Deviation from an idealised model should also indirectly give evidence of deviation from idealised behaviour where PCT plots are not available.

An alternative approach to estimating the permeability is also available using the Richardson equation. As has been mentioned elsewhere in this chapter, equation 5.1 provides a general form of the Richardson equation, where *n* can be varied. The variation of *n* is used to compensate for this change in the relationship, and is effectively an attempt to tie chemical potential (and not concentration) to the gas pressure. The determination of *n* for this is done semi-empirically as shown in (Morreale *et al.*, 2003) where flux data is plotted against the pressure differential raised to the power *n* ($P_u^n - P_d^n = \Delta P^n$). The value used for *n* is varied until the R^2 value for the linear trend is maximised, different values of *n* are available in the literature (Morreale *et al.*, 2003)(Al-Mufachi, Rees and Steinberger-Wilkens, 2015), however the vast majority reported are n=0.5, with values of 0.62 and 0.68 also stated for palladium .

The limitation of this model is that whilst it can be used to predict the permeability as a composite property, it is incapable of producing data on the diffusivity or solubility without further information. Data on hydrogen solubility (H/M) in the form of PCT curves can be combined with the permeability to give data on the diffusivity under specified conditions.

The obvious drawback to this situation is that it requires experimental data, and thus cannot be utilised as a primary source of membrane investigation, due to the dependence on prior testing. However, it provides a simple method for calculating a relatively accurate permeability value whilst accounting for the deviation from ideal behaviour – this model is used in chapter seven during the analysis of the experimental results.

5.2.1 Hydrogen Solubility in Vanadium and Vanadium Alloys

Amongst others (Steward, 1983), citing (Veleckis and Edwards, 1969), reports limits to the Sievert behaviour of the group V metals; with temperature below 300 °C and pressures above 0.1 bar resulting

in deviation from the idealised behaviour. PCT diagrams and solubility data for the vanadium-hydrogen system can be found across multiple sources for varying conditions (Chang and Wert, 1973)(Dolan, 2010)(Veleckis and Edwards, 1969) and (Shim *et al.*, 2013). It is clear to see that deviation from Sievert's behaviour is severe even under moderate conditions; with H/V atomic ratios shown to be significantly over 0.4 at pressures as low as 1 bar at temperatures in the range of interest.

Vanadium alloys show a significantly different trend to pure vanadium, with much lower H/M atomic ratios at considerably higher pressures. Of particular interest to this work is the effect of increasing aluminium and nickel content.

(Shim *et al.*, 2013) shows through model predictions that the addition of nickel and aluminium reduces hydrogen solubility significantly in the system, with the diffusivity/diffusion coefficient also shown to decrease with increasing nickel or aluminium content. It is assumed a ternary mixture of vanadium, nickel and aluminium will result in the same reduction. A similar conclusion of decreasing solubility for increasing aluminium content can be drawn from (Suzuki *et al.*, 2016), where a diagram is presented depicting H/M ratios for a temperature of 773K at various pressures. (Ozaki *et al.*, 2003a) suggests that hydrogen solubility is more affected by the addition of aluminium than nickel.

Data for hydrogen solubility in V-Ni alloys is more readily available but with some disagreement on the H/M ratio/solubility displayed by the alloy. For V-Ni alloys at pressures of up to 7 bar the H/M ratio is shown to be less than 0.1 in both (Dolan, 2010) and (Dolan *et al.*, 2011), whereas work done by the same group appears to suggest that this is not the case (Dolan, McLennan and Way, 2012). The study completed by Shim et al referenced above also shows significant deviation from idealised behaviour at modest pressures; with the calculated values deviating from idealised behaviour at pressures as low as 3 bar approximately.

To investigate this ambiguity it was decided to model the V-Ni membrane assuming idealised behaviour in a pure hydrogen feed. By comparing this to the experimental data collected in chapter six it was hoped that the limits to the idealised behaviour could be determined experimentally.

5.3 Surface Interactions and Their Impact on Membrane Behaviour

So far this chapter has focussed on modelling membranes in which bulk diffusion acts as a limiting factor. This requires the acceptance of a number of conditions to validate the predictions; chief amongst these is that the surface interactions are not rate limiting.

However, there exist a number of situations in which this is not the case; examples of this include feed gases with multi-component mixtures and membrane operation at temperatures where the permeate flux is not diffusion limited. Evidence of the latter can be found in (Caravella, Barbieri and Drioli, 2008), where adsorption and desorption are suspected to provide limits to hydrogen permeation at low temperatures. Multi-component mixtures are discussed below.

One of the key aspects of this PhD study is the consideration of varying the catalytic coating on the surface of the membrane. As such, this section attempts to model the impact of this variation and give consideration to how this may affect the overall hydrogen permeability under the conditions of interest to this project.

5.3.1 Palladium and Palladium Alloy Coatings

Palladium coatings have long been used where a catalytic presence is required for hydrogen dissociation and adsorption. Before considering the material itself, it is worthwhile to recall the rate equations for adsorption and surface-to-bulk transfer:

$$R_{ads} = 2\Gamma S(\theta) \qquad \text{(Equation 3.31)}$$

$$R_{s-b} = N_s N_b \nu_0 e^{\frac{-E_{s-b}}{RT}} \theta(1 - X) \qquad \text{(Equation 3.38)}$$

For adsorption the bombardment rate and the sticking coefficient are the driving forces. The relationship between the sticking coefficient and surface coverage was described in chapter three, where it was stated that for pure palladium the value of S_0 is equal to 1. It is assumed that a Pd-Ag coating provides the same value for S_0 and that the same relationship is maintained. As with other published works such as (Caravella, Barbieri and Drioli, 2008)(Ward and Dao, 1999), it is assumed that there is no activation barrier for hydrogen adsorption on palladium.

As the bombardment rate is independent of the membrane material this relationship should be considered as a function of the operational parameters solely. The bombardment relationship considered here assumes a pure hydrogen feed, with a mixed feed considered later in section 5.3.3.

Thus for both the palladium and palladium-silver coating it is assumed that the adsorptive rate will be identical, due to the independence of the bombardment rate and the assumed identical nature of the modelled adsorption rate.

When considering the second process in permeation however, surface to bulk transfer, the behaviour between the two coatings begins to deviate due to their differing physical properties. An ideal starting place to investigate this deviation is the value of ν_0, the pre-exponential factor utilised in the rate equation for surface to bulk transfer. The value of ν_0 is determined through the use of the following equation, shown in chapter three:

$$\nu_0 = \frac{\beta_0 T^{0.25}}{Q} \frac{1-\theta}{\theta} \sqrt{\frac{\theta_{HH} S_0}{S(\theta)}} \qquad \text{(Equation 3.65)}$$

The value for ν_0 is shown to be dependent on both temperature and surface coverage,

As this relationship is dependent on the bulk-to-surface pre-exponential factor (β_0) it is required that this must be calculated also. The relationship used to calculate β_0 was established in chapter three, here it is given as:

$$\beta_0 = \frac{4D_0}{a^2 N_b (1-\theta)} \qquad \text{(Equation 5.3)}$$

The constant β_0 is shown to be dependent on surface coverage but independent of temperature, unlike the surface-to-bulk constant. This allows for easy calculation of the value of β_0 with the use of available data.

The values for D_0, a and N_b for both palladium and a 80Pd-20Ag coat are taken from (Catalano, Giacinti Baschetti and Sarti, 2010), with figures 5.6 and 5.7 included of show the impact of varying surface coverage (θ) on the resultant value of β_0.

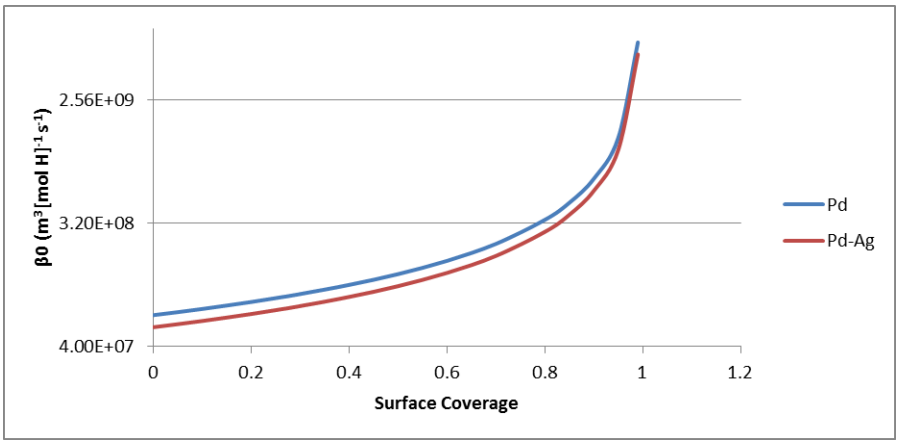

Figure 5.6 – Value of factor β_0 over varying surface coverage

The graph shows that the pre-exponential factor is heavily dependent on surface coverage. Due to the pressures utilised in membrane separation; the surface coverage is likely to be high (over 0.9) figure 5.7 shows this range in greater detail.

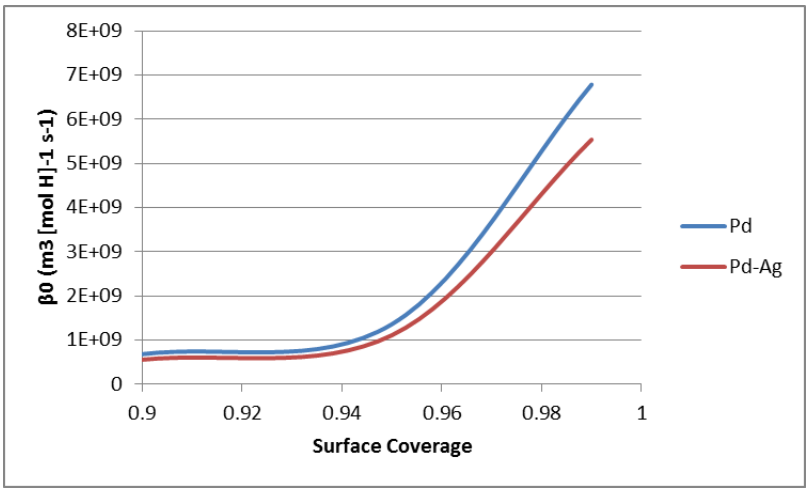

Figure 5.7 – Value of factor β_0 over the surface coverage range of interest

As the value for the surface-to-bulk factor (v_0) is expressed within the model as a ratio dependent on the value of β_0 it is possible to infer various conclusions from the graphs above. As previously stated, the value for β_0 is shown to increase dramatically with surface coverage and therefore the value of v_0 will also increase with surface coverage.

It can be seen that for the alloy the value of β_0 (and v_0) is lower under all surface coverages; this is due to the addition of silver in the palladium crystal structure reducing the diffusivity potential (D_0) whilst increasing the lattice parameter and reducing the bulk density (lower N_b). Studying the figures in (Catalano, Giacinti Baschetti and Sarti, 2010) shows that an increasing amount of silver content in the alloy results in further decreases of bulk site concentration and diffusivity whilst further increasing the lattice parameter.

Whilst this may raise immediate questions on why silver alloys have been of so much interest in research, the same question can be answered through analysis of the activation energies. The activation energy for bulk diffusion and the bulk-surface-bulk rates all follow a similar pattern, with the energy required dropping with increasing silver content up to 25% before increasing again. This drop in activation energy leads to a higher rate constant (D, β_0 and v_0) for hydrogen transition.

Continuing with the use of the models to evaluate materials that offer the most potential for use as membranes, it can be seen that once again identifying materials with the lowest barriers to the

transport processes is more important than the consideration of various physical aspects such as bulk and surface site density.

As this work utilises Pd-Ag primarily as a catalytic coating it is the bulk-surface-bulk reactions that are of most interest as it is assumed the bulk of the coating will be thin enough not to impact the transfer rate.

The rate equation for surface-bulk transfer is given above, and as shown previously the rate equation for bulk-to-surface transfer is similar to this in nature:

$$R_{b-s} = N_s N_b \beta_0 e^{\frac{-E_{b-s}}{RT}} X(1-\theta) \qquad \text{(Equation 3.46)}$$

For both transition rate equations, it is possible to consider the rate equation as the sum of three parts:

- A surface term, consisting of N_s and a Θ term (dependent on the process considered) that defines the hydrogen surface concentration.
- A bulk term, consisting of N_b and an X term (again, dependent on the process considered) that defines the hydrogen bulk concentration.
- A rate constant in the standard Arrhenius form.

The rate constant can therefore be seen as governing the rate of transition between the two states, with availability of sites also having an impact. It is well understood that the surface-bulk/bulk-surface reaction is very fast and is ultimately not found to be rate limiting in permeation modelling. This is logical, as although the jump from surface to bulk or bulk to surface requires activation, only a small distance must be travelled by each individual hydrogen atom, unlike transport through the bulk where each atom must traverse the entire crystal.

It is also worthwhile to note that the relationship between the pre-exponential factors used in the model is dependent on Sievert conditions – deviation from this causes the relationship between Θ and X to falter as shown by the more soluble metals in group V.

The final surface process to be considered is that of re-combinative desorption. Unlike the surface-bulk-surface reactions or adsorption, desorption was shown to be rate limiting in the idealised Sievert conditions modelled by Ward and Dao and in the additional calculations of Caravella et al and Catalano et al.

Deviation from idealised Sievert's behaviour appears to be primarily dependent on the thickness of the membrane, with thinner membranes showing deviations from bulk limited transfer at lower

temperatures. The change from bulk limited to desorption limited behaviour coincides with the saturation of the downstream surface, as would be expected – under these conditions no further increasing amount of hydrogen can diffuse through the bulk. The deviation from bulk diffusion behaviour at lower temperatures can be explained for thinner membranes - as there is less bulk material to cross hydrogen can permeate quicker through the bulk, resulting in saturation of the downstream surface (as the rate of bulk diffusion overtakes the rate of desorption).

As it has been established how a saturated lower surface interacts, it is now possible to turn to the final operational parameter not discussed so far with respect to its impact – pressure. Pressure on both sides of the membrane is shown to have an impact on surface coverage, with downstream pressure of more interest here.

Both surfaces of the membrane are modelled as having adsorption and desorption at steady state with the permeating flux being the difference between the two reactions. If a higher downstream pressure is accounted for in the model, this has significant impact on the surface coverage. To demonstrate the impact of upstream and downstream pressure 2 differing membrane separation systems have been modelled; both use a pure hydrogen feed, with a palladium membrane and both have a membrane thickness of 100 µm. The only differences are the pressures both upstream and downstream; a system with upstream pressure of 1 bar and downstream pressure of 1 Pascal (rounded to 0 bar on the graph in figures 5.8 and 5.9 below) has been modelled similar to that used in other published models. This is compared to a system with 10 bar upstream pressure and 1 bar downstream. This model was constructed as part of this investigation and the surface coverage upstream (figure 5.8) and downstream (figure 5.9) have been included on graphs below.

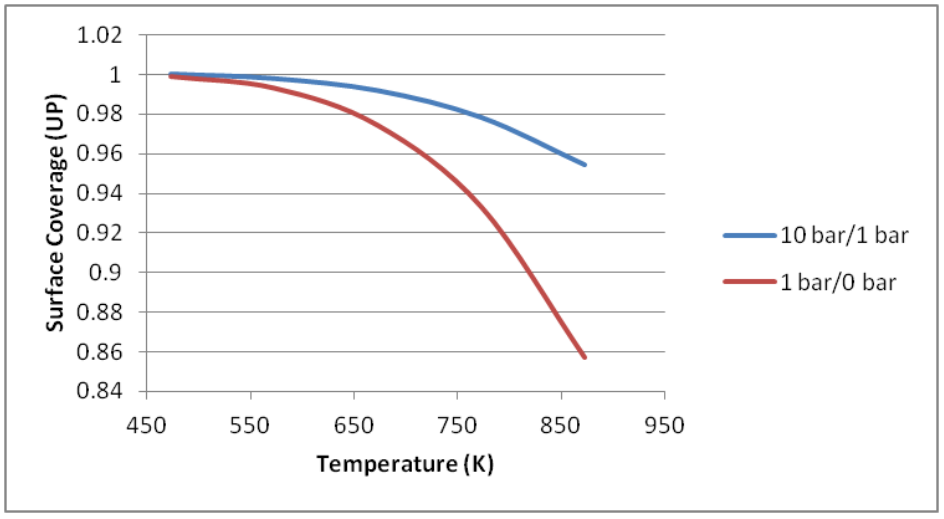

Figure 5.8 – Upstream surface coverage calculated under differing operating pressures

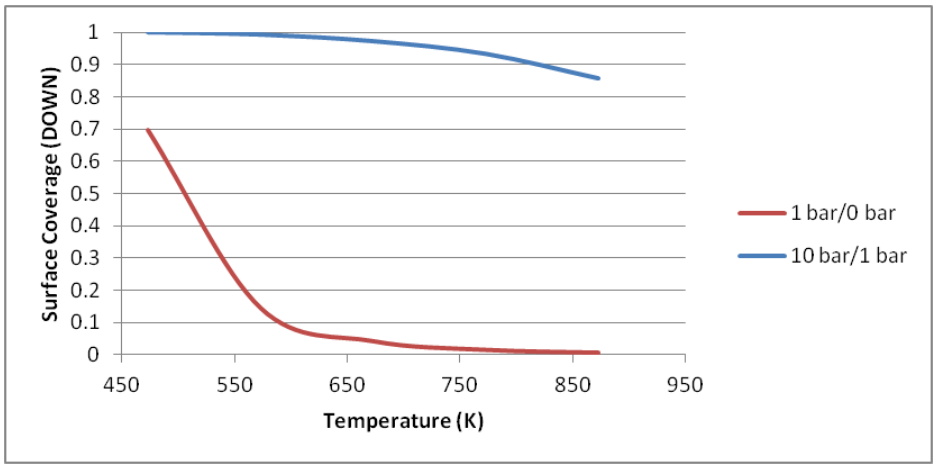

Figure 5.9 – Downstream surface coverage calculated under differing operating pressures

The 10 bar upstream 1 bar downstream was chosen to represent operational conditions investigated as part of this thesis; with this being the highest pressure tested.

As can be seen for the upstream surface, coverage follows a similar pattern under both conditions, with a higher surface coverage found for the higher pressure under all conditions above the temperatures investigated. This is not surprising as a higher pressure equates to a higher bombardment rate, thus even at a reduced sticking probability surface coverage is higher.

Of much more interest however is the downstream surface, where even atmospheric pressure results in an increase in surface coverage over the temperature range of primary interest. It is important to note that surface coverage is not complete, but it is nevertheless very high and the advantages to operating at a reduced pressure become apparent almost immediately.

A significant conclusion to be drawn from this in terms of the experimental work undertaken as part of this thesis is that under the test conditions utilised the membranes investigated are expected to be bulk-limited in terms of permeate flux.

This is of significance, as the decision was made to not operate under a vacuum on the permeate side (unlike the vast majority of data reported for both palladium and non-palladium membranes) during the experimental work undertaken in this study. This decision was made as the use of a vacuum system requires a greater input of energy thus reducing the efficiency of the separation process. Alongside this any industrial system requiring vacuum operation would incur a greater capital cost alongside greater maintenance costs also – therefore if it is possible to avoid such a system this should be done.

Reducing the barrier to desorption is shown to suppress the temperature at which desorption limited behaviour occurs. This is demonstrated throughout the literature where various activation energies

are modelled for desorption of hydrogen from the membrane surface. This is done in part as it appears that the energy for desorption is difficult to measure empirically with the value being dependent on multiple physical factors ranging from the crystal structure to the presence of any contaminants.

As shown in figure 5.8 and 5.9, when operating pressures are increase even moderately, a significant impact on the surface coverage is predicted; if the activation energy can be reduced at these higher temperatures a reduction in the surface coverage can be attained ensuring that the membrane remains in the bulk-diffusion limited phase. By remaining in the bulk-limited phase, the permeating flux is shown to be significantly greater for the same temperature.

The previously stated difficulties in collecting accurate desorption data are somewhat problematic for the construction of an accurate model especially in desorption limited systems. Desorption with respect to palladium has been mentioned above, with data the most widely available for this due to the material being of significant interest. The other coating of interest in this section is palladium-silver; where data is not as available in the literature. A suggestion for the desorption energy is provided in (Catalano, Giacinti Baschetti and Sarti, 2010), where the activation energies investigated are about half that for pure palladium. However it must be noted that no estimate for the value of the pre-exponential constant, k_0, is made – an assumption that the value for this is the same as for pure palladium can be made although this is somewhat limited. If the value for the activation energy for palladium-silver is to be believed than a membrane coated with palladium-silver as a catalytic coat would see a suppression of its desorption-limiting temperature in comparison to that of a pure palladium coating.

A final comment of note to be added is a brief acknowledgement of potential model limitations. One potential limitation of the model not considered so far is that the models, including the improved variations, model the surface site area in a relatively simplistic manner. When considering the number of surface sites a simple relationship is used consistently by all groups; where the surface site density is given as a function of the bulk density:

$$N_s = \frac{N_b^{2/3}}{N_A^{1/3}}$$

Whilst this simplistic method is acceptable in situations where surface adsorption/desorption are not limiting, questions can be asked about the validity in cases where this is not true. It is worthwhile to note that published models for thick membranes appear to be accurate under the specified conditions suggesting that the surface site calculation is acceptable. Many of the permeation models available display conditions in which desorption is the rate limiting step, once again these models appear to be

accurate (for palladium) in these situations, suggesting that the surface site approximation works under these conditions also.

A precautionary tone is taken here however, as the palladium-silver alloy surface has been shown to offer a different structure to that of pure palladium. Electroless plating of palladium and palladium-silver by (Hatlevik *et al.*, 2010) and that undertaken in this work show significant differences in the surface structure. The work of (Serra *et al.*, 1998) suggests that Pd-Ag membranes/coatings offer increased rates of hydrogen adsorption and desorption, as does the work of (Pick and Sonnenberg, 1985).

As the structure of the surface is not only affected by the material of construction but the method of construction it is essentially impossible to consider a more involved model for this; as with other works it is assumed that the simplistic surface site calculation is a close enough approximation for this work.

5.3.2 Oxidised Silver as a Membrane Catalytic Coating

It is important to note that a number of assumptions made about hydrogen adsorption on palladium cannot be made as readily for silver coated membranes. As stated in the above section, hydrogen adsorption onto palladium is assumed to be free from an activation barrier – this is unlikely to be the case for oxidised silver. Therefore alterations to the model are required; (Pick and Sonnenberg, 1985) provide an alternative equation for the sticking coefficient:

$$S(\theta) = S_0 e^{\frac{-2E_C}{RT}} \qquad \text{(Equation 5.4)}$$

Where E_c is the activation energy for dissociation (kJ mol^{-1}) and the remaining factors have already been described. The value for S_0 for oxidised silver is not available; however a possible alternative is to use the value for silver itself, with (Qin and Whitten, 2005) being one potential source of required values. Pick & Sonnenberg in the aforementioned paper suggest that the value of S_0 for most clean metal surfaces is close to unity, although the presence of oxygen may negate this. The value of E_c for oxidised silver would be dependent on the silver to oxygen ratio trapped in the metal lattice, with values suggested in (Mohammad *et al.*, 2008) and (Xu, Greeley and Mavrikakis, 2005) showing a significant reduction in the activation energy for 0.75Ag-0.25O in comparison to pure silver.

Whilst further study of the oxidised silver dissociative adsorption model would be considered valuable, it has been determined to be outside of the scope of this thesis primarily due to the lack of information available to build even an approximate model. Without data on the surface-bulk-surface transport

mechanism accurate modelling is not feasible, however if the coating is shown to be promising future work could potentially improve this.

As the membranes tested experimentally as part of this work have been coated in both silver and palladium, comparisons of the permeate flux data can yield some limited information about the silver coating.

By testing both coatings on identical bulk membranes under conditions known to be bulk-flux limited (pure hydrogen feed) significant variations in the volume of permeate collected would indicate that the surface of the membrane is responsible for the limiting of the flux.

5.3.3 The Impact of Multi-Component Mixtures on Permeability

The impact of multi-component mixtures can be considered as a two-fold issue. First, the addition of multiple non-hydrogen components will reduce the hydrogen partial pressure for a fixed system pressure thus reducing the driving force for diffusion by reducing the concentration/chemical potential of hydrogen. Secondly, the interaction of other gases with the surface of the membrane will result in the blocking of surface sites by non-permeating species. It is worthwhile noting that the second reason given here can be seen as an umbrella term to cover various physical phenomena; (Peters *et al.*, 2008) gives details on the contributing factors for carbon dioxide/monoxide interactions with the surfaces. The effects of concern as described by Peters et al are:

- **Surface effect of CO_2/CO:** The surface effect is described as the impact of surface adsorption of the species on the membrane. This effect is not uniform and is dependent on both the membrane material and the gas species; for palladium containing surfaces the surface effect of CO is significantly greater than that of CO_2.
- **Concentration polarisation:** Concentration polarisation is caused by the formation of concentration gradients due to the permeation of hydrogen through the membrane. As hydrogen can permeate whilst other species cannot, poor mass transfer can lead to a build-up of a boundary-surface layer with a high concentration of carbon dioxide/monoxide. This can lead to a depletion of the hydrogen on the upstream membrane surface, and can lead to changes of the concentration profile internally in the membrane affecting the permeating flux rate.
- **Depletion of hydrogen:** This factor refers to bulk depletion of hydrogen (the reduction of the overall hydrogen concentration in the bulk gas on the feed side) resulting in a change in the hydrogen potential gradient.

(Peters *et al.*, 2008) displays the above as fractions of the total resistance to permeation, alongside the resistance provided by the palladium membrane and the support layer for a thin membrane. As Peters et al conducted experiments on thin, supported palladium-silver membranes the effect of each factor is likely to be different to that for the membranes considered in this work but the factors having an impact will be consistent.

Before considering how to model the above factors it is possible to draw conclusions from the work of Peters et al that are relevant to the design of membrane separation units. As this work is focussed on thick membranes the contribution of resistance from the membrane support can be negated, and it can safely be assumed that the contribution of the membranes resistance to permeation will be greater, reducing the impact that the addition of other gaseous species has.

To limit the effect of concentration polarisation ensuring good mass transfer is critical, to compensate for this the membrane separation unit was designed in a manner in which a turbulent hydrogen rich feed gas will be utilised to supply the membrane with a constant flow rate of feed gas used to limit polarisation (and depletion). By supplying the feed gas continuously this also eliminates the effect of depletion, at the cost of losing overall hydrogen recovery efficiency (although this is not a target of interest in this work).

Upon identification of the factors affecting permeation, it is possible to consider methods for modelling this over a wider range of conditions. Unlike the models considered above, multi-component mixtures can be seen as having diffusion limited by upstream adsorptive processes; instead of bulk diffusion of downstream desorption. Numerous options are available, with the Stefan-Maxwell theory used in (Caravella, Barbieri and Drioli, 2008) and the method of (Pérez *et al.*, 2015), or the simplistic use of a mass transfer coefficient modelled by (Ward and Dao, 1999). Details are provided where they are used in this work.

One potential concern for modelling the surface limitations is the dependence on semi-empirical data that varies greatly not only with the composition of the feed gas and the surface membrane but also with the design of the enclosure. This has led to most efforts on the modelling of permeation of multi-component gas mixtures utilising collected experimental/empirical data to predict performance.

5.4 Utilising the Ward and Dao Model for Modelling Membranes

In (Ward and Dao, 1999) a model, discussed previously in chapter three, is proposed to predict hydrogen permeation behaviour in palladium membranes. In this section efforts have been made to utilise this model for a non-palladium-based membrane, a vanadium-alloy (85V-15Ni) membrane alongside the modelling of a palladium membrane that was also tested. The operational parameters used to model the membranes are the equivalent of the test conditions investigated experimentally, with temperatures between 573 K and 773 K (300 – 500 °C) and feed-side pressures between 2 and 10 bar investigated, with the permeate-side pressure fixed at 1 bar. Using these conditions allows for direct comparisons between the data sets with a pure hydrogen feed; experimental data can then be utilised to investigate the deviation from idealised behaviour in a multi-component feed mixture.

The limits to the Ward and Dao model have been acknowledged earlier in this chapter and in chapter three; as such efforts have been made to model a V-Ni membrane under conditions that can are expected to follow valid Sievert law behaviour. Deviations between experimental data and the model predictions of Ward and Dao are more pronounced for thin membranes (where bulk diffusion is not the rate determining step), however as only thick membranes were considered and utilised in this body of work the impact of this deviation was found to be minimal.

5.4.1 The Modelling of the Pd Bulk Membrane

As mentioned previously in this chapter a palladium membrane was modelled as part of this work using the model of Ward and Dao. Utilising data from (Caravella, Barbieri and Drioli, 2008), a model was constructed to predict the behaviour of a 100 µm thick membrane as tested experimentally as part of this PhD study, with the results found in chapter 6. A summary of key model values has been included in table 5.5.

Table 5.5 – Table containing key model constants, values taken from (Caravella, Barbieri and Drioli, 2008)(Ward and Dao, 1999)

Description	**Symbol**	**Value**	**Units**
Activation Energy - Surface-Bulk	E_{sb}	55647	J mol^{-1}
Activation Energy - Diffusion	E_{diff}	22175	J mol^{-1}
Activation Energy - Bulk-Surface	E_{bs}	22175	J mol^{-1}
Activation Energy - Desorption	E_{des}	41840	J mol^{-1}

Description	Symbol	Value	Units
Surface Site Concentration	N_s	2.77E-05	[mol Pd] m^{-2}
Molar Density	N_b	1.13E+05	[mol Pd] m^{-3}
Diffusion Pre-exponential Factor	D_0	2.90E-07	m^2 s^{-1}
Desorption Pre-exponential Factor	$K_{0\,des}$	4.80E+17	m^2 [mol H]$^{-1}$ s^{-1}
Surface-Bulk Pre-exponential Factor	v_0	Equation 3.65	m^3 [mol H]$^{-1}$ s^{-1}
Bulk-Surface Pre-exponential Factor	β_0	Equation 5.3	m^3 [mol H]$^{-1}$ s^{-2}
Initial Sticking Coefficient	S_0	1	Dimensionless
Pairwise Interaction Energy	w	2092	J mol^{-1}
Adsorption Relation Constant	K_w	0.05	Dimensionless

The data in table 5.5 was used to generate the five mass flux equations previously described in chapter three, with mass balances taken in effect at five locations:

1. Upstream surface
2. Upstream bulk (immediately below the surface)
3. Across the bulk (bulk diffusion)
4. Downstream bulk (immediately below the surface)
5. Downstream surface

Predicting the permeate flux downstream was done as an iterative process. The five mass flux equations were then solved sequentially by setting the mass flux of each equal to the steady-state permeate flux, providing values for the upstream surface coverage (Θ_u), bulk upper and lower hydrogen concentration (X_u and X_d respectively) and then the downstream surface coverage (Θ_d).

The final mass balance was then used to provide a value for permeate hydrogen concentration (and ultimately pressure); this value could then be compared to the actual downstream pressure. If there was any discrepancy between the values, a new value for the steady state flux was inserted and the process repeated until the P_d value from the model was consistent with the actual value calculated through the adjusted gas law (PV=nRTZ, with Z taken to be 1.0006).

This methodology was used to solve the model in all instances, with both the Pd and V-Ni membrane.

Figure 5.10 is included to give a summary of the predicted fluxes for the palladium membrane calculated under various conditions for comparison with experimental results in chapter seven. The graph shows the predicted permeate flux for a 100 µm membrane, with a constant downstream hydrogen partial pressure of 1 bar and varying upstream hydrogen pressure and temperature.

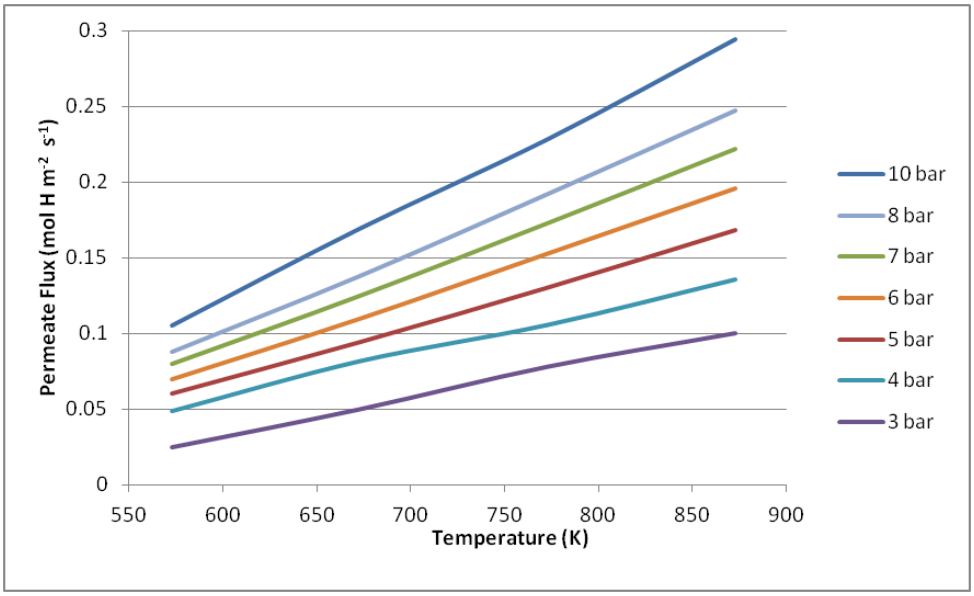

Figure 5.10 – Predicted permeate flux for a 100 µm thick palladium membrane under various operational temperatures and various upstream hydrogen pressures

A number of different pressures are shown within the operational range, with clear and expected trends shown clearly. An increase in both pressure and temperature produces an increase in the predicted flux, with the relationship being very close to linear in nature. Figure 5.11 shows the same data as figure 5.10, but here the relationship between the permeate flux and the pressure is the primary plot.

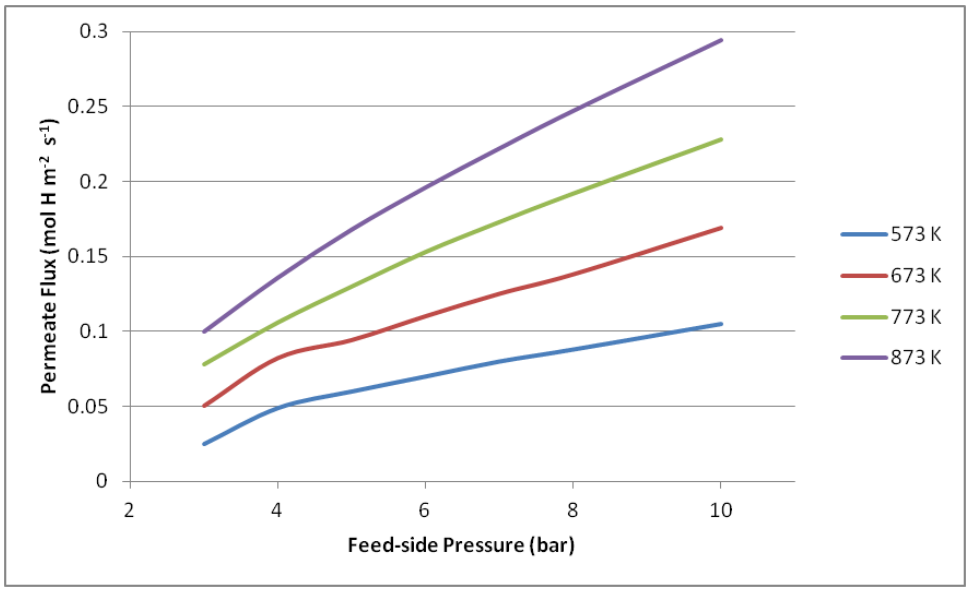

Figure 5.11 – Predicted permeate flux for a 100 µm thick palladium membrane under various operational temperatures and various upstream hydrogen pressures

Displaying the data in this manner shows the characteristic curve expected as pressure increases, however the behaviour of the palladium membrane at lower temperatures and pressures is shown to vary slightly from that expected. This may be an error in calculation or the model, or it could be related to the changing conditions within the membrane where the reduction of hydrogen solubility has a different effect under more moderate pressures.

Alongside the plots above, graphs can be drawn to show the changes in surface coverage and bulk metal hydrogen concentration. Figure 5.12 below shows an example of this, with the feed-side surface coverage displayed for various conditions, the general trend remains constant, however at higher feed pressures the upstream surface retains a higher coverage. At low temperatures, all of the isobars included begin to converge towards unity, however the model does not predict this to become a limiting factor under the conditions tested experimentally.

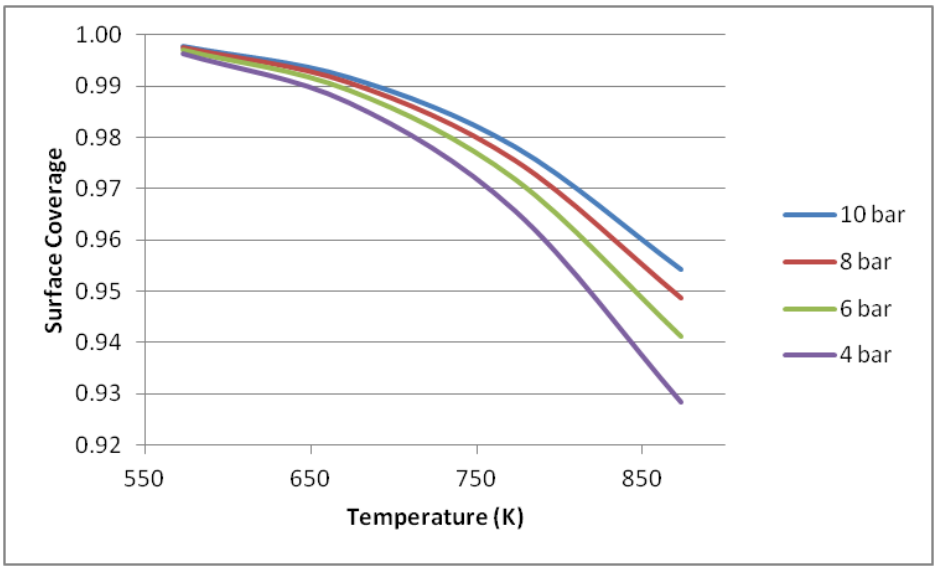

Figure 5.12 – Predicted feed-side surface coverage for a palladium membrane under various operating conditions

Figure 5.13 shows the hydrogen to metal ratio values predicted by the model under various conditions, with the feed-side (labelled UP) and the permeate-side (labelled DOWN) values included on the graph for comparison.

The model shows a number of expected results, the solubility of hydrogen is shown to decrease significantly with increasing temperature and the solubility of hydrogen is shown to increase with an increase in pressure. There is minimal variation in the value for X_d, this is reasonable as the permeate side pressure is assumed to be constant. As the values for $X << 1$, it can be expected that the model should provide a reasonable prediction of the generated permeate flux experimentally.

The decrease in solubility with increasing temperature is scalar, with this having the largest real effect on higher pressures. This is a useful feature in terms of designing potential palladium based membranes. As has been stated, a high H/M ratio can result in permanent, irreparable damage to the membrane, by increasing the operational temperature it is possible to subdue the solubility of hydrogen in the metal with the added effect of increasing hydrogen diffusivity. For palladium membranes, the model predicts that the net effect of increasing diffusivity overcomes the reduction in solubility resulting in an increased permeability – as is shown experimentally also. By identifying the highest possible H/M ratio in which damage can be avoided, it is then possible to identify a maximum operating differential for any given temperature (to maximise the permeate flux), similar to what is done by (Suzuki *et al.*, 2016) for vanadium based membranes. By identifying the maximum value, separation and permeation can be kept towards the maximum feasible efficiency under any condition.

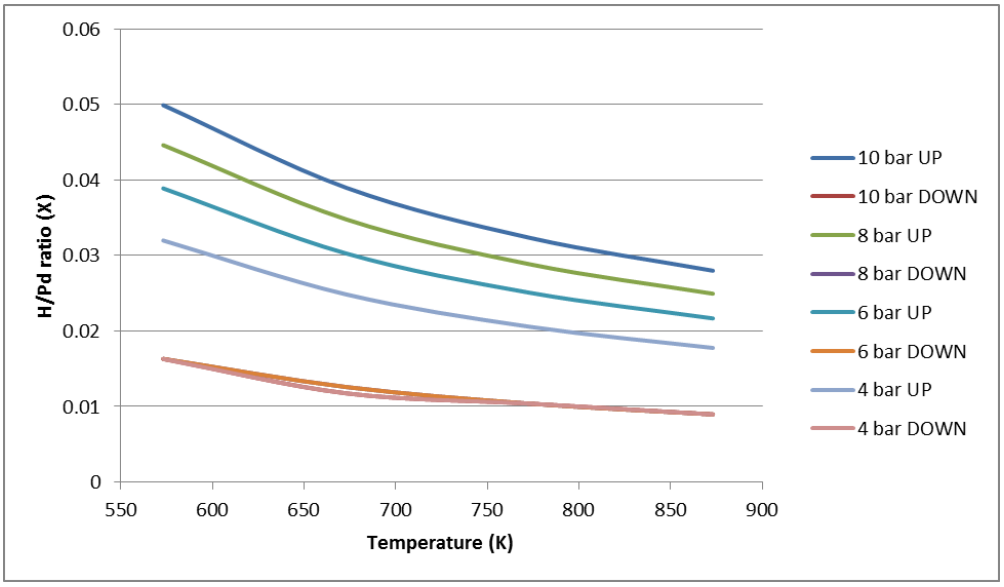

Figure 5.13 – Predicted H/Pd ratios for a palladium membrane under various operating conditions

Finally, figure 5.14 shows the downstream/permeate-side surface coverage, to validate that the membrane under the conditions specified would be operating in the diffusion limited phase and not desorption.

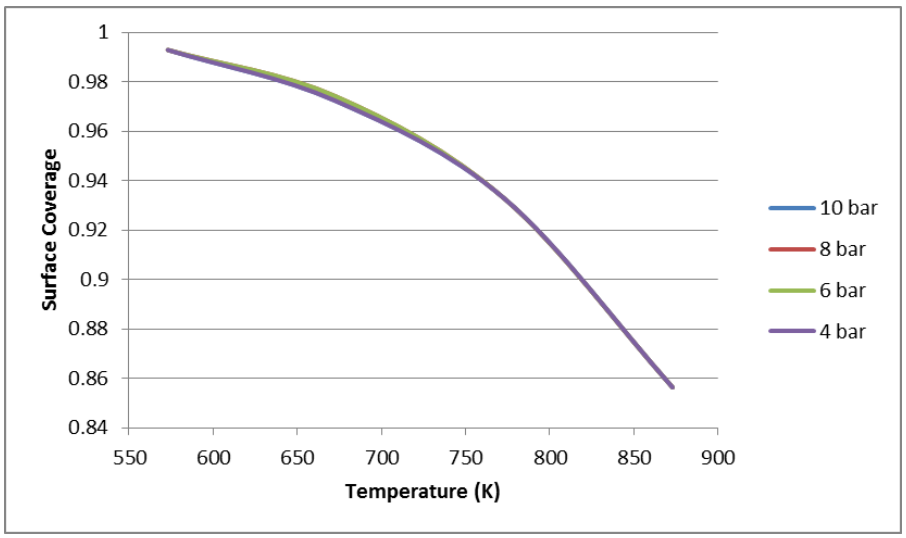

Figure 5.14 – Predicted downstream surface coverage for a palladium membrane under various operating conditions

As can be seen, whilst coverage approaches unity at the downstream surface it is not reached under any condition. The figure also shows that there is little to no variation in downstream coverage with varying upstream pressure, this is expected as the downstream pressure was kept constant at 1 bar.

In summary, the model shows that for palladium-based membranes a high operating temperature is desirable, with the limit of this likely to be tied to the mechanical properties of the alloy itself. A higher temperature allows for a higher diffusivity and ultimately a higher permeability, even if hydrogen

solubility in the alloy is decreased. The decrease in solubility (and reduction of the driving force) can be overcome by increasing the pressure differential, in this work this is done by increasing the feed-side pressure whilst ensuring that the H/M ratio never reaches a point in which damage occurs. This may be of particular interest for use with the operation (steam reformation, gasification) considered here, where the pressure and temperature range are likely to be dictated by the primary process.

5.4.2 The Modelling of the V-Ni Bulk Membrane

The hydrogen solubility of the V-Ni membranes was discussed earlier in this chapter, and the limit to the application of idealised Sievert's law behaviour is suggested to be somewhere within the range of operational pressures investigated as part of this work. This section sets out a range of predicted permeate fluxes for various operating conditions to be compared with experimental data in a later chapter.

The behaviour of vanadium-based membranes has been shown to be significantly different from that of palladium based ones and this is reflected accordingly in the model.

Before the model could be constructed, the relevant model parameters/constants had to be collected and collated. The figures can be found in table 5.6. It was chosen to model a membrane consisting of a bulk alloy of 85V-15Ni and hence the activation energy for bulk diffusion and the constant D_0 reflects this. The values D_0 and E_{diff} were taken from (Zhang *et al.*, 2003), with the figures providing diffusion coefficients similar in scale to those included in (Dolan, 2010).

As the membrane to be used experimentally is coated with a palladium-based coating, this has been incorporated into the model in the form of modelling the V-Ni membrane with a palladium coating. A number of reasonable assumptions are made at this point, the first is that the catalytic coating is thin enough to not impact the overall permeation rate – in other words the membrane remains bulk limited. This is reasonable as an assumption since the reaction rates for the adsorption, desorption and surface-bulk-surface reactions are significantly higher under the conditions of interest than those of bulk permeation. An assumption is made that there is no miscibility issues that reduce hydrogen permeation between the palladium and the vanadium alloy and also that the two layers whilst acting as a singular phase remain distinct – no ternary palladium, vanadium and nickel alloy with different properties is formed that would alter the behaviour of the membrane.

As the model now has two distinctive layers with different thermodynamic properties, care must be taken to select the data that best represents the physical membrane. As stated above V-Ni

thermodynamic properties will be used for the bulk permeation, whilst adsorption and desorption will be modelled based solely on the behaviour of the palladium surface coating. Whilst N_s was taken as the value for palladium, N_b was calculated from the molar densities of vanadium (0.118 mol cm^3) and nickel (0.152 mol cm^3) using the molar percentage ratio present in the alloy (V 85%, Ni 15%).

This leaves the surface-bulk-surface reactions, where the scenario is more complex due to the transition between the two distinct metal regions. Considering the activation energies, it was decided to model the surface-bulk reaction with the activation energy taken from palladium. This was done to represent the energy required for hydrogen to jump from the surface site to the bulk, where it is assumed that the activation energy represents the initial energy required for hydrogen to make an interstitial jump from palladium. Secondly, this assumes that the identity of the site the hydrogen atom is jumping to has no effect on the activation energy. For bulk-surface, the activation energy utilised is the equivalent to the V-Ni diffusion energy, as in the original model the activation energy for diffusion was used as the activation energy for bulk-surface jumps. The same assumptions as before are made in that the activation energy is only representative of the hydrogen atoms origin and that the destination site has no effect.

This leaves the calculation of the pre-exponential constants; as before β_0 can be calculated using equation 5.3. The surface-bulk constant ν_0 can be calculated using the original expression but with a modification to account for the difference in solubility between palladium and the vanadium-nickel alloy.

In chapter three the relationship between the parameters β_0 and ν_0 is discussed in more detail, a central part of the relationship is the dependence on the Sievert/solubility constant. With the Sievert/solubility constant calculated using equation 3.64:

$$K_S = e^{\frac{\Delta\overline{H_H^0}}{RT}} e^{\frac{-\Delta\overline{S_0^0}}{2R}} \qquad \text{(Equation 3.64)}$$

Where $\Delta\overline{H_H^0}$ represents the enthalpy of hydrogen absorption under standard conditions (J mol^{-1}) and $\Delta\overline{S_0^0}$ is the entropy of hydrogen absorption under standard conditions (J mol^{-1}). As the equivalent figures were not available for the V-Ni membrane in question the solubility constant, K_s was taken from the experimental data of (Ozaki *et al.*, 2003b). This can then be substituted into the equation 3.64, where the right hand sides of equations 3.64 (the Sievert constant) and 3.59 are equated as done by (Ward and Dao, 1999).

Table 5.6 below contains the key figures used throughout this model; as before, data relating to palladium is taken from (Caravella, Barbieri and Drioli, 2008) and data on vanadium-nickel is taken from (Ozaki *et al.*, 2003b).

Table 5.6 – Table containing key model constants, values taken from (Caravella, Barbieri and Drioli, 2008)(Ward and Dao, 1999)

Description	**Symbol**	**Value**	**Units**
Activation Energy - Surface-Bulk	E_{sb}	55647	J mol^{-1}
Activation Energy - Diffusion	E_{diff}	10900	J mol^{-1}
Activation Energy - Bulk-Surface	E_{bs}	10900	J mol^{-1}
Activation Energy - Desorption	E_{des}	41840	J mol^{-1}
Surface Site Concentration	N_s	2.77E-05	[mol Pd] m^{-2}
Molar Density	N_b	1.23E+05	[mol M] m^{-3}
Diffusion Pre-exponential Factor	D_0	4.25E-08	m^2 s^{-1}
Desorption Pre-exponential Factor	$K_{0\,des}$	4.80E+17	m^2 [mol H]$^{-1}$ s^{-1}
Surface-Bulk Pre-exponential Factor	ν_0	Equation 3.65	m^3 [mol H]$^{-1}$ s^{-1}
Bulk-Surface Pre-exponential Factor	β_0	Equation 5.3	m^3 [mol H]$^{-1}$ s^{-2}
Initial Sticking Coefficient	S_0	1	Dimensionless
Pairwise Interaction Energy	w	2092	J mol^{-1}
Adsorption Relation Constant	K_w	0.05	Dimensionless

The membrane modelled in figure 5.15 is modelled with the same thickness as the membranes tested experimentally, with a thickness of 250 µm with the modelled temperatures and pressures modelled reflecting those tested experimentally. As with the palladium membrane, the V-Ni membrane is modelled with a constant downstream pressure and a variable temperature and feed-side pressure.

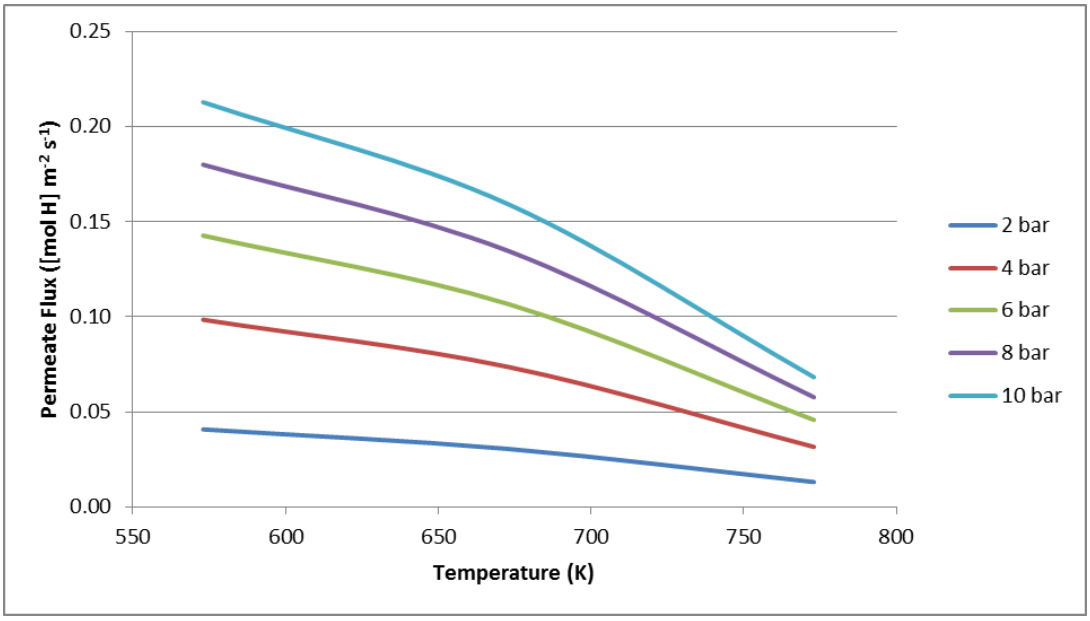

Figure 5.15 – Predicted permeate flux for a 250 µm thick V-Ni membrane modelled on used experimental conditions

As can be seen, unlike the palladium membrane modelled previously the V-Ni membrane is shown to reduce in permeability at higher temperatures. This is consistent with the experimental measurements seen elsewhere in publications. The significantly higher permeability of the V-Ni membrane is demonstrated clearly when compared to the values for the palladium membrane shown in figure 5.10. The V-Ni membrane modelled offers a similar maximum permeate rate to the palladium membrane, but at a significantly increased thickness – 250 µm in comparison to the 100 µm palladium membrane. For comparison, figure 5.16 below models a V-Ni membrane with a thickness of 100 µm. As can be seen the predicted flux is significantly higher, however this has not been verified through experimentation as part of this study.

As has been discussed previously, it is clear to see that whilst the diffusivity of the membrane is shown to increase over the temperature range studied, from 4.31 $x10^{-9}$ m^2 s^{-1} at 573 K to 7.79 $x10^{-9}$ m^2 s^{-1} at 773 K, the significant drop in hydrogen solubility leads to an overall reduction in permeability.

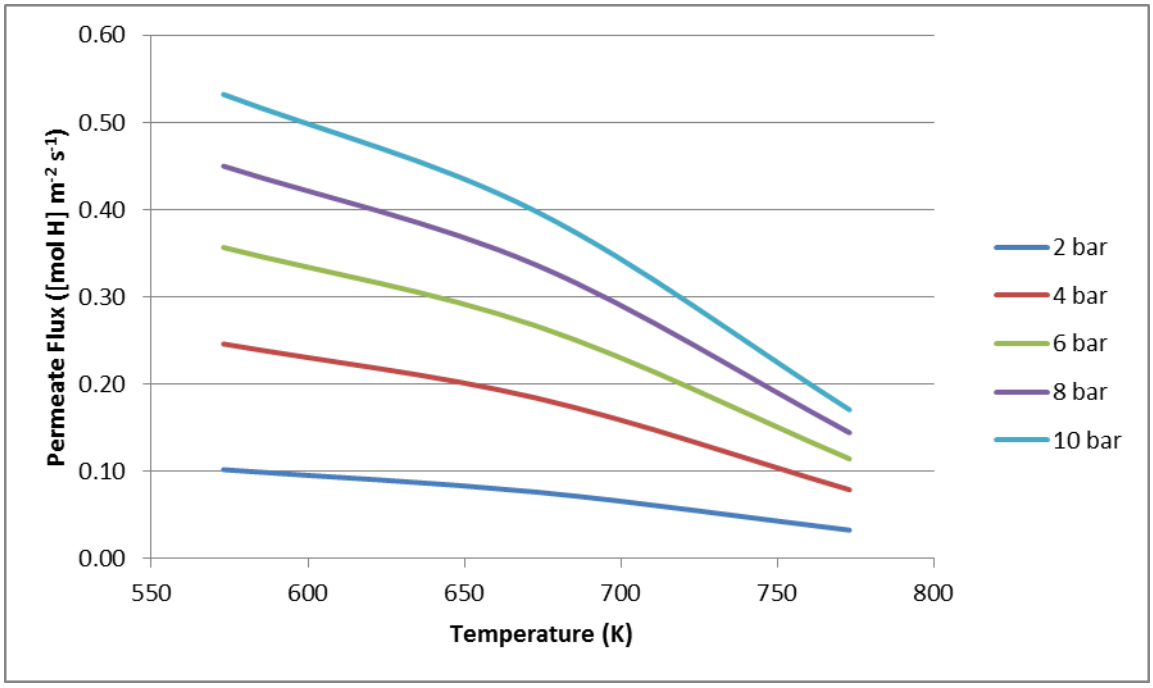

Figure 5.16 – Predicted permeate flux for a 100 µm thick V-Ni membrane modelled on used experimental conditions

As with the palladium membrane, values for X and Θ were produced through the use of the model, of most interest are the values of X_u and X_d shown in figure 5.17.

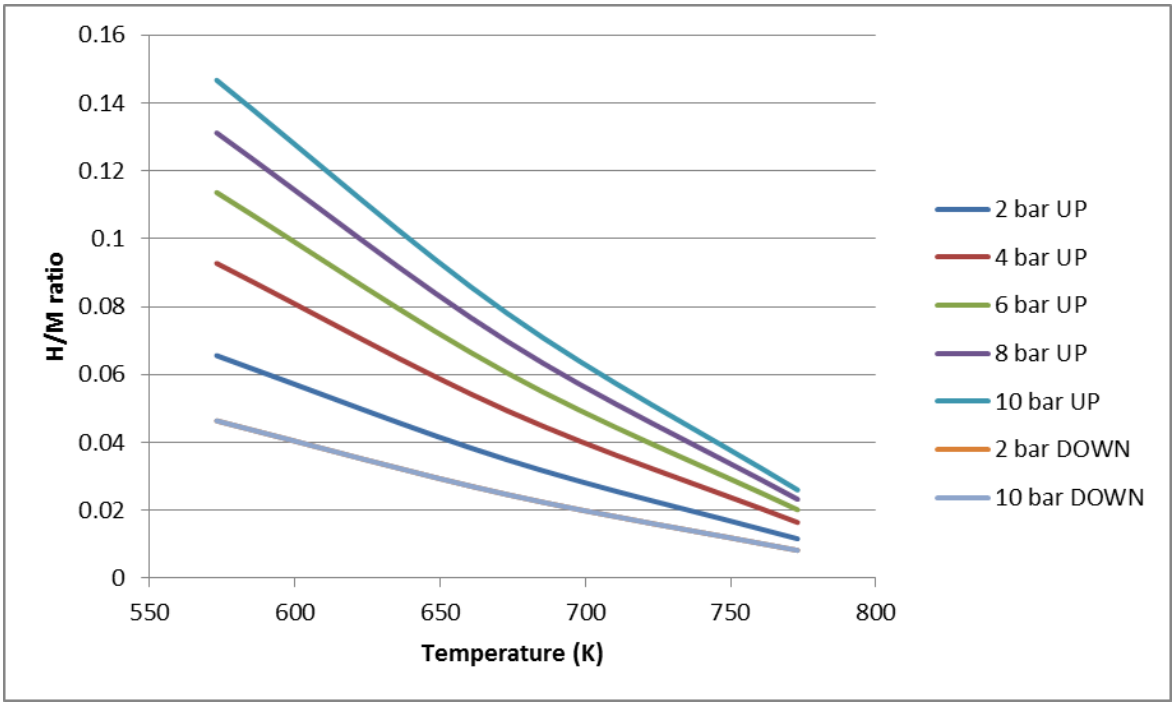

Figure 5.17 – Predicted X values (H/M ratio) upstream and downstream for various operational conditions for a 250 µm thick membrane

As can be seen, at the lower temperatures the H/M ratio under higher pressures is significantly higher than for the palladium membrane modelled in section 5.4.1. This is expected to a degree, as 10 bar is theorised to show some deviation from Sievert-type behaviour, where the condition of X << 1 is not true. What can be seen however is that the H/M ratio decreases sharply as temperature is increased, as before the change in the value is proportional, therefore having the largest real effect on the highest feed-side pressures investigated.

As before, the permeate side H/M ratio is shown to be near constant, as the downstream pressure is held constant at 1 bar throughout the model. The graphs showing surface coverage have not been included in this section, as they show no significant variation from figures 5.11 and 5.13. This similarity is explained by the use of palladium as a surface material, resulting in the adsorption and desorption processes being consistent regardless of the bulk material.

After completion of the models for both palladium and for the V-Ni membrane the results were compared to the experimental data collected. This comparison can be found in chapter seven.

5.5 Summary of the Chapter

In this chapter various aspects of the theory of hydrogen permeation membranes are explored for a number of potential membrane bulk materials and coatings. Individual aspects of the theory behind permeation are explored independently to investigate their potential impact on real world behaviour of metallic membranes.

The Ward and Dao model for hydrogen permeation through a palladium membrane was constructed and used to predict the behaviour of palladium membranes under various conditions that have been tested experimentally as part of this work.

A new model for the permeation of hydrogen through vanadium-nickel, palladium-coated membranes was then constructed – based on the principles and equations outlined by Ward and Dao. The results of the model were tested and validated experimentally under various operating conditions, as shown in chapter six.

5.6 Chapter Five Reference List

Al-Mufachi, N. A., Rees, N. V. and Steinberger-Wilkens, R. (2015) 'Hydrogen selective membranes: A review of palladium-based dense metal membranes', *Renewable and Sustainable Energy Reviews*. Elsevier, 47, pp. 540–551. doi: 10.1016/j.rser.2015.03.026.

Barrer, R. M. (1939) 'The Permeability of Metal Membranes to Diatomic Gases', *The London, Edinburgh, and Dublin Philosophical Magazine and Journal of Science*, 28(188), pp. 353–358. doi: http://dx.doi.org/10.1080/14786443908521189.

Caravella, A., Barbieri, G. and Drioli, E. (2008) 'Modelling and simulation of hydrogen permeation through supported Pd-alloy membranes with a multicomponent approach', *Chemical Engineering Science*, 63(8), pp. 2149–2160. doi: 10.1016/j.ces.2008.01.009.

Catalano, J., Giacinti Baschetti, M. and Sarti, G. C. (2010) 'Hydrogen permeation in palladium-based membranes in the presence of carbon monoxide', *Journal of Membrane Science*. Elsevier B.V., 362(1–2), pp. 221–233. doi: 10.1016/j.memsci.2010.06.055.

Chang, H. . and Wert, C. . (1973) 'The solubility and trapping of hydrogen in vanadium', *Acta Metallurgica*, 21. Available at: http://www.sciencedirect.com/science/article/pii/0001616073901648 (Accessed: 9 September 2014).

Dolan, M. D. (2010) 'Non-Pd BCC alloy membranes for industrial hydrogen separation', *Journal of Membrane Science*. Elsevier B.V., 362(1–2), pp. 12–28. doi: 10.1016/j.memsci.2010.06.068.

Dolan, M. D., Kellam, M. E., McLennan, K. G., Liang, D. and Song, G. (2013) 'Hydrogen transport properties of several vanadium-based binary alloys', *International Journal of Hydrogen Energy*. Elsevier Ltd, 38(23), pp. 9794–9799. doi: 10.1016/j.ijhydene.2013.05.073.

Dolan, M. D., McLennan, K. G. and Way, J. D. (2012) 'Diffusion of atomic hydrogen through V-Ni alloy membranes under nondilute conditions', *Journal of Physical Chemistry C*, 116(1), pp. 1512–1518. doi: 10.1021/jp208691x.

Dolan, M. D., Song, G., Liang, D., Kellam, M. E., Chandra, D. and Lamb, J. H. (2011) 'Hydrogen transport through V85Ni10M5 alloy membranes', *Journal of Membrane Science*. Elsevier B.V., 373(1–2), pp. 14–19. doi: 10.1016/j.memsci.2011.02.028.

Flanagan, T. B., Wang, D. and Shanahan, K. L. (2007) 'The role of non-ideality in H permeation

through membranes', *Scripta Materialia*, 56(4), pp. 261–263. doi: 10.1016/j.scriptamat.2006.10.029.

Hatlevik, Ø., Gade, S. K., Keeling, M. K., Thoen, P. M., Davidson, a. P. and Way, J. D. (2010) 'Palladium and palladium alloy membranes for hydrogen separation and production: History, fabrication strategies, and current performance', *Separation and Purification Technology*, 73(1), pp. 59–64. doi: 10.1016/j.seppur.2009.10.020.

Katsuta, H. and McLellan, R. (1979) 'Diffusivity permeability and solubility of hydrogen in platinum', *Solid State Communications*, 29(8), p. ii. doi: 10.1016/0038-1098(79)90687-2.

Kim, K.-H., Shim, J.-H. and Lee, B.-J. (2012) 'Effect of alloying elements (Al, Co, Fe, Ni) on the solubility of hydrogen in vanadium: A thermodynamic calculation', *International Journal of Hydrogen Energy*. Elsevier Ltd, 37(9), pp. 7836–7847. doi: 10.1016/j.ijhydene.2012.01.117.

Lloyd, P. B., Kress, J. W. and Tatarchuk, B. J. (1997) 'Surface and bulk interactions of hydrogen with copper', *Applied Surface Science*, 119(3–4), pp. 275–287. doi: 10.1016/S0169-4332(97)00179-7.

Marchi, C. S. and Somerday, B. P. (2012) *Technical Reference for Hydrogen Compatibility of Materials*. Available at: http://www.sandia.gov/matlsTechRef/chapters/SAND2012_7321.pdf.

Mohammad, A. B., Yudanov, I. V., Lim, K. H., Neyman, K. M. and Rösch, N. (2008) 'Hydrogen activation on silver: A computational study on surface and subsurface oxygen species', *Journal of Physical Chemistry C*, 112(5), pp. 1628–1635. doi: 10.1021/jp0765190.

Morreale, B. D., Ciocco, M. V, Enick, R. M., Morsi, B. I., Howard, B. H., Cugini, A. V and Rothenberger, K. S. (2003) 'Morealle 2003 Journal of Membrane Science bulk Pd', 212, pp. 87–97.

Ockwig, N. W. and Nenoff, T. M. (2007) 'Membranes for hydrogen separation.', *Chemical reviews*, 107(10), pp. 4078–110. doi: 10.1021/cr0501792.

Ozaki, T., Zhang, Y., Komaki, M. and Nishimura, C. (2003a) 'Hydrogen permeation characteristics of V-Ni-Al alloys', *International Journal of Hydrogen Energy*, 28(11), pp. 1229–1235. doi: 10.1016/S0360-3199(02)00251-3.

Ozaki, T., Zhang, Y., Komaki, M. and Nishimura, C. (2003b) 'Preparation of palladium-coated V and V-15Ni membranes for hydrogen purification by electroless plating technique', *International Journal of Hydrogen Energy*, 28(3), pp. 297–302. doi: 10.1016/S0360-3199(02)00065-4.

Pérez, P., Cornaglia, C. A., Mendes, A., Madeira, L. M. and Tosti, S. (2015) 'Surface effects and CO/CO2 influence in the H2 permeation through a Pd–Ag membrane: A comprehensive model',

International Journal of Hydrogen Energy, 40(20), pp. 6566–6572. doi: 10.1016/j.ijhydene.2015.03.106.

Perry, R., Green, D. and Maloney, J. (2008) *Perry's chemical engineers' handbook*. Available at: http://www.lavoisier.fr/livre/notice.asp?ouvrage=1037804 (Accessed: 6 November 2013).

Peters, T. A., Stange, M., Klette, H. and Bredesen, R. (2008) 'High pressure performance of thin Pd-23%Ag/stainless steel composite membranes in water gas shift gas mixtures; influence of dilution, mass transfer and surface effects on the hydrogen flux', *Journal of Membrane Science*, 316(1–2), pp. 119–127. doi: 10.1016/j.memsci.2007.08.056.

Phair, J. W. and Donelson, R. (2006) 'Developments and design of novel (non-palladium-based) metal membranes for hydrogen separation', *Industrial and Engineering Chemistry Research*, pp. 5657–5674. doi: 10.1021/ie051333d.

Pick, M. a. and Sonnenberg, K. (1985) 'A model for atomic hydrogen-metal interactions — application to recycling, recombination and permeation', *Journal of Nuclear Materials*, 131(2–3), pp. 208–220. doi: 10.1016/0022-3115(85)90459-3.

Qin, C. Y. and Whitten, J. L. (2005) 'Adsorption of O, H, OH, and H2O on Ag(100)', *J. Phys. Chem. B*, 109(18), pp. 8852–6. doi: 10.1021/jp044067a.

Serra, E., Kemali, M., Perujo, A. and Ross, D. K. (1998) 'Hydrogen and deuterium in Pd-25 Pct Ag alloy: Permeation, diffusion, solubilization, and surface reaction', *Metallurgical and Materials Transactions A: Physical Metallurgy and Materials Science*, 29(13), pp. 1023–1028. doi: 10.1007/s11661-998-1011-3.

Shim, J. H., Ko, W. S., Kim, K. H., Lee, H. S., Lee, Y. S., Suh, J. Y., Cho, Y. W. and Lee, B. J. (2013) 'Prediction of hydrogen permeability in V-Al and V-Ni alloys', *Journal of Membrane Science*. Elsevier, 430, pp. 234–241. doi: 10.1016/j.memsci.2012.12.019.

Steward, S. A. (1983) *Review of hydrogen isotope permeability through materials*. doi: 10.2172/5277693.

Suzuki, A., Yukawa, H., Nambu, T., Matsumoto, Y. and Murata, Y. (2014) 'Consistent description of hydrogen permeability through metal membrane based on hydrogen chemical potential', *International Journal of Hydrogen Energy*. Elsevier Ltd, 39(15), pp. 7919–7924. doi: 10.1016/j.ijhydene.2014.03.123.

Suzuki, A., Yukawa, H., Nambu, T., Matsumoto, Y. and Murata, Y. (2016) 'Analysis of pressure-

composition-isotherms for design of non-Pd-based alloy membranes with high hydrogen permeability and strong resistance to hydrogen embrittlement', *Journal of Membrane Science*. Elsevier, 503, pp. 110–115. doi: 10.1016/j.memsci.2015.12.030.

Suzuki, T. and Takata, K. (1993) 'Permeation of hydrogen in vanadium: II: Theoretical details', *Materials Science and Engineering: A*, 163, pp. 99–105. Available at: http://www.sciencedirect.com/science/article/pii/092150939390583Z (Accessed: 9 September 2014).

Veleckis, E. and Edwards, R. (1969) 'Thermodynamic properties in the systems vanadium-hydrogen, niobium-hydrogen, and tantalum-hydrogen', *The Journal of Physical Chemistry*, 7(9). Available at: http://pubs.acs.org/doi/abs/10.1021/j100723a033 (Accessed: 10 September 2014).

Völkl, J. and Alefeld, G. (1978) 'Diffusion of hydrogen in metals', in *Hydrogen in metals 1*, pp. 321–348. doi: 10.1007/3540087052_51.

Ward, T. and Dao, T. (1999) 'Model of hydrogen permeation behavior in palladium membranes', *Journal of Membrane Science*, 153(January 1998), pp. 211–231. Available at: http://www.sciencedirect.com/science/article/pii/S0376738898002567 (Accessed: 18 February 2014).

Xu, Y., Greeley, J. and Mavrikakis, M. (2005) 'Effect of subsurface oxygen on the reactivity of the Ag(111) surface', *Journal of the American Chemical Society*, 127(37), pp. 12823–12827. doi: 10.1021/ja043727m.

Zhang, G. X., Yukawa, H., Watanabe, N., Saito, Y., Fukaya, H., Morinaga, M., Nambu, T. and Matsumoto, Y. (2008) 'Analysis of hydrogen diffusion coefficient during hydrogen permeation through pure niobium', *International Journal of Hydrogen Energy*, 33(16), pp. 4419–4423. doi: 10.1016/j.ijhydene.2008.05.062.

Zhang, Y., Ozaki, T., Komaki, M. and Nishimura, C. (2003) 'Hydrogen permeation of Pd-Ag alloy coated V-15Ni composite membrane: Effects of overlayer composition', *Journal of Membrane Science*, 224(1–2), pp. 81–91. doi: 10.1016/j.memsci.2003.07.005.

6 Experimental Results

This chapter contains details on all of the experimental results gathered throughout this PhD study. Details on the test methodology and membrane construction can be found in chapter four. The results are analysed in greater detail in chapter seven.

6.1 Experimental Results – Palladium Membrane, Hydrogen Feed

The first permeation tests were conducted on palladium membranes, to ensure that the permeation testing equipment was suitable for use and to provide a bench mark to measure other membranes against. Large amounts of permeability data for palladium is available for comparison, however one concern was that unlike many reported permeabilities the testing undergone as part of this thesis did not apply a vacuum against the permeate side thus possibly limiting the permeation rate. This was done to investigate the use of a low energy, passive membrane process; however, it is conceded that any real membrane permeation process would require eventual pressurisation of the hydrogen before use (increasing total energy usage during separation).

This section and the remaining sections of this thesis will provide the experimental results gathered throughout this study. Experimental results are grouped based on the membrane tested and the composition of the feed gas. However, in instances where no positive result could be returned for the membrane under any condition only one section has been included to show the range of the study. Further analysis of the results can be found in chapter seven.

The membrane active area was recorded for each membrane to allow for calculation of flux in a cm^3 per cm^2 basis. The active area was determined by the total area of the membrane exposed to the feed; this was set by the circular area exposed to the feed on the inside circumference of the copper gasket.

Calculation of the flux was determined by collecting a specified volume of gas and measuring the amount of time required; this data was then manipulated into a total membrane flux (cm^3 min^{-1}) before calculating the per unit area flux. From this data a molar flux can be calculated for comparison with the flux predicted from the model shown in chapter five; the permeability of the membrane can also be calculated and compared to values given in the literature (as can be seen in chapter seven).

6.1.1 Experimental Data: Constant Pressure and Variable Temperature

All tests in this section were conducted on membranes with a thickness of 100 µm (0.1 mm) and for this test a constant feed side pressure of 9 bar gauge (10 bar absolute) was applied to the membrane. As the feed was pure hydrogen there was no need for to open the needle valve (vent), as there was no carbon dioxide present to influence surface adsorption of hydrogen (through the mechanisms previously described).

Table 6.1 contains the time taken to collect 10 cm^3 of gas using the measuring tube. The test was conducted twice on separate occasions to ensure consistency; with each measurement completed three times (giving a total of six data points under each condition).

Table 6.1 – Table the time required (seconds) for 10 cm^3 of permeate to be collected

Temp (°C)	1	2	3	4	5	6	Average (s)
300	29.1	27.1	28.7	27.7	27.9	28.5	28.2
350	17.0	19.5	20.2	20.1	20.0	19.9	19.5
400	14.8	12.8	13.0	13.5	13.4	13.2	13.5
450	10.5	11.1	11.5	10.3	11.1	11.2	11.0
500	9.8	9.3	9.7	9.8	9.6	10.0	9.7
550	7.9	7.9	8.0	7.7	8.1	7.8	7.9

To calculate the permeate flux on a per minute basis the following equation was used:

$$\frac{60 \text{ x (vol collected)}}{\text{Average time taken}} = \text{permeate flux } [\text{cm}^3 \text{ min}^{-1}] \qquad \text{(Equation 6.1)}$$

The expression above is a relatively simple conversion utilising the average time to collect the specified volume and the volume itself to calculate the per minute flux (hence the factor of sixty). This number can then be divided by the active area of the membrane (2.27 cm^3) to give the flux per unit area, these figures can be seen in table 6.2 below.

Table 6.2 – Table showing the calculation of the permeate flux rate

Temp (°C)	Average (s)	[Cm^3 H_2] min^{-1}	[Cm^3 H_2] min^{-1} cm^{-2}
300	28.2	21.3	9.4
350	19.5	30.8	13.6
400	13.5	44.6	19.7
450	11.0	54.8	24.1
500	9.7	61.9	27.3
550	7.9	75.9	33.5

Figure 6.1 below displays the per unit area flux, with this being the preferred method for presenting results throughout this section now that the methodology for producing the graph has been discussed. Tables containing data have been included where necessary, with a full set of numerical results presented in a tabular format can be found in appendix one at the end of this thesis.

As predicted by the models discussed and developed in earlier chapters of this thesis, an increase in temperature for palladium membrane systems results in an increasing permeate flux. As the membrane tested is thicker than 10 µm it is deemed to be a thick palladium membrane and as defined by chapter two the rate determining step is that of bulk diffusion. Leading on from this, the temperatures utilised in this test are above that of predicted desorption-limited behaviour by Ward and Dao, therefore it can reasonably be assumed that for palladium membranes the rate is determined by the bulk diffusion.

As shown in chapter three, diffusion has long been modelled as a temperature dependent Arrhenius-type relationship, where an increase in temperature results in an increase in the diffusion coefficient until an asymptote is reached as shown in chapter five (above the temperature range investigated here). An increasing diffusion coefficient leads to a proportional increase in the permeate flux, as shown both experimentally and theoretically.

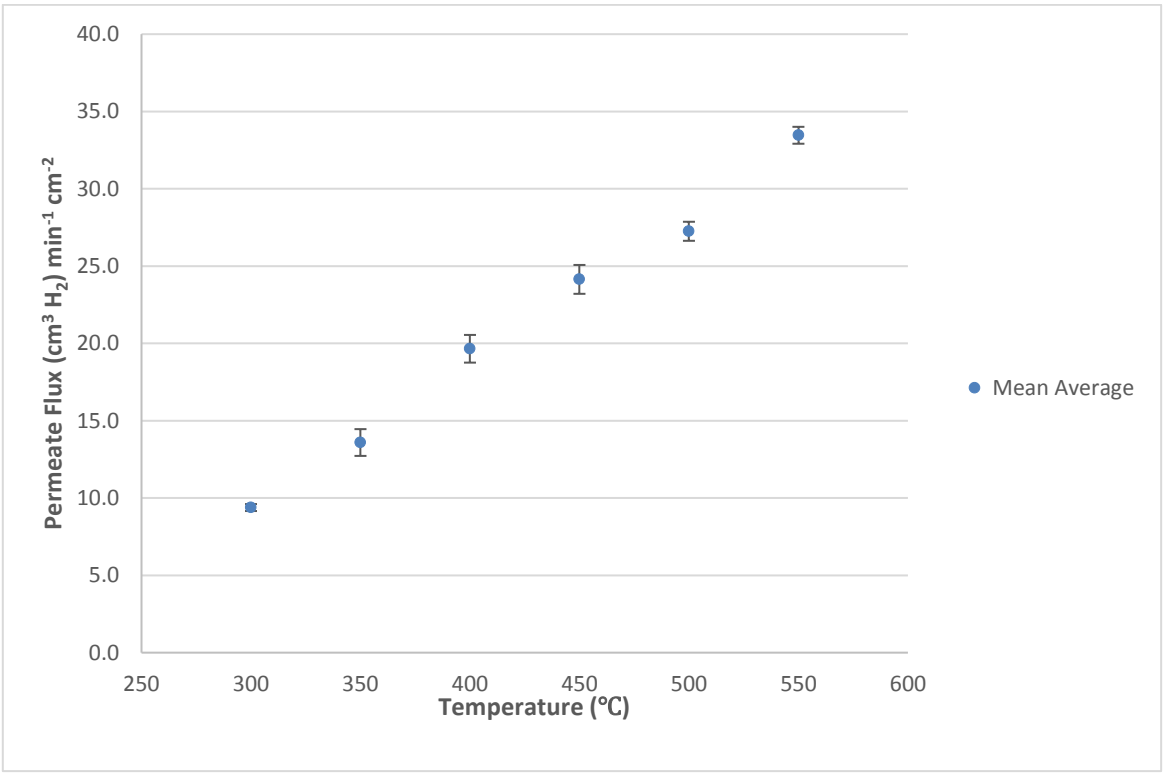

Figure 6.1 – Permeate flux for a feed-side pressure of 10 bar (abs) at varying temperatures

The graph in figure 6.2 contains the minimum; maximum and the average permeate fluxes for each of the temperatures above, taken from the six data points collected for each condition.

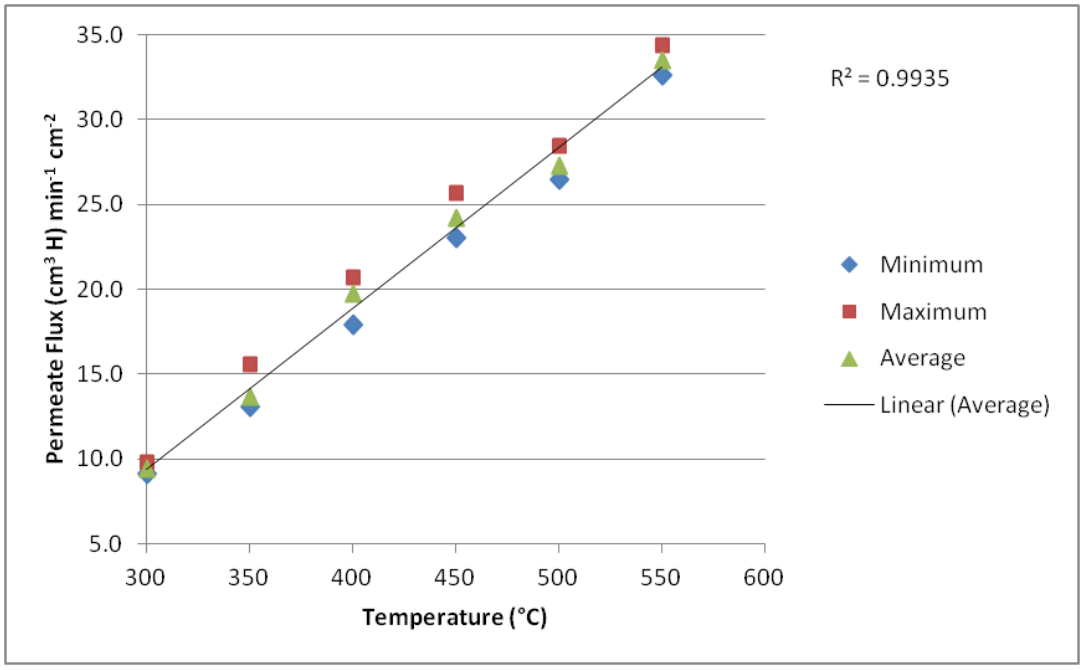

Figure 6.2 – Minimum, maximum and average (mean) permeate flux values for a feed-side pressure of 9 bar at varying temperatures.

This graph suggests good agreement of the test data, with the spread of maximum and minimum being relatively small. Table 6.3 below includes the standard deviation of the area flux to give an indication on confidence levels. The numbers show relatively good agreement in most cases.

Table 6.3 – Table containing the maximum, minimum and average flux rates for each temperature and the standard deviation of each dataset.

Temperature (°C)	Maximum value [$Cm^3 H_2$] $min^{-1} cm^{-2}$	Minimum value [$Cm^3 H_2$] $min^{-1} cm^{-2}$	Average value [$Cm^3 H_2$] $min^{-1} cm^{-2}$	Standard Deviation [$Cm^3 H_2$] $min^{-1} cm^{-2}$
300	9.8	9.1	9.4	0.22
350	15.5	13.1	13.6	0.87
400	20.6	17.9	19.7	0.90
450	25.7	23.0	24.2	0.93
500	28.4	26.4	27.3	0.62
550	34.3	32.6	33.5	0.55

The maximum standard deviation is 0.93 (cm^3 H_2 min^{-1} cm^{-2}); resulting in a maximum variance of 0.87 suggesting a generally tight spread for the data collected. Figure 6.16 shows that if a linear, first order fit is applied to the data an R^2 value of 0.9935 is given.

Table 6.4 details the average time taken to collect 50 cm^3 of gas using the rotameter and the calculation of the permeate flux. This test was done to check the accuracy of the measuring tube test and to ensure consistency of the permeate flux with a larger sample size. Once again the test was completed twice on separate occasions with three measurements taken each time to ensure consistency.

Table 6.4 – Permeate flux data for the calculated using the rotameter measuring method, 50cm^3 of gas collected.

Temperature (°C)	Average time to collect 50 cm^3 of permeate (s)	Membrane total [cm^3 H_2] min^{-1}	Per unit area [cm^3 H_2] min^{-1} cm^{-2}
450	58.9	51.0	22.5
500	50.2	59.8	26.3
550	40.3	74.4	32.8

Table 6.5 details the average time taken to collect 250 cm^3 of gas using the rotameter (and the calculated permeate flux), or one full rotation of the analogue display. This was done to further ensure accuracy of the small volume tests by minimising the effect of using a manual timer through the increase of the time taken to collect the sample, resulting in the estimated error being a smaller percentage of the total. Once again the test was completed twice on separate occasions with three measurements taken each time to ensure consistency.

Table 6.5 – Permeate flux data for the calculated using the rotameter measuring method, 250cm^3 of gas collected.

Temperature (°C)	Average time to collect 250 cm^3 (s)	Membrane total [cm^3 H_2] min^{-1}	Per unit area [cm^3 H_2] min^{-1} cm^{-2}
450	288.1	52.1	22.9
500	251.2	59.7	26.3
550	203.1	73.9	32.5

The graph in figure 6.3 below shows the calculated flux from each method for comparison of the data collected. The graph clearly shows good agreement between the values suggesting that all three measurement methods are accurate in relation to each other, bar the 10 mL measuring tube

calculated flux where the values are 1.5 cm^3 and 1.1 cm^3 greater than the 50 cm^3 and 250 cm^3 rotameter values, respectively.

If it is argued that the measurement that utilised the largest volume (and therefore the longest time) is the most accurate, this would give the measuring tube as overestimating the produced volume by 4.8 %. It appears that the measuring tube method consistently overestimates in comparison with the rotameter across all temperatures but the variation is always within 4.8 % of the 250 cm^3 rotameter value.

The permeate gas temperature for each test was measured and, in both instances, the permeate gas temperature collected in the measuring tube (16 °C and 15 °C for each test day) was higher than that of the rotameter (14 °C on both test days); assuming the same molar flux for both tests then a slightly higher volume would be expected. The potential for error of the test tube figures should be noted when considering any results collected using this method.

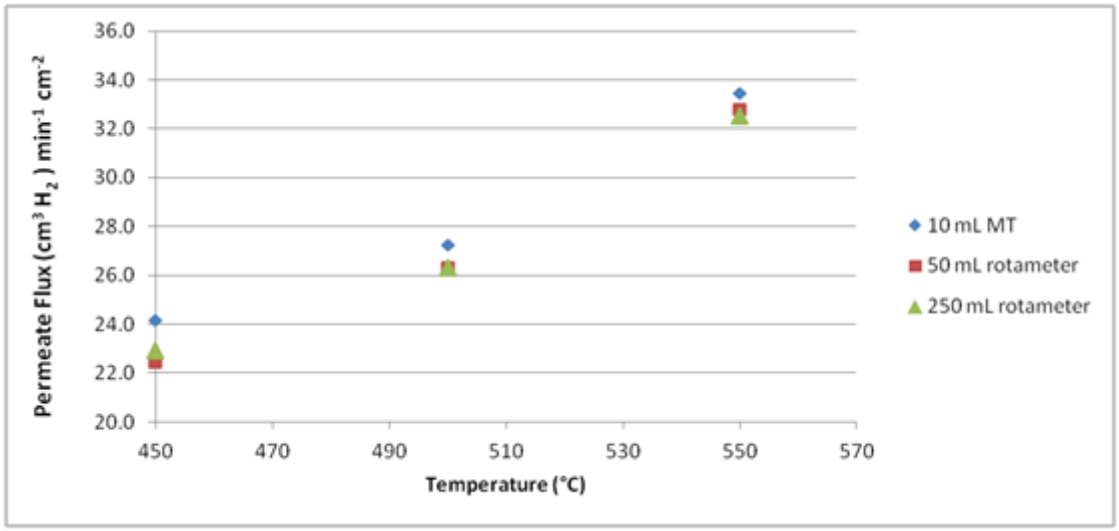

Figure 6.3 – Graph showing the calculated permeate flux rates per unit area using the three different measurement methods.

6.1.2 Experimental Data: Variable Pressure and Constant Temperature

All tests in this section were conducted on uncoated palladium membranes with a thickness of 100 µm (0.1 mm); a constant temperature was applied in each test with the feed pressure varied. The temperature for each test is given with each set of results.

Table 6.6 below shows the average time taken for permeation at each pressure, with a constant operating temperature of 400 °C maintained. Included in the table is the permeate flux rate and the

standard deviation to give an indication of variance as above. As before, the test was repeated on two separate occasions with three sets of data taken from each test for each condition (to give a total of six data sets).

Table 6.6 – Results from variable feed pressure test: hydrogen feed, palladium membrane, 400 °C temperature

Feed Pressure (bar)	**Membrane Flux [Cm^3 H_2] min^{-1}**	**Area Flux [Cm^3 H_2] min^{-1} cm^{-2}**	**Standard Deviation [cm^3 H_2] min^{-1} cm^{-2}**
2	6.4	2.8	0.02
3	11.3	5.0	0.07
4	15.1	6.7	0.06
5	19.7	8.7	0.11
6	24.9	11.0	0.23
8	33.5	14.8	0.30
10	44.6	19.6	0.87

The standard deviation was calculated to give an indication on confidence in the results, with most results showing little variance.

The permeate flux is shown to be heavily dependent on the feed side pressure; this was predicted by the models discussed and developed/utilised in earlier chapters of this thesis. As the feed side pressure increases and the permeate side pressure is kept constant, the partial pressure/concentration differential of hydrogen is increased resulting in a greater permeate flux as predicted by the models of Richardson and (Ward and Dao, 1999).

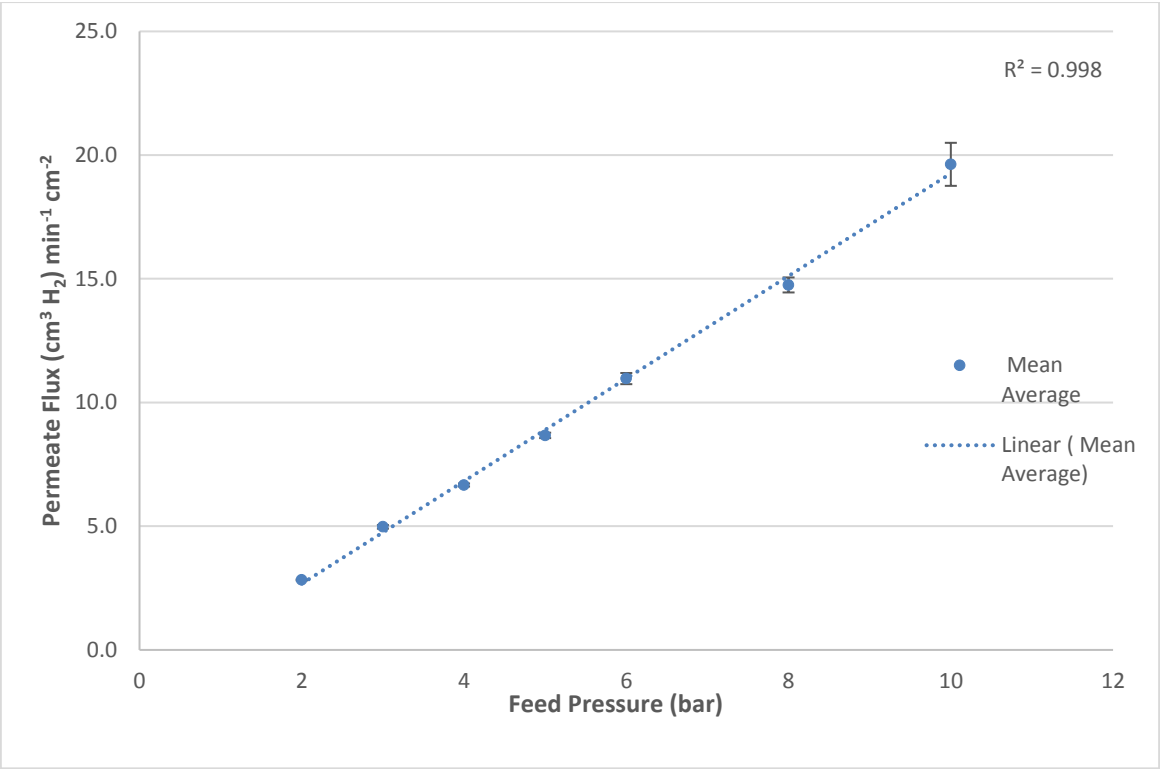

Figure 6.4 – Graph showing permeate flux at varying hydrogen feed-side pressures with an operational temperature of 400°C

Figure 6.4 displays the membrane area flux graphically. Once again, a first order relationship can be drawn from the data with a high R^2 value suggesting good statistical agreement. This is reasonable for the system tested, as the membrane is thick and not limited by surface (adsorption) or mass transfer processes, where a varying concentration differential can have a significant impact on permeate flux.

To further investigate the impact of pressure the experiment was repeated for the same test pressures at two other temperatures, 450 °C and 500 °C.

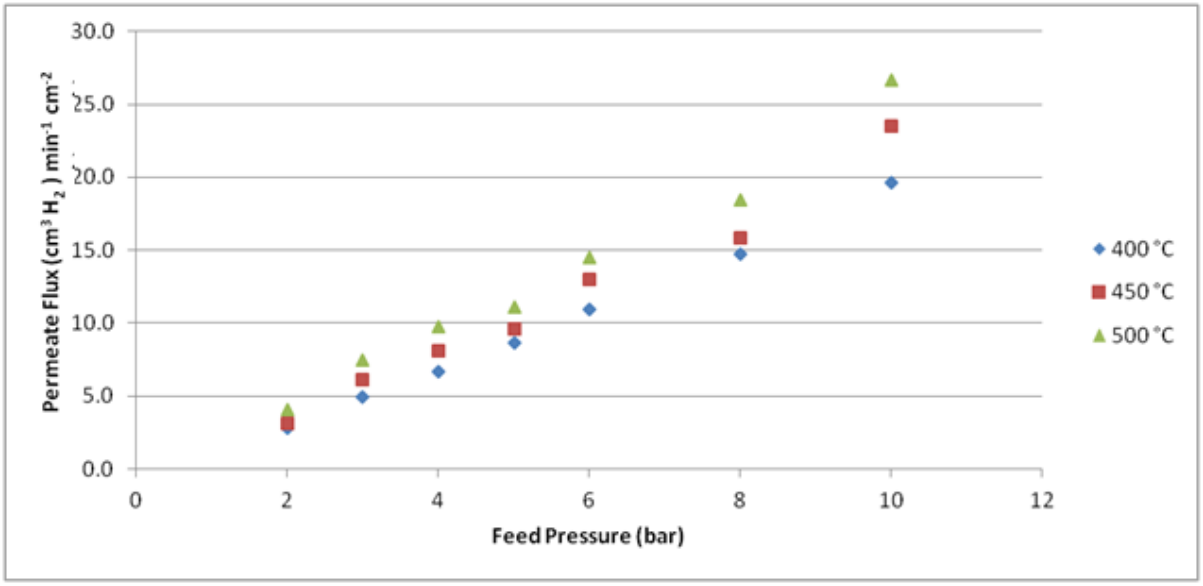

Figure 6.5 – Graph showing permeate flux at varying feed pressures for various operational temperatures

As can be seen in figure 6.5, similar patterns are shown for all three data sets, with a relatively linear/first order relationship for increasing pressure. As expected and as can be seen in the section above, increasing temperature results in an increasing permeate flux. Whilst the difference between the permeate fluxes of the 400 °C and the 500 °C increases in terms of raw numbers, the scaled/percentage difference between the two stays relatively similar:

- (1 bar feed pressure): Permeate flux at 500 °C / Permeate flux at 400°C = 4.1/2.8 = 1.45
- (9 bar feed pressure): Permeate flux at 500 °C / Permeate flux at 400°C = 26.7/19.6 = 1.36

This is once again expected due to the first order nature of the increase in flux when either pressure or temperature is increased.

6.1.3 Permeation Rate Stability Testing: Palladium with Hydrogen Feed

Further testing was conducted at a constant pressure and with constant temperature to investigate the stability of the permeation rate over the length of one test cycle. Using conditions of 10 bar feed pressure and 450 °C operating temperature, readings of the permeate flux were calculated every fifteen minutes for five hours. The results of this are shown in figure 6.6.

As highlighted previously in this thesis, membrane longevity is a serious barrier to technological readiness. As has been stated in the overview for this chapter investigating membrane longevity was not in the scope of this project. However, a preliminary investigation into the reusability of membranes was undertaken. This was done by re-testing the same palladium membrane for multiple

runs. Due to the fusion of the palladium membrane to the copper gaskets it was decided to not dismantle the enclosure and inspect the membrane at risk of losing the gas-tight seal of the enclosure. To test longevity, the test was repeated four times with the flux recorded every fifteen minutes for five hours; with each test being taken approximately one day after the previous.

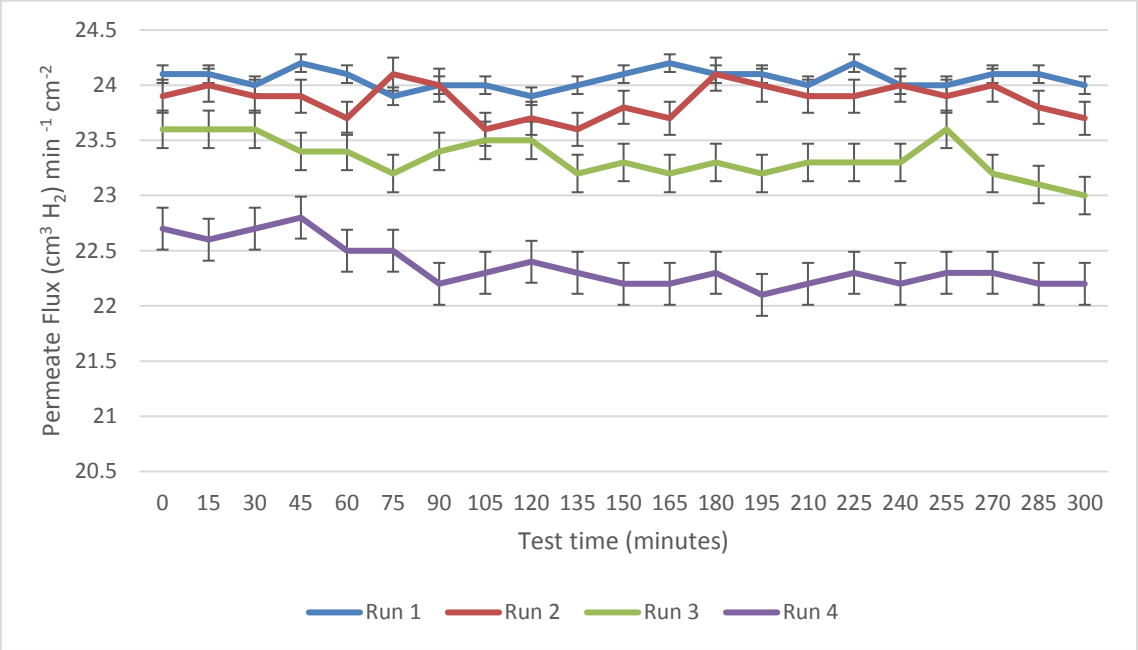

Figure 6.6 – Permeate flux recorded for repeated palladium membrane tests with 10 bar feed pressure and an operating temperature of 450 °C

The graph in figure 6.6 is insightful; the first test (blue line) shows little if any degradation of the flux over the test period. Continuation of the tests sees a gradual decline, with a more pronounced drop in the permeate flux found during the final fourth run. Further evidence of this can be found by studying the standard deviation of each run; shown in table 6.7 (and on figure 6.6) below.

Table 6.7 – Standard deviation of the permeate flux tests

Run	Standard Deviation [Cm^3 H_2] min^{-1} cm^{-2}
1	0.08
2	0.15
3	0.17
4	0.19

As can be seen, the standard deviation begins to increase as the number of tests conducted on the membrane is increased. This increase in deviation suggests a more varied flux, and when combined

with the data presented in figure 6.6 it is clear to see that this variation is a result of declining performance.

This degradation was expected to a degree, with the most likely cause to be hydride damage to the membrane. Whilst the tests were conducted at a temperature well above those likely to lead to hydride formation the likelihood is that small amounts of hydrogen, trapped in the enclosure or the membrane itself as it cools, could form hydrides - leading to performance loss. Over time, the dislocation of palladium from its crystal structure (due to hydride formation, as discussed in chapter two) will cause a drop in performance as detailed in chapter two. A noticeable drop off is somewhat concerning, as this would suggest that the membranes cannot be cycled repeatedly - which may be a problem when planned down-time for maintenance or inspection of a unit is required, or when a supply of feed cannot be consistently guaranteed.

If as theorised above, the drop-off can be associated with hydride formation during cooling, managing operational use may be able to prevent this.

The membranes could be kept at operating temperature where possible or, if they do need to be cooled, it could be done in the presence of an inert sweep gas.

6.2 Experimental Results – Palladium Membrane, Mixed Feed

Upon completion of testing with a pure hydrogen feed, palladium membranes were tested with the previously mentioned 40 vol. % hydrogen 60 vol. % carbon dioxide mixed feed gas. As for the pure hydrogen feed system described above, the results reported here vary from those most commonly reported because the downstream is not held in a vacuum. To accurately investigate the impact of the addition of carbon dioxide the tests reported here mirror those undertaken and described in section 6.6 above; with the only major difference being the inclusion of gas chromatograph data to provide details on the hydrogen purity in the permeated flux.

6.2.1 Experimental Data: Constant Pressure and Variable Temperature

As in the previous section a palladium membrane of 100 µm (0.1 mm) thickness was used for the test. A constant feed side pressure of 9 bar (10 bar absolute) was maintained, mirroring the tests undertaken in the previous sub-section to allow for comparison of the results. To prevent a build-up of carbon dioxide and ensure good mass transfer kinetics a feed flow rate of 50 cm^3 min^{-1} was utilised. Figure 6.7 shows the average flux rate measured for each temperature.

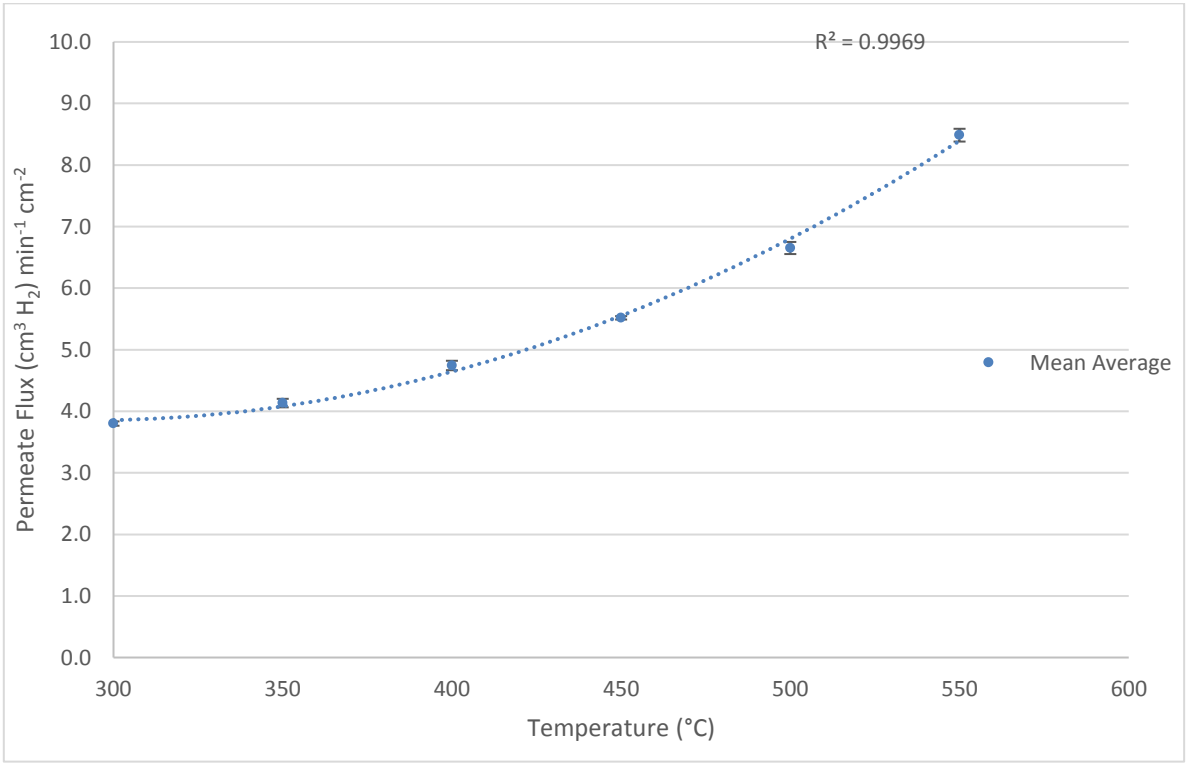

Figure 6.7 – Graph showing average permeate flux for a constant feed pressure of 9 bar and varying temperature

The graph shows a similar trend to that of the corresponding graph in the previous section (figure 6.1), with the increasing temperature resulting in an increasing permeate flux as expected. However unlike in the pure feed test, where a first order relationship was clearly apparent, the relationship between the temperature and the permeated flux appears to be second order; with a second order polynomial showing stronger R^2 correlation (0.9969) compared to the first order R^2 value of 0.9264. A summary of the raw data is given in table 6.8.

Table 6.8 – Table showing significant statistical data for the tests undertaken under the specified conditions

Temperature (°C)	Maximum value [Cm^3 H_2] min^{-1} cm^{-2}	Minimum value [Cm^3 H_2] min^{-1} cm^{-2}	Average value [Cm^3 H_2] min^{-1} cm^{-2}	Standard Deviation [Cm^3 H_2] min^{-1} cm^{-2}
300	3.8	3.7	3.8	0.04
350	4.2	4.0	4.1	0.07
400	4.9	4.7	4.7	0.08
450	5.6	5.5	5.5	0.03
500	6.8	6.5	6.7	0.10
550	8.6	8.3	8.5	0.10

As can be seen from the table the results are once again consistent; with the tabulated values for each condition having a minimal spread and the standard deviation further strengthens this conclusion. This suggests that this change in relationship is measurable and consistent and therefore it must be accounted for.

As the only difference between the two tests is the presence of carbon dioxide on the feed side it must be assumed that this is the causal factor. This leaves two possibilities to be considered, the first is that the mass transfer of hydrogen from the bulk to the surface is inhibited by carbon dioxide in such a way that a second order relationship is formed. The second possibility is that of surface kinetics, with carbon dioxide blocking active sites through binding and unbinding of the molecule to surface sites resulting in a change to the temperature/flux relationship to second order or pseudo-second order. Alternatively, a combination of the two effects could result in the change.

6.2.2 Experimental Data: Constant Temperature and Variable Pressure

The results presented in this section include the first no permeate flux (“no flow”) results discussed as part of this thesis. Two temperatures were tested, 400 and 450 °C, and in both instances no flow

was gathered for feed side pressures of 5 bar or less. Figure 6.8 shows the generated permeate fluxes for each condition.

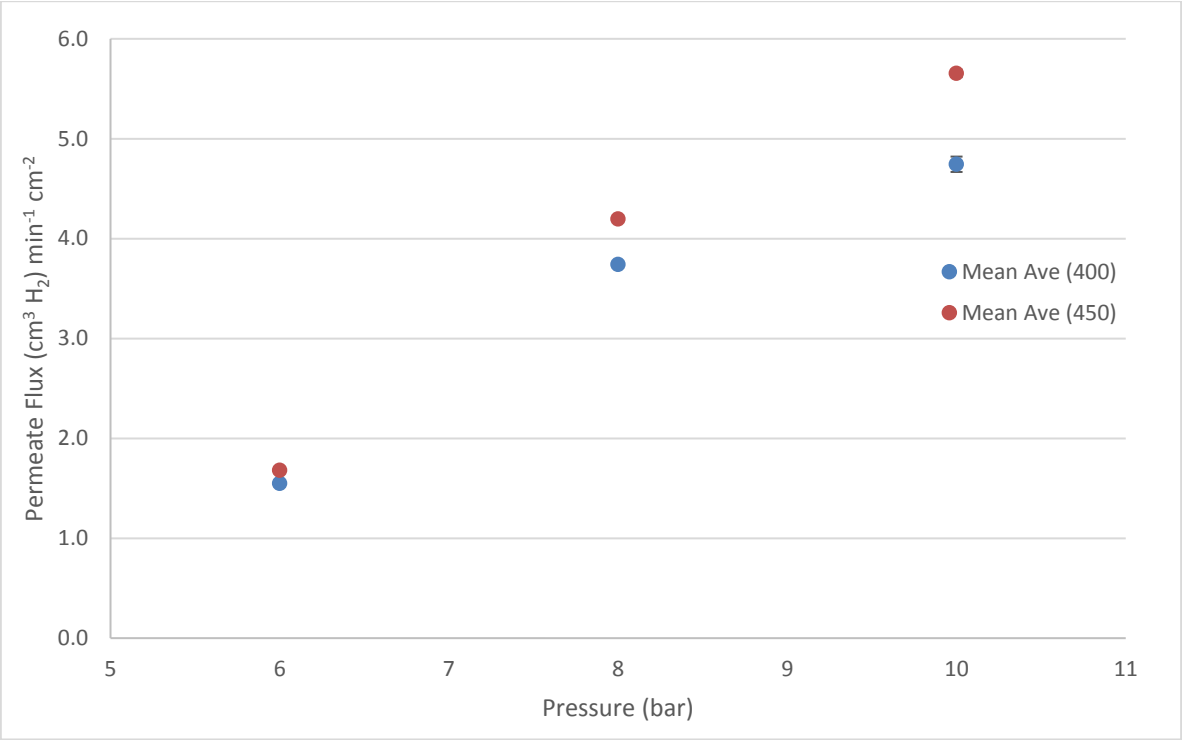

Figure 6.8 – Permeate fluxes achieved at 400 °C (blue) and 450 °C (red) for varying feed pressure

As expected, increasing the feed side pressure results in an increase in the permeate flux; with both temperatures behaving in a consistent manner. These results were expected and are consistent with the findings from the previous pure hydrogen feed tests.

Once again, the standard deviation and calculated variance for each test was low, suggesting consistent performance and reasonable data reliability.

6.2.3 Permeation Rate Stability Testing: Palladium with Mixed Feed

Mirroring the test undertaken in section 6.1.3, palladium membranes were cycled multiple times as before, to investigate the drop in permeate flux over time. The results of this test have been included in figure 6.9 below, to allow for comparison the test was with the same feed side pressure (10 bar) and operating temperature (450 °C) as in the previous test.

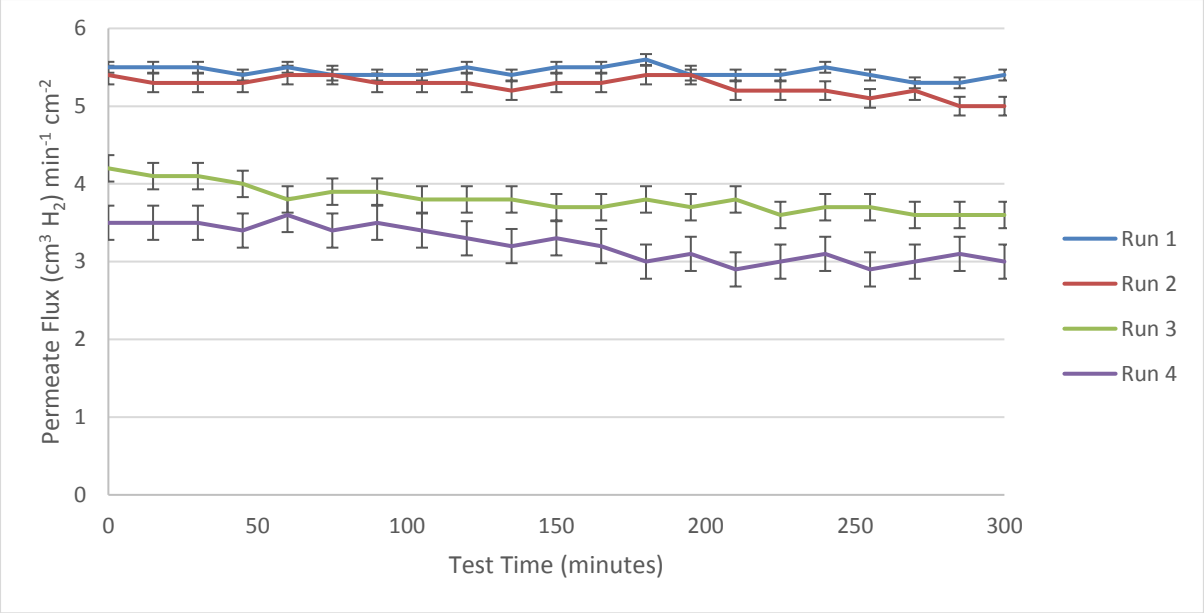

Figure 6.9 - Permeate flux recorded for repeated palladium membrane tests with 10 bar feed pressure and an operating temperature of 450 °C

As shown for the pure hydrogen tests conducted above the drop off between cycles is pronounced after multiple runs. Here, the drop off is significant and most noticeable between runs two and three. The performance loss from the first run to the final run is significant, with the flux dropping approximately 45% from the highest to the lowest value measured.

Table 6.9 – Standard deviation of the permeate flux tests

Run	Standard Deviation [Cm^3 H_2] min^{-1} cm^{-2}
1	0.07
2	0.12
3	0.17
4	0.22

The standard deviations of performance for each run are included once again (table 6.9) to show that performance is not only poorer after multiple cycles, but also less stable.

6.2.4 Analysis of Permeate Composition

Tests were undertaken on various samples detailed in table 6.10 below; the tests were undertaken following the methodology detailed earlier in chapter 4.

Table 6.10 – Hydrogen permeate purity (%) for various samples collected over the course of the Pd membrane tests

Sample Number	Sample Details	Hydrogen Purity (%)
1	Sample collected during variable temperature test run one	99.9%
2	Sample collected during variable temperature test run two	99.9%
3	Sample collected during variable pressure test run one	99.9%
4	Sample collected during longevity test one	99.9%
5	Sample collected during longevity test four	99.8%

As can be seen in the table, the hydrogen purity is very high and rather stable, with the only measured difference being found during the fourth longevity test; and this variance is within the error margin given by the calibration gas.

The high hydrogen purity is expected due to the relative thickness of the membranes. As detailed in chapter two, only hydrogen is transported at any measurable level through the metal grain with transport of other atoms (such as the carbon and oxygen in carbon dioxide) being transported mainly through the grain boundaries, if at all. In chapter two, the majority of the palladium membranes discussed were thinner than those utilised in this body of work and as such resulted in lower hydrogen permeate purities, although it must be noted they are not much lower. Other thick palladium based membranes such as those studied by (Dunbar, 2015) and (Tsai *et al.*, 2015) show similar selectivity of hydrogen over other components such as carbon dioxide and helium.

6.3 Experimental Results – Silver Coated Group V metals

After extensive testing of palladium membranes, tests on vanadium and niobium ("the group Vb metals") were undertaken. This section contains all the results relating to the testing of oxidised silver membranes under all the conditions investigated. As stated previously, the thickness of the silver coating was 200 nm; with this thickness expected to be capable of providing the required surface catalysis whilst not limiting the bulk diffusion. The coating was conducted by Wallwork HT with the oxidisation completed at the Buxton test facility – as stated previously.

6.3.1 Experimental Results: Uncoated and Pure Silver Coated Group V Membranes

It was decided to run tests on un-coated vanadium and niobium membranes alongside membranes coated with silver (but not oxidised) to investigate the effect of the proposed coating. The following experimental results were achieved:

- Uncoated vanadium membranes achieved no measurable permeate flux with a 9 bar hydrogen feed at temperatures ranging from 200 °C to 550 °C.
- Uncoated niobium membranes achieved no measurable permeate flux with a 9 bar hydrogen feed at temperatures ranging from 200 °C to 550 °C.
- Silver coated vanadium membranes achieved no measurable permeate flux with a 9 bar hydrogen feed at temperatures ranging from 200 °C to 550 °C.
- Silver coated niobium membranes achieved no measurable permeate flux with a 9 bar hydrogen feed at temperatures ranging from 200 °C to 550 °C.

As can be seen, none of these tests were successful, as was expected before testing. Therefore, the permeate flux produced by the oxidised silver membranes can be attributed to the oxidisation of the coating and not to any latent permeability.

The results were as expected and predicted from the literature review in chapter two. For vanadium and niobium, a combination of the ready formation of surface oxides and the lack of catalytic dissociation results in no measurable permeation. For the silver coated membranes, silver itself is shown to not activate the dissociation of hydrogen as detailed before.

6.3.2 Experimental Results: Oxidised Silver Coated Group V Membranes; Hydrogen Feed

Upon completion of the initial tests the silver coated membranes were oxidised as described in section 6.5. Preliminary tests were conducted at temperatures of 300 °C and above, however no flux was established due to the decomposition of Ag-O at these temperatures. Further tests were conducted at lower temperatures, significantly below the ideal operating temperatures for membrane separation and the target operating temperature range set by the US DoE.

Whilst the low operating temperature would not be ideal, if a reasonable permeate flux could be established, system control and energy recovery could allow for low-temperature operation with minimal energy loss. The temperature range used is towards the maximum suggested by (Garner and Reeves, 1954); where 200 °C is seen as the maximum stable operating temperature. The results for both niobium and vanadium coated in Ag-O are shown in figure 6.10 below.

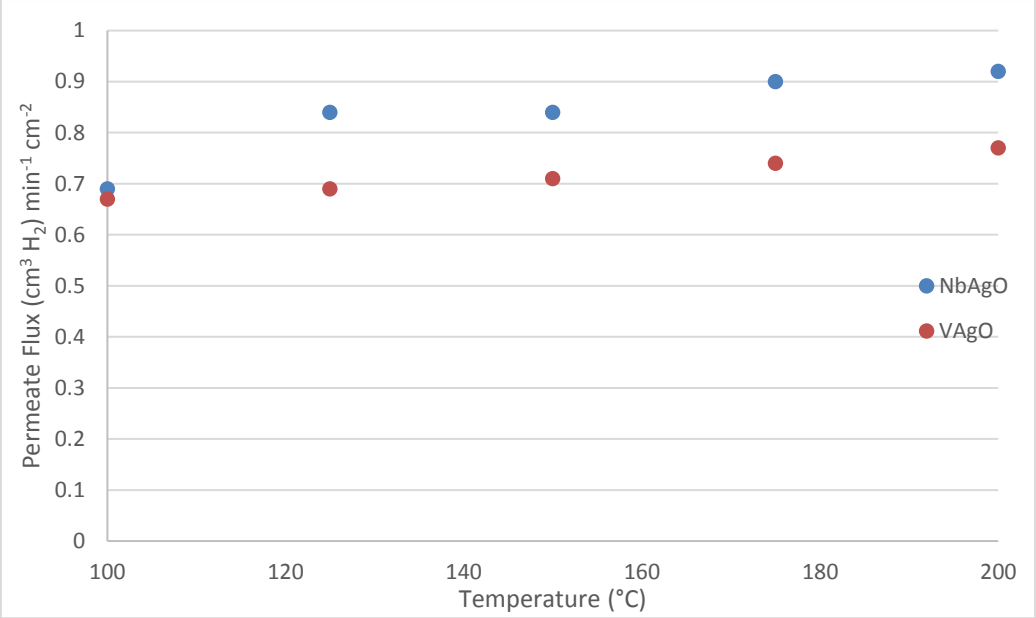

Figure 6.10 – Graph showing measured permeate flux for Ag-O coated group V metals at varying operating temperatures

As can be seen the membranes did deliver a measurable permeate flux at 10 bar, but even the highest permeate flux rate is only a small fraction of the permeate flux measured for palladium at an operating temperature of 300 °C and 10 bar (figure 6.1), the poorest performing palladium operating temperature.

The coating was also discovered to be relatively unstable. Whilst no time data was recorded with regards to longevity, it is estimated that operation of the membrane was possible for around 30 minutes before the permeate flux ceased. This is possibly due to the reduction of the Ag-O coating with this being an expected potential outcome due to the reducing capability of hydrogen.

The activation of the dissociation process is theorised by (Xu, Greeley and Mavrikakis, 2005) by the presence of oxygen in the Ag(111) surface, however it appears that this state is not stable for longer term use. (Mohammad *et al.*, 2007) and (Mohammad *et al.*, 2008) suggest a similar activation of the dissociation, however it is noted in this work that surface oxygen will likely be removed as H_2O.

6.3.3 Experimental Results: Oxidised Silver Coated Group V Membranes; Mixed Feed

After testing the oxidised coating with a pure hydrogen feed, testing was conducted on a mixed feed supply. However, no flux could be established for the membranes with a H_2/CO_2 mixed feed operation. The cause of this is believed to be a combination of the low permeability of the Ag-O coated membranes and the lower hydrogen partial pressure of the mixed feed, resulting in a poor level of performance, in which no measurable flux could be obtained.

It appears that the reduction of oxygen in the surface and sub-surface lattice occurs at a rate that is not sustainable for use with hydrogen separation membranes. Future tests on such a coating may be warranted on low temperature membranes, such as those based on tantalum (where the critical temperature for hydride formation is low). The application of a silver oxide coat through an alternative process may produce better results, but this direction has not been pursued as part of this thesis. Such a coating could in theory be applied through the use of PVD and related plasma oxidation methods (Cassar, Matthews and Leyland, 2012).

6.4 Experimental Results – Silver-Palladium Coated Niobium Membrane

Upon completion of the oxidised silver tests, the alternative coating consisting of palladium and silver was investigated. This section contains the results of the initial investigation of this coating, where varying compositions of palladium and silver were tested to identify an optimal coating. The palladium and silver were deposited using electroless plating as discussed above; where the methodology followed provided the expected deposition rates. These rates were used to gauge how long to leave the membrane in the coating bath for, with the exact composition determined using the EDX in the SEM.

As with the palladium tests discussed earlier in this chapter, each test was repeated six times with the average value taken. The standard deviation for each data set was calculated to assess consistency as has been done in the previous sections.

Niobium membranes were coated with the following three compositions:

1. 100% palladium, with the EDX Spectrum included in figure 6.25 below.

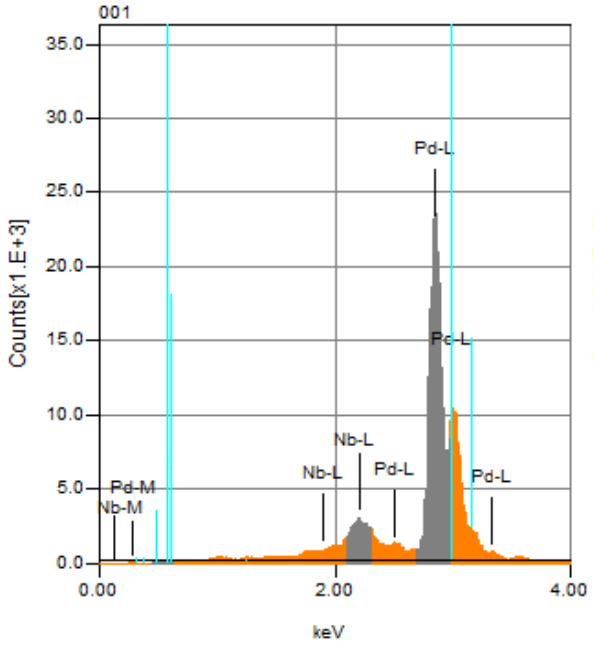

Figure 6.11 – EDX graph showing the surface composition for a 100Pd coated Nb membrane

2. 76.3% palladium; 23.7 % silver, with the EDS Spectrum included in figure 6.26 below.

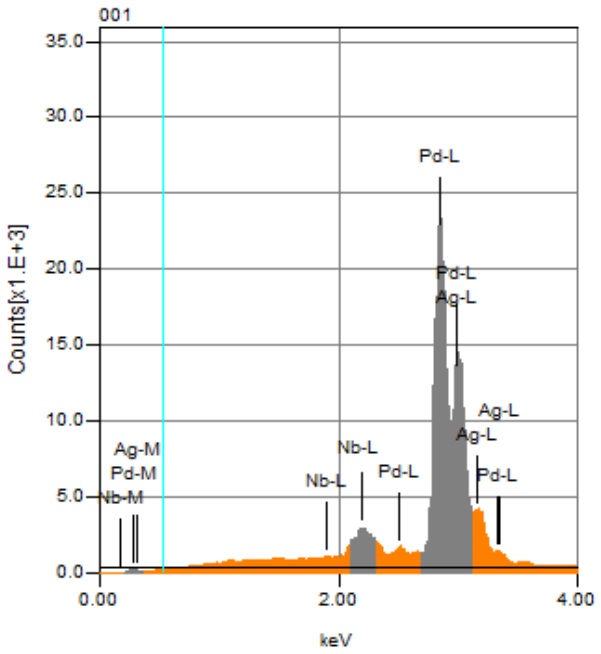

Figure 6.12 - EDX graph showing the surface composition for a 77Pd23Ag coated Nb membrane

3. 55.2% palladium; 44.8% silver, with the EDX Spectrum included in figure 6.27 below.

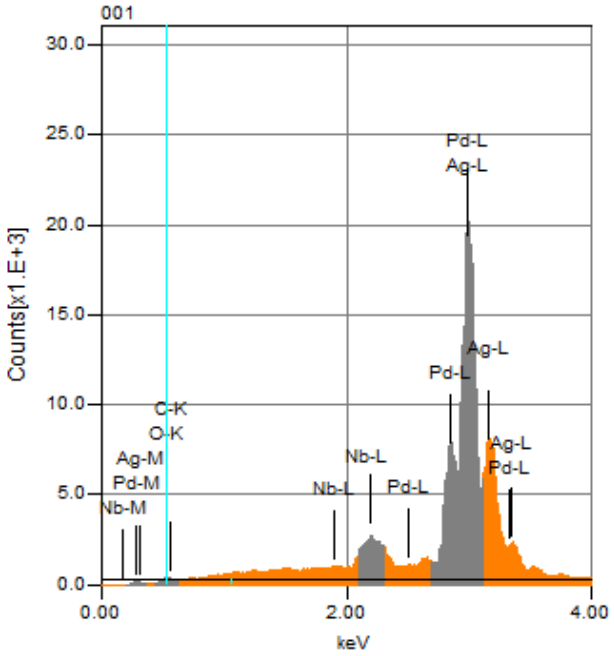

Figure 6.13 - EDX graph showing the surface composition for a 55Pd45Ag coated Nb membrane

Figure 6.13 shows a small amount of contamination with carbon and oxygen contamination on the surface, it is believed that this did not have an impact on the performance of the membrane in general.

The coatings are estimated to be 800 – 1800 nm in thickness from the deposition times. A pure palladium coating was utilised as a control for comparison with the PVD coatings (and with literature data). The second coating (76.3% palladium) was utilised as it is the optimum palladium-silver alloy composition for hydrogen permeation as detailed extensively in chapter two. Finally, a near 50-50 Pd-Ag alloy was utilised to investigate the performance loss in the case of excessive silver presence. In the case of Pd-Ag membranes the presence of excessive silver in the alloy results in a significant loss of performance.

The EDX spectra for all three membranes show a small peak for niobium; whilst this has been noted it is assumed to not have an effect on the behaviour of the membrane. The peak can be attributed to the penetration of the high energy EDX electron beam, with the beam detecting the composition of the bulk (niobium) below the surface. This is expected due to the X-ray effect of the EDX.

6.4.1 Experimental Results: Pd-Ag Coated Niobium with Pure Hydrogen Feed

Each of the three membranes described above were tested on a variable temperature basis; with a constant feed side pressure of 3 bar (absolute) applied to the 0.1 mm thick membrane. A relatively low hydrogen pressure was used due to the known issues of embrittlement for niobium. Early attempts had tried to utilise a higher hydrogen pressure but fracturing of the membrane was found to be a problem.

Figure 6.14A below shows the results of the permeation tests for each of the three coatings in pure hydrogen. Figure 6.14B shows only the Pd100 and Pd76 coatings to display the standard deviation of both graphically. For the Pd100 and Pd76 coatings the permeate volume collected was 50 cm^3 and for the Pd55 coating the permeate volume collected was 10 cm^3.

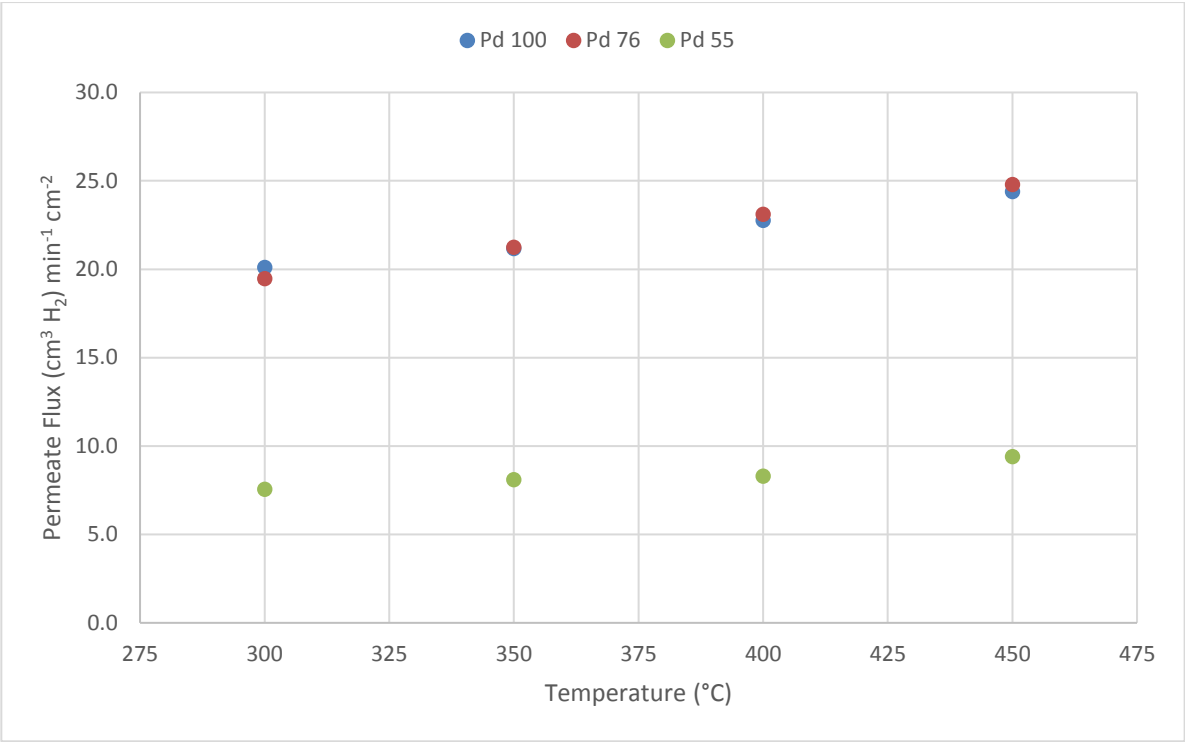

Figure 6.14A – Graph showing permeate flux for each of the three coated Nb membranes (Pure H_2 feed)

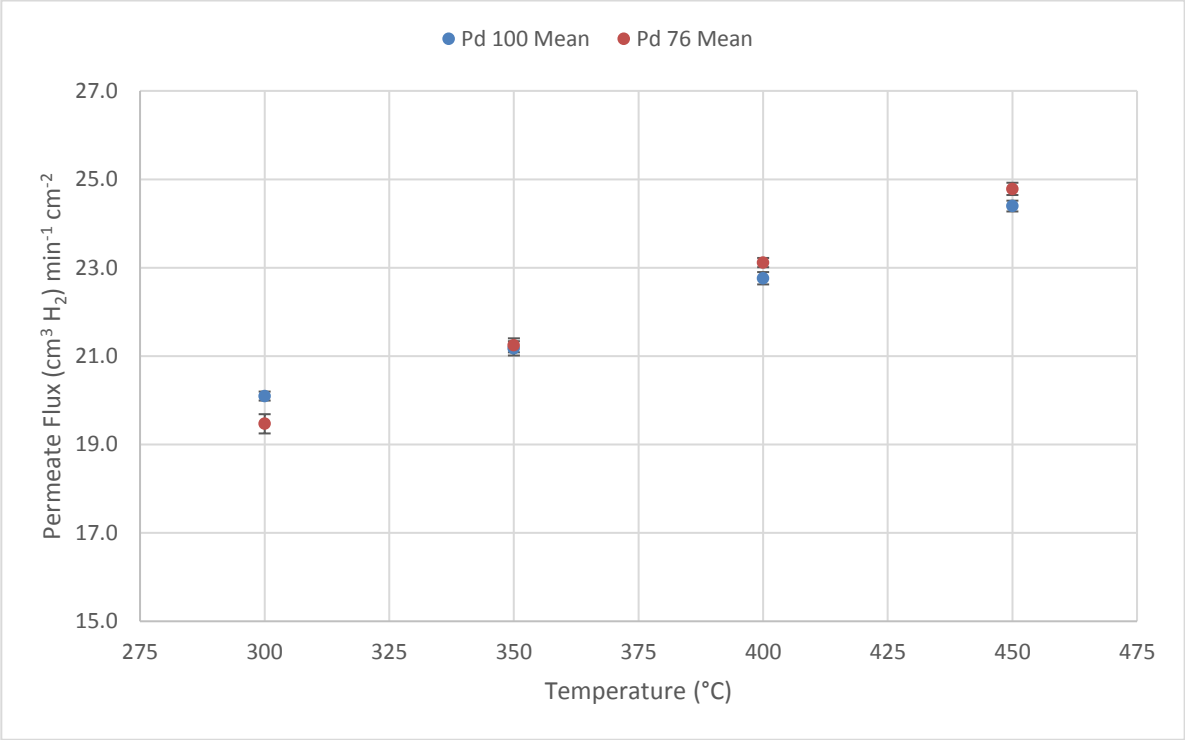

Figure 6.14B – Graph showing permeate flux and standard deviation for Pd 100 and Pd 76 (Pure H_2 feed)

In figure 6.14A, two trends are immediately apparent; the first is that little difference can be found between the performance of the pure palladium coated membrane (Pd100) and the Pd76 coating. Figure 6.14B plots the standard deviation alongside the mean values from figure 6.14A, the overlap or near overlap of the error bars at most temperatures tested shows that with reasonable confidence it can be assumed that no significant difference in membrane performance can be found between the two coatings. The consistency between both across the temperature range is shown in the graph and this suggests that the substitution of silver (at this concentration) does not result in any impedance of the flux or result in any loss of catalytic ability. However, unlike Pd-Ag bulk membranes increasing the silver content does not result in an increasing flux.

Such a result suggests that the membrane is bulk-diffusion limited. This is expected due to the experimental conditions investigated; a thick membrane, a relatively high hydrogen concentration and elevated temperatures were expected to result in such behaviour. This view can be supported further with data from literature; (Serra *et al.*, 1998) suggest that, in conditions where the surface processes are rate limiting, a 75Pd-25Ag alloy would perform better than a pure palladium membrane. Thus with the catalytic coatings performing equally, it would suggest bulk-diffusion limitation is in effect.

The second trend is the significant drop off in membrane performance for the highest silver/lowest palladium content. This was considered as a potential outcome, as Pd-Ag membranes suffer from decreased permeability when the optimum silver content is surpassed, as shown by others such as (Hatlevik *et al.*, 2010) and (Knapton, 1977).

With the behaviour of Pd-Ag membranes extensively studied, it is tempting to extrapolate from this and to conclude the same outcome before even running a test. A first glance at the results included shown in figure 6.14 would suggest that this conclusion holds; however, when inspecting the data in more detail, questions can be raised on whether such a view is a little facile. This inspection and the resultant discussion can be found in chapter seven.

What can be concluded from the results here is that there is a drop off in membrane performance when the silver content is increased. Such a drop in performance would suggest that the membrane was operating on a surface-limited basis. Table 6.11 below shows the standard deviation for each result collected.

Table 6.11 – Standard Deviation for the area flux of each membrane

Standard Deviation ([cm^3 H_2] cm^{-2} min^{-1})			
Temp (°C)	**Pd 100**	**Pd 76**	**Pd 55**
300	0.10	0.22	0.10
350	0.16	0.16	0.15
400	0.14	0.11	0.16
450	0.12	0.14	0.20

6.4.2 Experimental Results: Pd-Ag Coated Niobium with Mixed Feed

Tests were also conducted on the niobium coated membranes with the mixed hydrogen and carbon dioxide feed. For consistency each of the membranes tested as part of this section were identical to the membranes tested in section 6.9.1; this was done by ensuring all the coating for the membranes was undertaken at the same time in the same plating baths.

To be consistent with prior tests it was decided to use a hydrogen partial pressure on the feed side of 3 bar, this equated to a total pressure of 7.5 bar. The results for the tests are shown below in figure 6.15.

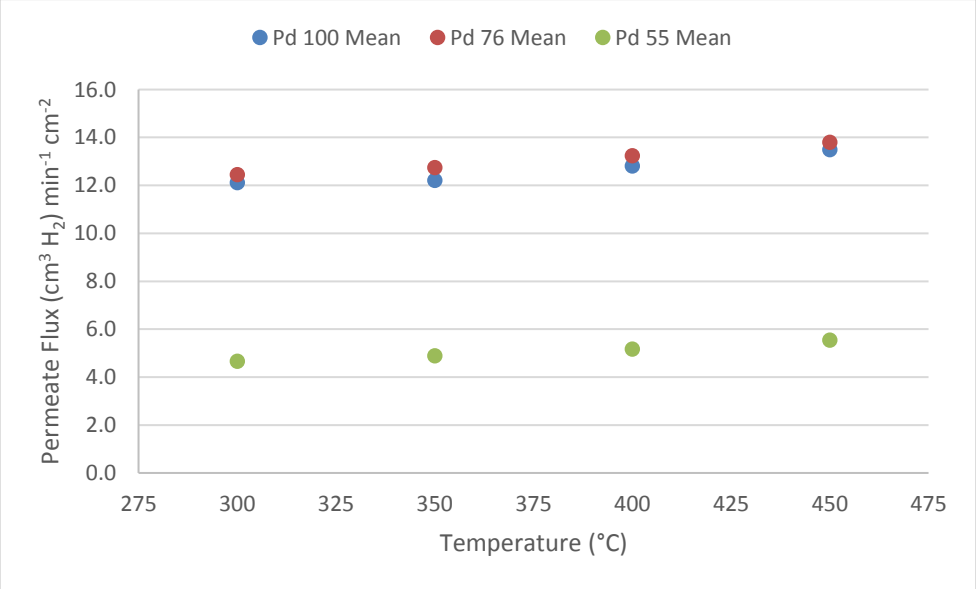

Figure 6.15A – Graph showing permeate flux for each of the three coated Nb membranes (H_2/CO_2 feed)

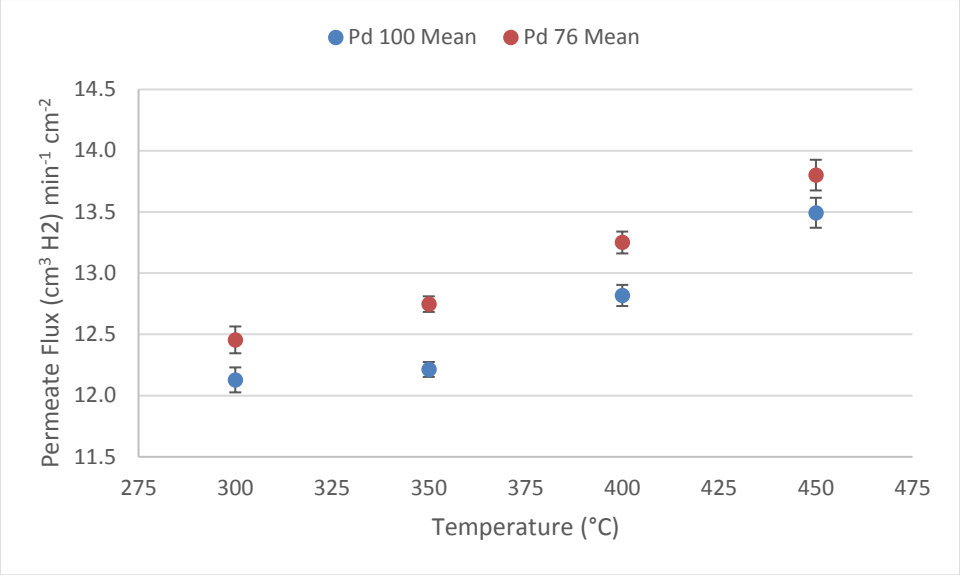

Figure 6.15B – Graph showing permeate flux for each of the three coated Nb membranes (H_2/CO_2 feed)

Figure 6.15A shows a similar pattern to figure 6.14A, with the Pd100 and Pd76 coated membranes outperforming the Pd55 coating. However, unlike in hydrogen feed only tests there does appear to be a slight difference in performance between the Pd100 and the Pd76 coating. This can be seen more clearly in figure 6.15B, where the standard deviation has been plotted with the mean average.

Under all conditions tested the Pd76 coated membrane appears to perform better, with an increase in area flux ($cm^3\ cm^{-2}\ min^{-1}$) found at each temperature. The difference in performance is shown in table 6.12 below. The increase is relatively small, but is consistent enough to suggest that it may be more than simple variance.

Possibilities for this difference are discussed in chapter seven, where such a discourse is more relevant. It should be noted that the main reason for substitution of Pd is purely financial, should the increase be proven to be more than coincidental this would merely be an added benefit.

Table 6.12 – Table showing the difference in performance between the Pd100 and Pd76 coated membranes with a mixed gas feed

Area flux area flux ([$cm^3\ H_2$] $cm^{-2}\ min^{-1}$)			
Temperature (°C)	**Pd100**	**Pd76**	**Increase (%)**
300	12.1	12.5	2.7
350	12.2	12.7	4.4
400	12.8	13.3	3.4
450	13.5	13.8	2.3

Finally, the permeate through each membrane in the mixed test was tested for hydrogen purity. Table 6.13 contains the results of the test, showing a high hydrogen purity for each test was achieved.

Table 6.13 – Table of permeate purity test results for Nb membranes

Membrane	**Hydrogen permeate purity (%)**
Pd100 coated niobium	99.9
Pd76 coated niobium	99.9
Pd55 coated niobium	99.9

6.5 Experimental Results – Palladium-Silver Coated Vanadium Alloy Membranes

The final permeation tests were undertaken on palladium and silver-coated vanadium alloys, with the alloys used being 85V-15Ni and 85V-10Ni-5Al as detailed earlier in this chapter. These alloys were chosen for the reasons detailed in chapter two, namely their promising permeate flux characteristics and their increased resistance to hydride damage over pure group V metals.

The silver palladium coating prepared on these membranes was determined by the best performing membranes from section 6.4 above; where the target coating composition is 77% palladium and 23% silver. Once again, the exact surface composition was determined through the use of the EDX detector. All membranes were coated for the same length of time, to ensure consistency in the thickness and composition of the coatings.

The composition of the coatings was analysed before usage. Energy-dispersive X-ray spectroscopy (EDX) tests were conducted on both types of membrane to ensure that the different alloy composition didn't result in differing deposition rates. Results were returned by the SEM in tabular, map and spectra form; examples of the spectra and maps have been included.

A 77.3Pd-22.7Ag coating was deposited on the V-Ni membrane, figure 6.16 shows the energy dispersive X-ray spectrum used to confirm the exact ratio of Pd to Ag found in the catalytic coating. The peak can be attributed to the penetration of the high energy EDX electron beam, with the beam detecting the composition of the bulk (vanadium, nickel) below the surface. This is expected due to the X-ray effect of the EDX.

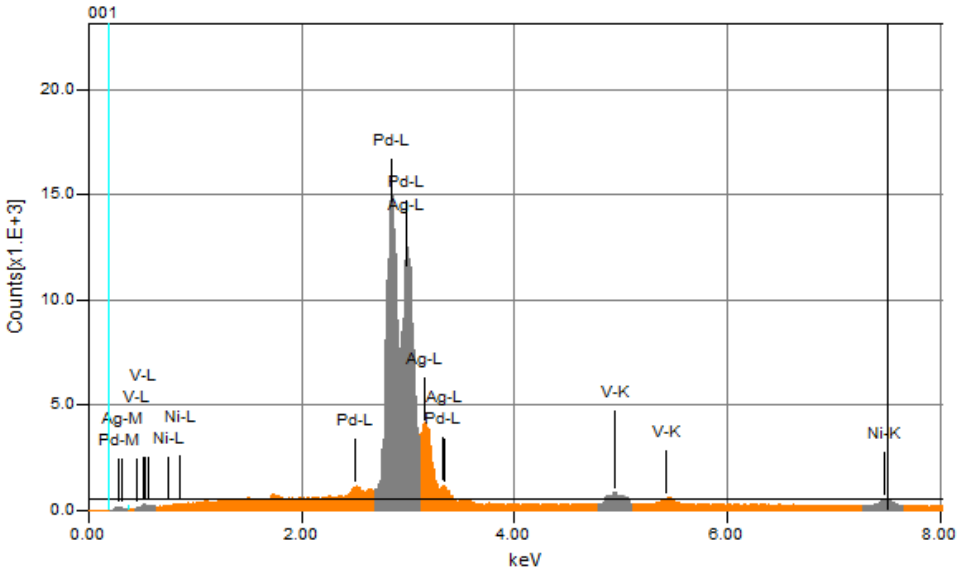

Figure 6.16 – EDX spectrum for V-Ni membrane with Pd77Ag23 coating

A 77.3Pd-22.7Ag coating was deposited on the V-Ni-Al membrane; figure 6.17 shows the energy dispersive X-ray spectrum used to confirm the exact ratio of Pd to Ag found in the catalytic coating. As with the V-Ni membrane, trace amounts of the bulk membrane components (V, Ni and Al) which is once again expected due to the penetration of the high energy electron beam from the EDX.

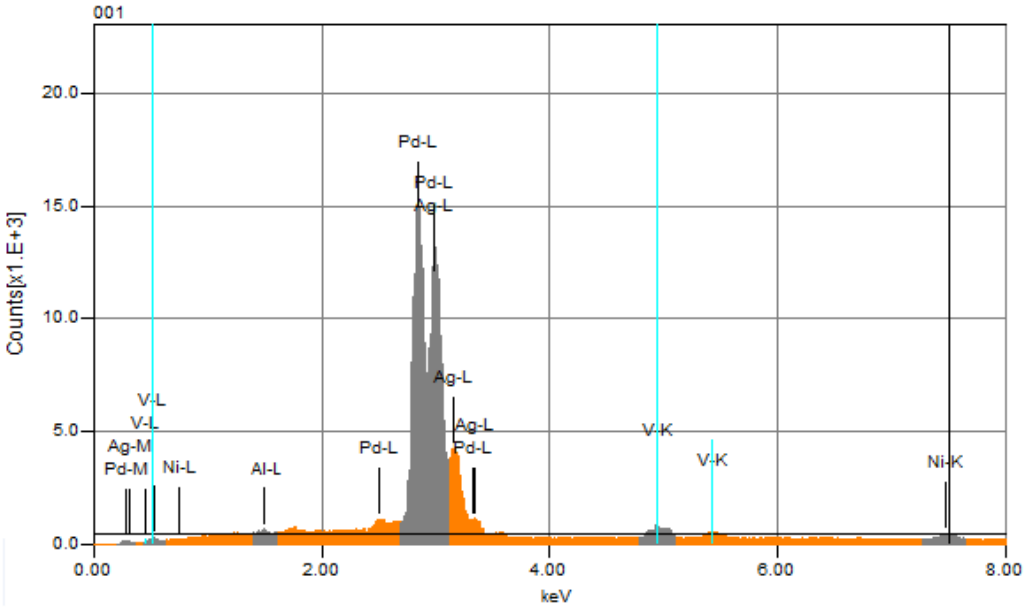

Figure 6.17 – EDX spectrum for V-Ni-Al membrane with Pd77Ag23 coating

It should be noted for all of the EDS spectra shown that the peaks for palladium and silver can overlap. Whilst this could be problematic the results given by the EDS are similar to those predicted from the deposition times for the electroless plating technique.

Maps of the surface were also produced to ensure that distribution of the catalyst was even, an example of this is shown in figure 6.18. The maps shown below are taken from a scan of the V-Ni membrane and show clearly the extent of the uniform nature of the coating after annealing.

Figure 6.18 shows the extent of the coating on the surface. The central image shows the secondary electron image, the purple image shows palladium, yellow shows silver, green shows nickel and red shows vanadium. The image shows that in some areas coverage was not as thick, suggesting future iterations may benefit from longer deposition.

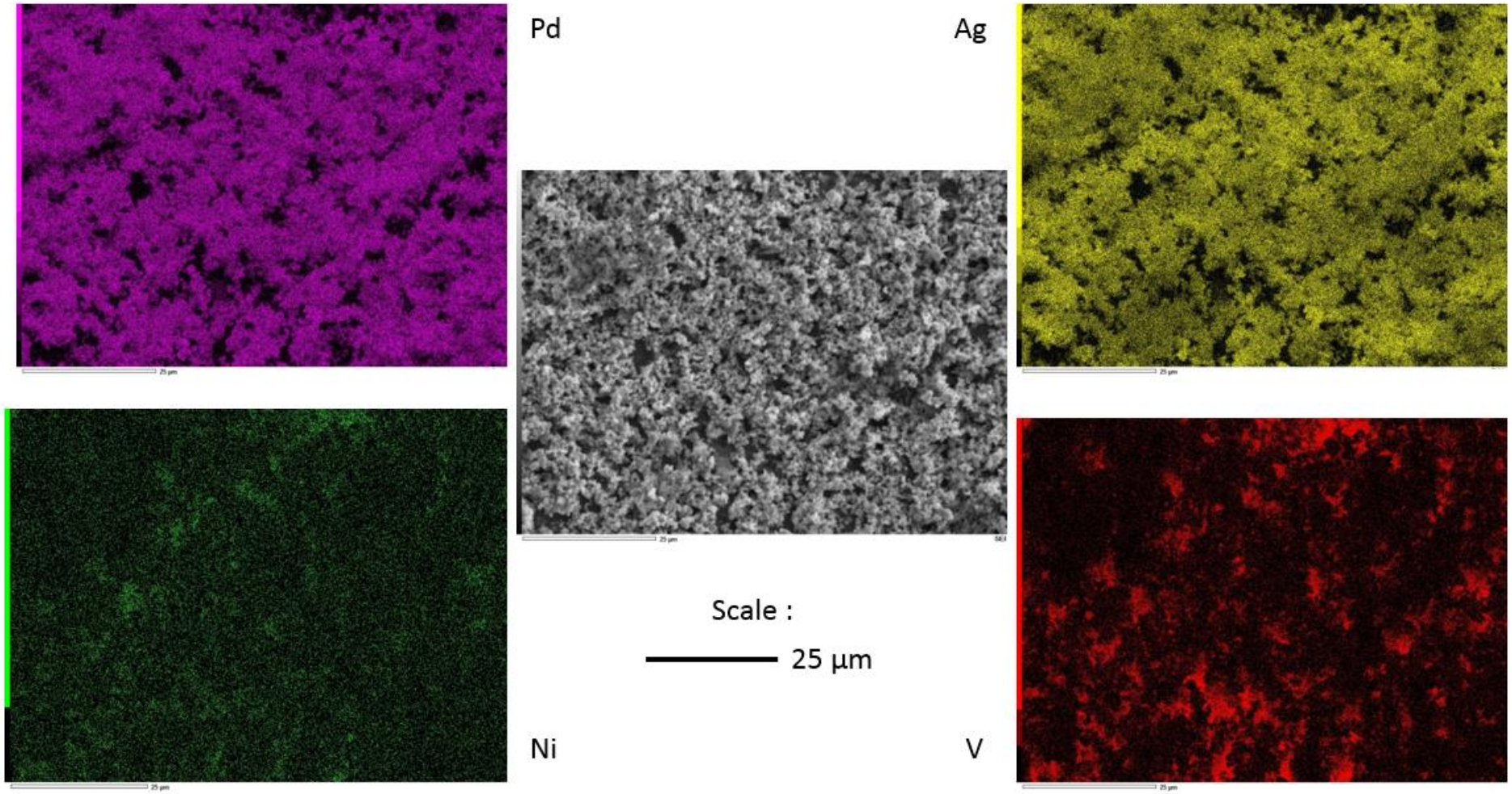

Figure 6.18 – EDX surface map of the coated V-Ni membrane

As tests were undertaken on thicker, 250 µm (0.25 mm), membranes, direct comparison with other collected results is not feasible. To make comparisons possible further analysis of the results is required and this has been given in chapter seven as it falls outside the scope of this results section.

Mirroring the palladium membranes investigated in section 6.1 and 6.2, tests were conducted at varying operating temperatures and varying feed side pressures. As with the palladium and niobium tests discussed earlier in this chapter, each test was repeated six times with the average value taken. The standard deviation for each data set was calculated to give an assessment of consistency as with each of the other data sets collected.

6.5.1 Experimental Results: Coated V-Ni Membrane with Pure Hydrogen Feed

The measured permeate flux values for the coated V-Ni membranes are plotted in figure 6.19. Tests were conducted at three different feed side pressures (4 bar, 7 bar and 10 bar absolute pressure) over the temperature range 300 to 425 °C. Whilst it was initially planned to investigate temperatures above this it was found that the membranes suffered significant and rapid loss of performance above these temperatures. This has been attributed to the mobility of palladium in the vanadium alloy at increased temperatures by other studies such as (Dolan *et al.*, 2011) and (Zhang *et al.*, 2003).

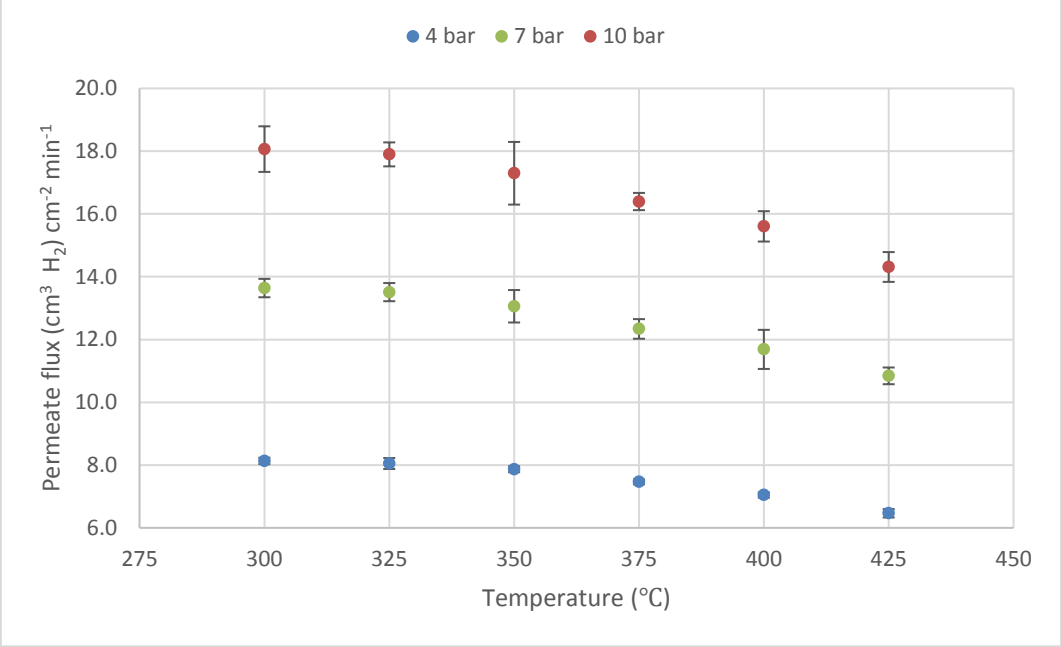

Figure 6.19 – Measured permeate flux for coated V-Ni membrane at various temperatures and pressures with pure hydrogen feed

As figure 6.19 shows the permeate flux decreased with increasing temperature for each pressure investigated. This can be explained by the decreasing hydrogen solubility in the bulk metal with increasing temperature.

The variance between the maximum and the minimum permeate flux values for each pressure investigated is also relatively small, in comparison to the flux changes recorded from tests on niobium and palladium in pure hydrogen. This would be somewhat expected due to the increased thickness reducing the scale of the flux; however, even after taking this into consideration the performance range is very narrow. This behaviour is similar to that detailed in (Dolan, McLennan and Way, 2012); where a 85V-15Ni membrane with a palladium coat was investigated and shown to provide similar behaviour over the temperature range.

A significant difference can be seen in the flux evolved for each feed side pressure, as would be expected. However, even with this difference the general trend appears to be relatively similar.

Included in table 6.14 below is the standard deviation for each set of results collected to give an indication of the consistency of the results gathered.

Table 6.14 – Standard deviation of area flux for the V-Ni membrane tests in pure hydrogen

Standard Deviation ([cm^3 H_2] cm^{-2} min^{-1})			
Temperature (°C)	**4 bar**	**7 bar**	**10 bar**
300	0.10	0.29	0.73
325	0.17	0.29	0.38
350	0.09	0.52	1.00
375	0.08	0.31	0.27
400	0.08	0.62	0.48
425	0.14	0.27	0.47

6.5.2 Experimental Results: Coated V-Ni Membrane with Mixed Feed

Tests with a mixed gas feed were once again undertaken, an absolute feed pressure of 10 bar was utilised for testing (resulting in a 4 bar partial pressure for hydrogen).

Figure 6.20 shows the results of the test undertaken. As with all other membranes each result was collected six times (3 readings, 2 tests).

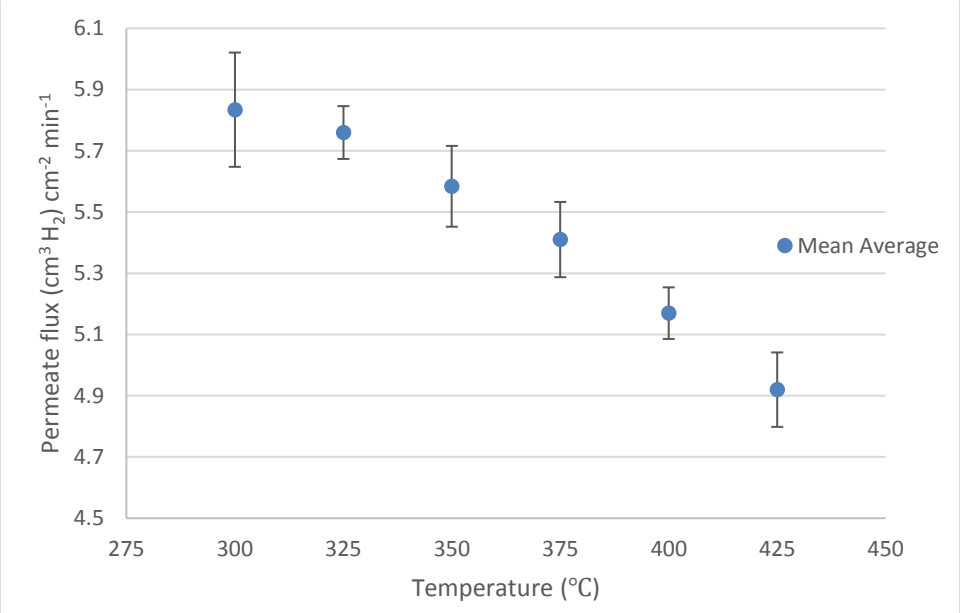

Figure 6.20 - Measured permeate flux for coated V-Ni membrane at various temperatures and pressures with mixed feed

The results show a relationship relatively similar to the pure feed, with direct comparison possible between this result and the pure 4 bar (absolute) pure hydrogen feed shown in figure 6.19.

Upon completion of the variable pressure and temperature tests, a number of runs were conducted on a single V-Ni membrane to test membrane longevity. The conditions used chosen were those that most reflected real operation (mixed gas feed) and those that produced the highest permeate flux (300 °C). As can be seen in figure 6.21 below, the membrane shows stable performance over the course of the three 8-hour tests undertaken. Whilst this is no real indication of long term stability this is a positive result nonetheless.

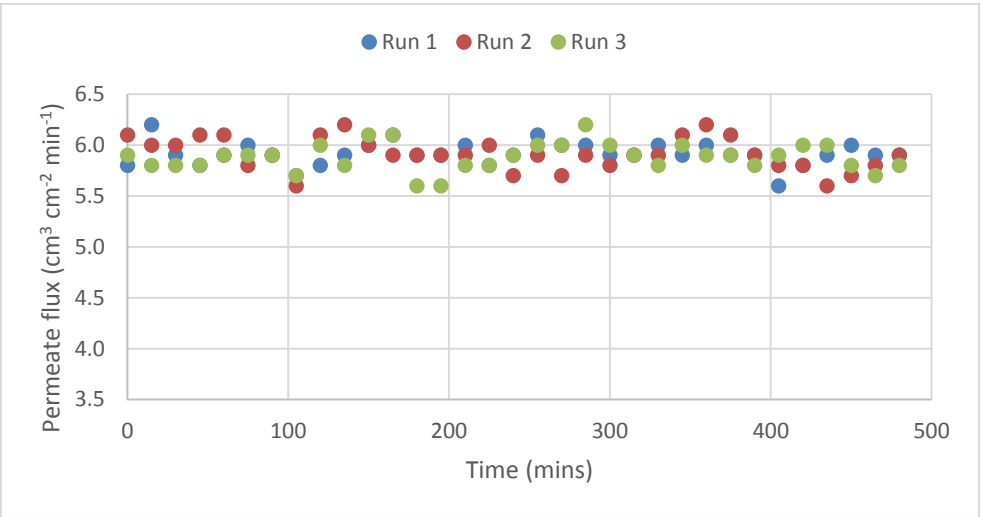

Figure 6.21 - Membrane longevity tests for V-Ni. Tests conducted with the mixed gas feed and with a temperature of 300 °C and a feed-side pressure of 10 bar

During the mixed feed tests permeate samples were taken for analysis to give a measure of hydrogen purity in the permeate. The gas chromatograph results are included in table 6.15 below.

Table 6.15 – Hydrogen permeate purity for V-Ni membrane as measured by the GC

Run	Description	H2 Purity (%)
1	Sample collected during permeate flux test 1	99.9
2	Sample collected during permeate flux test 2	99.9
3	Sample collected during longevity test run 1	99.9
4	Sample collected during longevity test run 3	99.9

As can be seen the permeate purity does not vary throughout any of the tests. This was expected due to the thickness of the membrane; with the gas chromatograph and calibration gas being the factors limiting further accuracy in the measured purity. The thickness of the membrane is sufficient to ensure a higher purity than 99.9% however this cannot be stated in absolute terms due to the mentioned limitations.

6.5.3 Experimental Results: Coated V-Ni-Al Membrane with Pure Hydrogen Feed

The measured permeate flux values for the coated V-Ni-Al is at varying temperatures are shown in figure 6.22 below. Tests were conducted between 300 °C and 400 °C and at 4 bar, 7 bar and 10 bar feed pressure. Tests above this temperature were attempted; however, as with the V-Ni membranes above, problems with mobility of the surface catalyst prevented successful completion.

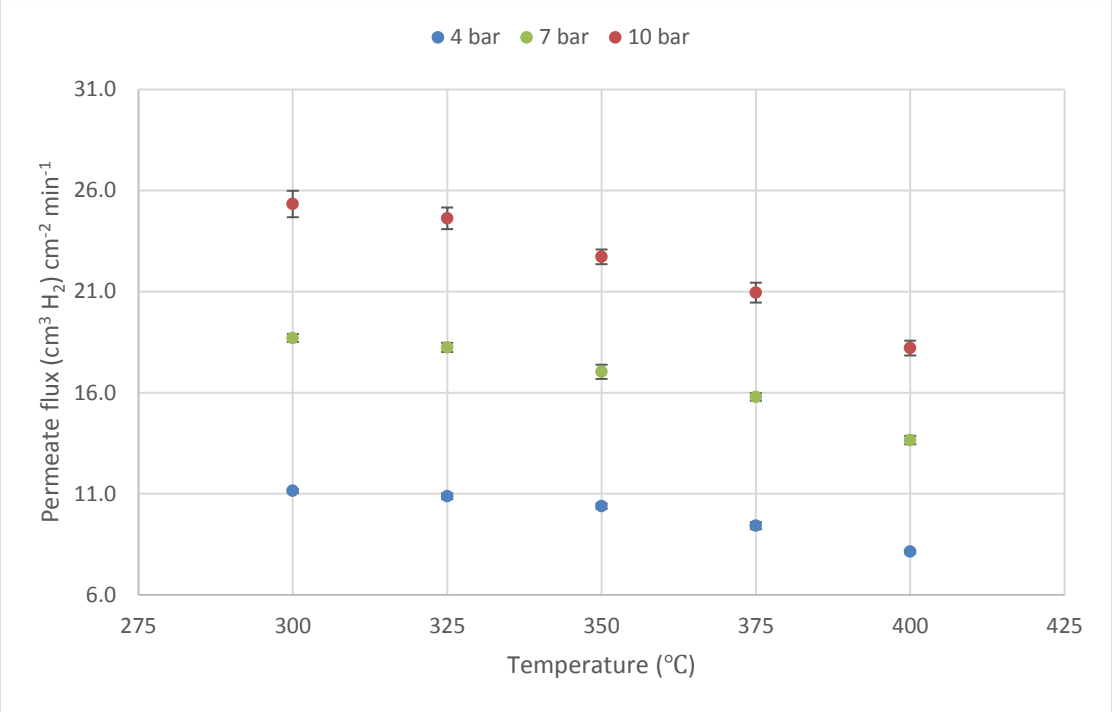

Figure 6.22 - Measured permeate flux for coated V-Ni-Al membrane at various temperatures and pressures with pure hydrogen feed

Figure 6.22 shows that the behaviour of the V-NI-Al membrane is somewhat similar to that of the V-Ni membrane tested above, with the general trend of the results being comparable. It should be noted however that the difference between the maximum and minimum flux achieved at each pressure is greater for the V-Ni-Al membrane. The flux values are also larger suggesting a higher permeability for the membrane, as was expected from reports of tests conducted under dilute conditions in other publications. The higher permeability is attributed to a higher hydrogen solubility in the ternary alloy, as established by (Dolan *et al.*, 2011).

The standard deviation of each set of results is given in table 6.16 below for reference.

Table 6.16 - Standard deviation of area flux for the V-Ni membrane tests in pure hydrogen

Standard Deviation (cm^3 cm^{-2} min^{-1})			
Temp (°C)	4 bar	7 bar	10 bar
300	0.09	0.20	0.65
325	0.14	0.22	0.54
350	0.13	0.35	0.36
375	0.17	0.19	0.49
400	0.08	0.21	0.37

6.5.4 Experimental Results: Coated V-Ni-Al Membrane with Mixed Feed

The final tests to be discussed in this chapter are those collected during the testing of the V-Ni-Al membrane with the mixed gas feed. As with the previous membranes a feed pressure of 10 bar absolute was used, giving a partial pressure of 4 bar hydrogen. The results for the variable temperature test are included in figure 6.23 below.

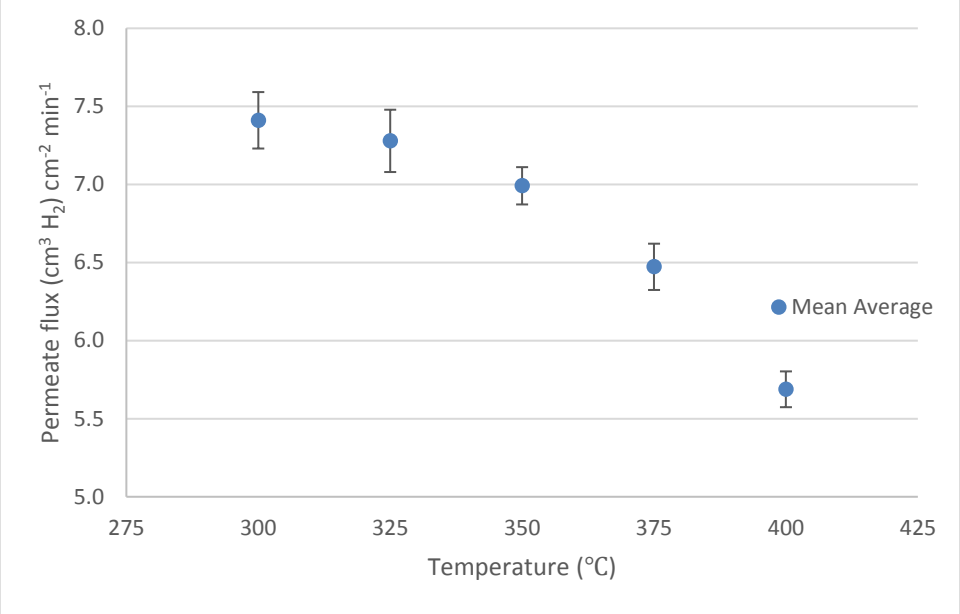

Figure 6.23 - Measured permeate flux for coated V-Ni-Al membrane at various temperatures and pressures with mixed gas feed

The results once again show a higher maximum area flux than the mixed feed test for V-Ni, consistent with the findings for the tests undertaken in the pure hydrogen feed tests. The achieved permeate flux is shown to drop with increasing temperature, as expected.

To be consistent with other membranes tested, a longevity test was performed on a V-Ni-Al membrane. The conditions utilised were the same as used in the test for V-Ni (300 °C, 10 bar absolute feed pressure utilising the mixed feed gas) and were conducted for the same length of time for comparison.

The results of the test can be seen in figure 6.24 below. The graph shows little variation and suggests no deterioration of the membrane for the duration of the tests or in subsequent cycles.

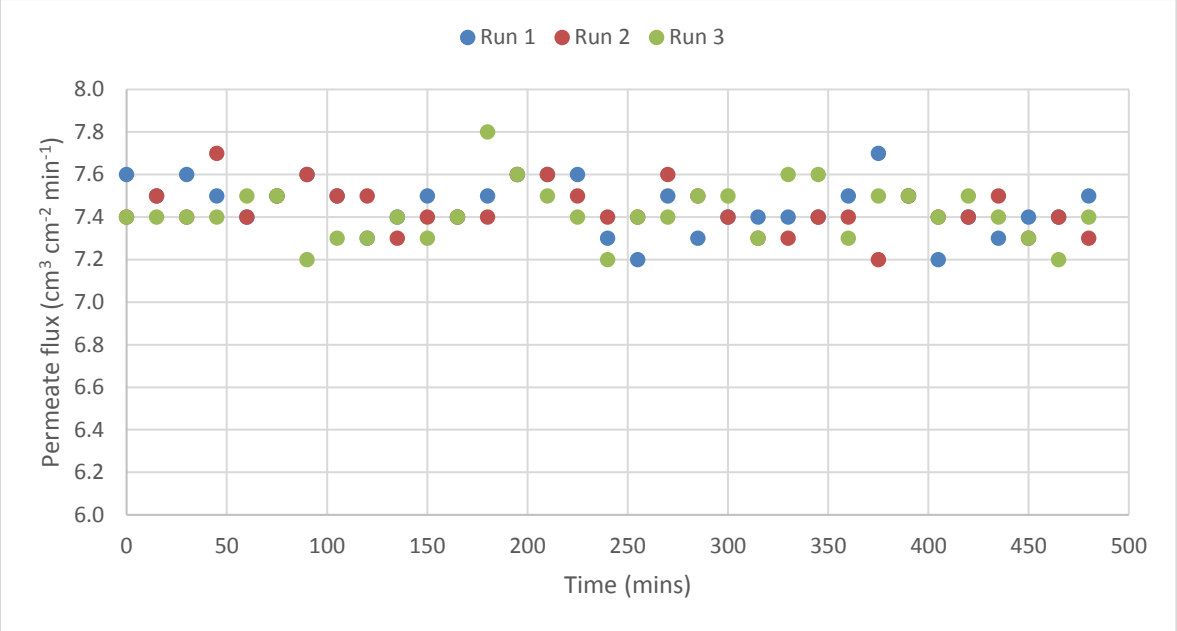

Figure 6.24 - Membrane longevity tests for V-Ni. Tests conducted with the mixed gas feed and with a temperature of 300 °C and a feed-side pressure of 10 bar

Finally, as with all mixed feed tests the gas chromatograph was used to test the permeate hydrogen purity. The test results are included in table 6.17 below.

Table 6.17 – Hydrogen permeate purity for V-Ni permeate as measured by the gas chromatograph

Run	Description	H2 Purity (%)
1	Sample collected during permeate flux test 1	99.9
2	Sample collected during permeate flux test 2	99.9
3	Sample collected during longevity test run 1	99.9
4	Sample collected during longevity test run 3	99.9

Once again, the permeate purity is shown to be 99.9%. The thickness of the membrane is once again cited for this purity due to the difficulty in transportation of carbon and oxygen across the membrane bulk.

6.6 Summary of the Experimental Chapter

Tests were conducted on a range of membranes; with each test repeated six times to allow for reasonable confidence in the consistency of the reported permeation flux figures. Alongside this, tests were run to investigate the permeate purity in mixed H_2/CO_2 feed tests. The membranes tested and the key findings of each are described below:

- **Palladium membranes** were tested to provide two main outcomes. The first was to ensure that the designed enclosure was fit for purpose, with the second being to provide a "yard-stick" with which other membranes tested could be compared.
- **Group V oxidised silver membranes** were tested to investigate the viability of using an oxidised silver coating as a surface catalyst for hydrogen dissociation to promote bulk diffusion. Ultimately the tests showed that the coating is unsuitable due to its instability in the test conditions; with no flow flux established in the required temperature range. Even when flow could be established at lower temperatures the coating proved to be unstable and the permeate flux fell way below the benchmark. The Ag-O coating is not considered to be of practical use and should not be considered for future use on vanadium/niobium alloys at elevated temperatures.
- **Pd-Ag coated niobium membranes** were tested to investigate the substitution of silver into the standard palladium coating to limit palladium usage. Tests found no drop in performance (in terms of permeate flux) for the Pd76 membrane coating in comparison to the pure palladium coating (Pd 100). A significant drop in membrane performance was found when a 55.2Pd-44.8Ag coating was used. The high solubility of hydrogen in niobium makes it unsuitable for use as a membrane, unless alloyed with other metals.
- **V-Ni and V-Ni-Al alloy membranes** were coated with the same "77Pd-23Ag" coating and the permeate flux was investigated. The membranes showed consistent performance over the tests, with V-Ni-Al membranes out-performing V-Ni membranes. The test conditions used in the mixed feed gas tests are unique to this work (as far as the author is aware).
- **All permeate samples collected from mixed feed operation** were analysed using the GC. The lowest measured hydrogen permeate purity was 99.8%. This high hydrogen purity was expected due to the thickness of the membranes limiting the potential for oxygen and carbon transport through the bulk and through the grain boundaries.

6.7 Chapter Six Reference List

Cassar, G., Matthews, A. and Leyland, A. (2012) 'Triode plasma diffusion treatment of titanium alloys', *Surface and Coatings Technology*. Available at: http://www.sciencedirect.com/science/article/pii/S0257897212008754 (Accessed: 7 November 2014).

Dolan, M. D., McLennan, K. G. and Way, J. D. (2012) 'Diffusion of atomic hydrogen through V-Ni alloy membranes under nondilute conditions', *Journal of Physical Chemistry C*, 116(1), pp. 1512–1518. doi: 10.1021/jp208691x.

Dolan, M. D., Song, G., Liang, D., Kellam, M. E., Chandra, D. and Lamb, J. H. (2011) 'Hydrogen transport through V85Ni10M5 alloy membranes', *Journal of Membrane Science*. Elsevier B.V., 373(1–2), pp. 14–19. doi: 10.1016/j.memsci.2011.02.028.

Dunbar, Z. W. (2015) 'Hydrogen purification of synthetic water gas shift gases using microstructured palladium membranes', *Journal of Power Sources*. Elsevier B.V, 297, pp. 525–533. doi: 10.1016/j.jpowsour.2015.08.015.

Garner, W. E. and Reeves, L. W. (1954) 'The thermal decomposition of silver oxide', *Transactions of the Faraday Society*, 50(254), p. 254. doi: 10.1039/tf9545000254.

Hatlevik, Ø., Gade, S. K., Keeling, M. K., Thoen, P. M., Davidson, a. P. and Way, J. D. (2010) 'Palladium and palladium alloy membranes for hydrogen separation and production: History, fabrication strategies, and current performance', *Separation and Purification Technology*, 73(1), pp. 59–64. doi: 10.1016/j.seppur.2009.10.020.

Knapton, A. (1977) 'Palladium alloys for hydrogen diffusion membranes', *Platinum Metals Review Rev*, (6), pp. 44–50. Available at: http://www.platinummetalsreview.com/pdf/pmr-v21-i2-044-050.pdf (Accessed: 5 February 2014).

Mohammad, A. B., Hwa Lim, K., Yudanov, I. V., Neyman, K. M. and R?sch, N. (2007) 'A computational study of H2 dissociation on silver surfaces: The effect of oxygen in the added row structure of Ag(110)', *Physical Chemistry Chemical Physics*, 9(10), p. 1247. doi: 10.1039/b616675j.

Mohammad, A. B., Yudanov, I. V., Lim, K. H., Neyman, K. M. and Rösch, N. (2008) 'Hydrogen activation on silver: A computational study on surface and subsurface oxygen species', *Journal of Physical Chemistry C*, 112(5), pp. 1628–1635. doi: 10.1021/jp0765190.

Serra, E., Kemali, M., Perujo, A. and Ross, D. K. (1998) 'Hydrogen and deuterium in Pd-25 Pct Ag alloy: Permeation, diffusion, solubilization, and surface reaction', *Metallurgical and Materials Transactions A: Physical Metallurgy and Materials Science*, 29(13), pp. 1023–1028. doi: 10.1007/s11661-998-1011-3.

Tsai, Y. C., Lin, C. C., Lin, W. L., Wang, J. H., Chen, S. Y., Lin, P. and Wu, P. W. (2015) 'Palladium based cermet composite for hydrogen separation at elevated temperature', *Journal of Power Sources*. Elsevier B.V, 274, pp. 965–970. doi: 10.1016/j.jpowsour.2014.10.085.

Ward, T. and Dao, T. (1999) 'Model of hydrogen permeation behavior in palladium membranes', *Journal of Membrane Science*, 153(January 1998), pp. 211–231. Available at: http://www.sciencedirect.com/science/article/pii/S0376738898002567 (Accessed: 18 February 2014).

Xu, Y., Greeley, J. and Mavrikakis, M. (2005) ‘Effect of subsurface oxygen on the reactivity of the Ag(111) surface’, *Journal of the American Chemical Society*, 127(37), pp. 12823–12827. doi: 10.1021/ja043727m.

Zhang, Y., Ozaki, T., Komaki, M. and Nishimura, C. (2003) ‘Hydrogen permeation of Pd-Ag alloy coated V-15Ni composite membrane: Effects of overlayer composition’, *Journal of Membrane Science*, 224(1–2), pp. 81–91. doi: 10.1016/j.memsci.2003.07.005.

7 Analysis and Discussion of Results

The preceding chapters have covered in detail both the modelling of selected membranes (chapter five) and experimental testing (chapter six) of membranes under a variety of conditions. This chapter is included to provide further analysis of those results alongside comparison of these results to those reported in similar studies.

7.1 Membrane Performance Targets

Before analysing and discussing the results collected in chapter six it is worthwhile revisiting the prior mentioned US DoE targets for membrane utilisation. As these targets provide some useful guidance for membrane performance and cost it is useful to include the figures of most interest again here (the values have been converted to SI units for ease of interpretation).

- **Desired minimum flux**: 0.025 m^3 m^{-2} s^{-1} (standard cubic metres)
- **Desired operating temperature**: 250 to 440 °C
- **Desired hydrogen purity**: 99.99%
- **Desired operating pressure**: 55 to 69 bar
- **Desired cost:** < \$2700 m^{-2}
- **Desired lifespan:** > 5 years

The minimum flux can be converted to a molar flux, utilising a temperature of 21 °C (as the original figure is given in scf and NIST state that this is given at this temperature), 1 mole of gas occupies 24.1 L. Converting from volume to moles gives a final figure of:

- 1.05 mol m^{-2} s^{-1} for the **desired permeate molar flux.**

Comparing the above figures with the collected results yields some immediate conclusions. The first is that the permeate purity figures established through GC testing are not accurate to give an idea on whether the membranes met the target, although the maximum purity achieved of 99.9% is adequate to 3 significant figures.

The membranes of most interest operated within the desired temperature range of 300 to 400 °C with no problems, however temperatures above this were not particularly viable due to the catalytic coating.

The desired pressures could not be tested at, as such the behaviour of the membranes under these conditions remains uncertain.

Comparisons to desired flux are best made in the relevant section of the discussion below; and comparisons of costs will be discussed (albeit briefly) in a later section.

7.2 Calculating Membrane Permeability and Other Comparable Figures

7.2.1 Introduction to the Metrics used in this Chapter

Whilst in the last chapter a large number of experimental results are supplied, these numbers alone offer little insight into membrane behaviour and more importantly, performance. As membranes were tested under a number of conditions it is difficult to compare raw permeate flux data and as such a more suitable, general metric is needed for comparison. In this instance two such metrics are of interest:

- **Membrane permeability**: This is the established method for comparison and can provide more insight into the individual components of the permeability too (solubility and diffusivity).
- **Thickness independent flux:** A second comparative metric used in this thesis is the thickness independent flux, which is calculated by multiplying the permeate flux by the thickness of the membrane. This is routinely reported in several publications and is of particular use for membranes tested under similar pressure and temperature conditions, but with different thicknesses (as has been done in chapter six).

One final note should be made in this section that all permeate flux values in the previous chapter are reported with the units $cm^3\ cm^{-2}\ min^{-1}$, for calculation of the permeability the molar flux rate is required, with units [mol H_2] $m^{-2}\ s^{-1}$. This does require some computation, with a need to convert the volume data collected to an equivalent amount of moles. Such a conversion is considered relatively trivial and so the computation is not repeated *ad nauseam* here but the method is stated. By measuring the temperature of the gas permeate, an equivalent volume for one mole can be calculated using the ideal gas law with a compressibility factor included for hydrogen (in this case Z = 1.0006). During testing the permeate flux temperature was recorded and efforts were made to cool the gas before measuring the volume in hope of gaining a more consistent outlet temperature and to prevent damaging the sample collection bags. By recording the permeate temperature at the point of measurement and assuming a constant atmospheric pressure of 101.3 kPa a volume equivalent for 1 mole of gaseous hydrogen permeate can be calculated using the ideal gas law. This volume can then be used to calculate the equivalent molar flow rate. An example is included below:

- Pd membrane, pure hydrogen feed (10 bar), 300 °C, volume: 9.4 $cm^3\ cm^{-2}\ min^{-1}$
- Temperature of permeate at measuring point: 26 °C
- Volume of 1 mole of permeate at the recorded temperature: 24.53 L mol^{-1}
- **Calculated molar flux of permeate (SI units): 9.4 / (60 x 2.45) = 6.18 x10^{-2} mol $m^{-2}\ s^{-1}$**

The factor 2.45 is changeable dependent on temperature with this incorporating the volume to molar conversion described. To allow for comparison with other measured values, the thickness independent flux is typically reported with the units [mol H_2] m^{-1} s^{-1}, where the permeate flux calculated above is multiplied by the thickness of the membrane.

7.2.2 Calculation of Membrane Permeability

As has been shown earlier in this thesis, permeability can be calculated using the equation:

$$J = \phi \frac{P_u^n - P_d^n}{t} \qquad \text{(Equation 5.1)}$$

Where the typical value for *n* is assumed to be 0.5 and the permeability, ϕ, is frequently given as a function of diffusivity (D) and the (Sievert) solubility (K_s). This leads to reporting permeability with units of mol m^{-1} s^{-1} $Pa^{-0.5}$. Utilisation of these parameters is widespread, even in conditions where the Sieverts law is known to falter for the reporting of the permeability of a membrane. As such, this will be used frequently throughout this chapter when determining the permeability of each membrane as it allows for simple comparison to literature sources.

Calculation of the permeability from the collected data is simple and as with the volume to permeate flux the methodology will be described here to remove the need to include trivial conversions repeatedly. Equation 5.1 can be re-arranged to give:

$$\phi = \frac{J}{\left(\frac{P_u^n - P_d^n}{t}\right)}$$

Assuming that *n* is 0.5, all of the information required to calculate permeability has been gathered throughout these tests. Extending the example in the prior section gives:

- Molar flux for test conditions = 6.18 $x10^{-2}$ mol m^{-2} s^{-1}
- Pressure up-stream = 10 bar; $P_u^{0.5}$ = 1000 $Pa^{0.5}$
- Pressure down-stream = 1.03 bar; $P_d^{0.5}$ = 318 $Pa^{0.5}$
- Membrane thickness = 1 x 10^{-4} m
- **Calculated permeability (SI units) = 9.07 x 10^{-9} mol m^{-1} s^{-1} $Pa^{-0.5}$**

For the calculation of the permeability in mixed gas feed tests only the partial pressure of hydrogen is of concern.

7.3 Discussion of Palladium Permeability Tests

There exists a large amount of data on the permeability of hydrogen through palladium. Tests have been conducted under many conditions, which provides a wealth of data for comparison to the data collected as part of this thesis.

As has been discussed previously, palladium is not suitable for use as a bulk membrane and as such the discussion in this section will be brief.

7.3.1 Calculating the Hydrogen Permeability of the Palladium Membrane (Pure H_2 Feed)

Figure 7.1 below shows the calculated permeability figures for the palladium membrane at various temperatures with a feed side pressure of 10 bar hydrogen absolute.

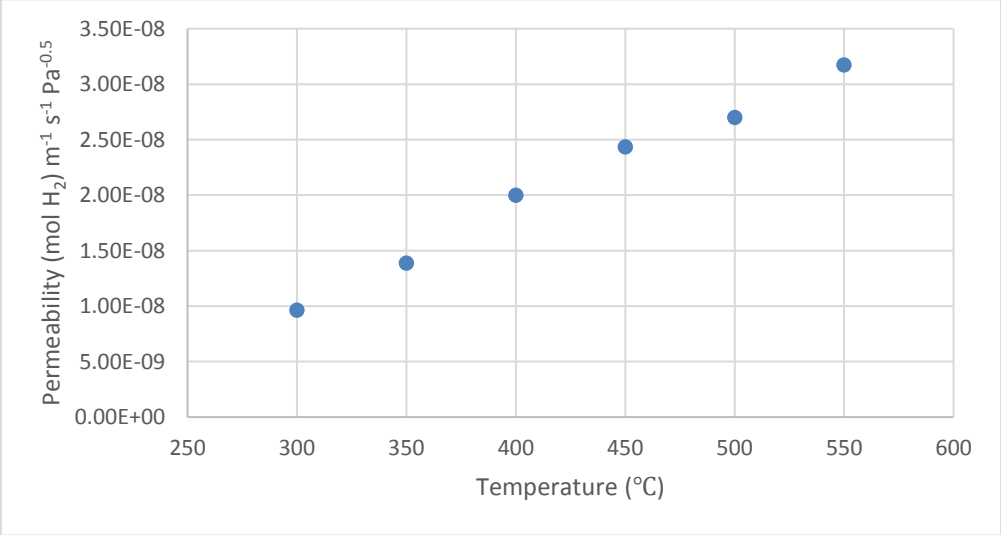

Figure number 7.1 – Calculated permeability for Pd membrane at 10 bar feed pressure and various temperatures

As can be seen the permeability increases as temperature increases, with the relationship appearing to show a relatively good agreement with a first order linear relationship. An increasing permeability with increasing temperature is hardly a surprise as it is well known that the diffusivity and solubility of hydrogen in palladium increases with increasing temperature.

Many literature values can be found for the permeability of palladium at various temperatures. (Morreale *et al.*, 2003) provides a collection of published permeabilities from various sources, including their own tests. Whilst much of this data concerns hydrogen in dilute conditions or low pressures, the data of Morreale et al was collected at high temperatures and hydrogen feed side

pressures of up to 2480 kPa. With such high feed side pressures, the data here is of great interest as it should make for a useful comparison. The publication provides an Arrhenius relationship for the permeability data collected; with the pre-exponential factor being stated as 3.31 x10^{-7} mol m^{-1} s^{-1} $Pa^{-0.5}$ with an activation energy of 13.81 kJ mol^{-1}. This data can be used to graph the permeability observed by Morreale et al, which can then be compared to the results of the tests undertaken here.

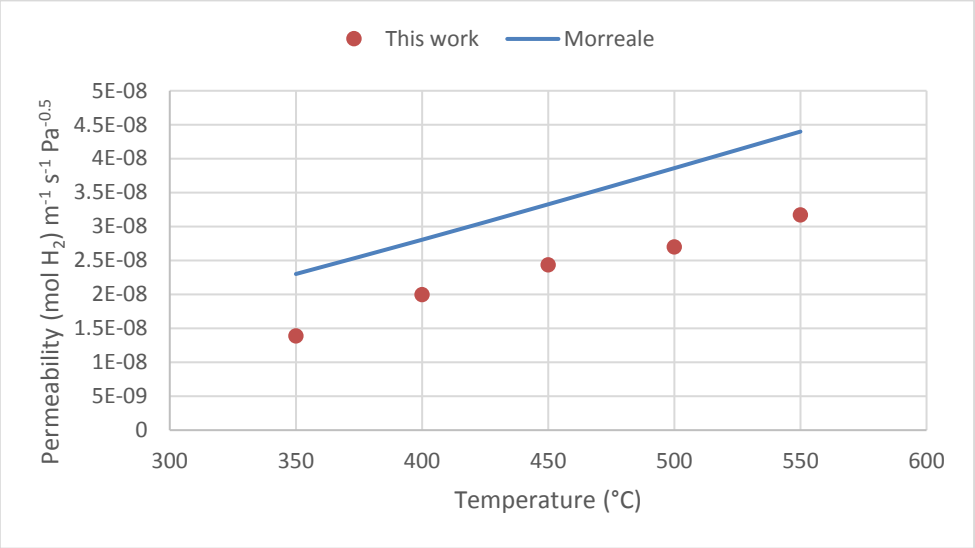

Figure 7.2 – Reported permeability data from (Morreale *et al.*, 2003), compared against data collected in this test

As can be seen in Figure 7.2 the trend is similar, however the values from the Morreale test are larger. This could be due to the higher test pressures used by Morreale.

As stated above, Morreale et al also provide data on other studies, with typical permeability values in the temperature range of interest being reported in the range of 1 x 10^{-8} to 4 x^{-8} mol m^{-1} s^{-1} $Pa^{-0.5}$. Similar values can be found in membrane technology review papers such as (Ockwig and Nenoff, 2007). Comparing the values calculated here to those presented elsewhere would suggest that the results are somewhat reliable as they are of the same order of magnitude as those reported previously.

As palladium is known to deviate from ideal Sievert behaviour at higher hydrogen concentrations, it was decided to investigate how the permeability changes with pressure. Chapter six presented results for variable feed side pressure tests. The results of the test can be found in figure 6.19, where the relationship between the feed side pressure and the flux is shown to be near linear. From the data presented the permeability at each feed side pressure was calculated, with the results given in figure 7.3 below.

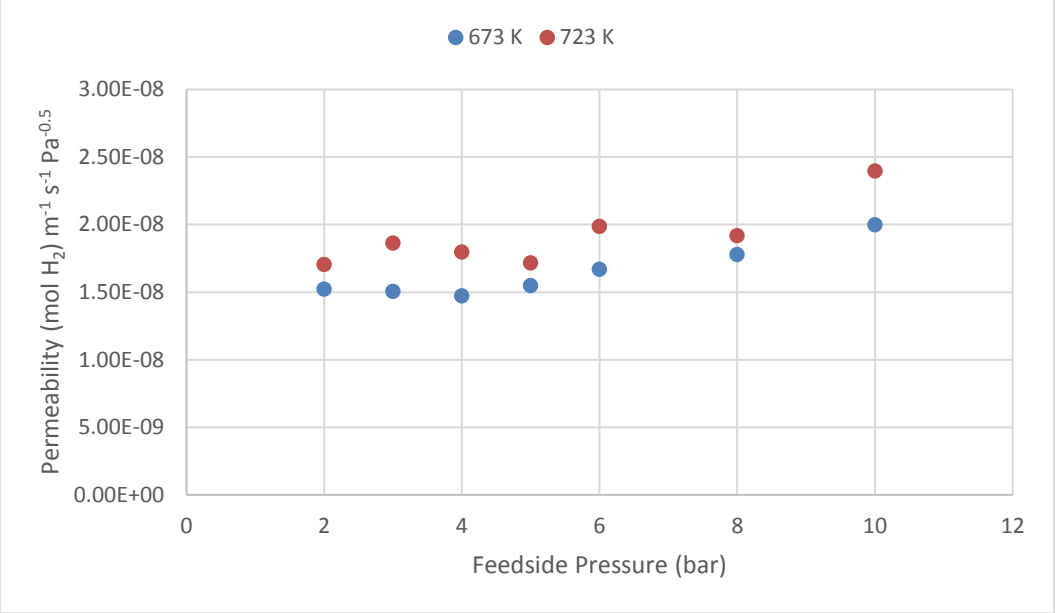

Figure 7.3 – Calculated permeability data for Pd membrane in pure hydrogen feed with varying feed side pressure

If Sievert's law is followed, then no there should be no changes to the permeability with changing feed pressure (as the downstream pressure is kept constant, changing the feed pressure changes the ΔP term). Figure 7.3 shows that this is not the case and that for both temperatures investigated the permeability begins to deviate above 6 bar. Such results suggest that the model studied in chapter five and three has significant limitations under non-dilute conditions for palladium.

7.3.2 Calculating the Hydrogen Permeability of the Palladium Membrane (Mixed Feed)

The calculated permeabilities for the palladium membrane with the mixed gas feed at various temperatures are given in figure 7.4 below.

The figure shows that the permeability for the mixed feed is lower under equivalent conditions for the pure feed. This is hardly surprising due to the presence of carbon dioxide, which will also adsorb to the surface and block hydrogen doing so, alongside causing mass transfer issues when hydrogen is depleted from the gas near to the surface.

Form the two data sets (pure H_2 and mixed H_2/CO_2 gas feed) a comparison can be drawn between a few equivalent data points, as shown in table 7.1.

Figure 7.4 also shows a different relationship between temperature and permeability compared to that for the pure feed. Whereas the pure feed shows a more linear relationship, the mixed feed shows

a greater increase in permeability for higher temperatures. This is unlikely to be a bulk diffusion effect, with the trend likely to be a product of the surface interactions of hydrogen and carbon dioxide.

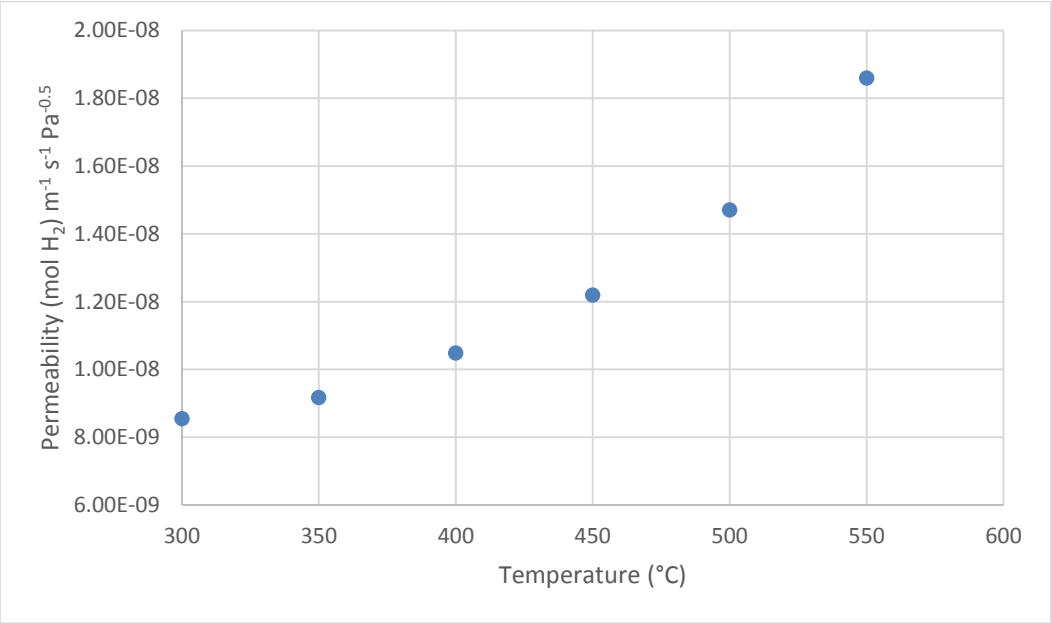

Figure 7.4 – Graph of calculated permeability for Pd membrane with mixed feed gas (10 bar feed pressure, 40% vol. hydrogen)

Table 7.1 – Table showing change in permeability for comparable conditions

Permeability (mol H_2) m^{-1} s^{-1} $Pa^{-0.5}$			
Temperature (°C)	**Pure H_2 feed**	**Mixed feed**	**Loss (%)**
400	1.47E-08	1.05E-08	28.8
450	1.80E-08	1.22E-08	32.1

The loss of permeability even at relatively low flux rates is significant. This is certainly problematic for any real world application where hydrogen will need to be separated from a multitude of gases. A number of factors are likely to impact the loss percentage, some of which it may be possible to mitigate; these factors are discussed later in this chapter.

7.4 Discussion of Niobium Permeability Tests

The tests conducted on the niobium membranes were done purely to investigate the impact of different catalytic coatings on the permeate flux, as such the variation of data collected was relatively minimal in comparison to that collected for the vanadium alloys.

The Ag-O coatings failed to produce any notable results and as such are not discussed in great detail here. As stated in the previous chapter, little hope is given for such a coating for future use particularly at elevated temperatures. This section will instead focus on the membranes that did produce some notable results. An interesting comparison can be made between the effectiveness of the coatings, with the PVD coating shown in figure 7.5B below shown to be a lot more uniform than the electroless Pd-Ag coating in 7.5A.

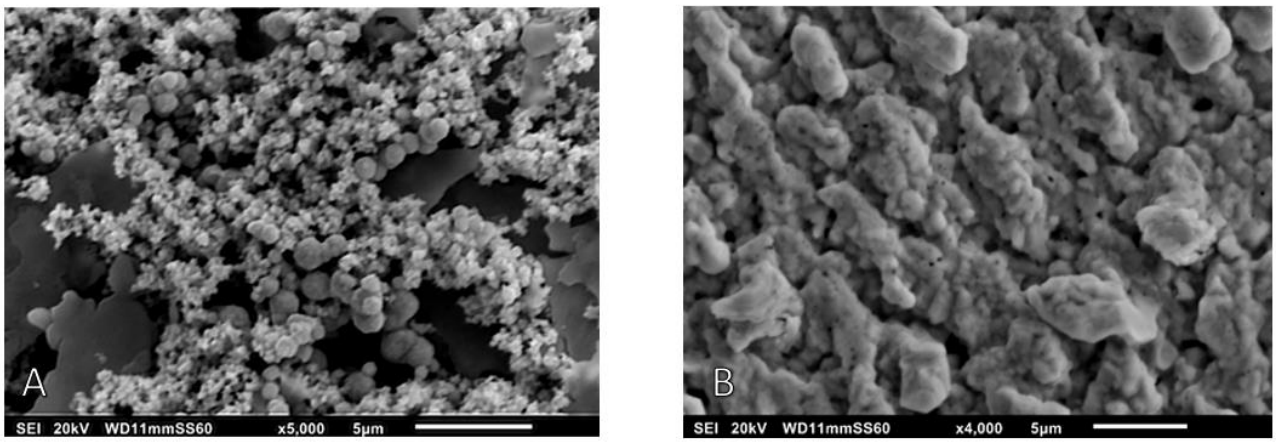

Figure 7.5 – SEM images of electroless plated Pd-Ag coating (A) and PVD silver coating (B)

The electroless plating sample is shown to have significant deficiencies (an area close to the edge of the membrane is inspected here) which suggests that the electroplating method needs to be refined. The PVD coating is shown to be significantly more uniform, co-deposition of silver and palladium for future tests via PVD may yield improved results.

7.4.1 Calculating the Hydrogen Permeability of the Niobium Membrane (Pure H_2 Feed)

Figure 7.6 below shows the calculated permeabilities of the Pd 100 and Pd 76 coated membranes. The results are shown to be near identical under all tested conditions, as would be expected from the flux data collected.

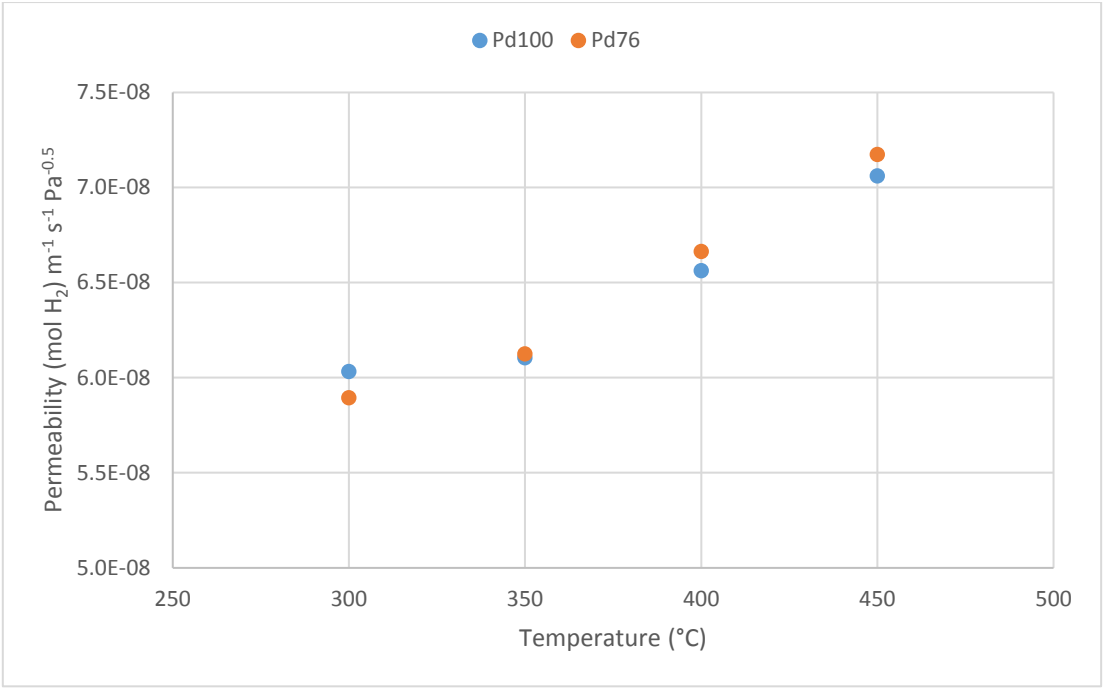

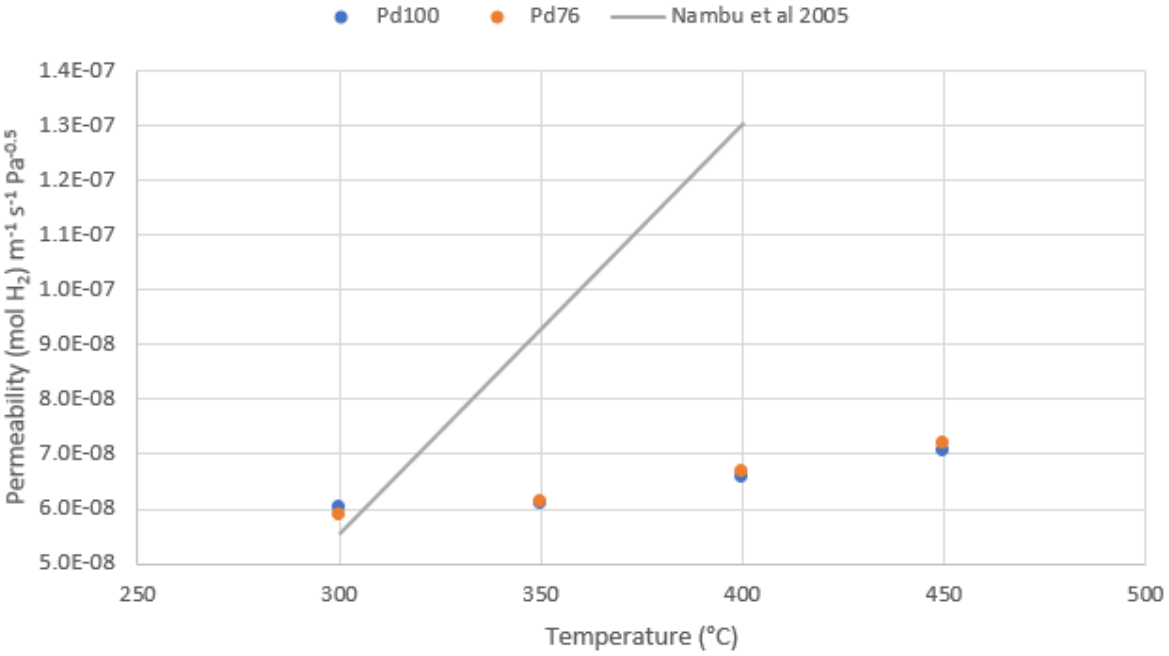

Figure 7.6 – Graphs of calculated permeability for the PdAg coated Nb membranes (H_2 feed)

Little data is available for direct comparison of the permeability of niobium under the conditions tested, however one example can be found in (Nambu *et al.*, 2005). In (Nambu *et al.*, 2005) hydrogen permeation is investigated through a niobium membrane, over the temperature range 200 °C to 400 °C at a pressure differential of 2 bar. The data is presented graphically in (Nambu *et al.*, 2005) and so only an approximate estimation can be made, with an approximate permeability of 5.5 x 10^{-8} (mol H_2) m^{-1} s^{-1} $Pa^{-0.5}$ at 300 °C and a maximum permeability of 1.3 x 10^{-7} (mol H_2) m^{-1} s^{-1} $Pa^{-0.5}$ at 400°C.

The lower end of these numbers are comparable to those given here, however there is some deviation between the permeability at the upper range. This deviation may be explained through damage to the coating or the membrane itself reducing permeability of the niobium membrane tested here. A similar trend is established in both (Nambu *et al.*, 2005) and the results of this work, with the permeability increasing exponentially as temperature increases.

7.4.2 Calculating the Hydrogen Permeability of the Niobium Membrane (Mixed gas feed)

As with the pure feed, the permeability of niobium was calculated for the mixed gas feed, the results of this can be seen in figure 7.7 below.

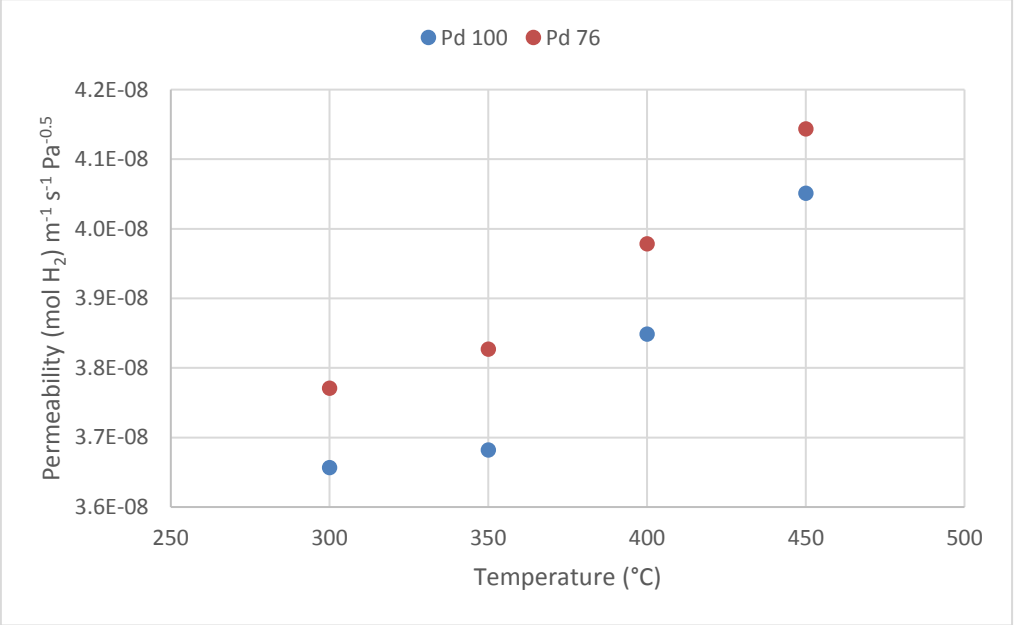

Figure 7.7 - Graph of calculated permeability for the PdAg coated Nb membranes (mixed feed)

As would be expected the permeability is lower for the mixed feed tests, the overall permeability is lowered by the presence of carbon dioxide through a combination of competitive surface adsorption and through the depletion of hydrogen in the near surface gas phase.

A comparison of the permeability for the Pd76 coated membrane is made in figure 7.8 below.

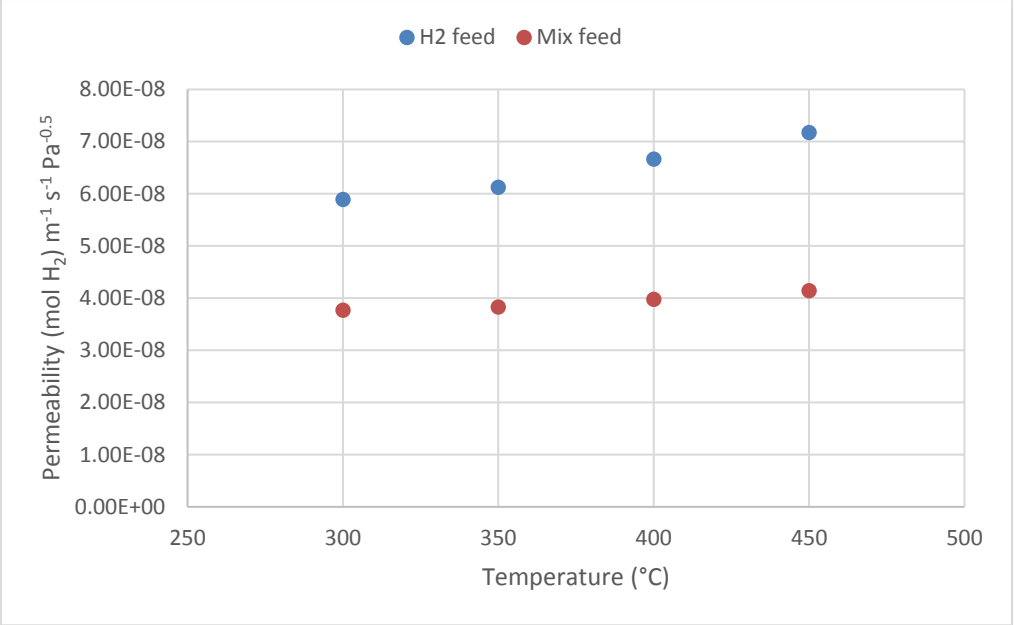

Figure 7.8 - Graph of calculated permeability for the PdAg coated Nb membranes under differing feed conditions

The amount of permeability "lost" over the temperature range investigated increases as the temperature (and flux) increases. At 300 °C, the mixed feed gas has a calculated permeability of 3.8 x 10^{-8} (mol H_2) m^{-1} s^{-1} $Pa^{-0.5}$ equal to 64% of the permeability for the pure hydrogen feed, calculated to be 5.9 x 10^{-8} (mol H_2) m^{-1} s^{-1} $Pa^{-0.5}$. At 450 °C, the percentage of the total drops to 58% - with the permeability for the mixed feed calculated to be 4.1 x 10^{-8} (mol H_2) m^{-1} s^{-1} $Pa^{-0.5}$ and the permeability of the pure hydrogen feed calculated to be 7.2 x 10^{-8} (mol H_2) m^{-1} s^{-1} $Pa^{-0.5}$. This is likely to be due to depletion of hydrogen in the gas phase near the membrane surface, hence why the loss of permeability is greater when the flux is greater.

Comparisons with literature data are again scarce. (Buxbaum and Marker, 1993) provided data for niobium permeability at a similar temperature (425 °C) with a total ΔP of 2.75 bar; with a mixed gas feed consisting of 73% hydrogen in methane (giving a ΔP of approximately 2 bar), the average permeability measured was 3.27 x 10^{-7} (mol H_2) m^{-1} s^{-1} $Pa^{-0.5}$. It is interesting to see that this value is larger than the value given by (Nambu *et al.*, 2005), recorded at a slightly lower temperature but with a pure hydrogen feed. As (Buxbaum and Marker, 1993) provide no data for tests in pure hydrogen, a comparison of the permeability loss is not possible although it is stated that the membrane has a lower permeability than the niobium substrate due to "transport resistance in the palladium, in the interfaces, and in the gas-phase".

Once again, the hydrogen permeability reported in the literature is significantly higher than the results gathered here at a similar hydrogen pressure differential and temperature. As stated before this could be attributed to issues with the surface catalytic coating (poor hydrogen transport to the bulk).

However, it should also be noted that Buxbaum uses a significantly higher hydrogen concentration (Buxbaum used a concentration of 73% H_2, compared to a 40% H_2 concentration used in this work), with this likely to lead to less of a loss of permeability through competitive adsorption. The impact of utilising CH_4 as a diluent instead of CO_2 may also have an impact, dependent on their interactions with the Pd/PdAg surface.

7.4.3 General Comments on Calculated Niobium Permeability

There are two noteworthy points that can be drawn from the permeability data presented above, and also the permeability data given by Buxbaum et al and Nambu et al.

The first relates to the scalar element of niobium permeability, namely that at the temperatures investigated in this work and by others the permeability is significantly lower than that predicted by studies where the dilute-hydrogen system diffusivity and solubility are considered.

Secondly, from the permeability data calculated above, it can be seen that the general trend of the hydrogen permeability increases as temperature increases. This trend is also established by Nambu et al; however his data is again somewhat different to that provided through tests on niobium under dilute conditions, where the permeability is shown to decrease.

(Zhang *et al.*, 2008) have also investigated such behaviour previously, where they concluded that not only does hydrogen solubility in the metal differ from Sievert behaviour (as is expected at any significant hydrogen partial pressure) but that the diffusion coefficient for hydrogen in niobium is smaller than the values reported from the dilute hydrogen solid solution tests.

This ultimately leads to the belief that the diffusion coefficient of niobium is not only just temperature dependent but also concentration dependent. Such a conclusion is well established for conditions in which hydrogen is highly soluble in metal (with the exact conditions being material and test condition dependent [i.e. temperature and hydrogen partial pressure]). (Zhang *et al.*, 2008) predicted a diffusion coefficient of approximately 2.95 $x10^{-9}$ (mol H_2) m^{-1} s^{-1} $Pa^{-0.5}$ at 500 °C, which is an order of magnitude lower than those reported through previous studies measured using the Gorsky effect (studies such as the aforementioned Voeckl 1972 paper); where the diffusion coefficient at 500 °C is estimated at 1.04 x 10^{-8} (mol H_2) m^{-1} s^{-1} $Pa^{-0.5}$.

This lower than expected diffusion coefficient and increasing permeability suggests that the hydrogen solubility in niobium must be significantly higher than expected. This raises some concerns about niobium's potential for use as a membrane material. A high hydrogen solubility is generally seen as a

poor quality for a membrane to possess due to the increased susceptibility to damage. If the diffusion coefficient is indeed significantly lower than the values reported from studies of the Gorsky-effect on dilute hydrogen systems, then the attractiveness of niobium as a potential membrane material certainly decreases. (Zhang *et al.*, 2008) reports that the diffusion coefficient of a Pd-Ag membrane is higher than that of pure niobium, albeit with significantly decreased hydrogen solubility. Such a result is surprising due to the different crystal structures of the materials, and raise doubts over its suitability for use.

As has been discussed in chapter two, niobium alloys have been tested by other groups. Typically, the formation of these alloys suppresses the hydrogen permeability of the group V metal, with this being the case for niobium also. For example, in chapter two a study on niobium alloyed with nickel and titanium is discussed; (Kishida *et al.*, 2008) found that the maximum permeability at 400 °C was approximately 2 $x10^{-8}$ mol m^{-1} s^{-1} $Pa^{-1/2}$. This value is significantly lower than the permeability found during this work at the same temperature, and when compared to the figures of Nambu et al and Buxbaum et al the permeability is found to be a factor of 10 smaller. This doesn't even account for the even higher permeabilities predicted by the Gorsky-effect studies mentioned above. Such a drop off in permeability may be explained by the lower than expected diffusivity of niobium.

This does not mean there is no hope for future niobium alloys, as mentioned briefly in chapter two amorphous niobium containing alloys have been found to perform well (in the limited studies that have taken place).

It should also be noted that many tests of the permeability of niobium have been undertaken using electro-chemical methods for the delivery of hydrogen, in such a test it would not be unreasonable to expect lower resistance to hydrogen transport (particularly at the surface, as dissolved hydrogen should behave in a similar fashion). With lower resistance to transport a higher permeability could be achieved, ultimately resulting in a higher permeability.

7.5 Discussion of Vanadium-Nickel Alloy Permeability Tests

Figure 7.9 shows the surface of the V-Ni membrane before and after coating.

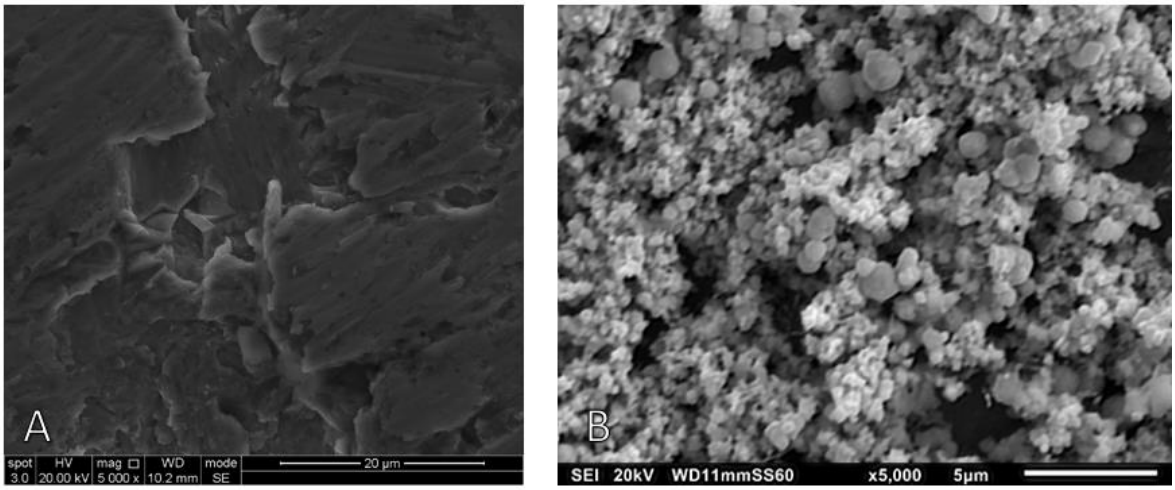

Figure 7.9 – SEM images of V-Ni membrane prior to coating (A) and after coating (B)

It is predicted from the image that the real surface area per m^2 should be higher for the coated membrane.

7.5.1 Calculating the Hydrogen Permeability of the V-Ni Membrane (Pure H_2 Feed)

Figure 7.10 below shows the calculated permeability values for the V-Ni membrane under pure hydrogen feed conditions at varying upstream pressures.

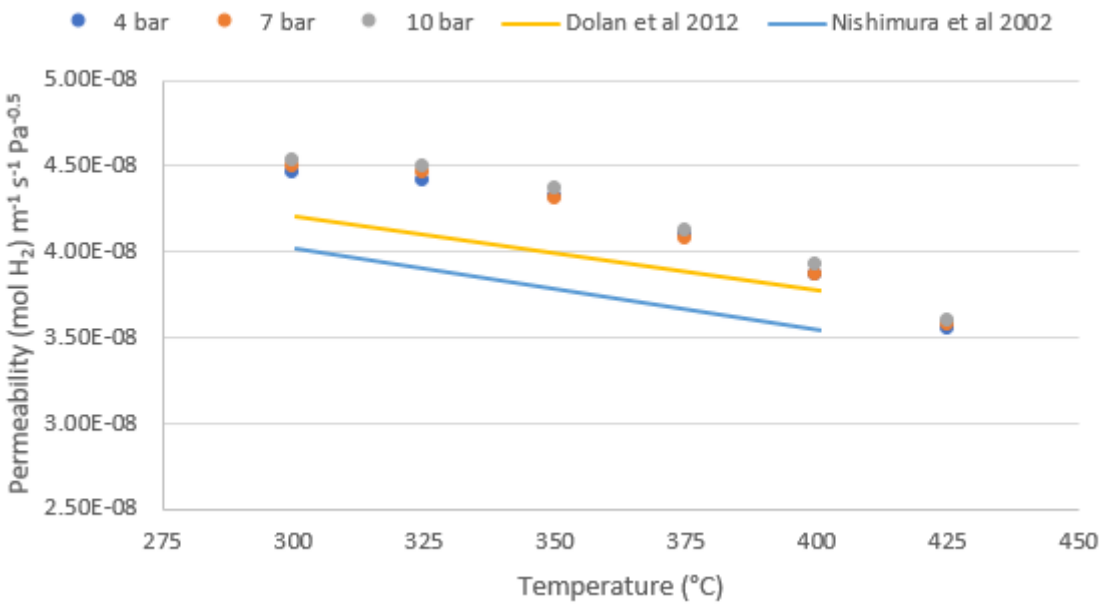

Figure 7.10 – Graphs showing calculated permeability for coated V-Ni membrane at various temperatures and pressures (pure H_2 feed)

The figure shows a decrease in permeability with increasing temperature, the most significant decrease being between 400 and 425 °C. The change in permeability between 400 and 425 °C is around 50% of the total for the change in permeability between 300 and 400 °C. This decrease may not be a function of the bulk permeability of the membrane, but of the surface.

As stated in chapter six, other sources have cited increased mobility of palladium in vanadium at temperatures above 400 °C, with this mobility forming a V-Pd alloy that drastically reduces hydrogen permeability (Dolan *et al.*, 2011). It should be noted however that other publications, such as (Alimov *et al.*, 2015) exist in which V-Pd alloys have been utilised as membranes themselves at similar temperatures. The bulk alloy may form a different phase with a different composition, but the potential for contradiction between the two schools of thought is something that should be investigated further.

A comparison of the permeability data presented above can be made against other sources. (Dolan, McLennan and Way, 2012) discusses the testing of various palladium coated V-Ni alloys under non-dilute hydrogen conditions. One of these alloys is an 85V-15Ni membrane comparable to those used in this investigation over a similar temperature range and a wide range of pressures.

The permeability of the 85V-15Ni membrane in Dolan et al is presented graphically and as such only approximate values can be drawn from the data; with such an estimation made more difficult by the large scale used in the figure (on the same graph Dolan et al publish permeability data that is a near

factor 10 greater, compressing the scale). The permeability for the 85V-15Ni membrane is found to be relatively consistent over all temperatures and pressure differentials investigated by (Dolan, McLennan and Way, 2012), with an approximate range of 3.7 to 4.2 x 10^{-8} mol m^{-1} s^{-1} $Pa^{-1/2}$, this data has been plotted on figure 7.11 for comparison. These figures show relatively good agreement with the data collected experimentally in this work, albeit with the data collected as part of this project producing a wider spread of permeabilities.

(Nishimura *et al.*, 2002) also provide permeability data, albeit at significantly lower operational pressures (0.8 bar feed pressure); with permeability figures in the range of 2 to 4 x10^{-8} mol m^{-1} s^{-1} $Pa^{-1/2}$. A final comparison can be made to (Hulme *et al.*, 2011), where a Pd-Ag coated 85V-15Ni membrane is tested with an inlet pressure of 1 bar and a vacuum is held on the permeate side. Hulme et al provides data at 200 °C, 300 °C and 400 °C with the latter two being of interest, with the permeability of both estimated to be in the range of 2.3 to 2.5 x10^{-8} mol m^{-1} s^{-1} $Pa^{-1/2}$ for a pure hydrogen feed.

As with the palladium tests, plots can be drawn to show the variation of the calculated permeability with not just temperature but also pressure. Such a plot has been included in figure 7.11 below.

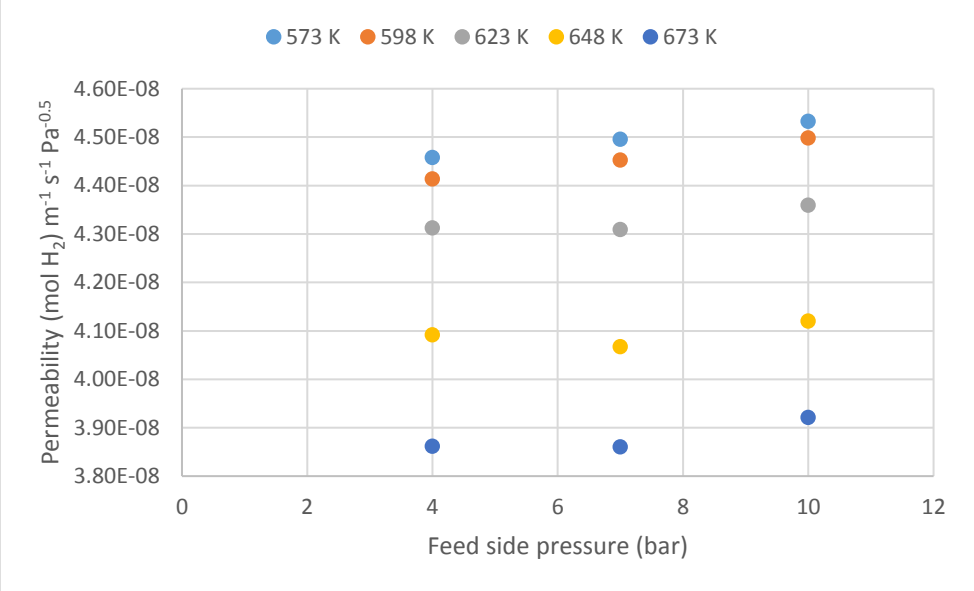

Figure 7.11 – Calculated permeability values for coated V-NI membranes at varying pressure

The figure suggests some variation with pressure, although the relative change is very small, even at 10 bar. As each data set begins to trend upwards at 10 bar, it is likely that at pressure above this Sieverts law does not hold. The model constructed in chapter 5.4.2 assumes that Sieverts law holds up until 10 bar pressure, and the figure above shows that this is arguably the limit for such an assumption. Beyond this, as was found with the palladium membrane, an alternative method for modelling the bulk diffusion must be utilised. The method of (Caravella, Barbieri and Drioli, 2008)

discussed in chapter three which incorporates chemical potential is likely to be a good choice. Future tests on V-Ni membranes with greater feed side pressures are needed to confirm whether or not pressures above 10 bar do result in deviation from ideal behaviour.

The flux data collected can also be compared to the model predicted flux and has been so in figure 7.12 below.

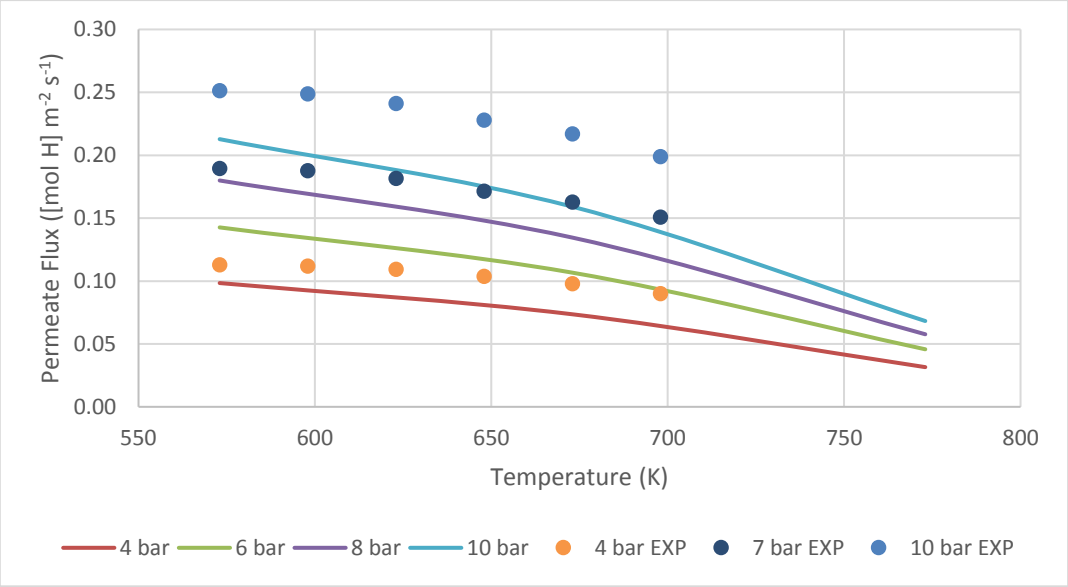

Figure 7.12 – Comparison of the model data and experimental data for V-Ni membrane (pure H_2 feed)

Figure 7.12 suggests that the model underestimates the evolved flux, when compared against the experimental values. If the membrane is bulk diffusion limited, this would suggest that the diffusion coefficient used in the model is potentially too small. Future work should include refining this value to fit the experimental data collected.

7.5.2 Calculating the Hydrogen Permeability of the V-Ni Membrane (Mixed Feed)

The calculated permeability of the V-Ni membrane tested under mixed gas conditions can be seen in figure 7.13 below.

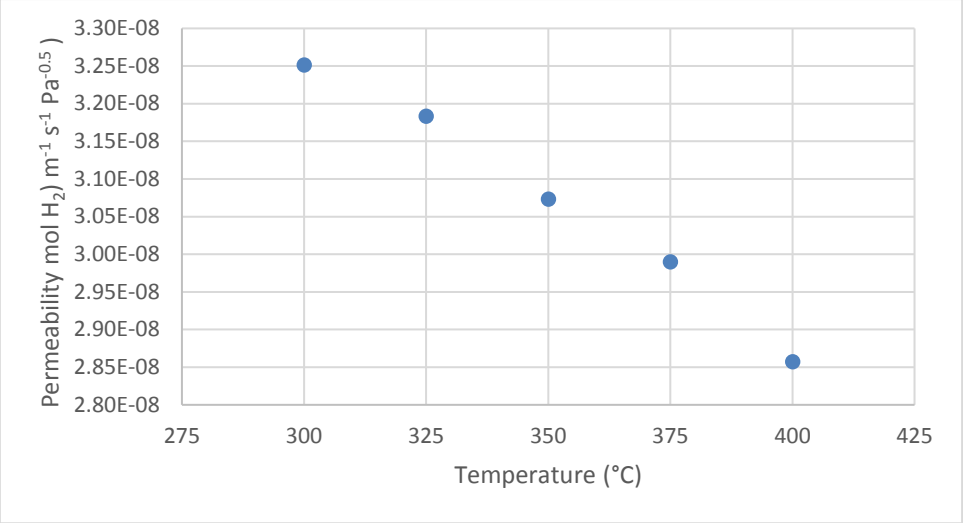

Figure 7.13 – Calculated permeability values for coated V-Ni membranes at varying temperature with mixed gas feed

Figure 7.13 shows that once again the presence of carbon dioxide reduces the permeability of the membrane when compared to a pure hydrogen feed of similar conditions (in this instance, the 4 bar pure hydrogen feed shown in section 7.5.1 above).

The extent of the reduction in permeability is not as high for the V-Ni membrane as for the other membranes investigated (comparing the 4 bar pure feed with the 4 bar partial hydrogen pressure of the mixed feed); a maximum decrease of 28.7% is calculated (at 350 °C), compared to a minimum decrease of 26 % (at 400 °C). It is believed that this is due to the membrane flux being smaller for the thicker membrane, resulting in lower depletion of hydrogen in the gas phase near the membrane surface. Whilst the palladium membrane also delivered a relatively small flux it is believed that the cold rolled surface of the membrane offered less 'real' surface area than the electroless deposited Pd-Ag surface. (Hulme *et al.*, 2011) also reports data on the effect of increasing CO_2 partial pressure on hydrogen permeability, where the permeability was found to drop by 1 $x10^{-8}$ mol m^{-1} s^{-1} $Pa^{-1/2}$ when the CO_2 concentration was increased from 0 to 30% at temperatures of 300 and 400 °C.

7.6 Discussion of Vanadium-Nickel-Aluminium Alloy Permeability Tests

An image of a coated V-Ni-Al membrane is included in figure 7.14 below.

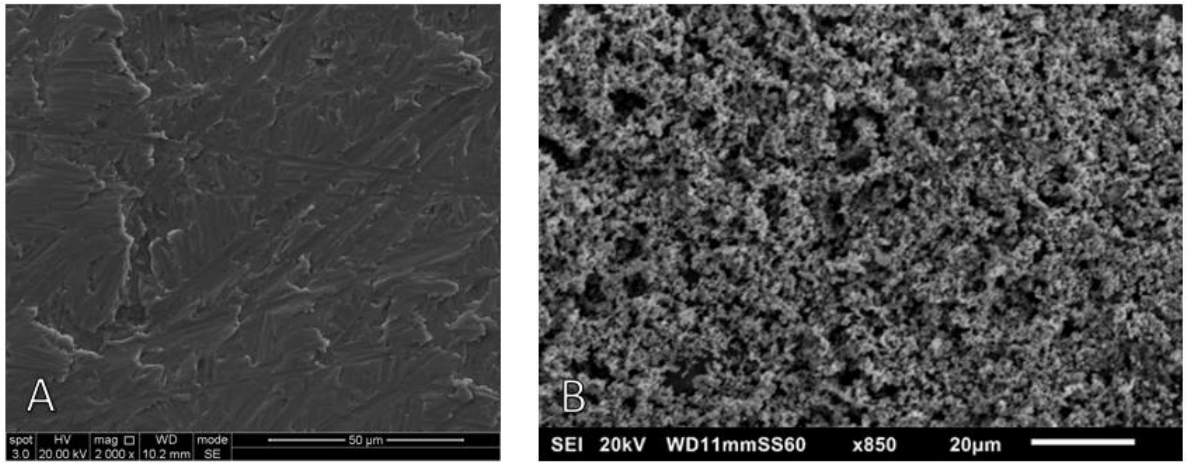

Figure 7.14 – SEM image of coated V-Ni membrane, before (A) and after (B) coating

As with the V-Ni membrane a greater surface area is expected for the coated membrane.

7.6.1 Calculating the Hydrogen Permeability of the V-Ni-Al Membrane (Pure H_2 Feed)

The calculated permeability for the coated V-Ni-Al membrane tested under pure hydrogen conditions is given in figure 7.15 below.

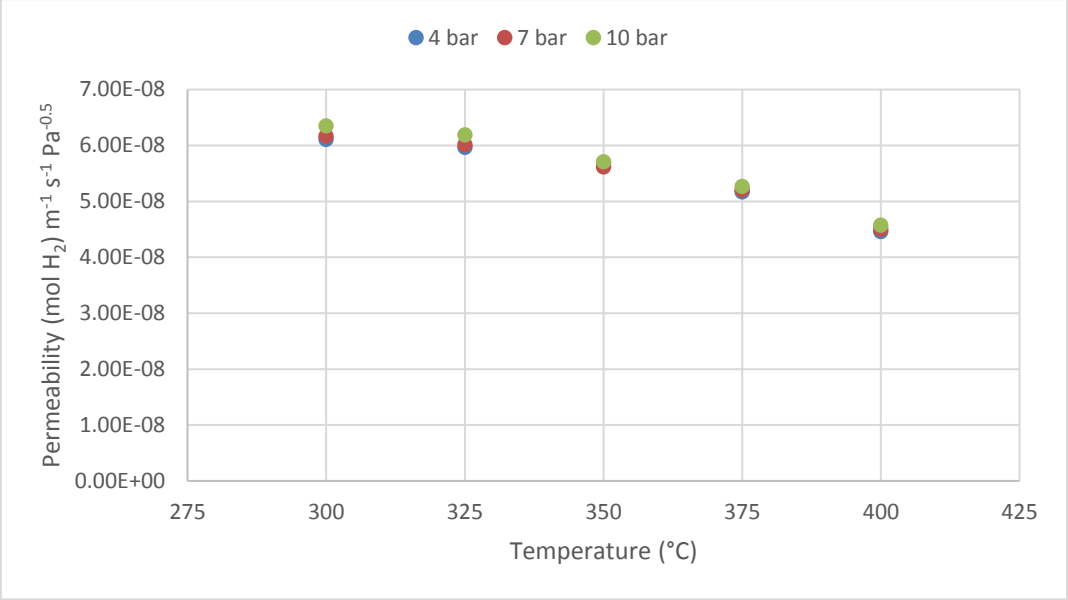

Figure 7.15 - Graph showing calculated permeability for coated V-Ni-Al membrane at various temperatures and pressures (pure H_2 feed)

As with the V-Ni alloy, the permeability of the Vi-Ni-Al membrane is shown to decrease with increasing temperature.

In both instances, the diffusivity of the membrane is expected to increase and as such the loss of permeability is likely to be due to a drop in hydrogen solubility. The calculated permeability for the V-Ni-Al membrane is higher than that of the V-Ni membrane when tested under the same conditions.

A similar result can be found in (Dolan *et al.*, 2011), where the permeability of several 85V-10Ni-5M (where M is a range of metals) membrane materials is reported. In the aforementioned study, the permeability of a 85V-15Ni membrane between 300 and 400 °C is reported to be between 2.0 and 2.5 $x10^{-8}$ mol m^{-1} s^{-1} $Pa^{-1/2}$ (in a similar range to some of the studies discussed in section 7.5 of this chapter), whilst a 85V-10Ni-5Al membrane has a reported permeability of 3.3 to 4.4 $x10^{-8}$ mol m^{-1} s^{-1} $Pa^{-1/2}$ over the same temperature range. Whilst the absolute numbers are smaller, the percentage increase in permeability is similar to that measured here.

Another example of tests on a V-Ni-Al membrane of similar composition can be found in (Ozaki *et al.*, 2003), where various ternary alloys of V-Ni-Al were tested at hydrogen feed side pressures of up to 200 kPa (only a pure stream of hydrogen was tested). The permeability of an 85V-10.5Ni-4.5Al membrane was reported for the temperature range of 200 °C to 400 °C, with the reported permeability ranging between approximately 5.5 and 7.5 $x10^{-8}$ mol m^{-1} s^{-1} $Pa^{-1/2}$. The same paper shows that an increasing amount of aluminium increases the permeability of the membrane, the 85V-15Ni membrane tested by Ozaki et al has a reported permeability ranging from 3.2 to 4.8 $x10^{-8}$ mol m^{-1} s^{-1} $Pa^{-1/2}$ (approximate values estimated from a graph), with results collected in the same 200 °C to 400 °C range.

As with the V-Ni membrane, tests were undertaken on the membrane with differing feed pressures, which allows for an investigation of the permeability change with respect to pressure at a constant temperature. Figure 7.16 contains the calculated permeabilities.

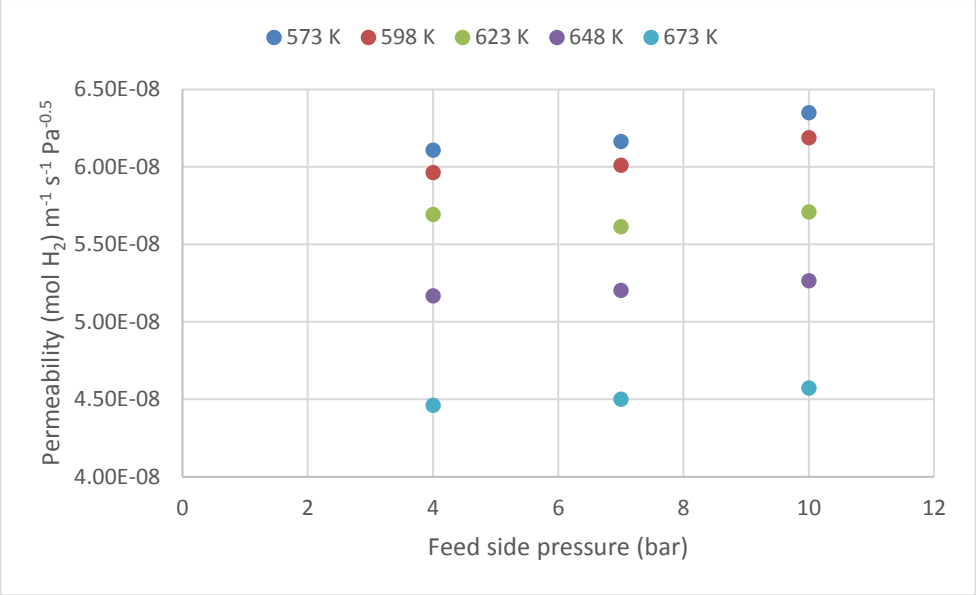

Figure 7.16 – Calculated permeability values for coated V-NI membranes at varying pressure

As with the V-Ni membrane, figure 7.16 shows less change in permeability with increasing hydrogen partial pressure than the Pd membrane but a noticeable shift up is present for the highest pressures tested. Once again, the this is amplified under conditions in which the hydrogen permeability is largest, suggesting that the increase in permeability may be due to an increase in hydrogen solubility (with higher hydrogen chemical potential at higher pressures).

A comparison of the change in the permeability between 4 bar and 10 bar feed pressure for both V-Ni and V-Ni-Al is given in table 7.2 below, where the average increase for the V-Ni-Al membrane is shown to be greater than that of V-Ni, suggesting more deviation from idealised behaviour.

Table 7.2 – Table showing change in permeability (as a percentage of 4 bar total)

% Increase in Permeability		
Temp (°C)	**V-Ni**	**V-Ni-Al**
300	1.67	3.98
325	1.90	3.80
350	1.09	0.29
375	0.70	1.90
400	1.54	2.48
Average	1.38	2.49

7.6.2 Calculating the Hydrogen Permeability of the V-Ni-Al Membrane (Mixed Feed)

As with all other membranes the permeability was calculated for the tests undertaken with a mixed gas feed of 40 vol% H_2 and 60 vol% CO_2. Figure 7.17 gives the calculated permeability for the membrane.

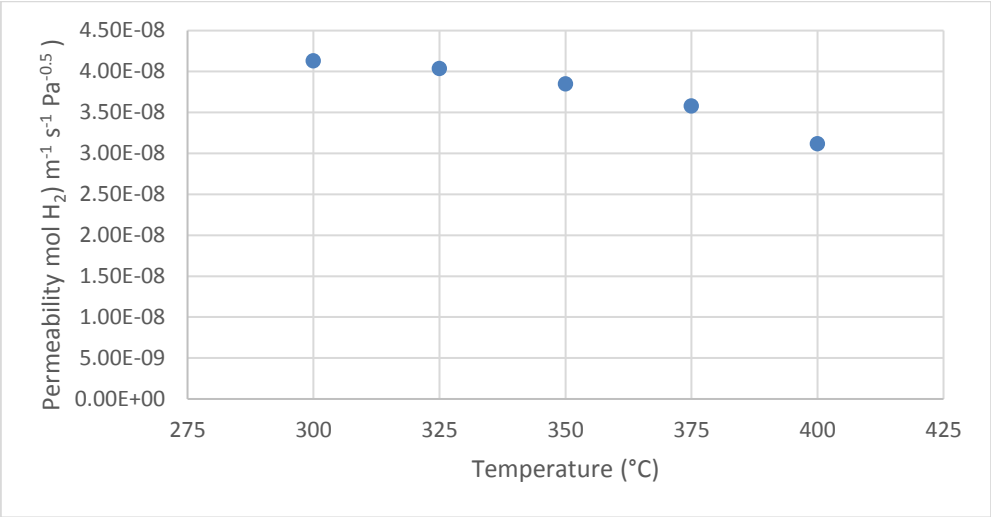

Figure 7.17 – Calculated permeability values for coated V-Ni membranes at varying temperature with mixed gas feed

As with the other membranes tested in this work, a percentage loss of permeability can be calculated in comparison to a pure H_2 feed. As with the V-Ni membrane, the lower temperatures investigated (those that deliver the highest membrane flux) were found to produce the largest loss of permeability. At 300 °C with a pure H_2 feed at 4 bar pressure a permeability of 6.1 x10^{-8} mol m^{-1} s^{-1} $Pa^{-1/2}$ was calculated/measured; for the mixed feed under similar conditions the permeability recorded is 4.1 x10^{-8} mol m^{-1} s^{-1} $Pa^{-1/2}$, a decrease of 32.4 %. No literature data could be found for comparison of the mixed feed V-Ni-Al membrane, however the decrease in permeability is comparable to the V-Ni membrane tests.

7.7 Overview of the Results

7.7.1 Summary of Permeability Data (H_2 Feed)

Upon completion of the permeability calculations it is now possible to produce a comparable summary graph of the useful values calculated. Figure 7.18 below shows such a graph for the values calculated from the pure hydrogen feed tests.

Whilst the permeability of the membranes supplied with the mixed feed is more representative of likely real-life behaviour, the tests in pure hydrogen are more useful for comparison to results collected by others.

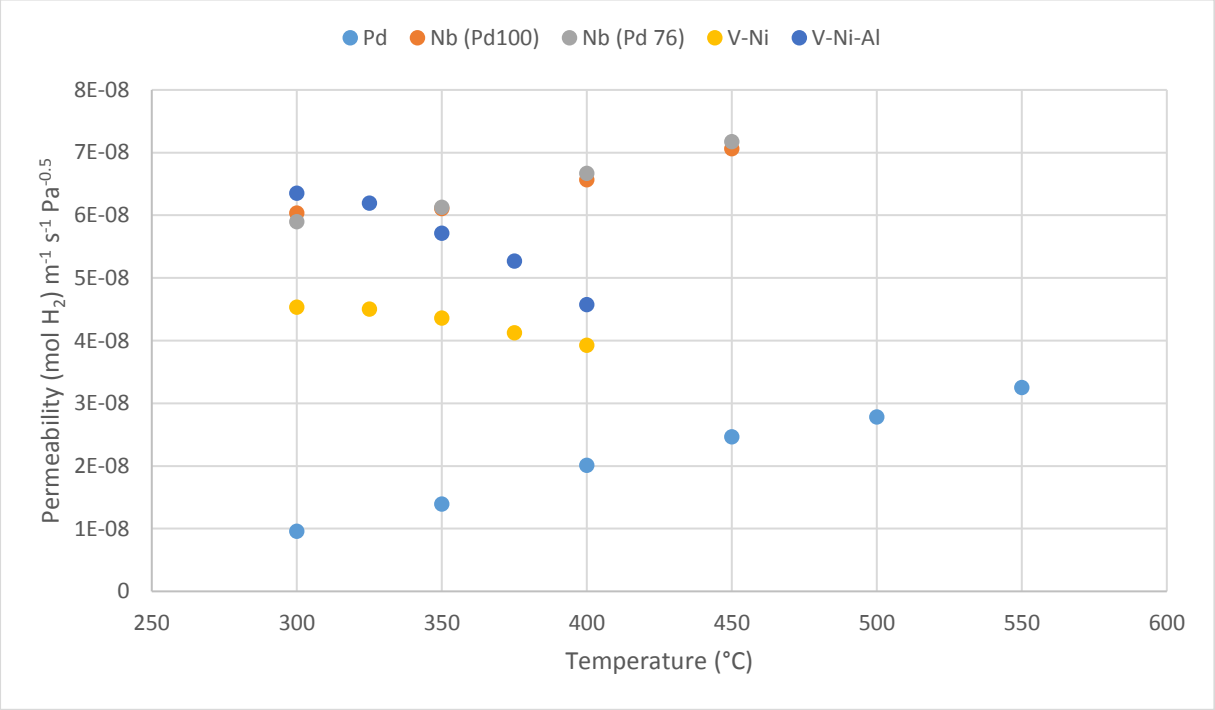

Figure 7.18 – Graph showing calculated permeabilities for various membranes with a pure H_2 feed

It is unsurprising to see that the highest permeabilities were achieved with the pure niobium membrane, even at moderate pressures the flux evolved was greater than that achieved by the other membranes. Of much more interest are the group V alloys where the membranes were found to be more stable during testing. The V-Ni-Al membrane tested actually produced a higher permeability than the niobium membrane at the lower end of the test temperature range. Such a result is encouraging, although more performance testing is required – preferably at higher pressures and for longer periods of time.

Whilst the V-Ni membrane did not show as good a performance as the ternary alloy it remains an interesting option. This membrane outperformed the palladium membrane and shows less of a reduction in permeability with increasing temperature, when compared to the V-Ni-Al membrane.

7.7.2 Summary of Permeability Data (Mixed Feed)

Figure 7.19 below includes a summary of selected measured permeabilities from tests under taken with the mixed feed conditions.

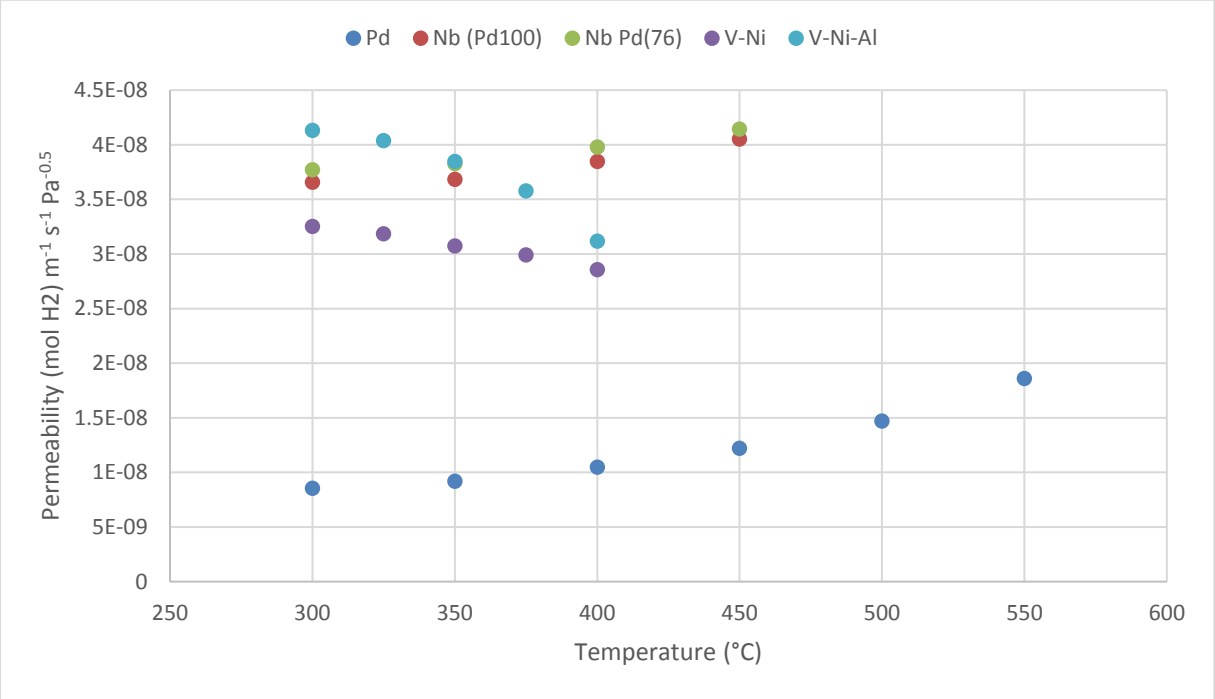

Figure 7.19 - Graph showing calculated permeabilities for various membranes with a pure mixed gas feed

Figure 7.19 shows similar trends to those shown in figure 7.18 for the corresponding membranes, as would be expected. In every instance the permeability of each membrane was found to be significantly lower than in the equivalent pure feed test (same hydrogen partial pressure differential over the membrane).

Once again, comparisons can be made across membrane materials – the Nb and V-Ni-Al membranes are comparable in their permeability at low temperatures and the V-Ni membrane out performs the Pd "yardstick" adequately too.

However, caution should be exercised when making comparisons between membranes. The graph shows that the niobium membranes suffered greater permeability loss than the vanadium alloy membranes, when comparing the maximum values from figures 7.18 and 7.19.

As both the Nb and V alloys had similar coatings it is expected that this difference is not so much a factor of the surface behaviour, but more likely due to hydrogen depletion. Table 7.3 is included to give an indication on how different the measured flux data is for each membrane. Since the depletion of hydrogen is higher at the higher fluxes it is unsurprising that this results in a larger drop in apparent permeability.

Table 7.3 – Table of membrane area flux for selected membranes

Measured membrane area flux ($cm^3\ cm^{-2}\ min^{-1}$)				
Temperature (°C)	**V-Ni**	**V-Ni-Al**	**Nb Pd100**	**Nb Pd76**
300	5.8	7.4	12.1	12.5
325	5.8	7.3		
350	5.6	7.0	12.2	12.7
375	5.4	6.5		
400	5.2	5.7	12.8	13.3
450			13.5	13.8

This behaviour is certainly something that warrants further investigation - especially when considering membranes for large scale separation.

7.7.3 Comparison of Flux and Permeability Data to the Established Targets

At the beginning of this chapter in section 7.1, a number of targets set by the US DoE were stated. Of particular interest to this work is the permeate flux target, initially given as a volume but translated into a target permeate molar flux. The target value is a flux of 1.05 mol $m^{-2}\ s^{-1}$ is stated, and this can be compared to the values calculated as part of this work. The maximum permeate flux for selected membranes is given as:

- Niobium membrane, pure H_2 feed at 450 °C: 0.18 mol $m^{-2}\ s^{-1}$
- Niobium membrane, mixed gas feed at 450 °C: 0.09 mol $m^{-2}\ s^{-1}$
- V-Ni membrane, pure H_2 feed at 300 °C: 0.12 mol $m^{-2}\ s^{-1}$
- V-Ni membrane, mixed feed at 300 °C: 0.04 mol $m^{-2}\ s^{-1}$
- V-Ni-Al membrane, pure H_2 feed at 300 °C: 0.17 mol $m^{-2}\ s^{-1}$
- V-Ni-Al membrane, mixed feed at 300 °C: 0.05 mol $m^{-2}\ s^{-1}$

As the figures stated are maximum values under the conditions investigated it is not possible to compare the values of each directly.

What is immediately apparent however is that under the conditions investigated in this PhD study no membrane delivers the required molar permeate flux. This is hardly surprising as the conditions tested under were modest and limited moderate pressures due to equipment and safety considerations. However, some extrapolations can be made from the data to give an indication of what conditions may be required to achieve the given target.

Pure niobium will not be considered, as this has been proven to not be a suitable material due to its high solubility, potentially leading to membrane failure. The temperature range will not vary from the range tested (which is incorporated in the DoE target temperature range) and thus the changeable factors are pressure differential and membrane thickness.

Taking the maximum permeability for both V-Ni and V-Ni-Al membranes (300 °C, 10 bar hydrogen feed pressure) the following modifications are proposed:

1. **Reduce membrane thickness to 0.1 mm**, **maintain same pressures**

At a thickness comparable to the Nb and Pd membranes investigated, the calculated flux for the V-Ni membrane increases from 0.12 to 0.31 mol m^{-2} s^{-1} and the flux for the V-Ni-Al membrane increases from 0.17 to 0.44 mol m^{-2} s^{-1}. Whilst this is a significant increase in flux, it does not yet meet the requirements.

2. **Reduce permeate side pressure to 0.5 bar through the use of a vacuum pump**

Reducing the permeate side pressure through the use of a vacuum pump is predicted to see the membrane permeate flux rise to 0.35 mol m^{-2} s^{-1} (V-Ni membrane) and 0.49 mol m^{-2} s^{-1} (V-Ni-Al membrane). Such a change only produces a relatively moderate increase, but should the membrane be operating in a downstream desorption limited state reducing the hydrogen partial pressure should reduce the bombardment rate and the surface coverage factor. This may then lead to a greater increase in flux than predicted from this exercise.

3. **Increase feed side pressure**

Whilst one alternative may be to further decrease the membrane thickness this is not explored here in the interest of ensuring that the membranes remain “thick”. Through preliminary calculations it was found that, by increasing the hydrogen feed side pressure to 35 bar, the desired molar flux rate could be reached for the V-Ni-Al membrane. This is a significant increase compared to the pressures tested as part of this thesis and the behaviour of the materials at these very high hydrogen concentrations remains relatively unknown. It should also be noted that the 35 bar pressure figure is suggested using

the pure hydrogen figure. For a mixed gas feed the total pressure will need to be higher to result in a hydrogen partial pressure of 35 bar.

If the membrane thickness were to be reduced to 0.075 mm (i.e. 75 μm) the required hydrogen pressure drops significantly from 35 to 22 bar. Finding a balance between membrane thickness and required pressure is likely to be a factor determined by the material's yield strength. Further studies into such properties would be advisable for any promising membrane material.

7.8 Chapter Seven Reference List

Alimov, V. N., Busnyuk, A. O., Notkin, M. E., Peredistov, E. Y. and Livshits, A. I. (2015) 'Hydrogen transport through V-Pd alloy membranes: Hydrogen solution, permeation and diffusion', *Journal of Membrane Science*. Elsevier, 481, pp. 54–62. doi: 10.1016/j.memsci.2015.01.058.

Buxbaum, R. and Marker, T. (1993) 'Hydrogen transport through non-porous membranes of palladium-coated niobium, tantalum and vanadium', *Journal of Membrane Science*, 85, pp. 29–38. Available at: http://www.sciencedirect.com/science/article/pii/037673889385004G (Accessed: 28 March 2014).

Caravella, A., Barbieri, G. and Drioli, E. (2008) 'Modelling and simulation of hydrogen permeation through supported Pd-alloy membranes with a multicomponent approach', *Chemical Engineering Science*, 63(8), pp. 2149–2160. doi: 10.1016/j.ces.2008.01.009.

Dolan, M. D., McLennan, K. G. and Way, J. D. (2012) 'Diffusion of atomic hydrogen through V-Ni alloy membranes under nondilute conditions', *Journal of Physical Chemistry C*, 116(1), pp. 1512–1518. doi: 10.1021/jp208691x.

Dolan, M. D., Song, G., Liang, D., Kellam, M. E., Chandra, D. and Lamb, J. H. (2011) 'Hydrogen transport through V85Ni10M5 alloy membranes', *Journal of Membrane Science*. Elsevier B.V., 373(1–2), pp. 14–19. doi: 10.1016/j.memsci.2011.02.028.

Hulme, J., Komaki, M., Nishimura, C. and Gwak, J. (2011) 'The effects of gas mixtures on hydrogen permeation through Pd–Ag/V–Ni alloy composite membrane', *Current Applied Physics*. Elsevier B.V, 11(4), pp. 972–975. doi: 10.1016/j.cap.2010.12.024.

Kishida, K., Yamaguchi, Y., Tanaka, K., Inui, H., Tokui, S., Ishikawa, K. and Aoki, K. (2008) 'Microstructures and hydrogen permeability of directionally solidified Nb-Ni-Ti alloys with the Nb-NiTi eutectic microstructure', *Intermetallics*, 16(1), pp. 88–95. doi: 10.1016/j.intermet.2007.08.001.

Morreale, B. D., Ciocco, M. V, Enick, R. M., Morsi, B. I., Howard, B. H., Cugini, A. V and Rothenberger, K. S. (2003) 'The permeability of hydrogen in bulk palladium at elevated temperatures and pressures', 212, pp. 87–97.

Nambu, T., Shimizu, N., Ezaki, H., Yukawa, H. and Morinaga, M. (2005) 'Hydrogen Permeation of Pure Niobium Metal in Highly Soluble Hydrogen State', *Journal of the Japan Institute of Metals*, 69(9), pp. 841–847. doi: 10.2320/jinstmet.69.841.

Nishimura, C., Komaki, M., Hwang, S. and Amano, M. (2002) 'V–Ni alloy membranes for hydrogen purification', *Journal of Alloys and Compounds*, 330–332, pp. 902–906. doi: 10.1016/S0925-8388(01)01648-6.

Ockwig, N. W. and Nenoff, T. M. (2007) 'Membranes for hydrogen separation.', *Chemical reviews*, 107(10), pp. 4078–110. doi: 10.1021/cr0501792.

Ozaki, T., Zhang, Y., Komaki, M. and Nishimura, C. (2003) 'Hydrogen permeation characteristics of V-Ni-Al alloys', *International Journal of Hydrogen Energy*, 28(11), pp. 1229–1235. doi: 10.1016/S0360-3199(02)00251-3.

Zhang, G. X., Yukawa, H., Watanabe, N., Saito, Y., Fukaya, H., Morinaga, M., Nambu, T. and Matsumoto, Y. (2008) 'Analysis of hydrogen diffusion coefficient during hydrogen permeation through pure niobium', *International Journal of Hydrogen Energy*, 33(16), pp. 4419–4423. doi: 10.1016/j.ijhydene.2008.05.062.

8 Conclusions and Further Work

8.1 Conclusions

The following conclusions are drawn from the previous seven chapters in this thesis:

- A number of negative effects can be attributed to the combustion of carbon-based fuels. One under-reported issue is that of the production of sub-micron particulate matter, which has been shown to have negative effects on health and causing death. It is concluded that a new energy vector is needed, particularly in urban areas where transport emissions of sub-micron particulate matter is high.

- Hydrogen offers potential as a versatile non-carbon energy vector, however SMR produced hydrogen currently requires prohibitively expensive separation for use of hydrogen in fuel cells. It is concluded that a technological gap exists for the development of a low-maintenance, low operating cost system capable of producing hydrogen to purities required for utilisation in fuel cells.

- Hydrogen separation membranes offer a potential alternative to existing hydrogen separation technology that would meet the criteria specified above. Polymer, ceramic and metallic membranes were considered in this work and it was concluded that metallic membranes offer the most promise in satisfying both the demand for a high flux and a high selectivity of hydrogen. However, existing metallic membranes are expensive due to their reliance on palladium and have yet to be commercialised on any large scale. It is clear that a need exists to develop metallic membranes that use little or no palladium.

- Group Vb metals offer promise as bulk membrane materials due to their high reported hydrogen permeabilities. These metals need to be alloyed to suppress hydrogen solubility and increase membrane stability and require a catalytic coat to promote hydrogen disassociation and re-association.

- It is concluded that nickel and aluminium are suitable alloying components for vanadium-based membranes. Previous works have utilised these materials in binary and ternary systems to suppress hydrogen solubility and the vanadium-based membranes tested in this work were

found to be stable under operating temperatures and pressures in the desired range. The permeability for the V-Ni and V-Ni-Al membranes tested in pure hydrogen feeds was found to be in a similar range to other reported figures in the same temperature range. Pd-Ag Coated V-Ni and V-Ni-Al membranes are shown to have a maximum apparent permeability of 3.3 $x10^{-8}$ mol m^{-1} s^{-1} $Pa^{-0.5}$ and 4.1 $x10^{-8}$ mol m^{-1} s^{-1} $Pa^{-0.5}$ when tested at 300 °C with a binary feed mixture of 60% vol CO_2 and 40% vol H_2.

- Tests conducted on bulk niobium membranes resulted in the calculation of hydrogen permeability significantly smaller than that predicted in dilute Gorsky-type studies. The permeability data (with a maximum value of 7.2 $x10^{-8}$ mol m^{-1} s^{-1} $Pa^{-0.5}$ in pure hydrogen test conditions) collected was compared to other non-dilute values given in literature and showed relatively good agreement at the lower end of test temperatures.

- A number of surface catalysts were investigated experimentally. It is concluded that oxidised silver is not a suitable surface catalyst for vanadium and niobium membranes with the evolved flux being far below target and incapable of performing in the target temperature range of 300 to 400 °C. Palladium and palladium silver alloys were also investigated, with little difference in performance found between the pure palladium (Pd 100) and the Pd 76 alloy coating. An increase in silver content to 45% (Pd 55) saw a significant drop in membrane performance (mirroring what is found in Pd-Ag bulk alloys); it is believed that this is due to the limitation of available active sites for hydrogen dissociation.

- For all membranes a significant drop in measured permeability was found when the binary gas mixture was used in tests. It is concluded that this drop is a function of two factors: competitive adsorption of carbon dioxide on the surface and the depletion of hydrogen in the gas phase near the membrane surface. As expected each membrane was found to offer excellent selectivity to hydrogen, with permeate hydrogen purity of up 99.9 % recorded.

- It is concluded that metallic membranes offer potential for use as hydrogen separation due to their excellent separation properties. Further testing is required on the bench scale to test longevity and to investigate the behaviour of the V-Ni and V-Ni-Al membranes at higher operational pressures to achieve the flux required for expected commercialisation.

8.2 Further Work

The most immediate issue to consider is the impact of other gases on hydrogen permeability. The results show a significant loss of permeability even under mild test conditions, if the target permeate flux of 1.05 mol m^{-2} s^{-1} is to be met from a mixed gas source, depletion of the near surface hydrogen concentration could become problematic. Such considerations are almost independent of the bulk permeability, but the surface is likely to play a significant role - as will optimal design of a membrane separator. Whilst both factors will have an impact, they will have more of an impact on differing elements of permeability loss.

The results presented in chapter six show that, even under conditions where hydrogen concentration depletion is likely to be relatively low (the vanadium alloy tests), a significant drop off in permeability is recorded, with a drop of at least 25% typical. Such a reduction is likely due to competitive surface adsorption. Whilst the focus of this thesis has been on the testing of membrane permeability it is worthwhile to give some brief comments on how this depletion effect might be reduced.

A surface coating material that binds/interacts weakly with non-hydrogen species could also be attractive for use, however this coating would still need to retain the catalytic properties that the Pd based coatings investigated show. Possible suggestions for materials to investigate include nickel alloys, as nickel has been successfully used as a coating in pure hydrogen tests previously (as discussed in chapter two), albeit with poorer performance than palladium alloys. The notion of using pure nickel has previously been dismissed by other groups (Dolan et al), however little consideration of nickel alloys appears to have been given. Other good candidate materials are likely to have weak CO_2, CO, H_2S and CH_4 (amongst other species) bond energies. DFT studies may provide a useful starting point for the investigation into potential coatings – such as those discussed briefly in chapter two of this work.

Alternatively, an ideal surface coating would have an increased real surface area per m^2 of membrane. One such way to achieve this could potentially be to roughen the surface of the membrane before coating, using either physical or chemical methods. The reasons for this can be seen in chapter five – an increase in the number of surface sites N_s allows for more adsorption (in this case more adsorption of the desired gas) and thus allows for more surface-to-bulk transfer and a higher measured permeate flux. Determining the best coating method for applying the surface catalyst should be seen as a priority. A number of surface coating techniques have been utilised in this work, and other alternatives exist beyond those tested, with varying success (predominantly due to the materials coated).

The electroless plating completed as part of this work was relatively rudimental but did garner some success. Improving this method (it would arguably be more useful to co-deposit Pd and Ag in one electroless bath to generate a more uniform coating if possible) and the development of a PVD co-deposition method for Pd-Ag for future tests would be beneficial. In this work, the Pd-Ag coat outperformed the pure Pd coating in the Nb tests undertaken, it is unknown as of now whether this was a quirk of the deposition method or a genuine improvement. Comparisons to published data under similar conditions are difficult due to the scarcity of relevant information.

Finally, the impact of hydrogen depletion should be considered in the design of membrane reactors. The flat disc test reactor utilised in this work has little promise for larger scale use, typical membrane reactor/separator designs incorporate tubular membranes and this is likely to remain the most feasible design. From the tests undertaken in this thesis it is believed that a good reactor design should incorporate:

- A large membrane surface area to gas volume ratio, as this would maximise contact with the surface.
- Multiple feed gas inlet points to allow for good mixing of the feed side gas and to prevent areas of low hydrogen concentration reducing overall membrane efficiency.
- The membrane should be modular to allow for shutting off of part of the separator if required, whether this be for maintenance or to cope with varying amounts of feed supply (if the amount of feed gas drops non-modular system will likely see a decrease in operational pressure reducing the efficiency of separation).

Figure 8.1 below gives an approximation of how an individual separation enclosure could operate, with the tube structure then housed in a structure similar to a shell and tube heat exchanger. The orange arrows represent the feed which would be supplied though an inner pipe and distributed along the length of the membrane. The red arrows represent the rejected gas phase and the green arrows represent the permeate.

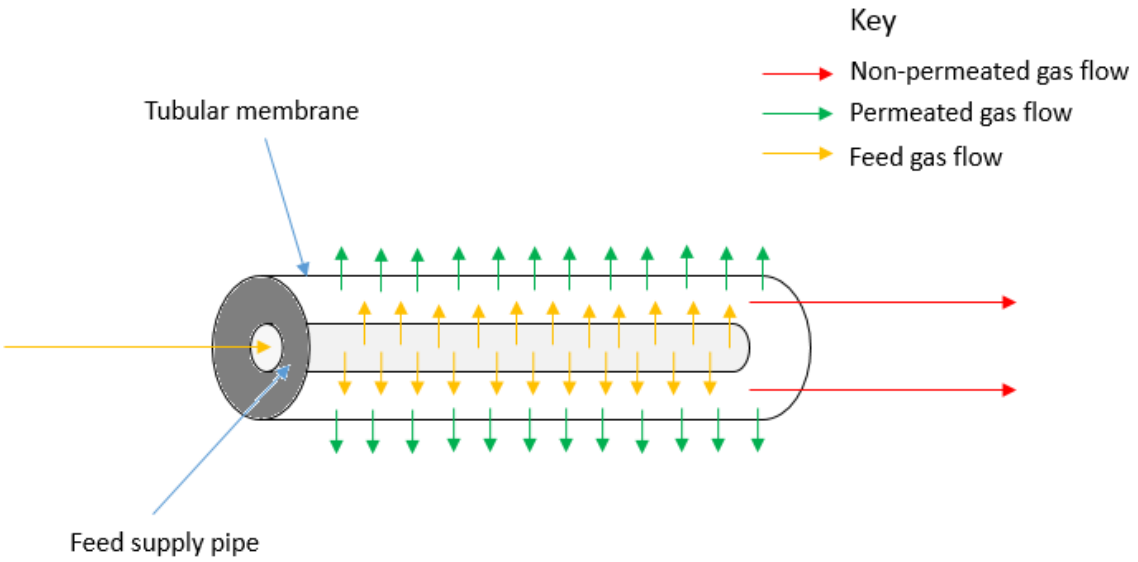

Figure 8.1 – Schematic of suggested membrane separator module design

It is suggested that the following tasks be completed as future work:

- Re-test the V-Ni and V-Ni-Al membranes under the same conditions with co-deposited PD-Ag coatings, preferably deposited through several different techniques to investigate the impact of coatings and their contribution to the measured permeate flux (i.e. do different coating methods produce different resistances to transport?). Comparing permeability data for different membrane coatings should give some indication on which coating method offers most promise. Of most importance is the testing of a co-deposited Pd-Ag PVD coating on a roughened membrane surface to increase effective surface area.
- Investigate V-Ni and V-Ni-Al membranes at the conditions discussed in chapter 7.7.3 to investigate the feasibility of the suggested membranes reaching established targets.
- Produce hydrogen solubility isotherms under non-dilute conditions for V-Ni and V-Ni-Al alloys to allow for the investigation of the H/M concentration and the development of more advanced models that incorporate chemical potential as a driving force and not hydrogen concentration. A suggested suitable methodology for the collection of these isotherms would be that used by Dolan et al previously mentioned (see section 5.1.1 and 7.5.1).

Design a suitable membrane reactor to minimise the effect of hydrogen depletion in mixed feed tests. Suggestions for how this could be done are given in above.